FUNCTIONAL AND PHYLOGENETIC SIGNALS IN THE PECTORAL GIRDLE OF THALATTOSUCHIA AND DYROSAURIDAE (CROCODYLOMORPHA)

ISAURE SCAVEZZONI, MICHELA M. JOHNSON, STÉPHANE JOUVE, AND VALENTIN FISCHER

ABSTRACT. Crocodylomorphs have colonized various environments from fully terrestrial to fully aquatic, making it an important clade among archosaurs. A remarkable example of the rich past diversity of Crocodylomorpha Hay, 1930 is the marine colonization undergone by several crocodylomorph lineages, particularly Thalattosuchia Fraas, 1901 during the Early Jurassic-Early Cretaceous, and Dyrosauridae de Stefano, 1903 during the Late Cretaceous-Early Eocene. Thalattosuchia represents the most impressive and singular marine radiation among Crocodylomorpha, occupying various ecological niches, before enigmatically disappearing in the Cretaceous. Dyrosauridae, on the other hand, is known for surviving the end-Cretaceous mass extinction in abundance but subsequently vanished. The evolutionary path undertaken by crocodylomorphs into the aquatic environments and the reasons for their disappearance outside marine extinction events during the Mesozoic remain a mystery. Despite a well-preserved fossil record, attention has primarily centered on craniodental adaptations, overlooking the swimming-related adaptations recorded in the postcranial skeleton.

This research primarily involves a comprehensive examination of the pectoral girdle of the most representative members of Thalattosuchia and Dyrosauridae, highlighting their evolutionary trajectories over time. Additionally, this work aims to test the phylogenetic signal residing in the postcranial anatomy of Crocodylomorpha. As such, the most recent and complete Crocodylomorpha phylogenetic dataset has been repurposed: 42 new postcranial characters have been added and several other have been revised to address our phylogenetic question. We stress that postcranial anatomy constitutes an important tool supply to better understand the relations of extinct crocodyliforms, but also offers insights on their development, ecology, and biomechanics.

CONTENTS

1. Introduction 2
2. Material & conventions 3
2.1. Orientation and terminology 3
2.2. Sampling 5
2.3. Phylogeny 13
2.4. Institutional abbreviations 14
3. The extant crocodylian shoulder articulation and musculature 14
4. Pectoral muscles of extant crocodylians 20
4.1. Coracoid 21
4.2. Scapula 22
5. Global measurement tables 24
6. The appendicular skeleton of thalattosuchians 28
6.1. *Turnersuchus hingleyae* Wilberg et al., 2023 28
7. The appendicular skeleton of thalattosuchians: metriorhynchoids 36
7.1. *Pelagosaurus typus* Bronn, 1841 36
7.2. *Thalattosuchus superciliosus* Blainville in Eudes-Deslongchamps and Blainville, 1852 42
7.3. *Gracilineustes leedsi* Andrews, 1913 54
7.4. *Rhacheosaurus gracilis* von Meyer, 1831 61
7.5. *Cricosaurus albersdoerferi* Sachs et al., 2021 63
7.6. *Cricosaurus bambergensis* Sachs et al., 2019 67

7.7. *Cricosaurus suevicus* Fraas, 1901 70
7.8. *Cricosaurus lithographicus* (Herrera et al., 2013b) Wagner, 1858 74
7.9. *Cricosaurus araucanensis* (Gasparini and Dellapé, 1976) Wagner, 1858 76
7.10. *'Metriorhynchus' brachyrhynchus* Eudes-Deslongchamps, 1867 79
7.11. *Geosaurus lapparenti* Debelmas and Strannoloubsky, 1957 84
7.12. *Dakosaurus maximus* Plieninger, 1846 87
7.13. *Tyrannoneustes lythrodectikos* Young et al., 2012 91
7.14. *Torvoneustes carpenteri* Wilkinson et al., 2008 96
8. The appendicular skeleton of thalattosuchians: teleosauroids 99
8.1. *Mycterosuchus nasutus* Andrews, 1913 99
8.2. *Aeolodon priscus* von Sömmerring, 1814 108
8.3. *Indosinosuchus potamosiamensis* Martin et al., 2019b 113
8.4. *Teleosaurus cadomensis* Lamouroux, 1820 116
8.5. *Platysuchus multiscrobiculatus* Berckhemer, 1929 119
8.6. *Macrospondylus bollensis* Jäger, 1828 125
8.7. *Charitomenosuchus leedsi* Andrews, 1909 131
8.8. *Neosteneosaurus edwardsi* Eudes-Deslongchamps, 1868 138
8.9. *Lemmysuchus obtusidens* Andrews, 1909 Johnson et al., 2017 146
8.10. *Machimosaurus hugii* von Meyer, 1837 153
9. The appendicular skeleton of dyrosaurids 156
9.1. *Anthracosuchus balrogus* Hastings et al., 2014 156
9.2. *Hyposaurus natator* Owen, 1849 159
9.3. *Dyrosaurus maghribensis* Jouve et al., 2006 169
9.4. *Congosaurus bequaerti* Dollo, 1914 175
10. Results 181
10.1. Myology 181
10.2. Phylogeny 183
11. Discussion 187
11.1. A range of shapes and movements 187
11.2. Phylogeny 189
12. Conclusions 191
13. Acknowledgements 195
References 196
List of Figures 203

1. Introduction

Within Thalattosuchia, two distinct clades with significantly different evolutionary histories can be identified: Metriorhynchoidea, which includes several highly pelagic forms (Fernández and Gasparini, 2008; Herrera et al., 2013a; Young et al., 2010; Wilberg, 2015a; Herrera et al., 2017), and Teleosauroidea, primarily consisting of semi-aquatic forms (Hua and De Buffrenil, 1996; Hua and Buffetaut, 1997; Johnson et al., 2018; Wilberg, 2015a; Foffa et al., 2019; Johnson et al., 2020). Derived metriorhynchoids (*i.e.* metriorhynchids) exhibit a range of unique features associated with a fully aquatic lifestyle, including laterally oriented orbits, pre-orbital salt glands, reduction of the forelimbs, paddle-like hindlimbs, loss of dermal ossification, and a hypocercal tail (similar to merriamosaurian ichthyosaurs and some advanced mosasaurs) (Young et al., 2010; Fernández and Gasparini, 2008; Herrera et al., 2013a; Wilberg, 2015a; Molnar et al., 2015; Young et al., 2020b,a). However, the posterior retraction of the external nares, a crucial feature for sustained swimmers, occurs relatively late in some metriorhynchids (Young

et al., 2020b). The evolutionary history of basal Metriorhynchoidea remains uncertain due to fragmentary fossil evidence (Wilberg, 2015a; Ősi et al., 2018; Aiglstorfer et al., 2019), obscuring the timing of these aquatic adaptations, which appear to follow a mosaic pattern (Wilberg, 2015b; Ősi et al., 2018; Aiglstorfer et al., 2019). Teleosauroids and the basal metriorhynchoid *Pelagosaurus typus* Bronn, 1841 are primarily known from Early Jurassic deposits (Pierce and Benton, 2006; Jouve, 2009; Young et al., 2016) but share some marine adaptations with more derived metriorhynchoids, such as a streamlined body and skull and reduced forelimbs (Young et al., 2011; Chiarenza et al., 2015; Ősi et al., 2018; Johnson et al., 2020, 2023). Teleosauroidea also underwent at least two transitions to a pelagic lifestyle with *Aeolodon* + *Bathysuchus* (Foffa et al., 2019) and *Machimosaurus* (Martin and Vincent, 2013; Young et al., 2014). Teleosauroids and *Pelagosaurus* likely employed axial subundulatory swimming, whereas metriorhynchids probably had a more efficient swimming mode near the thunniform side of the continuum (Young et al., 2010; Molnar et al., 2015). Additionally, many studies have compared the general morphology of thalattosuchians to that of other crocodyliforms (Wilberg, 2015a; Molnar et al., 2015; Wilberg et al., 2019), primarily due to a lack of comprehensive postcranial data on thalattosuchians, especially in cladistic datasets, where they account for at most 27% in the most recent datasets. This lack of data makes it difficult to reliably estimate the ecological diversity of the group over time, making it challenging to assess the impact of the debated Jurassic-Cretaceous boundary extinction (see Tennant et al. (2016); Fischer et al. (2012); Benson and Druckenmiller (2014)) on the ecological diversity of marine crocodyliforms at present.

Dyrosauridae, alongside Pholidosauridae, belongs to the extinct crocodyliform clade Tethysuchia, which spans the Late Jurassic to the Middle Eocene (Jouve and Jalil, 2020; Jouve, 2021). Dyrosaurids initially inhabited non-marine environments (Hastings et al., 2010, 2011, 2014; Jouve, 2021) before transitioning to a marine habitat with more advanced members (Schwarz et al., 2006; Jouve et al., 2008a; Schwarz-Wings et al., 2009; Jouve and Jalil, 2020; Jouve et al., 2021; Jouve, 2021). Dyrosaurid morphology differs from the pelagic adaptations observed in metriorhynchoids: dyrosaurids are characterized by highly flexible tails (Schwarz-Wings et al., 2009), robust girdles and limbs, ventral and dorsal osteodermal shields, tall neural spines, and thoracic hypapophyses (Langston, 1995; Jouve and Schwarz, 2004; Schwarz et al., 2006; Jouve et al., 2006; Schwarz-Wings et al., 2009). Dyrosaurids are believed to have originated in Africa (Barbosa et al., 2008; Jouve et al., 2008b; Hastings et al., 2014; Jouve et al., 2021) and were initially documented in the Turonian to Early Campanian Lapur Sandstone in northern Kenya (Sertich et al., 2006; Tiercelin et al., 2012) and the Campanian to Maastrichtian Shendi Formation in Sudan (Buffetaut et al., 1990; Salih et al., 2015). Dyrosaurids experienced multiple dispersal events from their place of origin, including three episodes of interchange with the Americas during the Late Cretaceous (Hastings et al., 2014; Jouve et al., 2021). The group survived the Cretaceous-Paleogene mass extinction (Bronzati et al., 2012, 2015; Hastings et al., 2014; Wilberg et al., 2019; Jouve and Jalil, 2020; Jouve, 2021) and ultimately went extinct around the Ypresian-Lutecian boundary (Buffetaut, 1978; Jouve et al., 2006; Jouve, 2007; Martin et al., 2019a; Jouve, 2021). Recent in-depth studies have shed light on the evolution (Jouve and Jalil, 2020; Jouve et al., 2021; Jouve, 2021) and ecological diversity (Jouve, 2021) of dyrosaurids. However, the postcranial anatomy of dyrosaurids remains understudied (Godoy et al., 2016) and would benefit from detailed investigation, as has been undertaken in some recent works (Jouve and Jalil, 2020; Jouve, 2021).

2. MATERIAL & CONVENTIONS

2.1. **Orientation and terminology.** To establish the orientation of the various bones in the postcranial skeleton, we've chosen a different approach than one based on the presumed resting posture of the extinct taxon (*e.g.*, refer to fig. 1). Instead, in our convention, we determine the bone orientations based on the body of the animal when it's lying flat, with its limbs positioned perpendicular to the body within the coronal plane. We've opted for this orientation method because it's straightforward to implement and ensures consistency, leading to more precise comparisons across different groups. We've included a

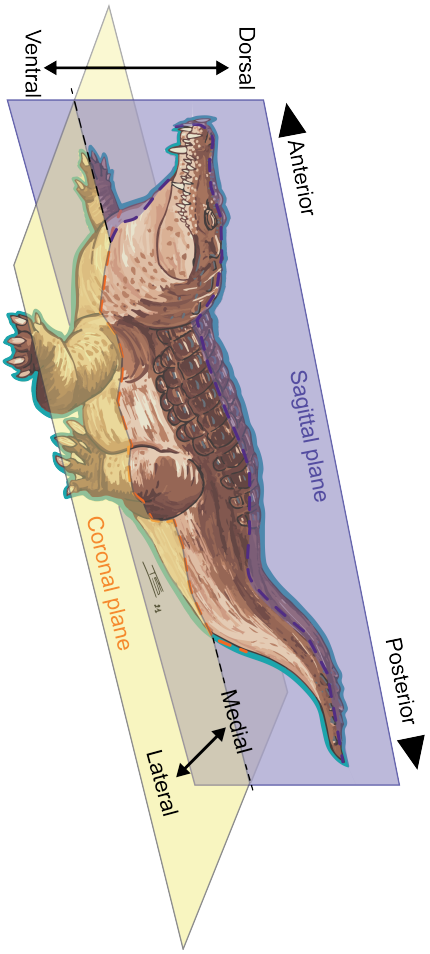


FIGURE 1. Schematic representation of a dyrosaurid (*Cerrejonisuchus improcerus*) illustrating the conventions of bone orientation based on the presumed resting pose of said taxa. Artwork by I.S. Picture modified from Scavezzoni and Fischer (2023).

schematic representation of a teleosauroid pectoral girdle in lateral view on fig. 2 to illustrate the impact of our conventions.

Terms employed:

- Anterior–posterior: ”Anterior” refers to the part of the bone closer to the front of the animal than the rear, while ”posterior” refers to the part of the bone closer to the rear of the animal than its front.;

- Dorsal–ventral: ”Dorsal” relates to the part of the bone closer to the animal’s back than its abdomen, whereas ”ventral” relates to the part of the bone closer to the abdominal side of the animal than its spine. For the scapula, the ventral margin also corresponds to the proximal margin. For the coracoid, the dorsal margin also corresponds to the proximal margin.

- Medial–lateral: ”Medial” refers to any part closer to the centre of the animal (along the sagittal or bilateral plane) than its flanks, and ”lateral” refers to any part situated farther away from the

centre of the animal. For the coracoid, the medial margin also corresponds to the distal margin.

- Proximal–distal: "Proximal" refers to the part of the bone close to the body stem of the animal (where the girdles meet), and "distal" refers to the extremity of the bone situated farther away from the stem. For the scapula, the distal margin also corresponds to the dorsal margin.

2.2. **Sampling.**

2.2.1. *Selection of specimens:* We selected the most representative specimens based on the completeness of their materials and/or the presence of an associated skull for further taxonomical identification (refer to tables 1 to 3).

2.2.2. *Measurement methods:* For most specimens, we conducted measurements using digital calipers with an approximate error of 0.1 mm. Additional measurements were obtained from 3D scans using the freely available software for data analysis and 3D measurement, GOM Inspect 2018.

2.2.3. *Surface Scan Data:* Surface scan data for the majority of specimens were acquired using the Creaform HandySCAN 300 surface laser scanner, which offers an accuracy of 0.2 mm. The surface model of *Acherontisuchus guajiraensis* was generated through photogrammetry using Meshroom version 2021.1.0 and assembled using Artec Studio 16. The models of the NJSM 23368 specimen of *Hyposaurus natator* Owen, 1849 were shared and scanned by Candice Stefanic using the structured light scanner Artec Space Spider, which offers an accuracy of up to 0.05 mm.

2.2.4. *3D modelling and repairs:* Blender (version 3.1.2) was employed for mirroring bones to achieve the preferred left polarity and to address obvious defects in certain portions. Bone reconstructions are based on phylogenetic closeness. The 3D girdle models presented in this work are available on ORBi, the institutional repository of ULiege.

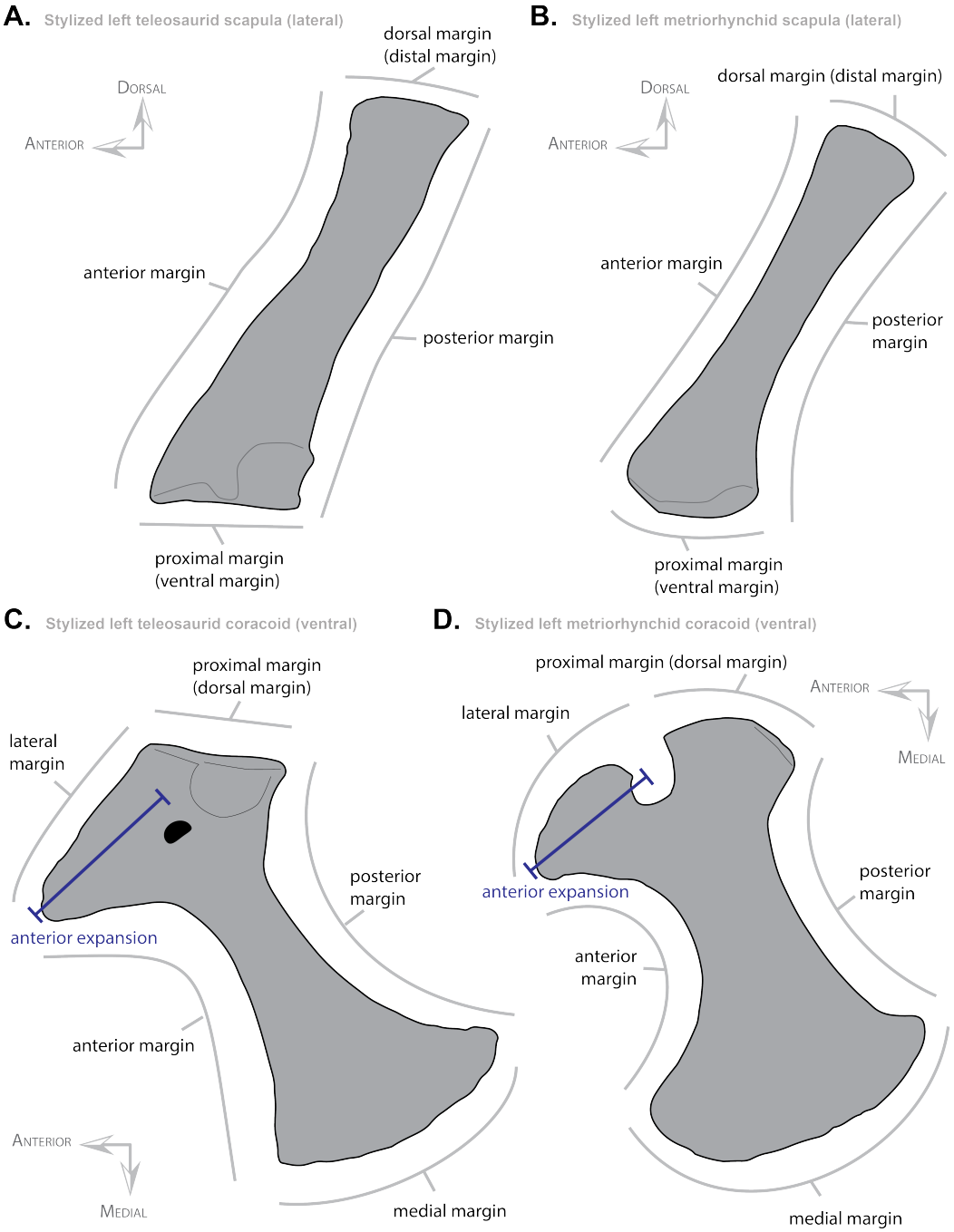


FIGURE 2. Schematic left teleosaurid and metriorhynchid pectoral girdle in lateral view as laying on a flat surface illustrating the orientation of each bone. **A & B** based on *Charitomenosuchus leedsi* NHMUK PV R 3806 and **C & D** based on the reconstruction of *Thalattosuchus* GLAHM V1146 from below. **A.** Stylized left scapula in lateral view; **B.** Stylized left scapula in lateral view; **C.** Stylized left coracoid in ventral view; **D.** Stylized left coracoid in ventral view. Terms in parentheses correspond to an alternative designation. The dark blue line indicates the anterior expansion of the coracoid head, which is measured from the anterior extremity of the scapulocoracoid synchondrosis surface.

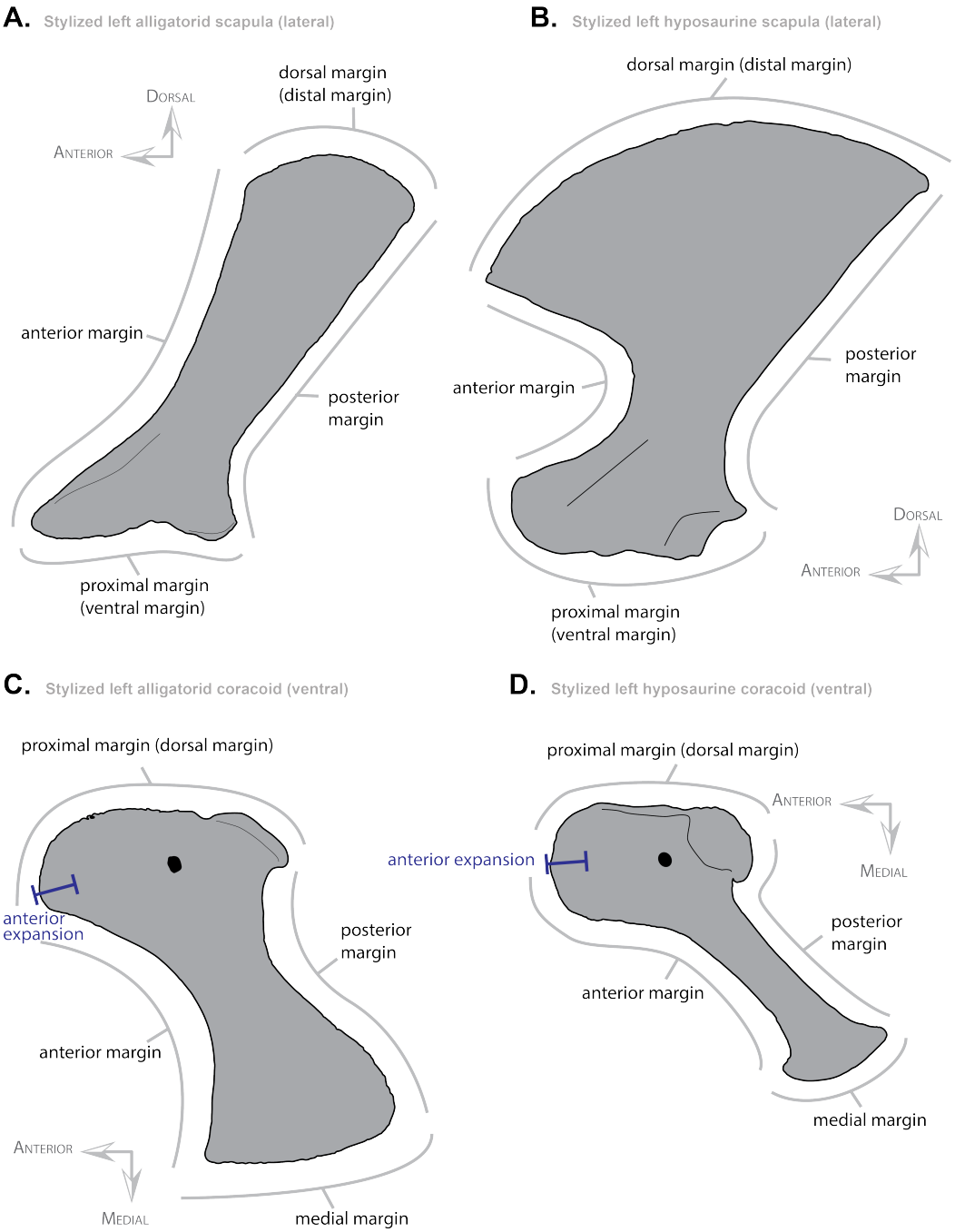


FIGURE 3. Schematic left alligatorid and hyposaurine pectoral girdle in lateral view as laying on a flat surface illustrating the orientation of each bone. **A & B** based on *Caiman crocodylus* NMW 30900 and **C & D** based on the reconstruction of *Congosaurus bequaerti* MRAC 1809 & MRAC 1811. **A.** Stylized left scapula in lateral view; **B.** Stylized left scapula in lateral view; **C.** Stylized left coracoid in ventral view; **D.** Stylized left coracoid in ventral view. Terms in parentheses correspond to an alternative designation. The dark blue line indicates the anterior expansion of the coracoid head, which is measured from the anterior extremity of the scapulocoracoid synchondrosis surface.

Species	Inventory number	Notes	Age	Formation	Location	Hypodigm	Completeness	References
Pelagosaurus typus	BRLSI M.1418		Jurassic (Toarcian)	Upper Lias Group	Strawberry Bank (England)	Referred	Skull & postcranium	(Pierce and Benton, 2006)
Pelagosaurus typus	BRLSI M.3578		Jurassic (Toarcian)	Upper Lias Group	Strawberry Bank (England)	Referred	Skull & postcranium	(Pierce and Benton, 2006)
Thalattosuchus superciliosus	GLAHM V1005		Jurassic (Middle Callovian)	Oxford Clay Fm	UK	Referred	Partial postcranium	GLAHM data portal
Thalattosuchus superciliosus	GLAHM V1146		Jurassic (Middle Callovian)	Oxford Clay Fm	UK	Referred	Partial postcranium	GLAHM data portal
Thalattosuchus superciliosus	PMU 35988					Referred	Nearly complete skeleton in 3D	
Thalattosuchus superciliosus	NHMUK PV R 1530		Middle or Upper Jurassic (Callovian or Oxfordian)	Oxford Clay Fm	UK	Referred	Partial cranium & postcranium	Young et al. (2020a)
Thalattosuchus superciliosus	GLAHM V1143		Jurassic (Middle Callovian)	Oxford Clay Fm	UK	Referred	Partial cranium & postcranium	GLAHM data portal, Young et al. (2020a)
Gracilineustes leedsi	NHMUK PV R 3014		Jurassic (Callovian)	Oxford Clay Fm	UK	Referred	Skull & postcranium	NHMUK data portal, Young et al. (2024)
Gracilineustes leedsi	NHMUK PV R 3015		Jurassic (Callovian)	Oxford Clay Fm	UK	Holotype	Skull & partial postcranium	NHMUK data portal, Young et al. (2024)
Rhacheosaurus gracilis	NHMUK PV R 3948		Late Jurassic (Tithonian)	Solnhofen Lithographic Limestone	Germany	Referred	Complete 2D skeleton	NHMUK data portal, Young et al. (2024)
'Metriorhynchus' brachyrhynchus	NHMUK PV R 4696	Part of skeleton R4763	Jurassic (Middle Callovian)	Oxford Clay Fm	UK	Referred	Fore paddle	NHMUK Data Portal
Cricosaurus albersdoerferi	BMMS-BK 1-2	Sachs et al. (2021)	Jurassic (Late Kimmeridgian)	Torleite Fm	Bavaria (Germany)	Holotype	Nearly complete skeleton in 2D	Sachs et al. (2021)
Cricosaurus bambergensis	NKMB-P-Watt14/274	Sachs et al. (2019)	Jurassic (Late Kimmeridgian)	Torleite Fm	Bavaria (Germany)	Holotype	Nearly complete skeleton in 2D	Sachs et al. (2019)
Cricosaurus suevicus	SMNS 9808		Jurassic (Late Kimmeridgian)	Nusplingen Plattenkalk	Nusplingen (Germany)	Lectotype	Nearly complete skeleton in 2D	Fraas (1902)

Cricosaurus lithographicus	MOZ-PV 5787	2D data courtesy of Dr. Herrera	Upper Jurassic (Tithonian)	Vaca Muerta Fm	Cerro Lotena and Bosque Petrificado (Argentina)	Holotype	Partial cranium & postcranium	Herrera et al. (2013b)
Cricosaurus araucanensis	MLP 72-IV-7-1	2D data courtesy of Dr. Herrera	Upper Jurassic (lower Tithonian)	Vaca Muerta Fm	Cerro Lotena and Bosque Petrificado (Argentina)	Holotype	Partial postcranium	Herrera et al. (2013a)
Geosaurus lapparenti	UJF-ID.11847j & UJF-ID.11852f		Early Cretaceous (Valanginian)	*peregrinus* ammonite zone	La Martre (Var), France	Holotype	Partial cranium & postcranium	Debelmas and Strannoloubsky (1957); Young and de Andrade (2009)
Dakosaurus maximus	SMNS 8203		Jurassic (Upper Kimmeridgian)	Nusplingen Limestone?	Staufen near Gingen (Germany)	Neotype	Partial cranium & postcranium	Fraas (1902); Young et al. (2020b)
Tyrannoneustes lythrodectikos	GLAHM V1145		Jurassic (Middle Callovian)	Oxford Clay Fm	UK	Holotype	Partial postcranium & teeth	Young et al. (2012)
Torvoneustes carpenteri	BRSMG Cd7203		Jurassic (Upper Kimmeridgian)	Kimmeridge Clay Formation	Westbury (UK)	Paratype	Partial cranium & postcranium	Wilkinson et al. (2008)

TABLE 1. List of metriorhynchoid specimens.

Species	Inventory number	Data source	Age	Formation	Location	Hypodigm	Completeness	References
Mycterosuchus nasutus	NHMUK PV R 2617		Jurassic (Middle Callovian)	Oxford Clay Fm	Peterborough (UK)	Holotype	Partial cranium & postcranium	Johnson et al. (2020)
Aeolodon priscus	MNHN.F.CNJ 78		Jurassic (Tithonian)	Canjuers lagerstatte (France)	Canjuers (France)	Neotype	Nearly complete skeleton in 2D	Johnson et al. (2020)
Aeolodon priscus	NHMUK PV R 1086		Jurassic (Tithonian)	Mörnsheim Fm	Daiting (Germany)	Holotype	Nearly complete skeleton in 2D	Johnson et al. (2020)
Indosinosuchus potamosiamensis	PRC-24	3D models courtesy of Dr. Suravech Suteethorn	Late Jurassic (?Tithonian)	Phu Kradung Fm	Phu Noi (Thailand)	Referred	Scapula	Martin et al. (2019b)
Teleosaurus cadomensis	NHMUK PV OR 31836		Jurassic (Bathonian)	Taynton Limestone Fm	Stonesfield (UK)	Referred	Scapula encased in matrix	NHMUK Data Portal
Platysuchus multiscrobiculatus	SMNS 9930		Jurassic (Toarcian)	Posidonia Shale Fm	Baden-Württemberg (Germany)	Holotype	Nearly complete skeleton in 2D	Westphal (1961)
Platysuchus multiscrobiculatus	UMH-0005		Jurassic (Toarcian)	Posidonia Shale Fm	Baden-Württemberg (Germany)	Referred	Nearly complete skeleton in 2D	
Platysuchus multiscrobiculatus	*Platysuchus multiscrobiculatus* Kloster Banz unnumbered specimen		Jurassic (Toarcian)?	Posidonia Shale Fm?	Baden-Württemberg (Germany)?	Referred	Nearly complete skeleton in 2D	
Macrospondylus bollensis	SMNS 54063		Jurassic (Toarcian)	Posidonia Shale Fm	Baden-Württemberg (Germany)	Referred	Pelvic girdle in 2D	SMNS data
Macrospondylus bollensis	SMNS 9428		Jurassic (Toarcian)	Posidonia Shale Fm	Baden-Württemberg (Germany)	Referred	Ischium	SMNS data
Macrospondylus bollensis	PMU 35980		Jurassic (Toarcian)	Posidonia Shale Fm	Holzmaden (Germany)	Referred	Nearly complete skeleton in 2D	PMU database
Charitomenosuchus leedsi	NHMUK PV R 3806		Jurassic (Middle Callovian)	Oxford Clay Fm	Peterborough (UK)	Referred	Nearly complete skeleton	Johnson et al. (2020)

Neosteneosaurus edwardsi	PETMG R178		Jurassic (Middle Callovian)	Oxford Clay Fm	Peterborough (UK)	Referred	Nearly complete skeleton	Johnson et al. (2020)
Neosteneosaurus edwardsi	NHMUK PV R 3701		Jurassic (Middle Callovian)	Oxford Clay Fm	Peterborough (UK)	Referred	Partial cranium & postcranium	Johnson et al. (2020)
Lemmysuchus obtusidens	NHMUK PV R 3169	Presumably belongs to R3168	Jurassic (Middle Callovian)	Oxford Clay Fm	Peterborough (UK)	Referred	Left coracoid	
Lemmysuchus obtusidens	NHMUK PV R 3168		Jurassic (Middle Callovian)	Oxford Clay Fm	Peterborough (UK)	Holotype	Partial cranium & postcranium	Johnson et al. (2017)
Machimosaurus spp.	SMNS 91415		Upper Jurassic (Lower Kimmeridgian)	Lacunosamergel Fm	Baden-Württemberg (Germany)	Referred	Skull & partial postcranium	(Young et al., 2014)
Machimosaurus spp.	BHN2R 1100					Lost Neotype of *Machimosaurus mosae*	Partial cranium & postcranium	Hua et al. (1993)

TABLE 2. List of teleosauroid specimens.

Species	Inventory number	Data source	Age	Formation	Location	Hypodigm	Completeness	References
Anthracosuchus balrogus	UF/IGM 68		Middle Paleocene	Cerrejón Fm	Colombia	Paratype	Partial cranium & postcranium	Hastings et al. (2014)
Hyposaurus natator	YPM VP.000985		Danian	Hornerstown Fm	Monmouth Co., NJ (USA)	Holotype	Partial cranium & postcranium	Troxell (1925)
Hyposaurus natator	YPM VP.000764		Danian	Hornerstown Fm	Gloucester Co., NJ (USA)	Type	Partial postcranium	Troxell (1925)
Hyposaurus natator	NJSM 23368		Danian	Hornerstown Fm	Gloucester Co., NJ (USA)	Referred	Almost complete skeleton	Dr. David Parris (*pers. comm.* August 2019)
Dyrosaurus maghribensis	OCP DEK-GE 254		Lower Eocene (Ypresian)	Phosphate mine of Mera el Arech (Oulad Abdoun Basin)	Morocco	Holotype	Partial cranium & postcranium	Jouve et al. (2006)
Dyrosaurus maghribensis	OCP DEK-GE 252		Lower Eocene (Ypresian)	Phosphate mine of Mera el Arech (Oulad Abdoun Basin)	Morocco	Referred	Partial cranium & postcranium	Jouve et al. (2006)
Dyrosaurus maghribensis	OCP DEK-GE 351		Lower Eocene (Ypresian)	Phosphate mine of Mera el Arech (Oulad Abdoun Basin)	Morocco	Referred	Partial cranium & postcranium	Jouve et al. (2006)
Congosaurus bequaerti	MRAC 1809 & MRAC 1811		Selandian	—	Landana, Angola	Holotype	Partial cranium & postcranium	Jouve and Schwarz (2004)

TABLE 3. List of dyrosaurid specimens.

2.3. **Phylogeny.** We modified the dataset of Young et al. (2024), which represents the most recent and comprehensive crocodylomorph dataset. We created three different phylogenetic matrices to estimate the phylogenetic strength of postcranial data: the first one containing only cranial characters from Young et al. (2024); the second one containing only postcranial characters and the last one combining both. Additional details can be found in the supplementary information (see files SUPP INF 1 and 2). Our analyses of those new datasets were conducted following a maximum parsimony framework using TNT v.1.5 (Goloboff and Catalano, 2016). Since implied weighting is considered a preferred approach which yields rigorous results under a maximum parsimony framework (Goloboff et al., 2018; Smith, 2019), we decided to follow this method to further limit the influence of homoplasy in our analyses. Implied weighting is an approach which adjusts the weight of each character in proportion to their level of homoplasy. As the increase of the k value decreases the penalty applied to homoplasic characters, we decided to use two values of the coefficient k (12) to assess the impact of different approaches of character weighting. But we also conducted equal weighting maximum parsimony analysis. In all our analyses, the maximum number of trees was increased to 100,000. Also, in order to pinpoint the islands containing the most parsimonious trees, we employed the new technology search with the following values: ratchet activated with 200 ratchet iterations; drift activated with ten cycles; five hits; and ten trees per replication. The tree bisection–reconnection algorithm was subsequently applied to thoroughly explore these islands, and the nodal support of our trees in the implied weighting framework was assessed through the use of symmetric resampling with a 33% change probability, generating differences in frequency across 10,000 replicates. In the R v.4.0.3 statistical environment (TEAM, 2013), we then timescaled the consensus trees with the following packages APE (Paradis et al., 2004), GEOSCALE, STRAP (Bell and Lloyd, 2015), and PALEOTREE (Bapst, 2012). This was accomplished using the minimum branch length (mbl = 3) method and taxon occurrence ages obtained from The Paleobiology Database (`https://paleobiodb.org`). Supplementary Information includes:

- the list of characters and taxa;
- the three matrices as nexus files: the postcranial dataset ('PostC.nex'); the cranial dataset ('C_only.nex'); and combined postcranial and cranial dataset ('Full.nex');
- the most parsimonious trees for k=12 for each dataset ('Trees' folder);
- the R script ('Phylo.R');
- the TNT scripts for each matrix for IW and EW ('Tnt_scripts' folder);
- and the taxon age file ('FAD_LAD.xls').

2.4. **Institutional abbreviations.** **AMNH** New York: American Museum of Natural History, USA;

BMMS Solnhofen : Bürgermeister-Müller-Museum Solnhofen, Germany;
BRLSI Bath: Bath Royal Literary and Scientific Institute, UK;
BRSMG Bristol: Bristol City Museum and Art Gallery, UK;

GLAHM Glasgow: Hunterian Museum and Art Gallery, UK;
LRM Lyme Regis: Lyme Regis Museum, UK;
MLP La Plata: Museo de La Plata, Buenos Aires, Argentina;
MNHN Paris: Muséum national d'Histoire naturelle, France;
MOZ Neuquén: Museo Juan Augusto Olsacher de Zapala, Argentina;
MRAC Tervuren: Musée Royal de l'Afrique Centrale, Belgium;
NHMUK London: Natural History Museum, England;
NJSM Trenton: New Jersey State Museum, USA;
NKMB Bamberg: Naturkunde-Museum Bamberg, Germany;
NMW Vienna: Naturhistorisches Museum Wien, Austria;

OCP DEK-GE Khouribga: Office Chérifien des Phosphates, Direction de l'Exploitation de Khouribga, Geologie-Exploitation, Khouribga, Morocco;
PETMG Peterborough: Peterborough Museum and Art Gallery, UK;
PMU Uppsala: Evolutionsmuseet – Uppsala universitet, Sweden;
PRC Maha Sarakham: Palaeontological Research and Education Centre, Maha Sarakham University, Thailand;
RBINS Brussels: Royal Belgian Institute of Natural Sciences, Belgium;
RVC London: Royal Veterinary College, University of London, UK;
SMNS Stuttgart: Staatliches Museum für Naturkunde, Germany;
UF/IGM Gainesville: **UF**, Florida Museum of Natural History, University of Florida, USA / **IGM**, Museo Geológico, at the Instituto Nacional de Investigaciones en Geociencias, Minería y Quimica, Bogotá, Colombia;
UJF Grenoble; Joseph Fourier University, France;
UMH Holzmaden : Urweltmuseum Hauff, Germany;
YPM New Haven: Yale Peabody Museum, USA.

3. THE EXTANT CROCODYLIAN SHOULDER ARTICULATION AND MUSCULATURE

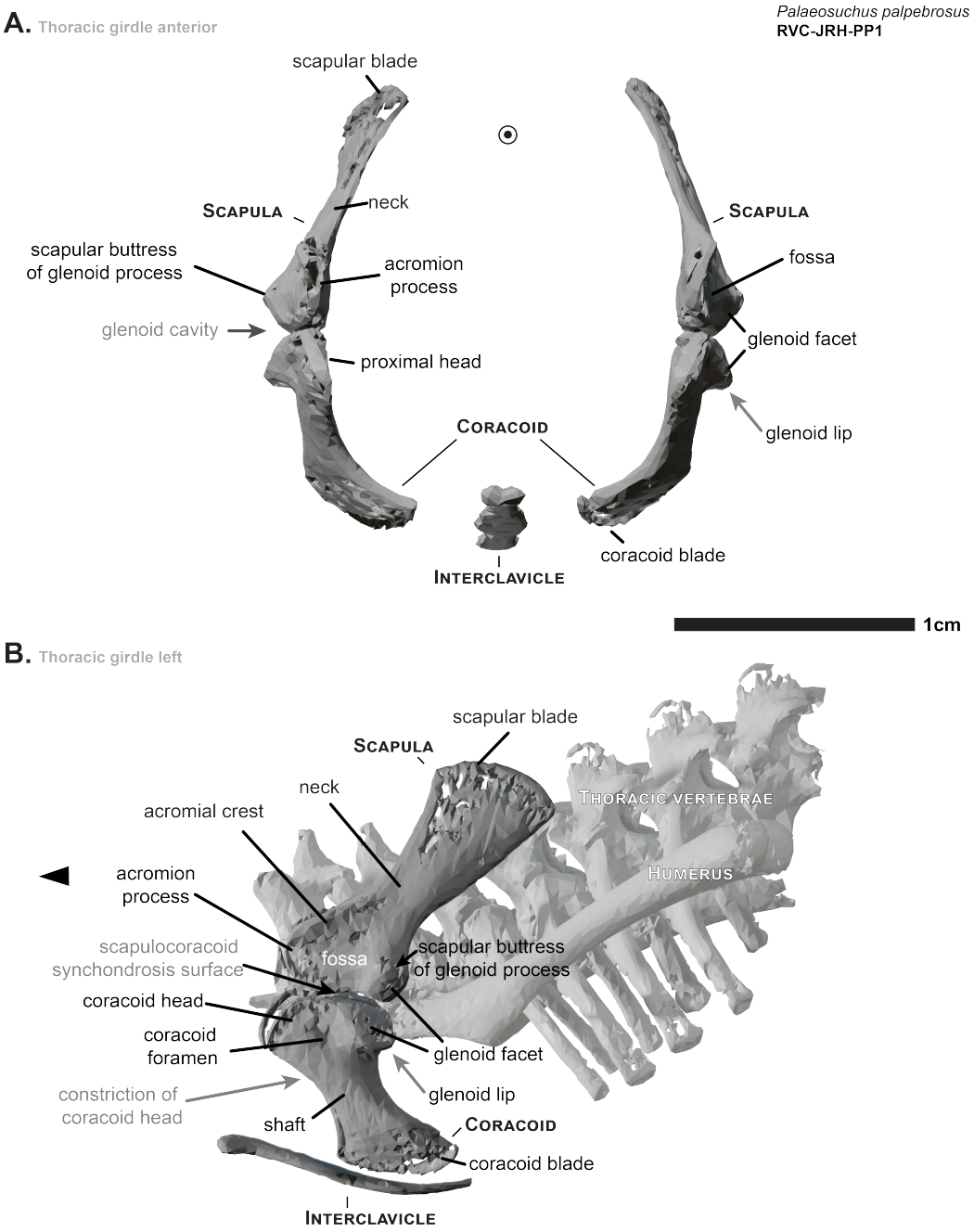


FIGURE 4. A snapshot of the pectoral girdle of the alligatoroid *Palaeosuchus palpebrosus* RVC-JRH-PP1 (3D models). **A.** In anterior view; **B.** In lateral view. Note the orientation of the scapula/coracoid. Target indicates anterior view. Grey arrow points anteriorly. CT scan courtesy of Professor John Hutchinson. Link: https://skfb.ly/6ByyV

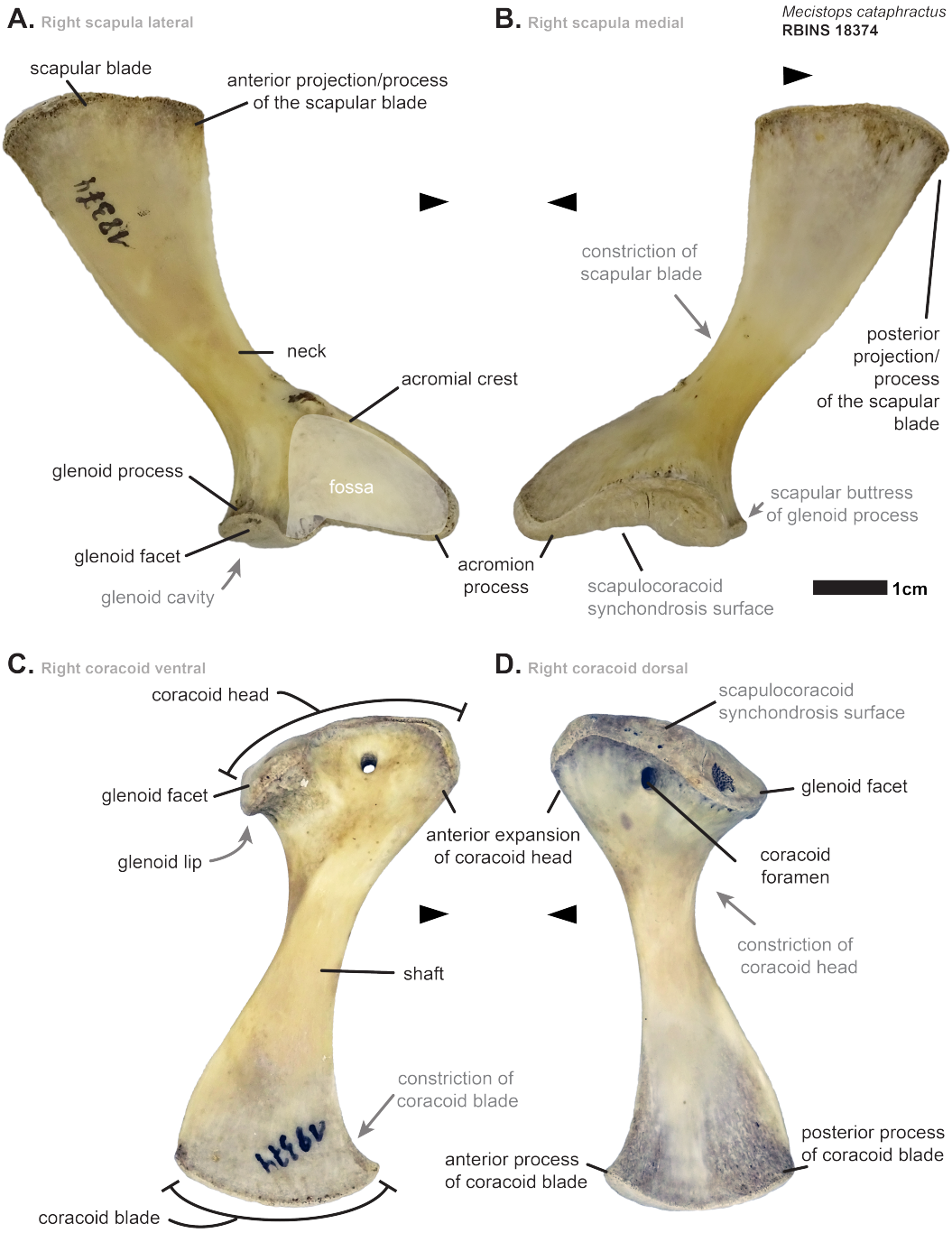


FIGURE 5. Right pectoral girdle of *Mecistops cataphractus* RBINS 18374 (photographs). **A.** Scapula in lateral view; **B.** Scapula in medial view; **C.** Coracoid in ventral view; **D.** Coracoid in dorsal view. Arrow points anteriorly.

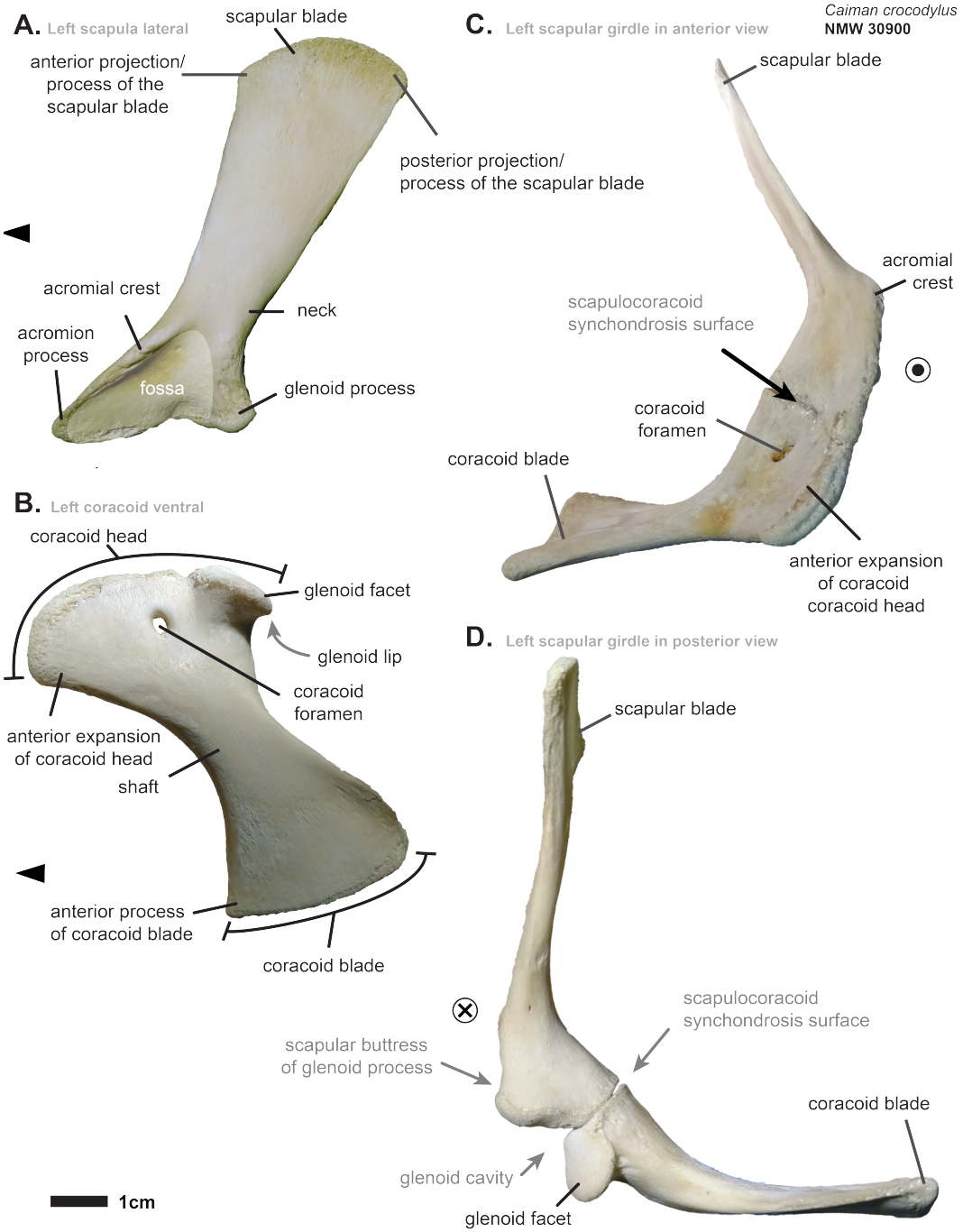


FIGURE 6. Left pectoral girdle of *Caiman crocodylus* NMW 30900 (photographs). **A.** Scapula in medial view; **B.** Coracoid in ventral view; **C.** Thoracic girlde in anterior view; **D.** Pectoral girdle in posterior view. Target indicates anterior. Cross indicates posterior. Arrow points anteriorly. Red dashed lines indicate missing parts.

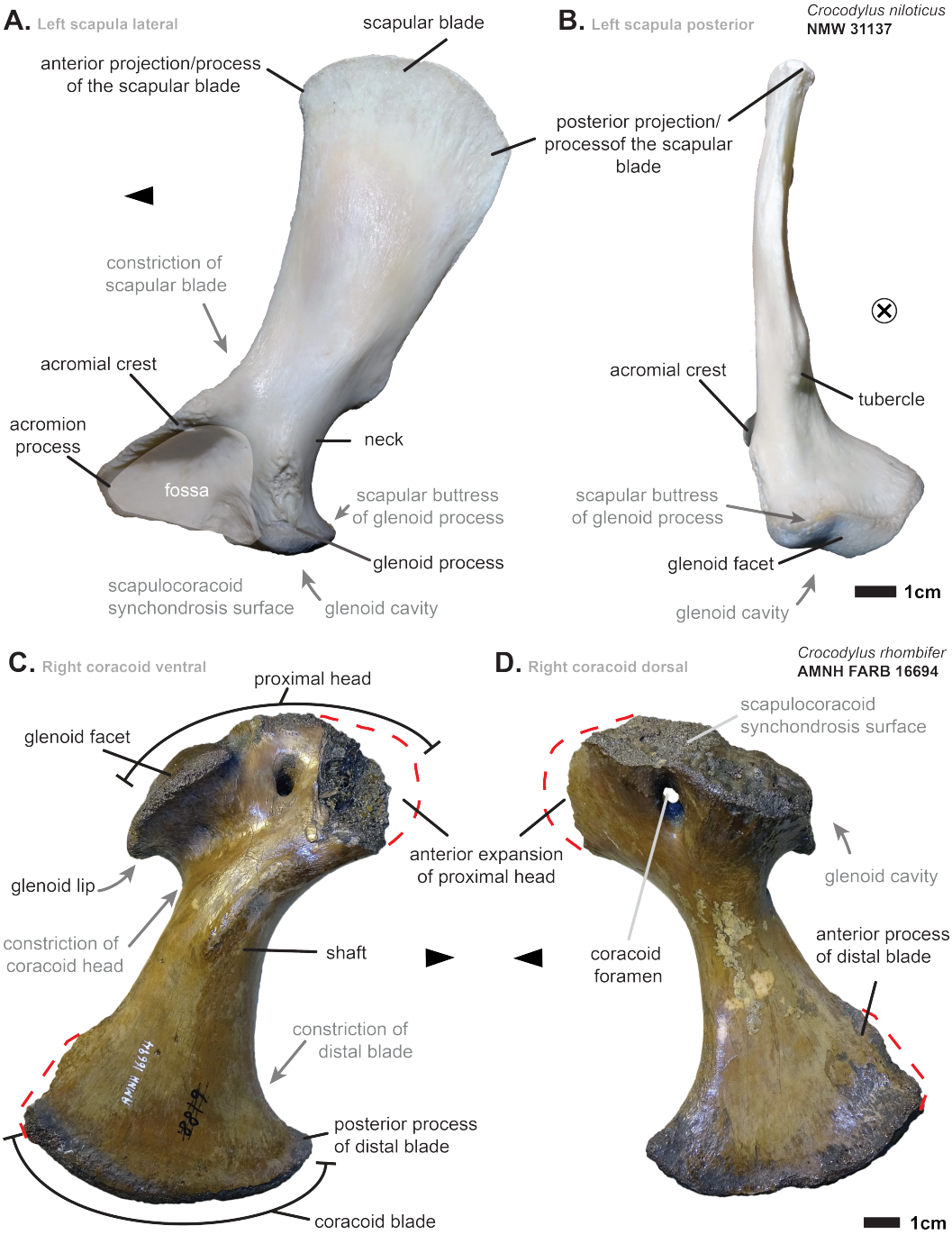


FIGURE 7. Left pectoral girdle of *Crocodylus niloticus* NMW 31137 (A&B) and *Crocodylus rhombifer* AMNH FARB 16694 (C&D) (photographs). **A.** Scapula in lateral view; **B.** Scapula in posterior view; **C.** Coracoid in ventral view; **D.** Coracoid in dorsal view. Cross indicates posterior. Arrow points anteriorly.

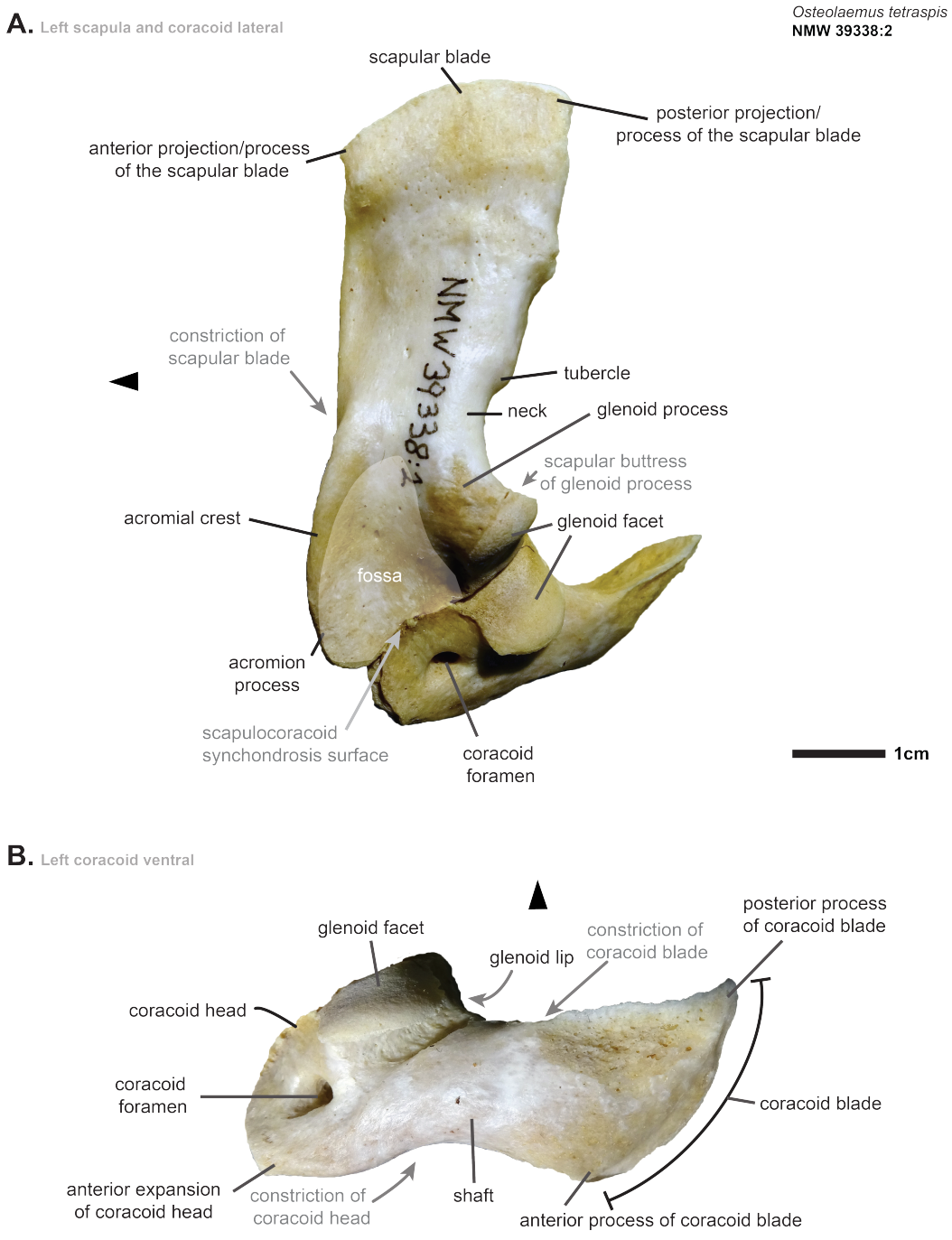


FIGURE 8. Left pectoral girdle of *Osteolaemus tetraspis* NMW 39338:2 (photographs). **A.** Scapula and coracoid in lateral view; **B.** Coracoid in ventral view. Arrow points anteriorly.

4. PECTORAL MUSCLES OF EXTANT CROCODYLIANS

Laterally, most of the surface of the scapular blade is occupied by the origin of *m. deltoideus scapularis* (shoulder abductor and flexor; Klinkhamer et al. (2017)) and that of *m. teres major* (shoulder abduction and flexion to minor degree; Klinkhamer et al. (2017)). The anterior surface of the scapular blade is covered by the insertion of the deep extrinsic muscle *m. levator scapulae* (Meers, 2003; Klinkhamer et al., 2017) which rotates the scapula anteriorly and also corresponds to an effective neck abductor. *M. levator scapulae* overlies *m. serratus ventralis cervicis* and *m. pectoralis* (Meers, 2003). *M. levator scapulae* is in turn overlaid by *m. trapezius* (Meers, 2003; Klinkhamer et al., 2017) which rotates the scapulocoracoid anteriorly and assists in the protraction of the forelimb for the high-walk (Meers, 2003; Romão and Santos, 2023). The posterior surface of the scapular blade is occupied by the insertion of *m. serratus ventralis thoracis* which is a pectoral girdle extensor (Klinkhamer et al., 2017). Medially, the insertions of the muscles *rhomboideus* (pectoral girdle adductor, elevator and also stabiliser; Michel et al. (2021)) and *serratus ventralis cervicus* (pectoral girdle flexors; Allen et al. (2014)) cover the dorsal-most portion of the scapular blade. The origin of the intrinsic muscle *m. subscapularis*, which is a shoulder extensor and shoulder stabiliser in extant crocodylians (Klinkhamer et al., 2017), extends over most the medial surface of the scapula. The origin of the intrinsic muscle *deltoideus clavicularis* (shoulder extensor) covers the anterior area of the scapula extending from the tip of the acromial crest (ventrally) up to the insertion of the LS and origin of the DS (dorsally). *M. deltoideus clavicularis* overlies *m. coracobrachialis brevis dorsalis* and the insertion of *deltoideus scapularis* (Klinkhamer et al., 2017). The origin of the intrinsic muscle *coracobrachialis brevis dorsalis*, which is a shoulder extensor and potentially joint stabiliser (Klinkhamer et al., 2017), lies along the acromial crest and underneath the origin of the *m. deltoideus clavicularis*. The tip of the acromion process bears laterally a portion of the origin of *m. supracoracoideus intermedius* and medially a portion of the origin of *m. supracoracoideus longus* (intrinsic muscle, shoulder extensor and, to a minor degree, adductor; Klinkhamer et al. (2017)). On the posterior margin of the scapula, the area of the neck constriction displays the origin of the *m. scapulohumeralis caudalis*, a shoulder abductor and intrinsic muscle (Klinkhamer et al., 2017). The origin of the elbow extensor (intrinsic muscle) *m. triceps longus caudalis pars scapularis* is found on the medial side of the scapula, near the origin of *m. subscapularis* and the insertion of *m. serratus ventralis thoracis* (Meers, 2003). The origin of the elbow extensor (intrinsic muscle) *m. triceps longus lateralis* is anchored above the glenoid process, near the origin of *m. scapulohumeralis caudalis* (Klinkhamer et al., 2017).

The largest muscle origin on the crocodylian coracoid extends ventrally from the coracoid foramen up to the coracoidal blade and corresponds to the intrinsic muscle *coracobrachialis brevis ventralis*, which is a shoulder and limb adductor (Klinkhamer et al., 2017). The insertion of the deep extrinsic muscle *costocoracoideus pars superficialis*, which retracts the coracoid (Meers, 2003) and constitutes a minor extensor of pectoral shoulder girdle (Klinkhamer et al., 2017), lies on the posterior margin of the coracoid next to the origin of the CBV (Meers, 2003; Klinkhamer et al., 2017). The deep extrinsic muscle *costocoracoideus pars profundus*, which is a pectoral girdle extensor (Klinkhamer et al., 2017) (and possibly retracts the coracoid Meers (2003)), inserts on the dorsal side of the coracoid shaft near the anterior margin of the bone (Meers, 2003; Klinkhamer et al., 2017). The origin of the intrinsic muscle *m. triceps longus caudalis pars coracoideus* (elbow extensor Meers (2003)) is also found on the dorsal side of the coracoid, near the base of the glenoid facet. The anterior expansion of the coracoid head displays the insertion of the muscle *omohyoideus* (which retracts the hyoid and possibly the tongue) at its extremity (Li and Clarke, 2015). As mentioned above, the origin of the intrinsic muscle *supracoracoideus intermedius* extends over both the scapula and coracoid. It lies on the ventral and surface of the coracoid and covers the anteriormost portion of the scapulocoracoid synchondrosis (Klinkhamer et al., 2017). On the dorsal side of the coracoid, the origin of *m. supracoracoideus longus* is also found along the anteriormost portion of the scapulocoracoid synchondrosis (Klinkhamer et al., 2017). The origin of the muscle

supracoracoideus brevis covers the ventral surface of the anterior expansion of the coracoid head, and extends over the area between the origins of *m. supracoracoideus intermedius* and *m. biceps brachii* and the insertion of *m. omohyoideus*. *M. biceps brachii*, a major elbow flexor (intrinsic muscle), possesses a small origin on the ventral side of the coracoid along the margin of the anterior expansion of the coracoid head, near its junction with the shaft of the coracoid (Klinkhamer et al., 2017).

The major muscle on the ventral side of the crocodylian shoulder corresponds to the thick and broad pectoral muscle (*m. pectoralis* – PEC), which inserts onto the tip of the deltopectoral crest of the humerus (Meers, 2003; Klinkhamer et al., 2017). The pectoral muscle is also often divided into two or three heads, which find their origin along the centre of the interclavicle, the mesosternum, and the portions of the thoracic ribs attaching to the sternum (and even sometimes the gastralia). *M. pectoralis* connects with *m. levator scapulae* anteromedially and is also partly covered by it. In comparison, *m. supracoracoideus longus* extends anterolaterally to *m. pectoralis*. *m. pectoralis* also covers other muscles like the *mm. costocoracoideus, sternocostalis, coracobrachialis brevis ventralis*, and part of the *m. biceps humerii* tendon (Meers, 2003). The pectoral muscle is hence not present on the scapula and coracoid but is a strong adductor of the humerus (Meers, 2003; Klinkhamer et al., 2017).

4.1. **Coracoid.** The following table (see table 4) contains the different muscle insertions and origins and their approximated function of the coracoid of extant crocodylians (see figs. 4 to 8).

Abbreviation	Full name	Type	Approximated function
COC	*Mm. costocoracoideus* complex	Insertion	Pull coracoid posteriorly to the sternum, caudal rotator of pectoral girdle (Meers, 2003).
COCS	*M. costocoracoideus pars superficialis*	Insertion	Retracts coracoid (Meers, 2003). Minor extensor of pectoral shoulder girdle (Klinkhamer et al., 2017). Deep extrinsic muscle (Meers, 2003; Klinkhamer et al., 2017).
COCP	*M. costocoracoideus pars profundus*	Insertion	Retracts coracoid (presumably) (Meers, 2003). Pectoral girdle extensor (Klinkhamer et al., 2017). Deep extrinsic muscle (Meers, 2003; Klinkhamer et al., 2017).
CBV	*M. coracobrachialis brevis ventralis*	Origin	Shoulder and limb adductor (Klinkhamer et al., 2017). Intrinsic muscle (Klinkhamer et al., 2017).
SC	*M. supracoracoideus*	Origin	Shoulder extensor and, to a minor degree, adductor (Klinkhamer et al., 2017). Intrinsic muscle (Klinkhamer et al., 2017).
BB	*M. biceps brachii*	Origin	Major elbow flexor. Intrinsic muscle (Klinkhamer et al., 2017).
TLC	*M. triceps longus caudalis pars coracoideus*	Origin	Elbow extensor. Intrinsic muscle (Meers, 2003).
Moh	*M. omohyoideus*	Insertion	Retraction of the hyoid, possible posterior movement of tongue involved (Li and Clarke, 2015).

TABLE 4. List of thoracic muscles of the coracoid of extant crocodylians (Meers, 2003; Klinkhamer et al., 2017).

4.2. **Scapula.** The following table (see table 5) contains the different muscle insertions and origins and their approximated function of the scapula of extant crocodylians (see figs. 4 to 8).

Abbreviation	Full name	Type	Approximated function
Rhm	*Rhomboideus*	Insertion	Pectoral girdle adductor, elevator and also stabiliser (Michel et al., 2021).
–	*M. trapezius*	Insertion	Rotates the scapulocoracoid cranially, assists in protraction of the forelimb (high walk) (Meers, 2003; Romão and Santos, 2023). Overlies LS (Meers, 2003; Klinkhamer et al., 2017).
LS	*M. levator scapulae*	Insertion	Cranial rotator of scapula and effective neck abductor. Overlies SVC *m. serratus ventralis cervicis* and PEC (Meers, 2003). Deep extrinsic muscle (Meers, 2003; Klinkhamer et al., 2017).
LD	*M. latissimus dorsi*	Insertion	Shoulder extensor (Allen et al., 2014). Overlies SVT *m. serratus ventralis thoracis* and the caudal fibers of *m. trapezius*. Possibly rotates and retracts humerus simultaneously (Meers, 2003).
SVC	*Serratus ventralis cervicus*	Insertion	Pectoral girdle flexors (Allen et al., 2014).
SVT	*Serratus ventralis thoracis*	Insertion	Pectoral girdle extensor (Klinkhamer et al., 2017). Deep extrinsic muscle (Meers, 2003; Klinkhamer et al., 2017).
TM	*M. teres major*	Origin	Shoulder abduction and flexion to minor degree (Klinkhamer et al., 2017). Overlies SHC. Intrinsic muscle (Klinkhamer et al., 2017).
DC	*M. deltoideus clavicularis*	Origin	Shoulder extensor. Overlies *m. coracobrachialis brevis dorsalis* as well as the insertion of *m. deltoideus scapularis* (Klinkhamer et al., 2017). Intrinsic muscle (Klinkhamer et al., 2017).
CBD	*M. coracobrachialis brevis dorsalis*	Origin	Shoulder extensor and potentially joint stabiliser (Klinkhamer et al., 2017). Intrinsic muscle (Klinkhamer et al., 2017).
DS	*M. deltoideus scapularis*	Origin	Shoulder abductor and flexor (Klinkhamer et al., 2017). Overlies SHC. Intrinsic muscle (Klinkhamer et al., 2017).
SHC	*M. scapulohumeralis caudalis*	Origin	Shoulder abductor. Intrinsic muscle (Klinkhamer et al., 2017).
SS	*M. subscapularis*	Origin	Shoulder extensor and shoulder stabiliser in extant crocodylians (due to its small size and limited mechanical advantage). Intrinsic muscle (Klinkhamer et al., 2017).
TLL	*M. triceps longus lateralis*	Origin	Elbow extensor. Intrinsic muscle (Klinkhamer et al., 2017).
TLC	*M. triceps longus caudalis pars scapularis*	Origin	Elbow extensor. Intrinsic muscle (Meers, 2003)
PEC	*M. pectoralis*	–	Not directly located on the scapula but is connected to LS anteromedially and is also partly overlaid by it (Meers, 2003). Powerful adductor of humerus. Superficial extrinsic muscle (Meers, 2003; Klinkhamer et al., 2017).

TABLE 5. List of pectoral muscles of the scapula of extant crocodylians (Meers, 2003; Klinkhamer et al., 2017).

5. GLOBAL MEASUREMENT TABLES

Taxon	Inventory number	H	ScB.l	Prox.l	CST	CST.d	SHAFT	SYN.l	SYN.w	ACR.l	GL.h	GL.w
Alligator sinensis	NMW 37 966	79.49	38.31	41.006	16.04	28.71	18.21	29.613	12.63	5.497	17.95	17.12
Crocodylus niloticus	NMW 31.137	122.51	51.658	58.572	24.88	38.9	18.54	46.416	23.65	6.82	19.77	19.04
Caiman crocodilus	NHMW 30 900	88.9	31.9	38.45	15.36	36.95	16.2	30.33	12.85	2.88	14.67	8.16
Osteolaemus tetraspis	NHMW 39338:2	59.82	24.35	26.55	15.312	22.64	NA	20.45	NA	2.734	10.41	13.907
Mecistops cataphractus	RBINS 18374	68.08	27.04	32.54	9.39	22.32	21.37	25.135	11.48	3.054	13.95	8.22
Congosaurus bequaerti	MRAC 1741	217.29	NA	114.54	49.95	70.96	73.63	75.739	29.69	21.583	38.498	28.97
Anthracosuchus balrogus	UF/IGM 68	207	147.96	96.8	56.16	53.45	111	72.743	15.73	10.414	21.09	21.64
Hyposaurus natator	YPM VP.000985	NA	NA	66.15	28.53	NA	NA	43.91	15.6	5.867	17.44	22.98
Hyposaurus rogersii	YPM VP.000764	NA	NA	76.69	NA	NA	NA	39.4	15.32	16.73	24.12	27.37
Hyposaurus natator	NJSM 23368	141.58	147.612	69.05	27.2	43.47	50.33	50.524	14.25	7.985	22.88	24.87
Dyrosaurus maghribensis	OCP DEK-GE 254	289.12	191.34	NA	54.22	113.2	NA	NA	NA	NA	36.64	40.07
Turnersuchus hingleyae	LRM 2021/45	70.58	NA	29.536	12.934	27.405	19.958	24.832	5.637	1.99	7.693	7.456
Pelagosaurus typus	BRLSI M.1418	11.192	5.66	4.46	2.251	4.68	3.66	3.014	NA	0.467	1.64	NA
Thalattosuchus superciliosus	PMU 35988	72.384	16.068	21.298	9.43	40.742	44.294	10.828	6.369	3.021	9.11	7.14
Thalattosuchus superciliosus	GLAHM V1146	90.427	19.2	28.106	11.958	54.212	53.924	15.89	5.71	2.986	11.082	9.54
Thalattosuchus superciliosus	GLAHM V1143	NA	NA	NA	NA	NA	NA	15.996	4.792	NA	8.512	7.833
Gracilineustes leedsi	NHMUK PV R 3014	58.212	6.934	17.049	4.436	39.293	33.787	12.481	2.761	3.118	7.199	3.739
Gracilineustes leedsi	NHMUK PV R 3015	68.337	12.126	21.604	7.351	40.19	43.849	16.372	2.703	3.994	6.965	4.499
Geosaurus lapparenti	UJF-ID.11847j	NA	NA	NA	NA	61.78	NA	31.475	14.305	NA	NA	17.345
Cricosaurus suevicus	SMNS9808	35.9	22.4	19.49	16.8	18.31	7	11.77	NA	3.08	7.25	NA
Cricosaurus albersdoerferi	BMMS-BK 1-2	47.35	NA	26.21	NA	NA	NA	13.72	NA	8.03	11.484	NA
Dacosaurus maximus	SMNS 8203	125.43	63.49	63.59	36.43	60.83	48.43	33	25.02	9.1	32.51	23.47
Torvoneustes carpenteri	Cd7203	NA	NA	NA	NA	NA	NA	26.82	11.12	17.327	22.88	18.62
Mycterosuchus nasutus	NHMUK PV R 2617	144.039	58.269	53.44	29.58	80.94	55.39	51.03	NA	0	27.56	19.48
Teleosaurus cadomensis	NHMUK PV OR 31836	109.65	21.41	44.09	19	50.17	62.93	35.036	NA	NA	NA	NA
Indosinosuchus potamosiamensis	PRC-24	113.773	42.562	39.903	16.163	63.268	45.93	26.596	21.66	8.082	16.079	15.593
Platysuchus multiscrobiculatus	SMNS9930	75.79	32.14	33.28	12.37	30.82	18.8	NA	14.16	4.37	13.45	9.35
Macrospondylus bollensis	SMNS 9428	66.99	NA	25.81	11.07	29.6	19.6	22.76	NA	1.98	10.3	9.36
Macrospondylus bollensis	PMU 35980	120.565	67.65	41.73	18.68	45.06	31.698	34.001	NA	6.404	NA	NA
Macrospondylus bollensis	SMNS 54063	128.98	65.04	47.134	19.62	44.76	45.94	39.64	NA	5.9	NA	NA
Charitomenosuchus leedsi	NHMUK PV R 3806	96.178	21.72	26.309	13.801	62.91	53.45	26.802	9.91	1.69	13.3	12.65
Lemmysuchus obtusidens	NHMUK PV R 3168	167	49.75	50.31	21.37	93.53	88.67	44.153	23.28	5.1	25.24	24.73
Neosteneosaurus edwardsi	NHMUK PV R 3701	88.197	27.59	29.08	12.99	47.406	46.77	20.896	11.04	3.104	14.667	12.713
'Steneosaurus' bollensis	SMNS 15712a	16.5	12.63	8.7	2.9	4.65	8.39	5.8	NA	0.8	2.4	NA

TABLE 6. List of measurements in mm of crocodyliformes scapulae. **H**: Maximum dorsoventral height; **ScB.l**: Scapular Blade maximum anteroposterior length; **Prox.l**: Proximal region maximum anteroposterior length; **CST**: Thinnest anteroposterior width of scapula; **CST.d**: Distance between proximal region and constriction of scapula; **SHAFT**: Dorsoventral extension of shaft; **SYN.l**: Anteroposterior length of scapulocoracoid synchondrosis surface; **SYN.w**: Mediolateral maximum width of scapulocoracoid synchondrosis surface; **ACR.l**: Anteroposterior extension of the acromion process; **GL.h**: Maximum height of the glenoid facet; **GL.w**: Maximum width (mediolaterally) of the glenoid facet (perpendicular to GL.h).

Taxon	Inventory number	H	Prox.l	CB.l	SHAFT	CST	ANG	CF.h	CF.w	SYN.l	SYN.w	GL.w	GL.h	AP.l
Alligator sinensis	NMW 37 966	67.82	39.02	38.59	NA	NA	NA	2.34	1.94	NA	NA	NA	NA	11.65
Caiman crocodilus	NMW 30 900	74.2	39.54	35.71	17.794	14.77	56	4.29	2.5	29.481	NA	NA	NA	15.389
Osteolaemus tetraspis	NMW 39338:2	47.24	29.604	27.537	9.029	13.858	49	3.327	4.733	23.929	NA	9.868	8.905	6.01
Mecistops cataphractus	RBINS 18374	68.87	28.66	27.97	14.132	8.547	59	2.69	2.38	14.86	11.98	12.9	10.68	3.484
Crocodylus rhombifer	AMNH FARB 16694	146.15	NA	82.31	NA	NA	61	8.74	5.31	34.89	37.87	42.47	29.85	11.875
Congosaurus bequaerti	MRAC 1741	177.76	97.37	54.05	98.983	21.105	39	7.68	5.4	75.958	29.25	44.05	26.82	15.321
Hyposaurus natator	YPM VP.000985	123.03	NA	NA	65.435	NA	NA	4.35	2.66	44.715	20.57	22.478	20.149	7.11
Hyposaurus natator	YPM VP.000764	173	76.35	36.96	105.48	17.966	39.3	7.54	5.04	26.7	17.3	25.39	20.97	10.07
Hyposaurus natator	NJSM 23368	127	63.31	28.44	73.783	14.246	41	7.12	5.64	51.227	15.983	30.535	23.225	9.119
Dyrosaurus maghribensis	OCP DEK-GE 254	253.16	NA	64.74	147.82	29.55	38	6.86	6.2	99.85	NA	NA	50.69	NA
Turnersuchus hingleyae	LRM 2021/45	NA	36.514	NA	NA	NA	30	2.888	2.405	22.451	6.627	9.775	10.352	12.927
Pelagosaurus typus	BRLSI M.1418	10.66	6.53	5.96	4.68	NA	71	0.4	0.4	NA	NA	NA	NA	2.12
Thalattosuchus superciliosus	GLAHM V1146	92.673	58.858	50.918	23.136	20.192	62	14.84	11.85	25.842	8.32	17.495	8.236	29.694
Thalattosuchus superciliosus	GLAHM V1005	68.765	42.985	NA	17.448	15.589	NA	9.904	NA	16.669	5.638	13.324	9.203	23.459
Thalattosuchus superciliosus	NHMUK PV R 1530	76.731	47.898	NA	20.282	17.922	NA	12.685	8.269	19.258	6.062	15.243	6.715	NA
Thalattosuchus superciliosus	PMU 35988	NA	NA	48.338	18.229	16.714	NA	NA	NA	NA	NA	13.588	9.357	16.857
Thalattosuchus superciliosus	GLAHM V1143	71.263	41.496	NA	19.829	16.196	62	9.657	NA	15.515	6.344	10.202	9.106	22.241
Gracilineustes leedsi	NHMUK PV R 3014	48.422	NA	29.643	12.945	8.801	NA	4.054	NA	14.578	4.753	5.415	4.588	16.272
Gracilineustes leedsi	NHMUK PV R 3015	NA	NA	NA	14.28	9.221	NA	NA	NA	NA	NA	6.525	5.838	NA
Rhacheosaurus gracilis	NHMUK PV R 3948	NA	NA	15.54	NA	NA	NA	NA	NA	NA	NA	NA	NA	7.07
Cricosaurus suevicus	SMNS 9808	42.09	24.8	24.19	12.31	9.716	78	NA	NA	NA	NA	NA	9.921	14.18
Cricosaurus albersdoerferi	BMMS-BK 1-2	59.224	37.876	40.561	12.817	14.963	75.019	1.988	1.55	14.646	NA	NA	11.81	21.314
Cricosaurus araucanensis	MLP 72-IV-7-1	67.702	45.572	48.895	17.658	17.611	72	3.401	5.144	NA	NA	7.8	15.146	26.671
Cricosaurus bambergensis	NKMB-P-Watt14/274	32.895	21.617	24.343	5.444	8.37	45	2.005	1.529	NA	NA	NA	6.12	11.962
Cricosaurus lithographicus	MOZ-PV 5787	NA	NA	NA	14.499	23.081	NA	NA	NA	NA	NA	NA	NA	NA
Metriorhynchus brachyrhynchus	NHMUK PV R 4696	75.243	NA	NA	20.786	16.507	50	11.898	NA	20.258	7.913	11.428	7.994	22.464
Dacosaurus maximus	SMNS 8203	178	79.34	NA	NA	NA	79	NA	NA	NA	NA	NA	NA	NA
Tyrannoneustes lythrodectikos	GLAHM V1145	95.292	NA	55.842	23.735	NA	67	13.585	NA	27.123	11.153	15.036	11.908	24.781
Mycterosuchus nasutus	NHMUK PV R 2617	150.268	87.578	NA	44.128	20.692	42.52	5.569	9.265	NA	18.181	28.014	17.651	50.948
Aeolodon priscus	NHMUK PV R 1086	21.79	10.016	10.98	9.384	3.844	40.24	1.1	0.91	4.228	NA	NA	NA	5.49
Platysuchus multiscrobiculatus	SMNS9930	92.86	40.65	33.83	32.556	NA	42	NA	NA	NA	NA	12.123	11.863	NA
Macrospondylus bollensis	SMNS 9428	NA	38.52	27.845	46.95	10.888	52	2.712	2.869	24.439	NA	13.139	7.484	13.975
Macrospondylus bollensis	PMU 35980	131.75	65.28	58.74	53.72	16.52	47.24	8.21	3.75	38.501	NA	NA	NA	28.644
Charitomenosuchus leedsi	NHMUK PV R 3806	98.619	48.647	48.91	38.028	13.102	49	2.14	2.263	26.487	11.942	15.638	13.811	30.633
Neosteneosaurus edwardsi	NHMUK PV R 3701	107.074	57.727	NA	46.81	15.495	53	3.024	3.53	32.127	11.513	21.556	15.814	31.541
'Neosteneosaurus edwardsi'	NHMUK PV R 3169	160.752	NA	NA	48.69	23.263	NA	4.011	4.996	44.604	13.6	30.788	19.036	NA
Machimosaurus spp.	SMNS 91415	179.49	82.844	NA	62.836	27.677	44.2	7.802	5.961	NA	NA	29.083	19.33	52.352

TABLE 7. List of measurements in mm of crocodyliformes coracoids. **H**: Maximum mediolateral height; **Prox.l**: Proximal region maximum anteroposterior length; **CB.l**: Coracoid Blade maximum anteroposterior length; **SHAFT**: Maximum mediolateral extension of shaft; **CST**: Thinnest anteroposterior width of coracoid; **ANG**: Angle formed between the scapulocoracoid synchondrosis surface and median of shaft; **CF.h**: Maximum height of coracoidal foramen (mediolateral); **CF.w**: Maximum width of coracoidal foramen (anteroposterior); **SYN.l**: Anteroposterior length of scapulocoracoid synchondrosis surface; **SYN.w**: Mediolateral maximum width of scapulocoracoid synchondrosis surface; **ACR.l**: Anteroposterior extension of the acromion process; **GL.w**: Maximum width (mediolaterally) of the glenoid facet (perpendicular to GL.h); **GL.h**: Maximum height of the glenoid facet; **AP.l**: Maximum extension of the anterior process of the coracoid head.

6. THE APPENDICULAR SKELETON OF THALATTOSUCHIANS

6.1. ***Turnersuchus hingleyae*** **Wilberg et al., 2023.** For measurements, see tables 6 and 7. The specimen is presumably a juvenile.

6.1.1. *Scapula.* The scapula of *Turnersuchus hingleyae* Wilberg et al., 2023 LRM 2021/45 (see Figures 9 to 11) bears several similarities with the scapula of basal metriorhynchoid *Pelagosaurus* BRLSI M.1418: its scapular blade is expanded (Wilberg et al., 2023), its neck shows a strong relative constriction, acromial crest seems present (Wilberg et al., 2023) along with underlying scapular fossa, and the anterior apex of the acromion process appears ventrally oriented. However, the scapula of *Turnersuchus* LRM 2021/45 departs from that of *Pelagosaurus* (BRLSI M.1418) in displaying a relatively straight posterior margin (Wilberg et al., 2023), and more importantly a strong posterior inclination in relation to the proximal portion of the bone. In this way, the scapula of *Turnersuchus* LRM 2021/45 brings to mind the scapula of several teleosauroids: *Mycterosuchus nasutus* Andrews, 1913 NHMUK PV R 2617, *Platysuchus multiscrobiculatus* Berckhemer, 1929 SMNS 9930 & UMH-0005, *Macrospondylus bollensis* Jäger, 1828 SMNS 54063, *Charitomenosuchus leedsi* Andrews, 1909 NHMUK PV R 3806, *Lemmysuchus obtusidens* Andrews, 1909 NHMUK PV R 3168, *Indosinosuchus potamosiamensis* Martin et al., 2019b PRC-24 (Martin et al., 2019b), etc. However, the wide scapular blade of *Turnersuchus* LRM 2021/45 further diverges from that of most teleosauroids (except *Platysuchus* SMNS 9930 & UMH-0005).

The anterior margin of the scapula of *Turnersuchus* LRM 2021/45 displays a strongly concave margin (Wilberg et al., 2023) whose apex appears to be located directly posteriorly to the mid-height of the bone. This, along with the straight posterior margin, result in a relatively distally positioned neck constriction as in the scapula of other thalattosuchians (*e.g.* *Pelagosaurus* BRLSI M.1418, *Thalattosuchus* GLAHM V1146, *Cricosaurus suevicus* SMNS 9808, *Dakosaurus maximus* SMNS 8203, *Mycterosuchus* NHMUK PV R 2617, *Platysuchus* SMNS 9930 & UMH-0005, *Macrospondylus* SMNS 54063, *Charitomenosuchus* NHMUK PV R 3806, *Lemmysuchus* NHMUK PV R 3168, *Indosinosuchus potamosiamensis* PRC-24, etc.). From the strong degree of concavity of the anterior margin also ensues a moderately elongated scapular neck between the fan-shaped extremity of the scapular blade and the proximal region of the scapula, similarly to the scapulae of *Pelagosaurus* BRLSI M.1418, *Geosaurus lapparenti* UJF-ID.11847j & UJF-ID.11852f, *D. maximus* SMNS 8203, *Mycterosuchus* NHMUK PV R 2617, and *Macrospondylus* SMNS 54063 within Thalattosuchia. From what is preserved, the scapular blade of *Turnersuchus* LRM 2021/45 appears to have been slightly domed as in the scapulae of *Pelagosaurus* BRLSI M.1418, *Thalattosuchus* GLAHM V1146, *C. albersdoerferi* BMMS-BK 1-2, *Mycterosuchus* NHMUK PV R 2617, *Charitomenosuchus* NHMUK PV R 3806, *Neosteneosaurus edwardsi* Eudes-Deslongchamps, 1868 NHMUK PV R 3701 & PETMG R178, and *Lemmysuchus* NHMUK PV R 3168. Hence, the anterior extremity of the scapular blade of *Turnersuchus* LRM 2021/45 was presumably located on the same level (*i.e.* distally) as the posterior corner (as in the scapula of *Pelagosaurus* BRLSI M.1418 or *Mycterosuchus* NHMUK PV R 2617 for example).

Ventrally, the neck of the scapula of *Turnersuchus* LRM 2021/45 gradually flares out to form the proximal region of the scapula, which mirrors its enlarged scapular blade. In this way, the scapula of *Turnersuchus* LRM 2021/45 resembles those of *Pelagosaurus* (BRLSI M.1418) and *Macrospondylus* (*e.g.* SMNS 54063). In the latter, the proximal region is shortened in relation to the scapular blade, which is also observed on the scapula of *Turnersuchus* LRM 2021/45. The proximal-most portion of the scapula of *Turnersuchus* LRM 2021/45 displays an acromion process similar to that of *Pelagosaurus* (BRLSI M.1418) and other teleosauroids in having its apex located ventrally, on the same plane as the scapulocoracoid synchondrosis surface (*e.g.* *Macrospondylus* SMNS 54063, *Charitomenosuchus* NHMUK PV R 3806, *Neosteneosaurus* NHMUK PV R 3701 & PETMG R178, *Ind. potamosiamensis* PRC-24, etc.). The dorsal margin of the acromion process is slightly convex as on the scapula of *Pelagosaurus* BRLSI

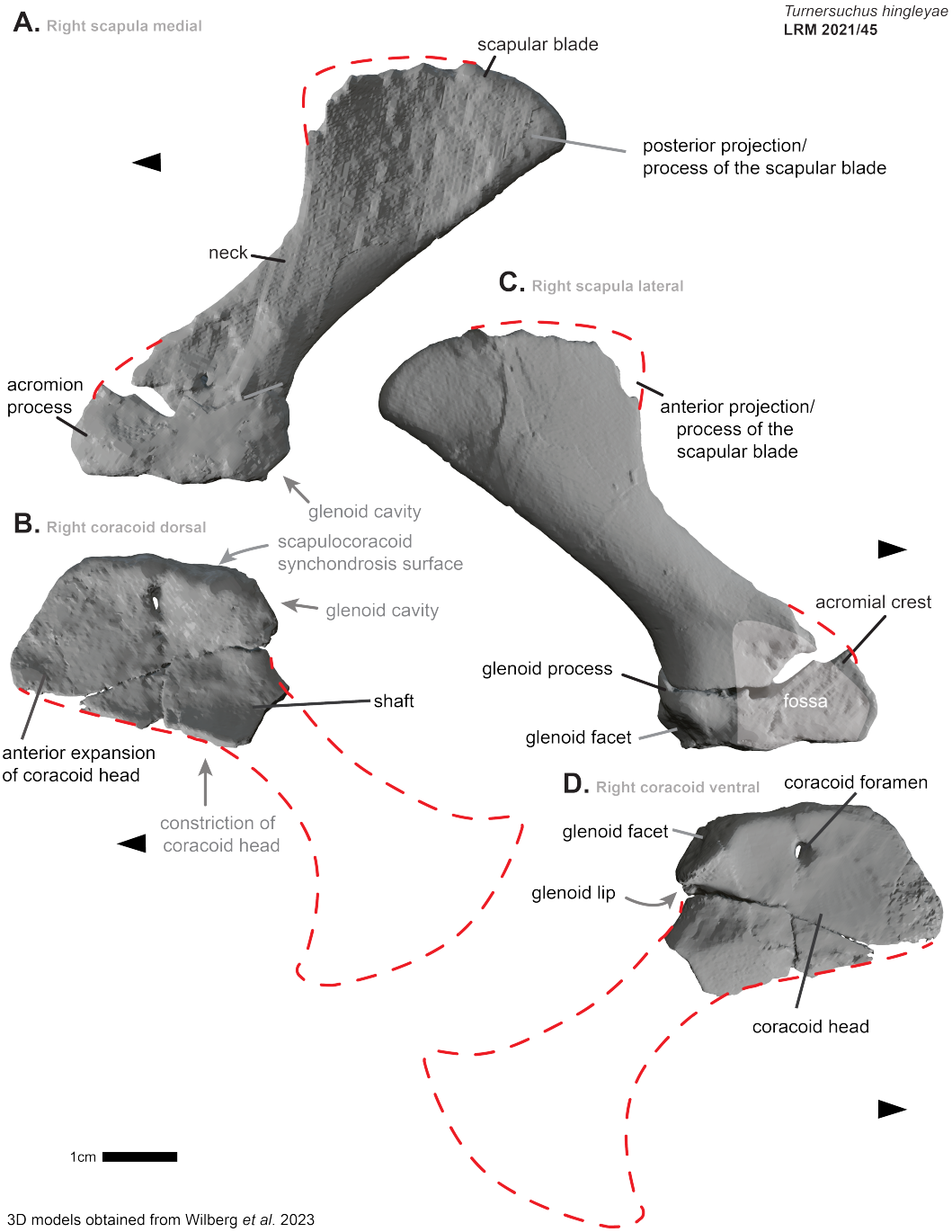


FIGURE 9. Pectoral girdle of *Turnersuchus hingleyae* LRM 2021/45 (3D models) (Wilberg et al., 2023). **A.** Left scapula in lateral view ; **B.** Left coracoid in ventral view ; **C.** Left scapula in medial view ; **D.** Left coracoid in ventral view. Arrow points anteriorly. 3D models from Wilberg et al. (2023). Red dashed lines indicate missing parts. Reconstruction of missing parts based on *Macrospondylus bollensis* PMU 35980.

M.1418, and is also slightly thickened mediolaterally. This thickening of the dorsal border is further emphasized by the presence of a shallow recessed area extending over the entire acromion process but which ends at the base of the glenoid process. The thickening of the dorsal border of the acromion process of the scapula of *Turnersuchus* LRM 2021/45 presumably corresponds to the acromial or deltoid crest.

The glenoid process of the scapula of *Turnersuchus* LRM 2021/45 slightly protrudes posteriorly, of lesser intensity than what is observed in the scapula of *Pelagosaurus* BRLSI M.1418. The glenoid facet of the scapula *Turnersuchus* LRM 2021/45 is positioned posteriorly as on the scapula of *Pelagosaurus* BRLSI M.1418, rather than strictly laterally as on the scapula of teleosauroids. The relatively planar surface of the glenoid facet of the scapula of *Turnersuchus* LRM 2021/45 could be an ontogenetic artefact still subjected to modifications (Brochu, 1992).

The scapulocoracoid synchondrosis surface of the scapula of *Turnersuchus* LRM 2021/45 displays a triangular outline due to the mediolateral thinning of the acromion process. Overall, the scapulocoracoid synchondrosis surface accounts for almost the entirety of the anteroposterior length of the proximal region of the scapula. Ventrally, the surface of the scapulocoracoid synchondrosis is strongly undulated and mirrors that of the coracoid so that both surfaces were interlocking. The presence of a rugose coracoid contact is perceived as an acquired ontogenetic change (Brochu, 1992).

6.1.2. *Coracoid.* The coracoid of *Turnersuchus* LRM 2021/45, see figs. 9, 10 and 12) possesses the typically short scapulocoracoid synchondrosis surface found in other thalattosuchians. In addition, the coracoid head of *Turnersuchus* LRM 2021/45 also displays the sharp and tapered anterior expansion as found in teleosauroids. The coracoid of *Turnersuchus* LRM 2021/45 differs from that of other thalattosuchians in displaying a smaller angular relation between the shaft of the coracoid and the scapulocoracoid synchondrosis surface.

The coracoid head of *Turnersuchus* LRM 2021/45 possesses an overall parallelepiped shape due to the relatively parallel lateral and medial margins. In addition, the lateral, medial and anterior margins are all rather straight which emphasizes the geometric shape of the coracoid head. The anterior expansion of the coracoid head of *Turnersuchus* LRM 2021/45 is triangular in shape which resembles teleosauroids, but contrasts with the forms observed in metriorhynchoids, dyrosaurids and extant crocodylians. Indeed, the anterior expansion of the coracoid of *Turnersuchus* LRM 2021/45 produces a sharp and acute corner with the median margin of the coracoid head. As a result, the total anteroposterior length of the coracoid head markedly exceeds that of the scapulocoracoid synchondrosis surface. This difference in length is a trait found in other thalattosuchians, although the shape of the coracoid head is more variable. Similar to other thalattosuchians, the coracoid head of *Turnersuchus* LRM 2021/45 displays a relatively thin dorsoventral thickness throughout its surface (especially the anterior expansion) giving it a plate-like appearance. In comparison, the dorsoventral thickness of the coracoid head of extant crocodylians and dyrosaurids is proportionally greater, but still becomes narrower anteriorly. This difference is presumably induced by the respective size of the scapulocoracoid synchondrosis surface, with thalattosuchians displaying a long and non-supporting anterior expansion whereas extant crocodylians and dyrosaurids bear the scapulocoracoid synchondrosis surface at full length. Another differing trait of the coracoid of *Turnersuchus* LRM 2021/45 compared to extant crocodylians and dyrosaurids is the lesser inclination of the coracoid foramen. Indeed, the dorsal and ventral apertures of the coracoid foramen of *Turnersuchus* LRM 2021/45 are almost entirely aligned. This feature is also found in other thalattosuchians, and the small thickness of the coracoid head presumably hampers any additional shifting of the apertures. On the coracoid of *Turnersuchus* LRM 2021/45, the location of the apertures is close to the margin of the scapulocoracoid synchondrosis surface, and is positioned around its mid-length. In other thalattosuchians, the apertures of the coracoid foramen are also relatively centered in relation to the scapulocoracoid synchondrosis surface

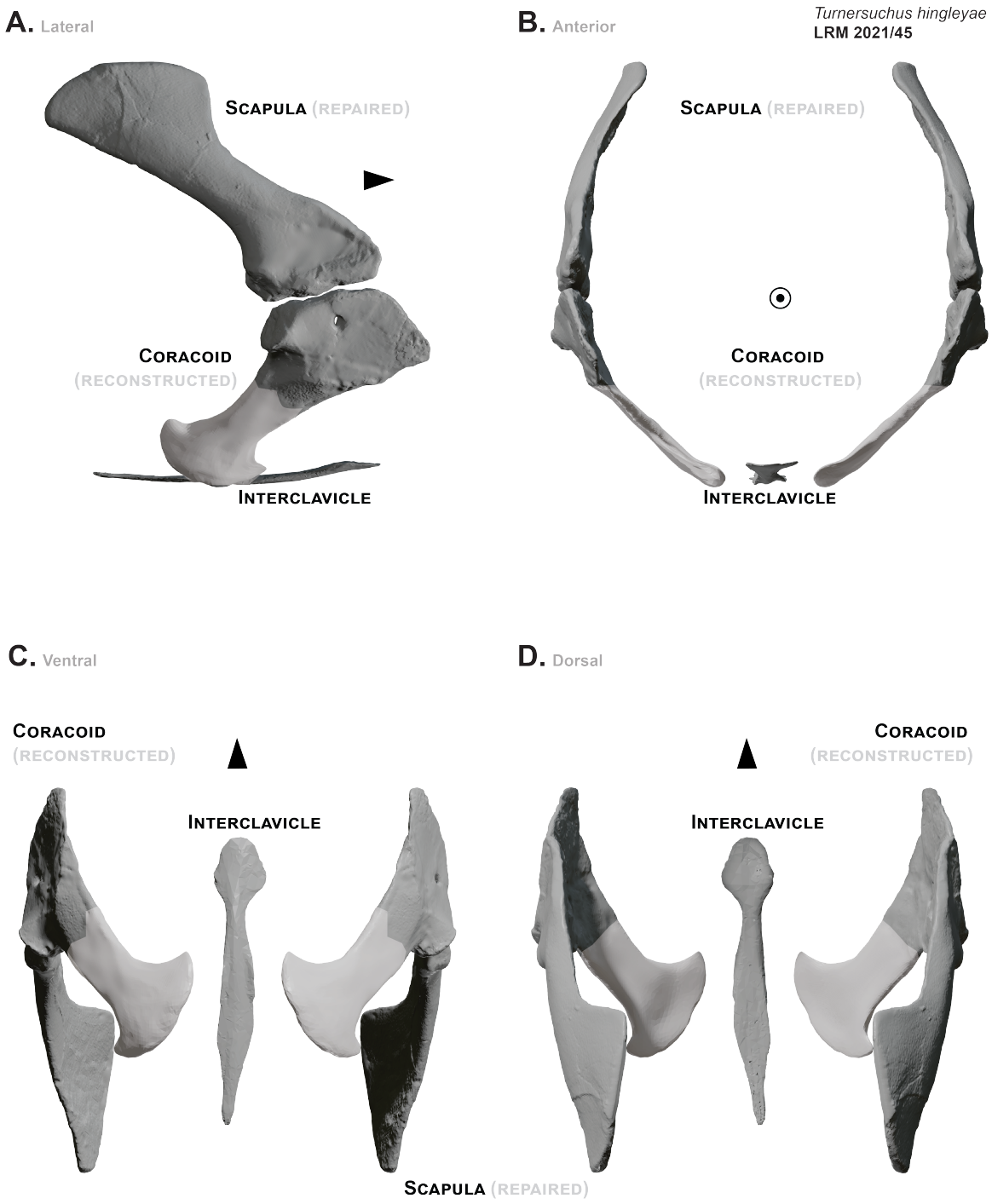


FIGURE 10. Reconstruction of the pectoral girdle of *Turnersuchus hingleyae* LRM 2021/45 (3D models). **A.** Lateral view; **B.** Anterior view; **C.** Ventral view; **D.** Dorsal view. Arrow points anteriorly. Target indicates anterior. The left scapula and coracoid are mirrored. Reconstruction of missing parts based on *Macrospondylus* PMU 35980.

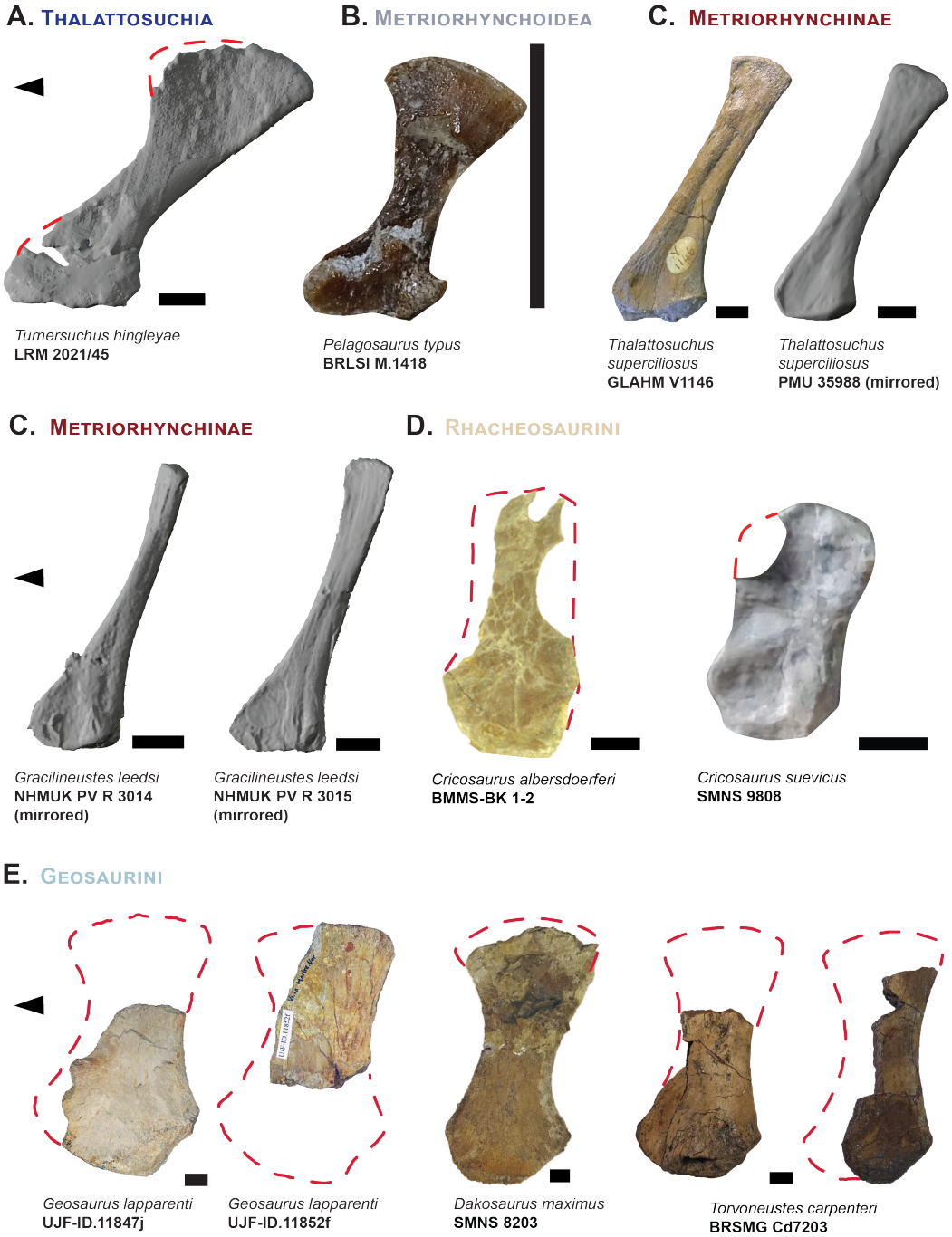


FIGURE 11. Comparative figure of basal thalattosuchian and metriorhynchoid scapulae. **A.** Thalattosuchia (3D model); **B.** Metriorhynchoidea (photograph); **C.** Metriorhynchinae (photograph and 3D models); **D.** Rhacheosaurini (photographs); **E.** Geosaurini (photographs). Arrow points anteriorly. Scale bars represent 1cm. Red dashed lines indicate missing parts.

but are more medially shifted and hence are found closer to the base of the shaft of the coracoid.

The scapulocoracoid synchondrosis surface of the coracoid of *Turnersuchus* LRM 2021/45 has the shape of a scalene right-angle triangle which becomes narrower anteriorly as the coracoid head becomes thinner. The hypotenuse side of this triangle corresponds to the dorsal margin of the scapulocoracoid synchondrosis surface, and hence its right-angle corner points ventrally. The thickest portion of the scapulocoracoid synchondrosis surface is found at the base of the glenoid process, and corresponds to the line perpendicular to the hypotenuse joining the right-angle corner. Posteriorly to this, the glenoid process keeps expanding to form the glenoid facet. The triangular outline of the scapulocoracoid synchondrosis surface is partly induced by the relative posterior to posteroventral position of the glenoid facet, which truncates the posterior extremity of the scapulocoracoid synchondrosis surface and creates an oblique posterior side. In most teleosauroid coracoids, the glenoid facet is strictly ventral and does not impact the shape of the scapulocoracoid synchondrosis surface, which hence displays a subrectangular posterior extremity and an overall parallelepiped shape (*e.g.* *Mycterosuchus* NHMUK PV R 2617, *Charitomenosuchus* NHMUK PV R 3806, *Neosteneosaurus* NHMUK PV R 3701, *Lemmysuchus* NHMUK PV R 3169, *Platysuchus* SMNS 9930, etc.). In comparison, metriorhynchoid coracoids also display a posterior or posteroventrally positioned glenoid facet similar to the coracoid of *Turnersuchus* LRM 2021/45 (*e.g.* *Pelagosaurus typus* BRLSI M.1418 and BRLSI M.3578, *Magyarosuchus fitosi* Ősi et al., 2018 (Ősi et al., 2018), *Thalattosuchus* GLAHM V1005, *Thalattosuchus* GLAHM V1146, *Thalattosuchus* PMU 35988, *Thalattosuchus* NHMUK PV R 1530, *C. albersdoerferi* BMMS-BK 1-2, *C. bambergensis* NKMB-P-Watt14/274, *C. suevicus* SMNS 9808, *'Metriorhynchus' brachyrhynchus* NHMUK PV R 4696, *D. maximus* SMNS 8203, *Tyrannoneustes lythrodectikos* GLAHM V1145). On the coracoid of *Turnersuchus* LRM 2021/45, the surface of the scapulocoracoid synchondrosis is undulated and interlocks with matching configurations on the scapula. In comparison, most thalattosuchian coracoids (*i.e.* metriorhynchoids and teleosauroids) tend to display a smoother scapulocoracoid synchondrosis surface, with the exception of the coracoid of *Platysuchus* SMNS 9930 which appears to possess a more irregular surface on both the scapula and coracoid.

The glenoid process of the coracoid of *Turnersuchus* LRM 2021/45 constitutes the dorsoventrally widest area of the bone, similar to other thalattosuchians, extant crocodylians and dyrosaurids. Due to the sub-circular shape of the glenoid facet of the coracoid of *Turnersuchus* LRM 2021/45, the thickest portion of the coracoid also coincides with the maximum diameter of the glenoid facet of the coracoid, as on the coracoid of *Magyarosuchus* (Ősi et al., 2018) and presumably that of *Pelagosaurus* (most complete specimens are partly encased in rock matrix), but also as in more derived metriorhynchoids (*e.g.* *C. suevicus* SMNS 9808, *Dakosaurus sp.* DMA-JP-2009/001, *Tyrannoneustes* GLAHM V1145, etc.). This feature is also observed in extant crocodylians, although the overall position of the glenoid facet differs from that of *Turnersuchus* LRM 2021/45 (*e.g.* *Palaeosuchus palpebrosus* RVC-JRH-PP1, *Mecistops cataphractus* RBINS 18374, *Caiman crocodylus* NMW 30900, *Crocodylus rhombifer* AMNH FARB 16694, *Osteolaemus tetraspis* NMW 39338:2, etc.). In comparison, the glenoid facet of teleosauroid coracoids has an elliptical outline with the longest axis, and hence width, being anteroposteriorly orientated in most taxa (*e.g.* *Mycterosuchus* NHMUK PV R 2617, *Platysuchus* SMNS 9930, *Macrospondylus* SMNS 9428, *Neosteneosaurus* NHMUK PV R 3701, *Lemmysuchus* NHMUK PV R 3169). However, in the teleosauroid *Charitomenosuchus* NHMUK PV R 3806 the thickest portion of the coracoid also corresponds to the maximum diameter of the glenoid facet as observed on the coracoid of *Turnersuchus* LRM 2021/45. As observed on the coracoids of the basal metriorhynchoids *Pelagosaurus* and *Magyarosuchus* (Ősi et al., 2018), the glenoid facet of the coracoid of *Turnersuchus* LRM 2021/45 is less expanded than in more derived thalattosuchians. Indeed, the area of the glenoid facet is proportionally small compared to the size of the coracoid head and also the glenoid process does not markedly protrude from the coracoid head, differing from extant crocodylians (*e.g.* *Palaeosuchus palpebrosus* RVC-JRH-PP1, *Mecistops cataphractus* RBINS 18374, *Caiman crocodylus* NMW 30900, *Crocodylus rhombifer* AMNH FARB 16694, *Osteolaemus tetraspis* NMW 39338:2, etc.) and dyrosaurids (*e.g.* *Hyposaurus*

natator NJSM 23368 and YPM VP.00095, *Dyrosaurus maghribensis* OCP DEK-GE 254, *Congosaurus bequaerti* MRAC 1811). In derived metriorhynchoids, the area of the glenoid facet of the coracoid shows a small increase in size and is also more protruding (*e.g. Thalattosuchus* GLAHM V1005, *Thalattosuchus* NHMUK PV R 1530, *'Me.' brachyrhynchus* NHMUK PV R 4696, *Tyrannoneustes* GLAHM V1145, *C. suevicus* SMNS 9808), whereas the glenoid facet of teleosauroids is markedly larger and prominent (*e.g. Mycterosuchus* NHMUK PV R 2617, *Platysuchus* SMNS 9930, *Macrospondylus* SMNS 9428, *Neosteneosaurus* NHMUK PV R 3701, *Lemmysuchus* NHMUK PV R 3169).

The medial portion of the coracoid of *Turnersuchus* LRM 2021/45 is not preserved. However, it is possible that the coracoid of *Turnersuchus* LRM 2021/45 possessed a relatively slender and rod-like shaft similar to the coracoids of the basal metriorhynchoids *Pelagosaurus* and *Magyarosuchus* (Ősi et al., 2018). However, the most important feature of the shaft of the coracoid of *Turnersuchus* LRM 2021/45 is its relative inclination, as it forms a markedly acute angle with the scapulocoracoid synchondrosis surface (around 30° angle). An acute angle (around 45°) between the long axis of the shaft of the coracoid and the scapulocoracoid synchondrosis surface is usually observed in dyrosaurids, but the teleosauroid *Platysuchus* SMNS 9930 also displays a similar configuration.

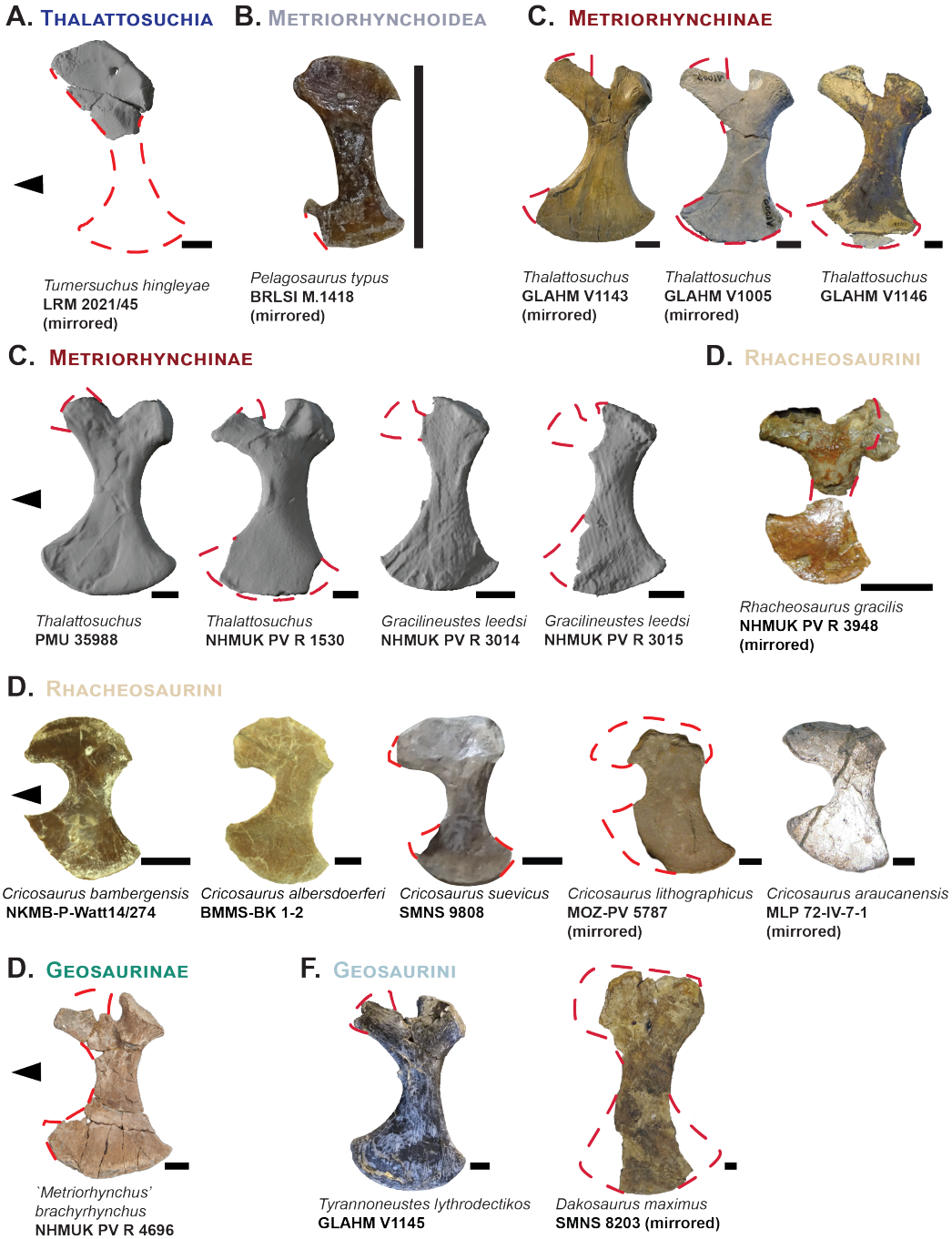


FIGURE 12. Comparative figure of basal thalattosuchian and metriorhynchoid coracoids. **A.** Thalattosuchia (3D model); **B.** Metriorhynchoidea (photograph); **C.** Metriorhynchinae (photographs first row – 3D models second row); **D.** Rhacheosaurini (photographs); **E.** Geosaurinae (photograph); **F.** Geosaurini (photographs). Arrow points anteriorly. Scale bars represent 1cm. Red dashed lines indicate missing parts.

7. THE APPENDICULAR SKELETON OF THALATTOSUCHIANS: METRIORHYNCHOIDS

7.1. ***Pelagosaurus typus* Bronn, 1841.** For measurements, see tables 6 and 7. The specimens correspond to juveniles.

7.1.1. *Scapula.* The scapula of *Pelagosaurus typus* (BRLSI M.1418 & BRLSI M.3578 see figs. 11, 13 and 14) resembles that of extant crocodylians (*e.g. Palaeosuchus palpebrosus* RVC-JRH-PP1 see fig. 4, *Mecistops cataphractus* RBINS 18374 see fig. 5, *Caiman crocodylus* NMW 30900 see fig. 6, or *Crocodylus niloticus* NMW 31137 see fig. 7) in displaying a short neck, a moderately flared out scapular blade and an overall similar proximal area (*i.e.* shallow acromial crest and scapular fossa, and well defined glenoid process). In this way, it strongly contrasts with that of other thalattosuchians and dyrosaurids.

The anterior and posterior margins of the scapula of *Pelagosaurus* BRLSI M.1418 and BRLSI M.3578 are both strongly concave. This feature is also found in the scapula of *D. maximus* SMNS 8203 (see fig. 11 E), and presumably in the scapulae of *Ge. lapparenti* UJF-ID.11847j & UJF-ID.11852f, and *Torvoneustes carpenteri* Wilkinson et al., 2008 BRSMG Cd7203 among metriorhynchoids. Basal teleosauroids such as *Mycterosuchus* NHMUK PV R 2617 and *Platysuchus* SMNS 9930 & UMH-0005 also possess scapulae with strongly concave margins. In comparison, modern crocodylians usually display a strong concavity for the anterior margin of their scapula whereas the posterior margin of their scapula is more sinusoidal. In *Pelagosaurus* BRLSI M.1418 & BRLSI M.3578, the apex of both the anterior and posterior margins of the scapula are almost facing one another around the mid-height of the bone, resulting in a slender and short neck. Indeed, the anteroposterior length of the constriction at its thinnest reaches about half of the anteroposterior proximal length of the scapula. In addition, the concurrence of both a strong concavity as well as the convergence of both extremities around the same position confines the extension of the neck, unlike in the more slender scapulae of *Thalattosuchus* PMU 35988, *Charitomenosuchus* NHMUK PV R 3806, *Neosteneosaurus* NHMUK PV R 3701, *Lemmysuchus* NHMUK PV R 3168.

In parallel, the overall similar concavity of both anterior and posterior margins of the scapula of *Pelagosaurus typus* BRLSI M.1418 & BRLSI M.3578 results in a moderately wide (*i.e.* extends as far anteriorly and posteriorly as the acromion and glenoid processes) and symmetrically fan-shaped scapular blade (see fig. 13). The scapular blade of *Pelagosaurus typus* BRLSI M.1418 & BRLSI M.3578 stands out from that of other thatattosuchians as it is proportionally greatly larger than the constriction of the neck (more than twice) while still being symmetrical anteroposteriorly. Among Thalattosuchia, only the scapulae of *D. maximus* SMNS 8203 and *Mycterosuchus* NHMUK PV R 2617 similarly show a scapular blade highlighted by a marked neck constriction although with a lesser intensity than in *Pelagosaurus* BRLSI M.1418 & BRLSI M.3578. As in most thalattosuchians (*e.g. Thalattosuchus* GLAHM V1146, *Thalattosuchus* PMU 35988, *Ge. lapparenti* UJF-ID.11847j & UJF-ID.11852f, *D. maximus* SMNS 8203, *Mycterosuchus* NHMUK PV R 2617, *Charitomenosuchus* NHMUK PV R 3806, and *Lemmysuchus* NHMUK PV R 3168), the dorsal surface of the scapular blade of *Pelagosaurus typus* BRLSI M.1418 & BRLSI M.3578 is slightly convex or domed, and is overall parallel to the ventral margin of the scapula (defined by the acromion process and scapulocoracoid synchondrosis surface, see fig. 13). Hence, the anterior and posterior corners of the scapular blade, marking the junction between the anterior and posterior margins with the dorsal margin of the blade, form acute corners both oriented anteroposteriorly.

Ventrally to the neck, is the proximal head of the scapula. The latter still comprises several pronounced features in *Pelagosaurus typus* BRLSI M.1418 & BRLSI M.3578 which gradually fade away in more derived metriorhynchoids (*e.g. Thalattosuchus* PMU 35988, *C. albersdoerferi* BMMS-BK 1-2, *C. suevicus* SMNS 9808, *Ge. lapparenti* UJF-ID.11847j & UJF-ID.11852f, *D. maximus* SMNS 8203, *D. maximus* SMNS 8203, etc.): acromion process, acromial crest, scapular fossa, glenoid process and scapula buttress. Indeed, the acromion and glenoid processes of the scapula of *Pelagosaurus typus* BRLSI M.1418 & BRLSI M.3578 both strongly protrude anteriorly and posteriorly from the neck of the scapula as in extant

crocodylians. In *Pelagosaurus* BRLSI M.1418 & BRLSI M.3578, the acromion process of the scapula shows an elliptic outline and culminates in a rounded apex pointing anteroventrally as in the scapula of *Palaeosuchus palpebrosus* (RVC-JRH-PP1, see fig. 4) or *Mecistops cataphractus* (RBINS 18374, see fig. 5). As a result, the ventral margin of the acromion process of the scapula of *Pelagosaurus typus* BRLSI M.1418 & BRLSI M.3578 is in line with (and gradually forms) the ventral margin of the scapulocoracoid synchondrosis surface, unlike in *Thalattosuchus* GLAHM V1146, *Thalattosuchus* PMU 35988, *C. albersdoerferi* BMMS-BK 1-2, *C. suevicus* SMNS 9808, *D. maximus* SMNS 8203, and *To. carpenteri* BRSMG Cd7203 for which the acromion process is either reduced or pointing anterodorsally. On the lateral surface of the acromion process and along its dorsal margin, there is a ridge called the acromial crest. In *Pelagosaurus* BRLSI M.1418 & BRLSI M.3578, the acromial crest runs along the entire acromion process and appears shallow as in extant crocodylians (*e.g. Palaeosuchus palpebrosus* RVC-JRH-PP1 see fig. 4, *Mecistops cataphractus* RBINS 18374 see fig. 5, *Caiman crocodylus* NMW 30900 see fig. 6, or *Crocodylus niloticus* NMW 31137 see fig. 7). The acromial crest of the scapula of *Pelagosaurus* BRLSI M.1418 & BRLSI M.3578, as in extant crocodylians, overhangs a shallow sub-triangular recessed region – the scapular fossa – which extends up until the glenoid process. In more derived metriorhynchoids, the scapular fossa becomes shallower and dorsally stretched (*e.g. Thalattosuchus* PMU 35988, *D. maximus* SMNS 8203; *To. carpenteri* BRSMG Cd7203, etc.).

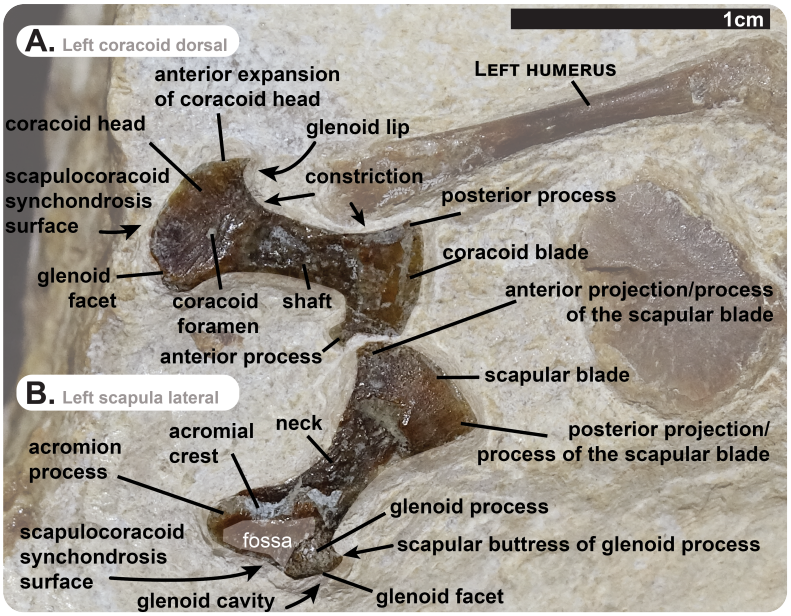
The glenoid process of the scapula of *Pelagosaurus typus* BRLSI M.1418 & BRLSI M.3578 forms a posteriorly protruding knob at the posteroventral corner of the scapula, which contrasts with that of other metriorhynchoids (*e.g. Thalattosuchus* PMU 35988, *C. suevicus* SMNS 9808, *Ge. lapparenti* UJF-ID.11847j & UJF-ID.11852f, *D. maximus* SMNS 8203, *To. carpenteri* BRSMG Cd7203, etc.). As a result, the glenoid process of the scapula of *Pelagosaurus typus* BRLSI M.1418 & BRLSI M.3578 displays a well developed scapular buttress.

In *Pelagosaurus* BRLSI M.1418 & BRLSI M.3578, the glenoid facet is dorsally tilted compared to the rest of the ventral margin of the scapula leading to a posteroventrally oriented articular facet as in other metriorhynchoids rather than mostly ventrally as in the extant crocodylians *Mecistops cataphractus* (RBINS 18374), and *Caiman crocodylus* (NMW 30900). The articular facet of the glenoid of the scapula of *Pelagosaurus typus* BRLSI M.1418 & BRLSI M.3578 is relatively planar, which could be an ontogenetic artefact (Brochu, 1992).

7.1.2. *Coracoid.* The coracoid of *Pelagosaurus* (see figs. 12 to 14) possesses a similarly sized proximal head and distal blade, as in extant crocodylians (*e.g. Palaeosuchus palpebrosus* RVC-JRH-PP1, *Mecistops cataphractus* RBINS 18374, *Caiman crocodylus* NMW 30900, *Crocodylus rhombifer* AMNH FARB 16694, etc.) but unlike dyrosaurids (*e.g. H. natator* NJSM 23368 or *Co. bequaerti* MRAC 1811).

The coracoid head of *Pelagosaurus* BRLSI M.1418 & BRLSI M.3578 appears symmetrical due to both the position and orientation of the shaft (which is centered and almost perpendicular to the scapulocoracoid synchondrosis surface) and the relatively similar outline of both extremities (*i.e.* the glenoid process and anterior expansion). Similar to other thalattosuchians, the coracoid head of *Pelagosaurus typus* BRLSI M.1418 & BRLSI M.3578 extends further anteriorly than the scapulocoracoid synchondrosis surface to form the anterior expansion. In *Pelagosaurus* BRLSI M.1418 & BRLSI M.3578, the anterior expansion forms a short and sharp hook, with a strongly convex lateral margin and markedly concave medial margin culminating into a curved and sharp extremity, strictly medially oriented. Several other metriorhynchoid taxa display a similarly shaped hooked anterior expansion, although larger in size: *C. albersdoerferi* BMMS-BK 1-2, *C. bambergensis* NKMB-P-Watt14/274, *C. suevicus* SMNS 9808, *Dakosaurus sp.* Rygol specimen. In extant crocodylians, the expansion of the coracoid head is proportionally less prominent and of differing shape (*e.g. Palaeosuchus palpebrosus* RVC-JRH-PP1, *Mecistops cataphractus* RBINS 18374, *Caiman crocodylus* NMW 30900, *Osteolaemus tetraspis* NMW 39338:2), with some bearing a similarly looking hooked-shape (*e.g. Palaeosuchus palpebrosus* RVC-JRH-PP1 and

Pelagosaurus typus
BRLSI M.1418



Pelagosaurus typus
BRLSI M.3578

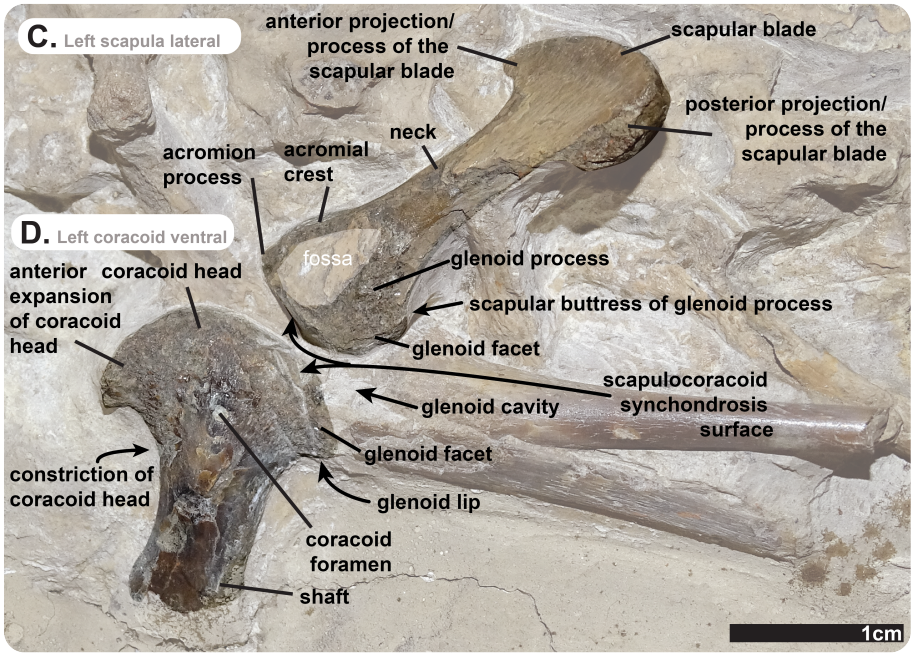


FIGURE 13. Pectoral girdle of *Pelagosaurus typus* BRLSI M.1418 (A&B) and *Pelagosaurus typus* BRLSI M.3578 (C&D) (photographs). **A.** Left coracoid in dorsal view; **B.** Left scapula in lateral view; **C.** Left scapula in lateral view; **D.** Left coracoid in ventral view.

Caiman crocodylus NMW 30900). In dyrosaurids, the anterior expansion is also proportionnally shorter than most thalattosuchians and sub-circular in shape (*e.g. H. natator* NJSM 23368 & YPM VP.00095, *Dy. maghribensis* OCP DEK-GE 254, *Co. bequaerti* MRAC 1811). In comparison, the anterior expansion of teleosauroids and the basal thalattosuchian *Turnersuchus* LRM 2021/45 is larger than *Pelagosaurus typus* BRLSI M.1418 & BRLSI M.3578 and triangular in shape. A short anterior expansion of the coracoid head is also observed in *Platysuchus* SMNS 9930, *Macrospondylus* SMNS 54063, SMNS 9428 & PMU 35980, and *Aeolodon priscus* von Sömmerring, 1814 NHMUK PV R 1086 & MNHN.F.CNJ 78, with *Aeolodon* NHMUK PV R 1086 possessing the shortest expansion.

Overall, the glenoid facet and scapulocoracoid synchondrosis surface of the coracoid of *Pelagosaurus typus* BRLSI M.1418 & BRLSI M.3578 are proportionally large and account for about two-thirds of the total anteroposterior length of the coracoid head. This contrasts with other thalattosuchians bearing more slender scapulae and subsequently reduced scapulocoracoid synchondrosis surfaces (*e.g. Thalattosuchus* PMU 35988, *C. albersdoerferi* BMMS-BK 1-2, *D. maximus* SMNS 8203, *Charitomenosuchus* NHMUK PV R 3806, *Neosteneosaurus* NHMUK PV R 3701, etc.). As mentioned above, the scapulocoracoid synchondrosis surface of extant crocodylians and dyrosaurids is markedly larger (in relation to the overall size of the coracoid head and glenoid facet) than in *Pelagosaurus typus* BRLSI M.1418 & BRLSI M.3578 and other thalattosuchians. In ventral and dorsal views, the junctions between the scapulocoracoid synchondrosis surface form two similar obtuse angles with the glenoid facet (posteriorly) and the anterior expansion, which contributes to the symmetrical morphology of the coracoid head. The exact outline of the scapulocoracoid synchondrosis surface of the coracoid of *Pelagosaurus* is unknown, but presumably resembled the triangular shape of *Turnersuchus* LRM 2021/45 due to the posteroventral position of the glenoid facet. The latter appears to possess and overall circular outline, but it is unclear if the widest portion of the coracoid head also corresponds to the maximum diameter of the glenoid facet as in *Turnersuchus* LRM 2021/45 and other metriorhynchoids. The glenoid facet of the coracoid of *Pelagosaurus typus* BRLSI M.1418 & BRLSI M.3578 appears relatively flat or slightly domed and forms an acute angle with the shaft. The glenoid facets on the scapula and coracoid of *Pelagosaurus typus* BRLSI M.1418 & BRLSI M.3578 almost meet at a right angle in lateral view, which creates a large glenoid cavity. The junction between the glenoid facet and the shaft of the coracoid forms a concave recess as in *Turnersuchus* LRM 2021/4 and *Magyarosuchus* (Ősi et al., 2018), rather than a faintly curved slope as in more derived metriorhynchoids (*e.g. Thalattosuchus* NHMUK PV R 1530, *Cricosaurus* species, *'Me.' brachyrhynchus* NHMUK PV R 4696, *Tyrannoneustes* Young et al., 2012 GLAHM V1145, etc).

In *Pelagosaurus* BRLSI M.1418 & BRLSI M.3578, the coracoid foramen forms a relatively small and circular opening on the ventral and dorsal surfaces of the coracoid head. It is overall positioned at the dorsoventral same level as the distal tips of the glenoid lip and anterior expansion, and hence is close to the base of the shaft of the coracoid as in other metriorhynchoids, but differing from *Turnersuchus* LRM 2021/45. The shaft of the coracoid of *Pelagosaurus typus* BRLSI M.1418 & BRLSI M.3578 (see fig. 13), extending from the constriction of the coracoid head and distal blade, is proportionally long and narrow. Indeed, the total proximodistal length of the shaft of the coracoid reaches about half of the total height of the bone, whereas its anteroposterior width retains the same thickness throughout its length giving the shaft of the coracoid a rod-like appearance. The minimal width of the shaft of the coracoid accounts for slightly less than half of its proximodistal length. Another great peculiarity of the shaft of the coracoid of *Pelagosaurus* BRLSI M.1418 is its orientation: it forms an angle of about 71° with the scapulocoracoid synchondrosis surface and hence appears relatively perpendicular, as in *D. maximus* SMNS 8203 and *C. suevicus* SMNS 9808.

The overall size and shape of the distal blade of the coracoid of *Pelagosaurus* BRLSI M.1418 mirrors that of the proximal head: its distal surface is convex and culminates in sharp extremities anteriorly and

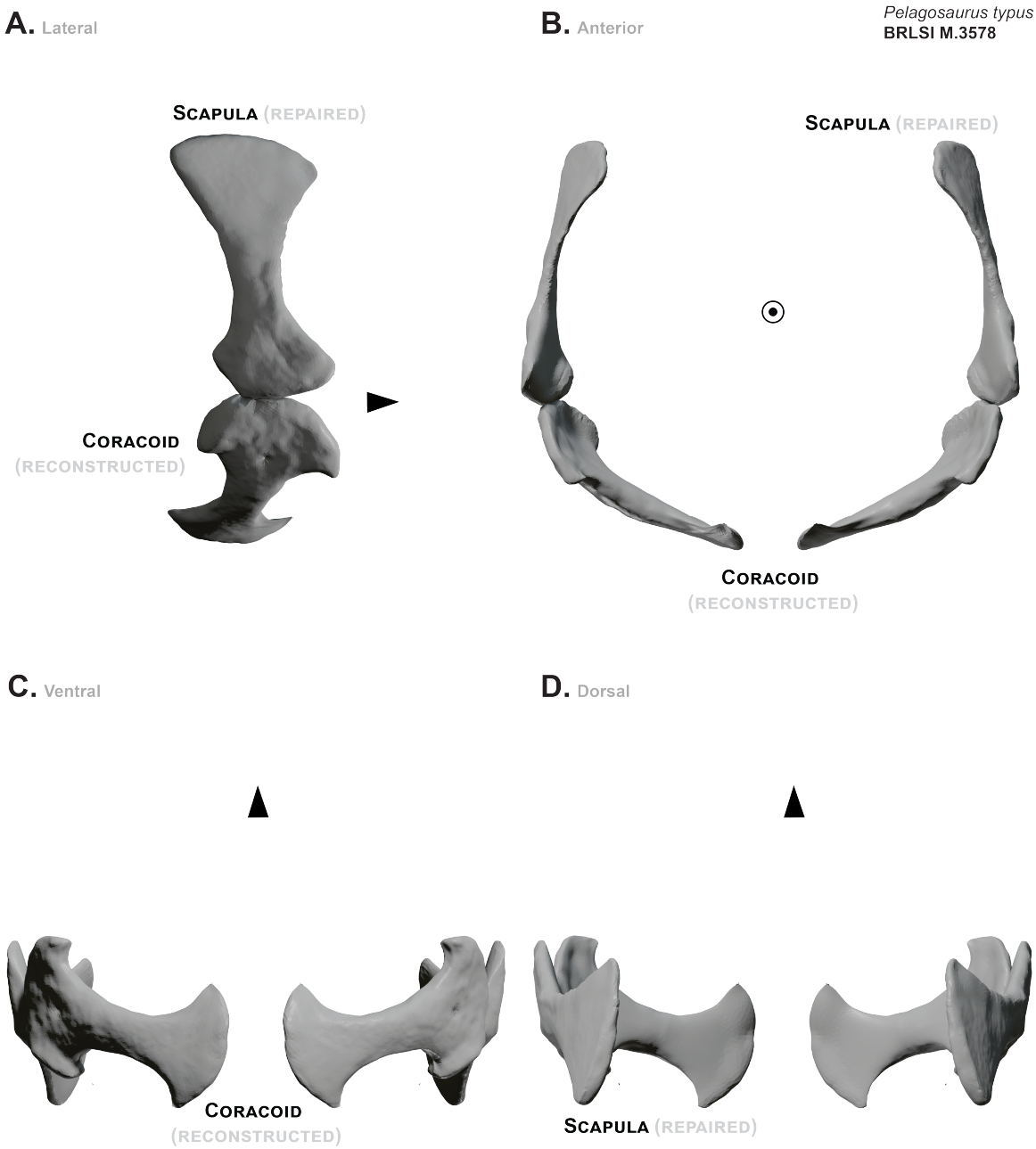


FIGURE 14. Reconstruction of the pectoral girdle of *Pelagosaurus* BRLSI M.3578 (3D models). **A.** Lateral view; **B.** Anterior view; **C.** Ventral view; **D.** Dorsal view. Arrow points anteriorly. Target indicates anterior. The right scapula and coracoid are mirrored.

posteriorly. The anterior corner of the distal blade is mainly oriented anteriorly and corresponds to the distal-most extremity. The posterior corner displays a strong proximal component in its orientation and is located relatively more proximately than the anterior corner. This positioning has an impact on the junction between the shaft of the coracoid and the distal blade: the anterior junction forms a smooth and gradual concave slope whereas the posterior junction shows a greater concavity. Other thalattosuchians also possess a strong anteroposterior asymmetry between the tips of their distal blade: *e.g. Rhacheosaurus* NHMUK PV R 3948, *C. bambergensis* NKMB-P-Watt14/274, *Aeolodon* NHMUK PV R 1086.

7.2. ***Thalattosuchus superciliosus*** **Blainville in Eudes-Deslongchamps and Blainville, 1852.** For measurements, see tables 6 and 7.

The fragmentary specimens GLAHM V1005 and GLAHM V1146 corresponding to a juvenile specimen GLAHM V1005 and isolated postcrania GLAHM V1146 from the Oxford Clay have not been included in the list of referred *Thalattosuchus* by Young et al. (2020a). Based on the morphological investigation of their pelvic and pectoral girdles and 3DGM analyses (Scavezzoni and Fischer, 2023), GLAHM V1005 and GLAHM V1146 have been assigned to *Thalattosuchus superciliosus* in this work.

However, GLAHM V1146 displays a unique humeral shape for *Thalattosuchus*. Since the associated girdle elements show no signs of abnormalities, such a difference in humeral shape could be the result of a pathology.

7.2.1. *Scapula.* The scapula of the *Thalattosuchus superciliosus* Blainville in Eudes-Deslongchamps and Blainville, 1852 specimens GLAHM V1146, PMU 35988 & GLAHM V1143 (see figs. 11 and 15 to 17 and also on the reconstruction figs. 18 to 20) is very gracile compared to that of most metriorhynchoids (*e.g. Pelagosaurus* BRLSI M.1418 & BRLSI M.3578, *C. albersdoerferi* BMMS-BK 1-2, *C. bambergensis* NKMB-P-Watt14/274, *C. suevicus* SMNS 9808, *Ge. lapparenti* UJF-ID.11847j & UJF-ID.11852f, *D. maximus* SMNS 8203 or *To. carpenteri* BRSMG Cd7203, etc.). Indeed, the scapula of GLAHM V1146 & PMU 35988 displays both a reduced proximal head and scapular blade, linked by an elongated and narrow shaft which is similar to what is observed in *G. leedsi* (NHMUK PV R 3014 & NHMUK PV R 3015). In comparison, several teleosauroids also possess a relatively slender scapula (*e.g. Mycterosuchus* NHMUK PV R 2617, *Ind. potamosiamensis* PRC-24, *Teleosaurus cadomensis* NHMUK PV OR 31836, *Neosteneosaurus* NHMUK PV R 3701, and *Lemmysuchus* NHMUK PV R 3168).

The total dorsoventral height of the bone is about three times (339.86% for PMU 35988; 321.74% for GLAHM V1146) larger than the anteroposterior length of the proximal head, and about four and a half times larger than the size of the scapular blade (450% for PMU 35988; 470% for GLAHM V1146). In GLAHM V1146 & PMU 35988, the shaft of the scapula accounts for 60% of the total height of the bone, which greatly contrasts with other metriorhynchoids (*e.g. Pelagosaurus* BRLSI M.1418 & BRLSI M.3578, *C. albersdoerferi* BMMS-BK 1-2, *C. bambergensis* NKMB-P-Watt14/274, *C. suevicus* SMNS 9808, *Ge. lapparenti* UJF-ID.11847j & UJF-ID.11852f, *D. maximus* SMNS 8203 or *To. carpenteri* BRSMG Cd7203, etc.). In addition, the shaft of the scapula of GLAHM V1146 & PMU 35988 displays long and relatively straight anterior and posterior margins, only subtlety concave, which give the shaft a rod-like appearance. The section of the shaft of the scapula of GLAHM V1146 & PMU 35988 is overall elliptic, with the longest axis oriented anteroposteriorly. The lateral surface of the shaft of the scapula displays a shallow sulcus throughout most of its length. Proximally, the sulcus widens to form the acromial scapular fossa.

Distally, the shaft of the scapula flares out a little to form the scapular blade, which is only slightly anteroposterioly larger than the shaft. The scapular blade of GLAHM V1146 & PMU 35988 appears similar to that of *Pelagosaurus* BRLSI M.1418 but at a smaller scale: the dorsal rim of the scapular blade is lightly domed and is overall perpendicular to the long axis of the shaft of the scapula. However, the anterior and posterior corners of the scapular blade in GLAHM V1146 & PMU 35988 do not constitute the mirror image of one another as in *Pelagosaurus* BRLSI M.1418. Indeed, the posterior corner shows a posterior margin directly in line with that of the shaft of the scapula, so that the transition between the two is smooth and almost imperceptible. On the contrary, the anterior corner displays an anterior margin with a slope drastically different from that of the shaft of the scapula, resulting in a more abrupt and angular transition. As a consequence, the anterior corner is relatively more protruding than the posterior corner.

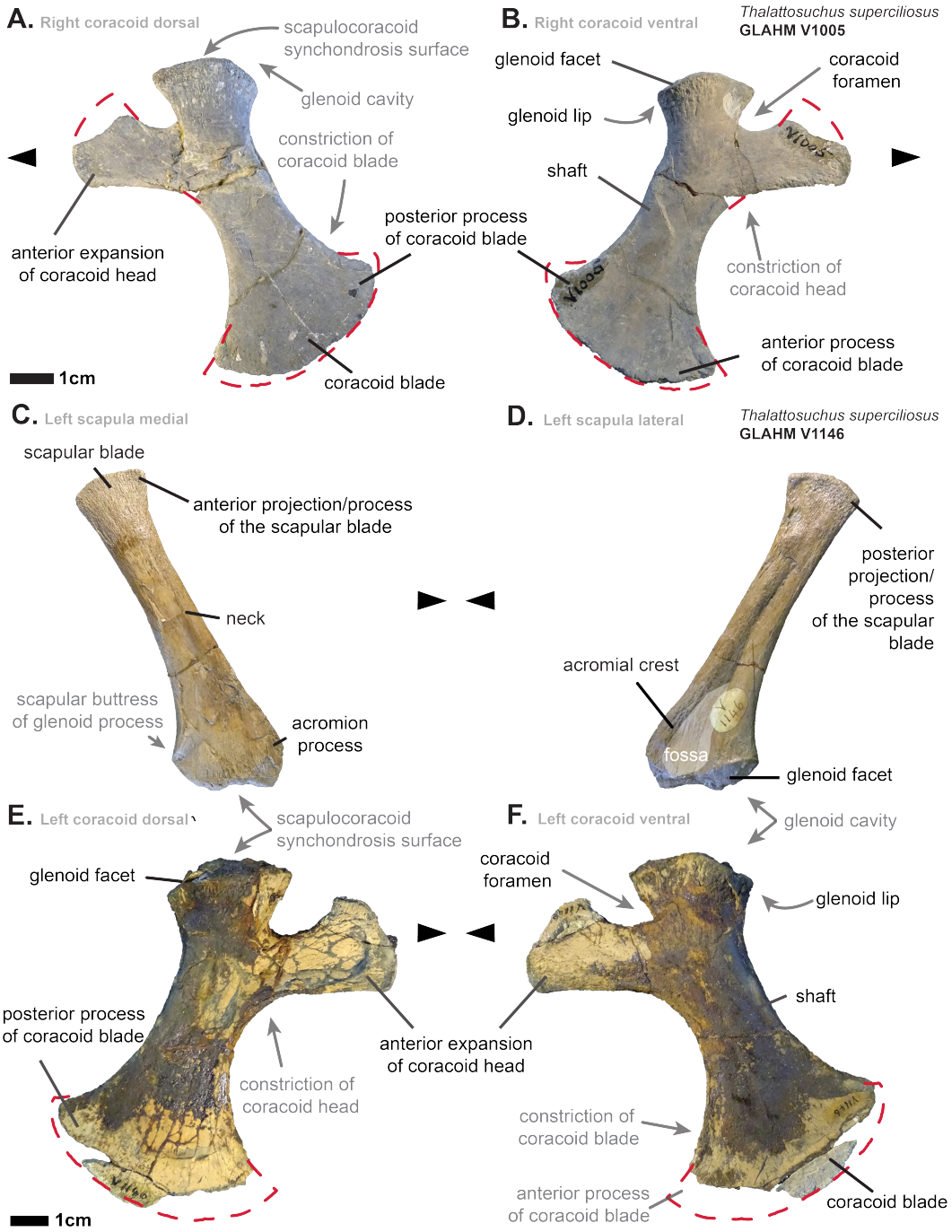


FIGURE 15. Pectoral girdle of *Thalattosuchus superciliosus* GLAHM V1005 (A&B; reconstruction of missing parts based on GLAHM V1146) and *Thalattosuchus superciliosus* GLAHM V1146 (C, D, E & F; reconstruction of missing parts based on GLAHM V1005) (photographs). **A.** Right coracoid in dorsal view ; **B.** Right coracoid in ventral view ; **C.** Left scapula in medial view ; **D.** Left scapula in lateral view ; **E.** Left coracoid in dorsal view ; **F.** Left coracoid in ventral view. Arrow points anteriorly. Red dashed lines indicate missing parts. Reconstruction of missing parts based on *Thalattosuchus superciliosus* GLAHM V1005.

Ventrally, the shaft of the scapula gradually widens as it transitions to the proximal portion of the scapula. The latter is constituted by the acromion process, scapular fossa, and glenoid process. As opposed to what was observed in *Pelagosaurus* BRLSI M.1418 & BRLSI M.3578, the acromion process, scapular fossa, and glenoid process of GLAHM V1146, PMU 35988 & GLAHM V1143 are markedly reduced as they only show a limited anteroposterior expansion. Indeed, in GLAHM V1146 & PMU 35988, the dorsal margin of the acromion process is directly in line with the anterior margin of the shaft of the scapula and follows its subtle curve. Hence, the acromion process does not appear to protrude from the shaft of the scapula. Unlike in *Pelagosaurus* BRLSI M.1418 & BRLSI M.3578, the dorsal margin of the acromion process of the scapulae of GLAHM V1146, PMU 35988 & GLAHM V1143 does not extend up until the ventral margin of the scapula, but rather forms an obtuse blunt corner at about the mid-height of the process. As a result, the acromion process of the scapulae of GLAHM V1146, PMU 35988 & GLAHM V1143 points directly anteriorly and not anteroventrally as in *Pelagosaurus* BRLSI M.1418 & BRLSI M.3578. A similarly shaped acromion process is found in other metriorhynchids (*e.g. G. leedsi* NHMUK PV R 3014 & NHMUK PV R 3015, *C. albersdoerferi* BMMS-BK 1-2, *C. suevicus* SMNS 9808, and *D. maximus* SMNS 8203). In GLAHM V1146 & PMU 35988, the length of the anterior protrusion of the acromion process (*i.e.* its extension anteriorly to the scapulocoracoid synchondrosis surface) is similar in length to the anteroposterior length of the glenoid facet. On the lateral surface of the scapula of specimens GLAHM V1146 & PMU 35988, along the dorsal margin of the acromion process, there is a subtle ridge corresponding to the acromial crest. As in other thalattosuchians, the acromial crest is strongly reduced and is mainly emphasized by the presence of the scapular fossa directly underneath it (*e.g. C. suevicus* SMNS 9808, *D. maximus* SMNS 8203, *Macrospondylus* SMNS 9428, *Neosteneosaurus* NHMUK PV R 3701, etc.). In GLAHM V1146 & PMU 35988, the scapular fossa is dorsoventrally longer than anteroposteriorly, presumably due to a short acromion process. The scapular fossa is limited to the anterior half of the scapula and ends where the glenoid process starts.

The scapulocoracoid synchondrosis surface is located on the ventral side of the scapula and extends in between the acromion and the glenoid processes. Similar to *G. leedsi* NHMUK PV R 3014 & NHMUK PV R 3015, the outline of the scapulocoracoid synchondrosis surface of GLAHM V1146, PMU 35988 & GLAHM V1143 possesses a subquadrangular posterior portion and a triangular anterior extremity. The shape of the latter is caused by the mediolateral thinning of the acromion process. In relation to the total dorsoventral extension of the bone, the scapulocoracoid synchondrosis surface of GLAHM V1146, PMU 35988 & GLAHM V1143 is proportionally short (just like the entire proximal region of the scapula) which contrasts with what is observed in *G. leedsi* NHMUK PV R 3014 & NHMUK PV R 3015. However, proportionally, the scapulocoracoid synchondrosis surface of GLAHM V1146, PMU 35988 & GLAHM V1143 corresponds to about half of the total anteroposterior length of the scapula proximally, which is larger than for the more derived metriorhynchids *D. maximus* SMNS 8203 and *To. carpenteri* BRSMG Cd7203.

Similarly to the acromion process, the glenoid process of the scapulae of GLAHM V1146, PMU 35988 & GLAHM V1143 does not appear to protrude from the shaft of the scapula and hence drastically stands out from that of *Pelagosaurus* BRLSI M.1418. In *G. leedsi* NHMUK PV R 3014 & NHMUK PV R 3015, the glenoid process is also modest and faintly protrudes from the shaft of the scapula, whereas the acromion process is strongly prominent. Yet, the dorsal margin of the glenoid process of the scapulae of GLAHM V1146, PMU 35988 & GLAHM V1143 does not exactly follow the curvature of the shaft of the scapula as its concavity is more pronounced, leading to a short but identifiable scapular buttress for the glenoid process. The articular facet of the glenoid is not aligned with the ventral surface of the scapulocoracoid synchondrosis surface, but is dorsally tilted as in other metriorhynchoids (*e.g. Pelagosaurus* BRLSI M.1418 & BRLSI M.3578, *C. albersdoerferi* BMMS-BK 1-2, *C. bambergensis* NKMB-P-Watt14/274, *C. suevicus* SMNS 9808, *Ge. lapparenti* UJF-ID.11847j & UJF-ID.11852f, *D.*

maximus SMNS 8203 or *To. carpenteri* BRSMG Cd7203, etc.). The angle between both surfaces is about 35° for GLAHM V1146, PMU 35988 & GLAHM V1143. The shape of the glenoid facet is elliptic with the longest axis oriented anteroposteriorly. As in other metriorhynchoids, the glenoid facet of the scapulae of GLAHM V1146, PMU 35988 & GLAHM V1143 is mainly oriented ventroposteriorly, but displays a small lateral component as well (see figs. 15 to 17). This type of orientation contrasts with most teleosaurids (*e.g. Mycterosuchus* NHMUK PV R 2617, *Macrospondylus* SMNS 9428, *Charitomenosuchus* NHMUK PV R 3806, *Lemmysuchus* NHMUK PV R 3168, etc.) which display a strongly laterally oriented facet.

7.2.2. *Coracoid.* The coracoid of *Thalattosuchus* (GLAHM V1005 and GLAHM V1146 see fig. 15; PMU 35988 and NHMUK PV R 1530 see fig. 16, and *Thalattosuchus* GLAHM V1143 see fig. 17; and see fig. 12) displays an atypical shape compared to most thalattosuchians: its coracoid head possesses an open coracoid foramen, which hence takes part in the outline of the bone. Within Thalattosuchia, the metriorhynchids *G. leedsi* NHMUK PV R 3014 (NHMUK PV R 3015 is too fragmentary),*'Me.' brachyrhynchus* NHMUK PV R 4696 and *Tyrannoneustes* GLAHM V1145 are the only other taxa known to possess an open coracoid foramen. Besides the open coracoid foramen, the coracoid of *Thalattosuchus* displays a relatively symmetrical silhouette with two similarly sized and shaped extremities: the coracoid head and coracoid blade.

The coracoid head of *Thalattosuchus* (all specimens, see figs. 18 to 20) possesses an open coracoid foramen which separates the coracoid head into two distinct processes. In *Thalattosuchus* (all specimens), the perforation forms a wide and deep indentation which extends slightly further than the mid-height of the coracoid head, similar to *Tyrannoneustes* GLAHM V1145 but differing from *G. leedsi* NHMUK PV R 3014 and *'Me.' brachyrhynchus* NHMUK PV R 4696 which possess a shallower indentation. The coracoid foramen of *Thalattosuchus* (all specimens) is almost aligned with the long axis of the shaft of the coracoid in most specimens (*i.e.* GLAHM V1005, PMU 35988, NHMUK PV R 1530) which is similar to *Tyrannoneustes* GLAHM V1145. In GLAHM V1146, the coracoid foramen is not exactly aligned with the long axis of the shaft of the coracoid but is slightly shifted anteriorly, as in *G. leedsi* NHMUK PV R 3014 and *'Me.' brachyrhynchus* NHMUK PV R 4696 but to a lesser extent. In *Thalattosuchus* (all specimens) and other metriorhynchids with an open coracoid foramen (*e.g. G. leedsi* NHMUK PV R 3014, *'Me.' brachyrhynchus* NHMUK PV R 4696, and *Tyrannoneustes* GLAHM V1145), the coracoid foramen bears an elliptic outline with markedly concave margins anteriorly and posteriorly corresponding to the sides of the anterior expansion and the posterior portion (including glenoid process) respectively. In *Thalattosuchus* GLAHM V1146, the anterior expansion and the posterior portion of the coracoid head both differ in size but still display a superficially similar axe-head outline, as in *Tyrannoneustes* GLAHM V1145. Indeed, the anterior expansion of the coracoid of *Thalattosuchus* (all specimens) is proportionally more elongated than the posterior portion (including the glenoid process), which has a broader appearance. As a result, the coracoid head is more expanded anteriorly than posteriorly, like the coracoid blade. In addition, the anterior expansion of the coracoid head is dorsoventrally thin like a blade as in other thalattosuchians, dyrosaurids, and extant crocodylians. However, in *Thalattosuchus* GLAHM V1146, the anterior expansion of the coracoid head constitutes the thinnest portion of the bone, similarly to other thalattosuchians (but unlike dyrosaurids and extant crocodylians in which the coracoid blade is the thinnest portion). The axe-head shape of the outline of the anterior expansion of the coracoid head is given by its relative lateral flaring and the shape of its lateral margin which is symmetrically convex (*i.e.* its apex is centered). The anterior margin of the anterior expansion of the coracoid head is relatively straight to slightly convex whereas its posterior margin (bordering the perforation) is markedly concave. The junction between the convex lateral margin and the anterior and posterior ones is achieved through protruding corners, which emphasizes the axe-head appearance of the process.

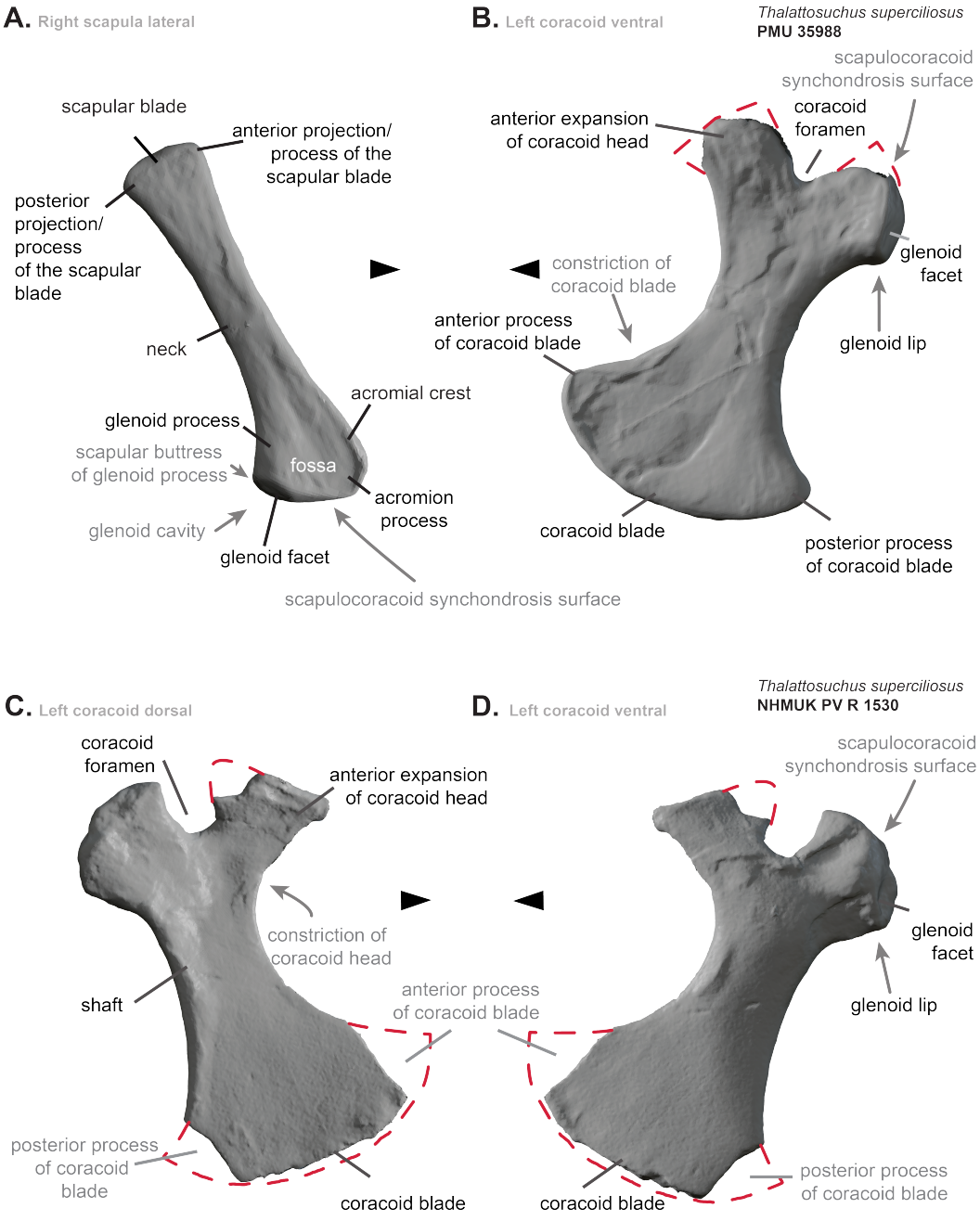


FIGURE 16. Pectoral girdle of *Thalattosuchus superciliosus* PMU 35988 (A&B) and *Thalattosuchus superciliosus* NHMUK PV R 1530 (C&D) (3D models). **A.** Right scapula in lateral view ; **B.** Left coracoid in ventral view ; **C.** Left coracoid in dorsal view ; **D.** Left coracoid in ventral view. Arrow points anteriorly. Red dashed lines indicate missing parts. Reconstruction of missing parts based on *Thalattosuchus superciliosus* GLAHM V1146 & GLAHM V1005.

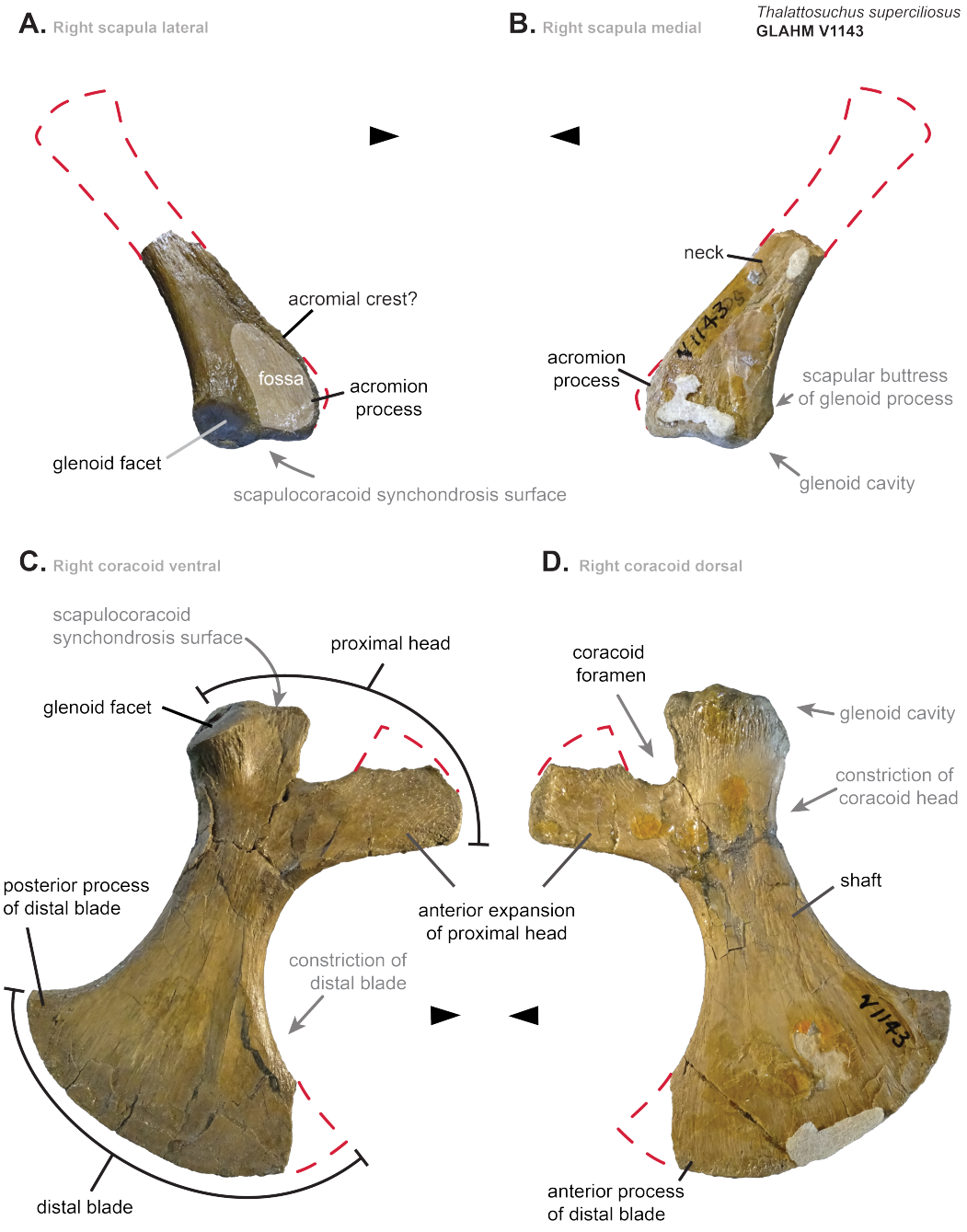


FIGURE 17. Pectoral girdle of *Thalattosuchus superciliosus* GLAHM V1143 (photographs). **A.** Right scapula in lateral view ; **B.** Right scapula in medial view ; **C.** Right coracoid in ventral view ; **D.** Right coracoid in dorsal view. Arrow points anteriorly. Red dashed lines indicate missing parts. Reconstruction of missing parts based on *Thalattosuchus superciliosus* GLAHM V1146.

The posterior portion of the coracoid head forms a relatively thick process which includes both the scapulocoracoid synchrondrosis surface and the glenoid process. The anteroposterior length of the extremity of the posterior portion is slightly larger than that of the anterior expansion (accounts for about 116% in GLAHM V1146), whereas its mediolateral extension is lesser (about one–third in GLAHM V1146 & GLAHM V1005). As a result, the lateral flaring of the posterior portion of the coracoid head is more intense than that of the anterior expansion. The shape of the posterior portion of the coracoid head in dorsal and ventral views appears similar to the anterior expansion but still slightly differs: both the anterior margin (bordering the coracoid foramen) and posterior margin are markedly convex, which emphasizes the salient appearance of the two corners binding the lateral margin. The latter is mainly formed by the scapulocoracoid synchondrosis surface as it accounts for about 78– 82 % (in GLAHM V1005 & GLAHM V1146 respectively) of the total anteroposterior length of the extremity of this portion. The remainder of the outline is formed by the glenoid facet, which slightly protrudes posteriorly in relation to the scapulocoracoid synchondrosis surface. The scapulocoracoid synchondrosis surface is greatly elongated anteroposteriorly (about three and a half times the dorsoventral width at mid-length), and has an overall triangular outline in GLAHM V1143, GLAHM V1146 and NHMUK PV R 1530 similar to *Tyrannoneustes* GLAHM V1145 and *G. leedsi* NHMUK PV R 3014. In GLAHM V1005, the scapulocoracoid synchondrosis surface possesses a more elliptic outline with rounded anterior and posterior extremities, which contrasts with the elliptical shape with sharp corners of the scapulocoracoid synchondrosis surface of the coracoid of *'Me.' brachyrhynchus* NHMUK PV R 4696. Proportionally, the overall extension of the scapulocoracoid synchondrosis surface of the coracoid of *Thalattosuchus* (observable on GLAHM V1146) is limited as it only accounts for less than half of the total anteroposterior length of the coracoid head. Similar to other metriorhynchids, this relative shortening of the scapulocoracoid synchondrosis surface mirrors the reduction of the scapula, which has a slender and rod-like appearance in *Thalattosuchus* (all specimens). In more derived metriorhynchids, the scapula becomes shorter and broader but the scapulocoracoid synchondrosis surface remains limited (*e.g. C. albersdoerferi* BMMS-BK 1-2, *C. suevicus* SMNS 9808, *Ge. lapparenti* UJF-ID.11847j & UJF-ID.11852f, *D. maximus* SMNS 8203, *To. carpenteri* BRSMG Cd7203, etc.). Several teleosauroids taxa also possess a slenderized scapula and subsequently shortened scapulocoracoid synchondrosis surface: *Ind. potamosiamensis* PRC-24, *Te. cadomensis* NHMUK PV OR 31836, *Charitomenosuchus* NHMUK PV R 3806, *Neosteneosaurus* NHMUK PV R 3701, *Lemmysuchus* NHMUK PV R 3169. In GLAHM V1146 and NHMUK PV R 1530, the scapulocoracoid synchondrosis surface is markedly scarred and displays a laterally protruding ridges along its main axis (*i.e.* anteroposterior). This ridge further divides the surface into a dorsal and ventral sub-area, which display strongly differing orientations as in *'Me.' brachyrhynchus* NHMUK PV R 4696 and *G. leedsi* NHMUK PV R 3014. In GLAHM V1005, the anteroposterior ridge of the scapulocoracoid synchondrosis surface is less prominent and the difference in the orientation of the dorsal and ventral sub-areas is less marked, which is similar to what is observed in *Tyrannoneustes* GLAHM V1145.

As in *'Me.' brachyrhynchus* NHMUK PV R 4696, the glenoid facet of the coracoid of *Thalattosuchus* is ovoid in shape and this appearance is clearly emphasized by the dorsoventral compaction of the bone (see GLAHM V1146 fig. 15, PMU 35988 & NHMUK PV R 1530 see fig. 16). This contrasts with the sub-circular one of the basal thalattosuchian *Turnersuchus* LRM 2021/45 and presumably other metriorhynchoids (*e.g. Pelagosaurus* BRLSI M.1418 & BRLSI M.3578, *Magyarosuchus* (Ősi et al., 2018), *G. leedsi* NHMUK PV R 3014 & NHMUK PV R 3015, *C. albersdoerferi* BMMS-BK 1-2, *Dakosaurus sp.* Rygol specimen, *Tyrannoneustes* GLAHM V1145, etc.). In GLAHM V1005, the glenoid facet displays a relatively more rounded outline due to a less dorsoventrally compressed state, and hence superficially resembles the glenoid facet of the coracoid of *Tyrannoneustes* GLAHM V1145. However, the total anteroposterior extension of the glenoid facet of the coracoid of GLAHM V1005 markedly exceeds its dorsoventral height which confers it an ovoid shape similar to other *Thalattosuchus* specimens. Hence, due to the shape of the glenoid facet, the maximum dorsoventral width of the coracoid of *Thalattosuchus*

(all specimens) coincides with the minor axis of the glenoid facet rather than the diameter (similar to most teleosauroids except *Charitomenosuchus* NHMUK PV R 3806 in which the glenoid facet is sub-circular). The glenoid facet of the coracoid of *Thalattosuchus* (all specimens) further differs from *Turnersuchus* LRM 2021/45, *Pelagosaurus* BRLSI M.1418 & BRLSI M.3578, and *Magyarosuchus* (Ősi et al., 2018) in being proportionally larger and positioned slightly more ventrally. Indeed, the glenoid process of the coracoid of *Thalattosuchus* (all specimens) forms a marked bulge on the ventral side of the coracoid and along the posterior border of the bone. The base of the glenoid process of the coracoid of *Thalattosuchus* (all specimens) is found along the line joining the base of the coracoid foramen and the base of the coracoid shaft along the posterior margin of the bone. From there, the glenoid process gradually increases in thickness as it flares out to form the glenoid facet laterally. The entire surface of the glenoid process (underlying the glenoid facet) is concave which gives the process a trumpet-shaped appearance. The glenoid process covers around two–thirds of the entire ventral surface of the posterior portion of the coracoid head; the remainder third of the surface displays the overall same dorsoventral thickness as the overlying scapulocoracoid synchondrosis surface. Due to the differences in shape and thickness of the two parts, their junction forms a hollowed area which is more or less marked: it is relatively subtle in GLAHM V1146 and PMU 35988, but it is more prominent in NHMUK PV R 1530 and GLAHM V1005 (in which it is even emphasized by a notch). The glenoid facet of the coracoid of *Thalattosuchus* (all specimens) is positioned posteroventrally as in other metriorhynchids, but which contrasts with more posterior facet of the coracoid of *Turnersuchus* LRM 2021/45, *Pelagosaurus* BRLSI M.1418 & BRLSI M.3578, and *Magyarosuchus* (Ősi et al., 2018). The anterior third of the surface of the glenoid facet of the coracoid of *Thalattosuchus* (all specimens) is slightly convex to flat, whereas the remainder posterior portion is noticeably concave similar to other metriorhynchids differing from the relatively flat surface of the glenoid facet of the coracoid of *Turnersuchus* LRM 2021/45, *Pelagosaurus* BRLSI M.1418 & BRLSI M.3578, and *Magyarosuchus* (Ősi et al., 2018). The concave area of the glenoid facet of the coracoid of *Thalattosuchus* (all specimens) comes close to the posterior margin, which hence does not form a bend nor displays a recurved margin as in dyrosaurids and extant crocodylians (and some teleosauroids like *Platysuchus* SMNS 9930 and possibly *Macrospondylus* SMNS 9428). Indeed, the glenoid margin of the coracoid of *Thalattosuchus* (all specimens) is thin and only forms a subtle bulge surrounding its ventral and posterior sides, as in *Turnersuchus* LRM 2021/45 and other metriorhynchoids. Anterodorsally, the junction between the glenoid facet and the scapulocoracoid synchondrosis surface is subtle as it only forms a smoothly domed surface as in other metriorhynchoids. In comparison, this junction forms a slight ridge in teleosauroids and a blunt corner in dyrosaurids.

The coracoid of *Thalattosuchus* (all specimens) appears slightly curved ventrally as in other thalattosuchians, dyrosaurids, and extant crocodylians. The anterior and posterior margins of the coracoid of *Thalattosuchus* (all specimens) are markedly concave which is responsible for the intense flaring of the lateral and medial extremities of the bone. The degree of concavity of the anterior margin of the coracoid of *Thalattosuchus* (all specimens) is larger than that of the posterior margin and the apex of each parabolic margin is relatively centered, similar to other metriorhynchids. As a consequence the shaft of the coracoid of *Thalattosuchus* (all specimens) is relatively slender like other metriorhynchids with an open coracoid foramen, which contrasts with the rod-like shaft of the more basal metriorhynchoids (*e.g. Turnersuchus* LRM 2021/45, *Magyarosuchus* (Ősi et al., 2018) and *Pelagosaurus* BRLSI M.1418 & BRLSI M.3578) and also differs from the proportionably short and thick shaft of the coracoid of metriorhynchids with a closed coracoid foramen (*e.g. C. albersdoerferi* BMMS-BK 1-2, *C. bambergensis* NKMB-P-Watt14/274, *C. suevicus* SMNS 9808, *C. lithographicus* MOZ-PV 5787, *C. araucanensis* MLP 72-IV-7-1, *D. maximus* SMNS 8203, etc.). Indeed, the anteroposterior width of the shaft of the coracoid at the constriction of *Thalattosuchus* (GLAHM V1146, NHMUK PV R 1530, GLAHM V1005, PMU 35988) is slightly inferior (about 88%) to the mediolateral extension of the shaft of the coracoid.

In comparison, the dorsoventral thickness of the shaft of the coracoid is narrower as it is about four-and-half times lesser than the mediolateral extension of the shaft. The shaft of the coracoid corresponds to the area of the bone connecting the coracoid head and coracoid blade whose anteroposterior width remains relatively constant (*i.e.* does not expands for more than 15% of the minimal anteroposterior width of the shaft). In teleosauroids, the shaft of the coracoid presents a slightly longer and more slender shape than in metriorhynchoids (*e.g.* *Mycterosuchus* NHMUK PV R 2617, *Aeolodon* NHMUK PV R 1086, *Platysuchus* SMNS 9930, *Macrospondylus* SMNS 9428, *Neosteneosaurus* NHMUK PV R 3701, *Machimosaurus* spp. see C on fig. 61).

Medially, the shaft of the coracoid of *Thalattosuchus* markedly flares out to form the coracoid blade. The latter presents an asymmetry in its shape anteriorly and posteriorly due to the differences in the degree of concavity of the anterior and posterior margins of the bone in GLAHM V1146, NHMUK PV R 1530 and GLAHM V1005. In PMU 35988, the anterior and posterior margins of the coracoid display more similar shapes. However, the coracoid blade is relatively symmetrical to the coracoid head as both display a short anterior expansion and a longer one posteriorly. This is also observed in other metriorhynchoids and teleosauroids. Hence, the coracoid blade of *Thalattosuchus* is anteroposteriorly large, but is also relatively broad mediolaterally with a height reaching about half of the total anteroposterior length of the blade. The shape of the medial extremity of the blade, where it must have connected to the sternum through cartilaginous structures, is noticeably convex with its apex centered. In comparison, other thalattosuchians and extant crocodylians also bear a broad axe-head shaped coracoid blade, whereas dyrosaurids display a shorter and narrower blade.

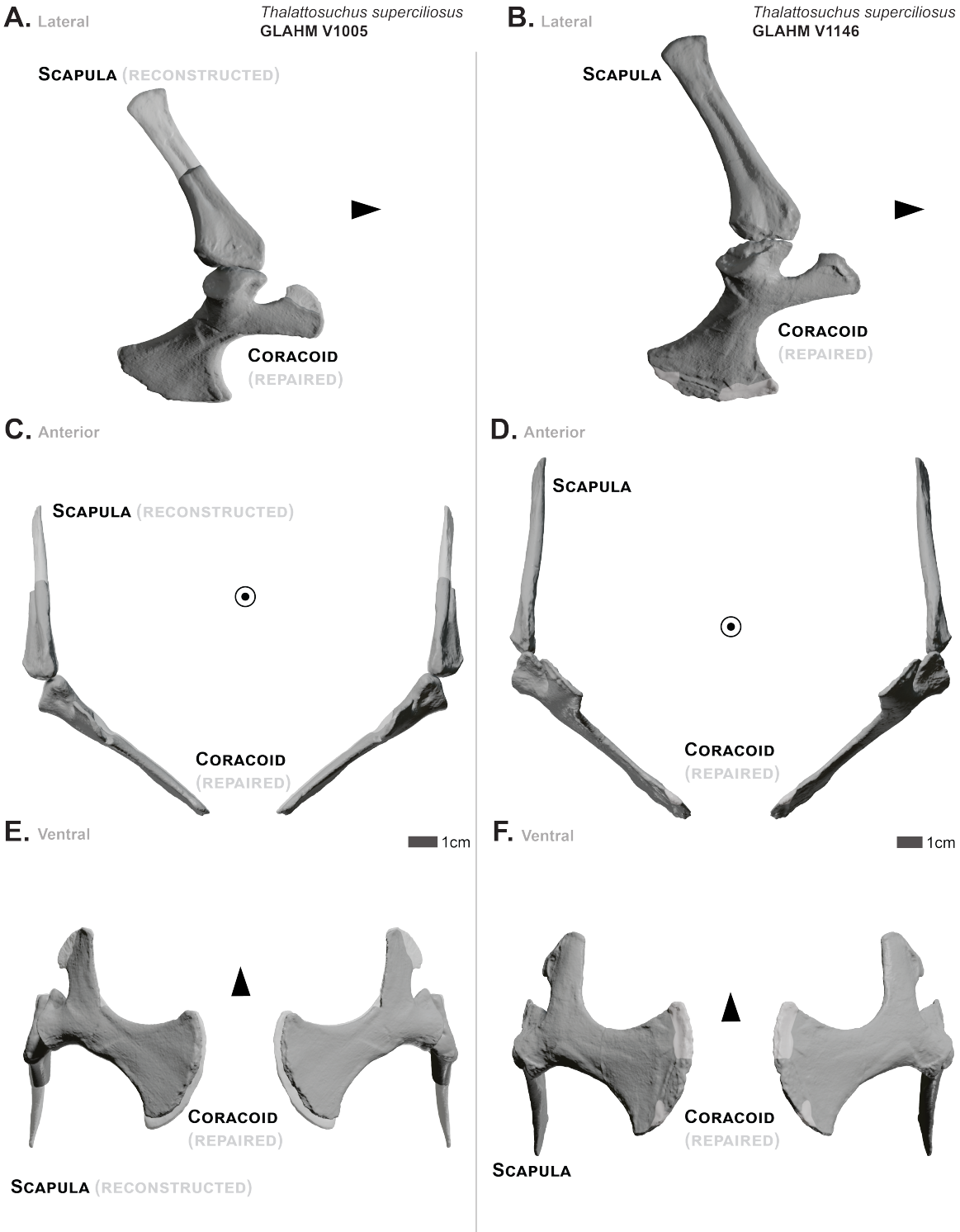


FIGURE 18. Reconstruction of the pectoral girdle of *Thalattosuchus superciliosus* GLAHM V1005 (A, C & E; reconstruction of missing parts based on GLAHM V1146) and *Thalattosuchus superciliosus* GLAHM V1146 (B, D, & F; reconstruction of missing parts based on GLAHM V1005) (3D models). **A.** Right lateral view GLAHM V1005; **B.** Right lateral view GLAHM V1146; **C.** Anterior view GLAHM V1005; **D.** Anterior view GLAHM V1146; **E.** Ventral view GLAHM V1005; **F.** Ventral view GLAHM V1146. Target indicates anterior. Arrow points anteriorly. The left scapula and coracoid of GLAHM V1005 are mirrored. The right scapula and coracoid of GLAHM V1146 are mirrored.

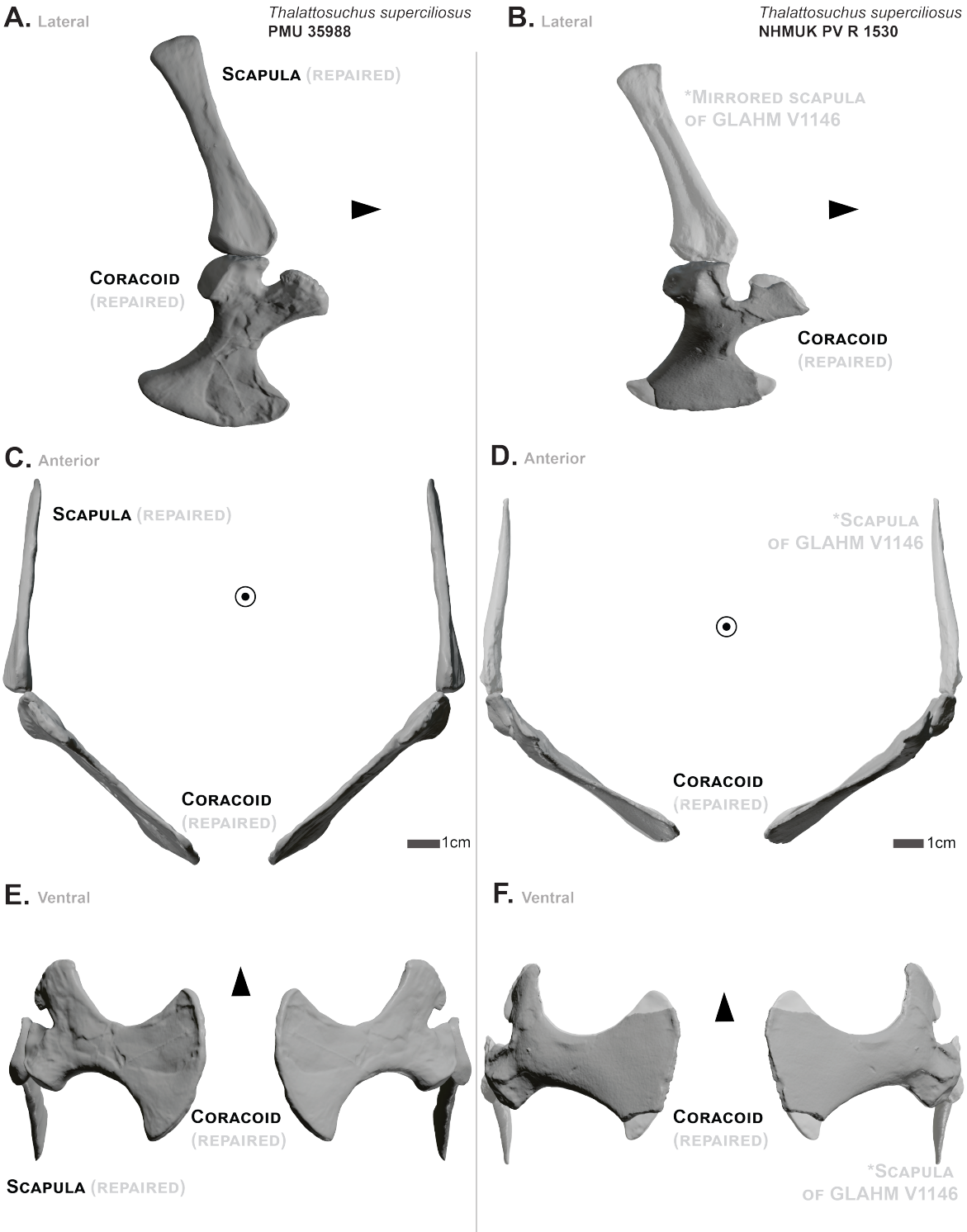


FIGURE 19. Reconstruction of the pectoral girdle of *Thalattosuchus superciliosus* PMU 35988 (A, C & E) and *Thalattosuchus superciliosus* NHMUK PV R 1530 (B, D, & F) (3D models). **A.** Right lateral view PMU 35988; **B.** Right lateral view NHMUK PV R 1530; **C.** Anterior view PMU 35988; **D.** Anterior view NHMUK PV R 1530; **E.** Ventral view PMU 35988; **F.** Ventral view NHMUK PV R 1530. Target indicates anterior. Arrow points anteriorly. The left scapula and right coracoid of PMU 35988 are mirrored. The right coracoid of NHMUK PV R 1530 is mirrored, and the scapula of *Thalattosuchus superciliosus* GLAHM V1146 is used in the reconstruction.

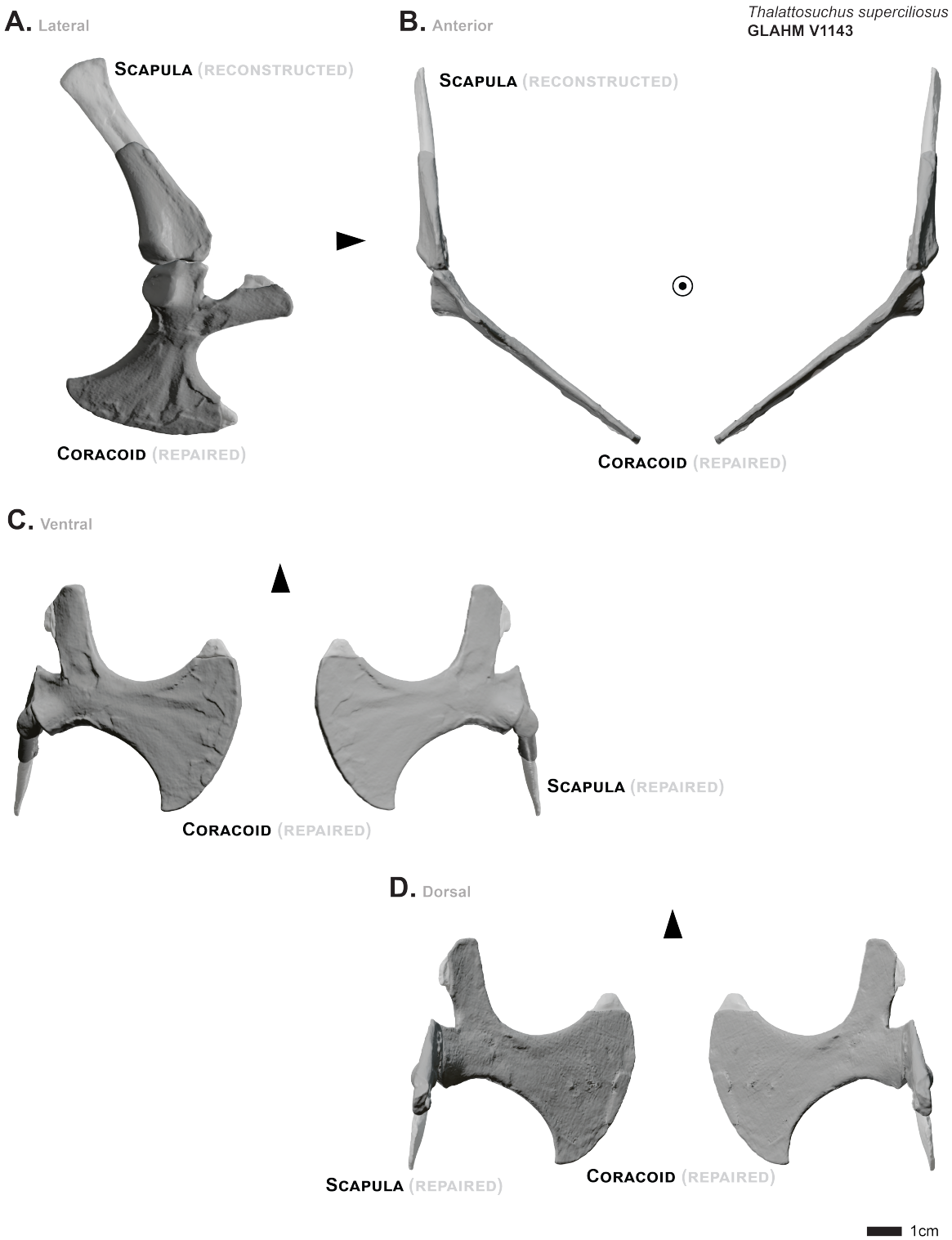


FIGURE 20. Reconstruction of the pectoral girdle of *Thalattosuchus superciliosus* GLAHM V1143 (3D models). **A.** Lateral view; **B.** Anterior view; **C.** Ventral view; **D.** Dorsal view. Arrow points anteriorly. Target indicates anterior. The left scapula and coracoid are mirrored. Reconstruction of missing parts based on *Thalattosuchus superciliosus* GLAHM V1146 & *Thalattosuchus superciliosus* GLAHM V1005.

7.3. ***Gracilineustes leedsi* Andrews, 1913.** For measurements, see tables 6 and 7. The specimens are likely juveniles based on their small size.

7.3.1. *Scapula.* The scapula of *Gracilineustes leedsi* NHMUK PV R 3014 & NHMUK PV R 3015 Andrews, 1913 (see figs. 11 and 21 to 23) possesses the typical rod-like silhouette of basal metriorhynchids induced by a long and thin shaft and relatively reduced scapular blade (*e.g. Thalattosuchus* GLAHM V1146 & PMU 35988). Yet, the scapula of *G. leedsi* NHMUK PV R 3014 & NHMUK PV R 3015 differs from that of other metriorhynchoids in displaying the combination of a markedly slender outline for a proportionally wide proximal region, a reduced glenoid facet and a marked distal twisting.

The anterior and posterior margins of the scapula of *G. leedsi* NHMUK PV R 3014 & NHMUK PV R 3015 presents an overall similar curvature throughout their length: the anterior margin is smoothly concave whereas the posterior margin is slightly convex. As a result, the anteroposterior thickness of the scapula remains relatively constant throughout most of its length which is similar to what is observed in *Thalattosuchus* GLAHM V1146 & PMU 35988 but contrasts with the short and broad shaped displayed by more derived metriorhynchids (*e.g. Cricosaurus* species, *D. maximus* SMNS 8203, *To. carpenteri* BRSMG Cd7203, etc.). Hence, *G. leedsi* NHMUK PV R 3014 & NHMUK PV R 3015 displays a strongly elongated shaft as it reaches around 59% of the total height of the scapula, as in *Thalattosuchus* (GLAHM V1146 59%; PMU 35988 61%) among metriorhynchids. However, the scapula of *G. leedsi* NHMUK PV R 3014 & NHMUK PV R 3015 departs from that of *Thalattosuchus* GLAHM V1146 & PMU 35988 in possessing a proportionally less expanded scapular blade as well as a more prominent acromion process. Indeed, the scapular blade of *G. leedsi* NHMUK PV R 3014 & NHMUK PV R 3015 does not markedly flare out distally (*i.e.* its anteroposterior width is close to that of the shaft of the scapula). As such, the anterior and posterior extremities of the distal blade of *G. leedsi* NHMUK PV R 3014 & NHMUK PV R 3015 form relatively smooth and blunt corners, with the anterior one being more rounded than the posterior one. This contrasts with the sharp and prominent ones of *Thalattosuchus* GLAHM V1146 & PMU 35988. Distally, the scapular blade of *G. leedsi* NHMUK PV R 3014 & NHMUK PV R 3015 displays a smoothly convex margin which is a trait also found in most metriorhynchids (except *D. maximus* SMNS 8203 and *Dakosaurus sp.* DMA-JP-2009/001). The surface of the scapular blade does not present any rugosity or ridges which could be attributed to an early ontogenetic stage like in extant crocodylians (Brochu, 1992). Unlike most metriorhynchoids, the scapular blade of *G. leedsi* NHMUK PV R 3014 (also clearly visible in the more flattened specimen NHMUK PV R 3015) displays a strong mediolateral twist which places the anterior corner more medially. This bending of the scapular blade of *G. leedsi* NHMUK PV R 3014 starts on the shaft of the scapula at around three–quarters of the height of the scapula. This strongly bend shape presumably hints at a slightly different position or inclination of the pectoral girdle for *G. leedsi* NHMUK PV R 3014 & NHMUK PV R 3015, seemingly more anterior, as it appears to mimic or hug the shape of the anterior constriction of the thoracic region towards the neck.

Unlike other metriorhynchids, the proximal region of the scapula of *G. leedsi* NHMUK PV R 3014 & NHMUK PV R 3015 shows a marked anteroposterior extension (especially in relation to its overall slenderness) but a relatively small glenoid facet. Indeed, the scapula of *G. leedsi* NHMUK PV R 3014 & NHMUK PV R 3015 bears a sharp and strongly prominent acromion process which accounts for about 18% of the total anteroposterior length of the proximal region of the scapula (this value reaches about 15% in *Thalattosuchus* GLAHM V1146 & PMU 35988). The dorsal and ventral margins of the acromion process of the scapula of *G. leedsi* NHMUK PV R 3015 & NHMUK PV R 3014 form relatively straight to slightly convex surfaces which anteriorly culminate to form a right-angle corner (broken in NHMUK PV R 3014). Similar to other metriorhynchids, the apex of the acromion process of the scapula of *G. leedsi* NHMUK PV R 3014 & NHMUK PV R 3015 is located around the mid height of the process, rather than being on the same level as the scapulocoracoid synchondrosis surface (as in teleosauroids).

The lateral surface of the scapula of *G. leedsi* NHMUK PV R 3014 & NHMUK PV R 3015 extending from the glenoid process to the acromion process displays a smoothly concave morphology throughout, as in *Thalattosuchus* GLAHM V1146, PMU 35988 & GLAHM V1143. However, the dorsal margin of the acromion process of the scapula of *G. leedsi* NHMUK PV R 3014 & NHMUK PV R 3015 is slightly more laterally prominent than the rest of the lateral surface, which then appears as a shallow or reduced crest as in *Thalattosuchus* GLAHM V1146, PMU 35988 & GLAHM V1143.

The scapulocoracoid synchondrosis surface of the scapula of *G. leedsi* NHMUK PV R 3014 & NHMUK PV R 3015 possesses an elliptic outline and constitutes most of the anteroposterior length of the proximal region (about 73–75%). It displays a slender silhouette with an oblong posterior extremity and triangular anterior one due to mediolateral thinning of acromion process. The relatively smooth aspect of the scapulocoracoid synchondrosis surface of the scapula could be attributed to an early ontogenetic stage like in extant crocodylians (Brochu, 1992). Unlike *Thalattosuchus* GLAHM V1146, PMU 35988 & GLAHM V1143, the scapulocoracoid synchondrosis surface of the scapula of *G. leedsi* NHMUK PV R 3014 & NHMUK PV R 3015 is mediolaterally thin, and bears an overall constant thickness throughout its length. The relative extension of the scapulocoracoid synchondrosis surface of the scapula of *G. leedsi* NHMUK PV R 3014 & NHMUK PV R 3015 is notably due to the size and strictly lateral position of the glenoid facet. Indeed, the latter displays an ovoid shape which is strongly reduced in size, especially compared to other metriorhynchids. As a result, the scapulocoracoid synchondrosis surface of the scapula of *G. leedsi* NHMUK PV R 3014 & NHMUK PV R 3015 extends medially to the glenoid facet. The overall small size of the glenoid facet of the scapula of *G. leedsi* NHMUK PV R 3014 & NHMUK PV R 3015 is also mirrored on the coracoid, although the latter displays a proportionally larger facet. The relatively planar articular surface of the glenoid facet could be attributed to an early ontogenetic stage like in extant crocodylians (Brochu, 1992).

7.3.2. *Coracoid.* The coracoid of *G. leedsi* NHMUK PV R 3014 Andrews, 1913 (see figs. 12 and 21) displays an open coracoid foramen, a slender shaft (also observable on NHMUK PV R 3015 see fig. 22), and a symmetrical coracoid blade similar to several metriorhynchids: *Tyrannoneustes* GLAHM V1145,*'Me.' brachyrhynchus* NHMUK PV R 4696 and *Thalattosuchus* (GLAHM V1005, GLAHM V1146, PMU 35988, NHMUK PV R 1530). However, the coracoid head of *G. leedsi* NHMUK PV R 3014 differs from the latter in possessing a series of distinct features: a proportionally small coracoid foramen, a greater constriction of the base of the anterior expansion and a short and broad posterior portion. The fragmentary state of the coracoid head of *G. leedsi* NHMUK PV R 3014 & NHMUK PV R 3015 prevents the assessment of mediolateral symmetry between the coracoid head and blade.

The coracoid of *G. leedsi* NHMUK PV R 3014 & NHMUK PV R 3015 (see figs. 21 to 23) possesses an open coracoid foramen as in *Tyrannoneustes* GLAHM V1145,*'Me.' brachyrhynchus* NHMUK PV R 4696 and *Thalattosuchus* (GLAHM V1005, GLAHM V1146, PMU 35988, NHMUK PV R 1530) but differing from *Cricosaurus* species (*e.g. C. albersdoerferi* BMMS-BK 1-2, *C. bambergensis* NKMB-P-Watt14/274, *C. suevicus* SMNS 9808, *C. araucanensis* MLP 72-IV-7-1) and *D. maximus* SMNS 8203 (as well as *Dakosaurus sp.* DMA-JP-2009/001 and Rygol specimen). However, the indentation of the coracoid head of *G. leedsi* NHMUK PV R 3014 and NHMUK PV R 3015, which corresponds to the coracoid foramen, is markedly shorter than in other metriorhynchids with an open coracoid foramen (*e.g. Tyrannoneustes* GLAHM V1145,*'Me.' brachyrhynchus* NHMUK PV R 4696 and *Thalattosuchus* GLAHM V1005, GLAHM V1146, PMU 35988 & NHMUK PV R 1530). Indeed, the maximum depth (mediolaterally) of the open coracoid foramen of *G. leedsi* NHMUK PV R 3014 accounts for about 8.7% of the total mediolateral height of the bone, whereas this number reaches about 16% in *Thalattosuchus* (GLAHM V1146 and NHMUK PV R 1530) and *'Me.' brachyrhynchus* NHMUK PV R 4696, and about 12.5% in *Tyrannoneustes* GLAHM V1145. In addition, the coracoid foramen of *G. leedsi* NHMUK PV R 3014 markedly departs from *Tyrannoneustes* GLAHM V1145,*'Me.' brachyrhynchus* NHMUK PV R

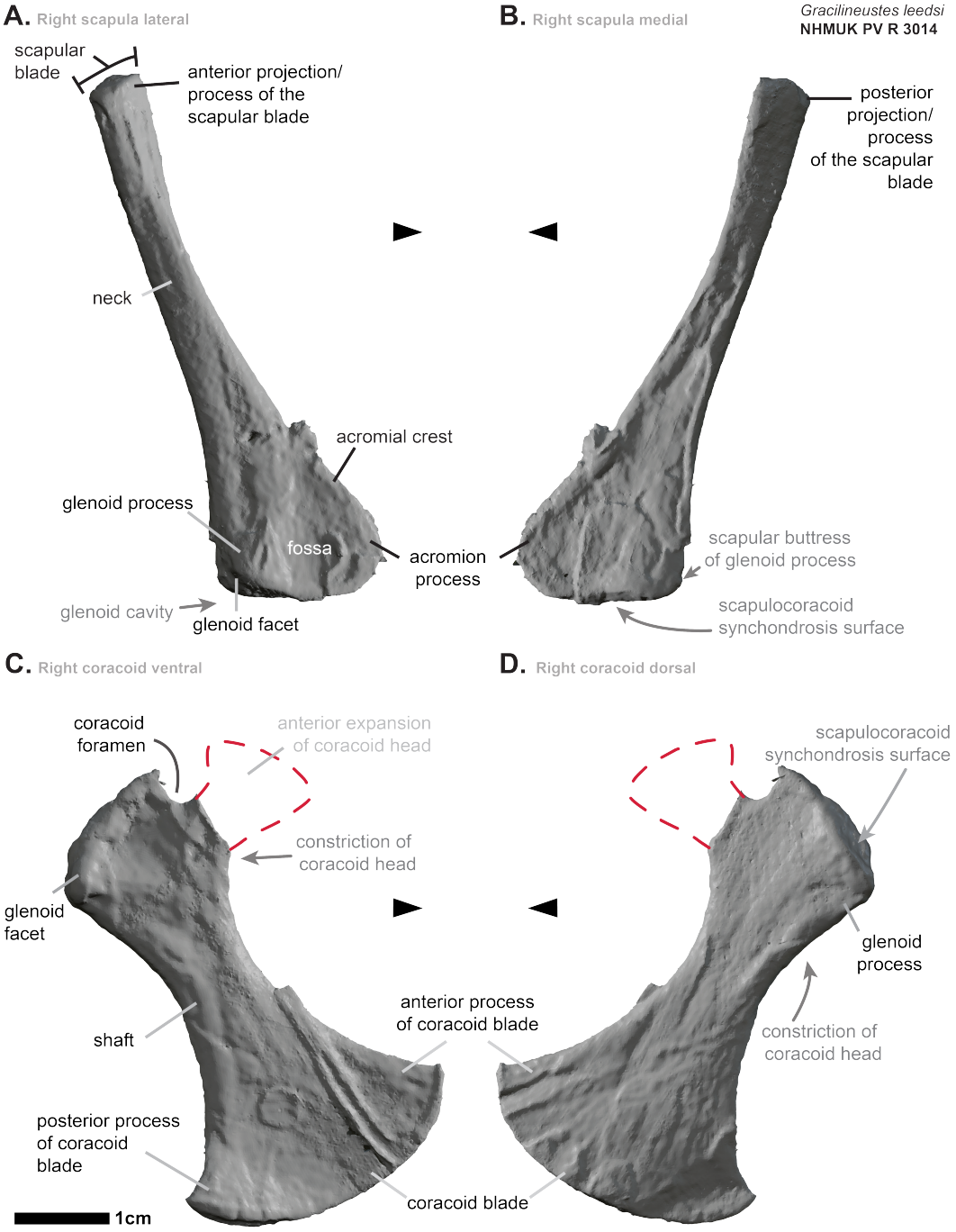


FIGURE 21. Pectoral girdle of *Gracilineustes leedsi* Andrews, 1913 NHMUK PV R 3014 (3D models). **A.** Right scapula in lateral view ; **B.** Right scapula in medial view ; **C.** Right coracoid in dorsal view ; **D.** Right coracoid in ventral view. Arrow points anteriorly. Scans courtesy of (c) The Trustees of the Natural History Museum, London. Red dashed lines indicate missing parts. Reconstruction of missing parts based on *Thalattosuchus superciliosus* GLAHM V1146.

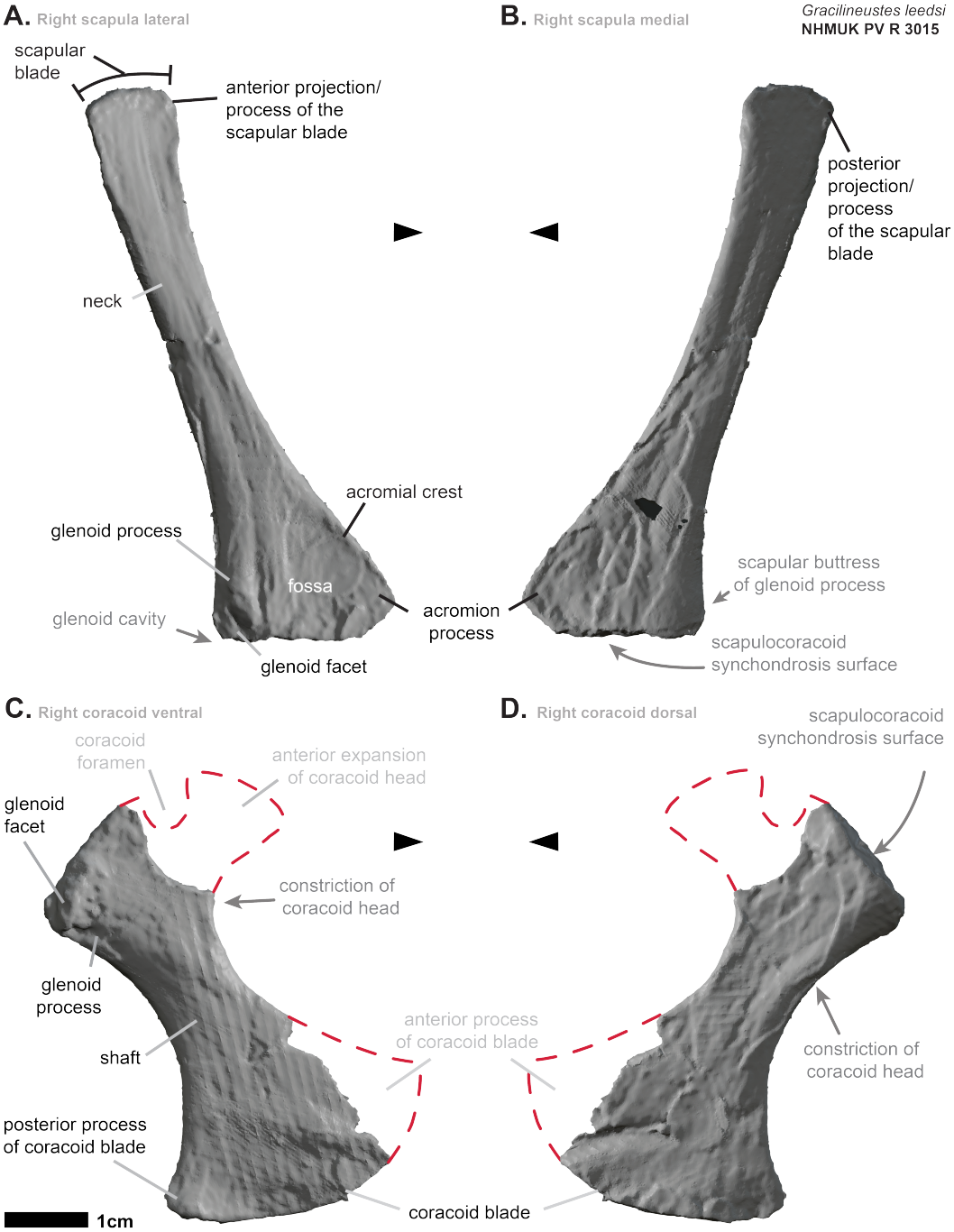


FIGURE 22. Pectoral girdle of *Gracilineustes leedsi* Andrews, 1913 NHMUK PV R 3015 (3D models). **A.** Right scapula in lateral view ; **B.** Right scapula in medial view ; **C.** Right coracoid in ventral view ; **D.** Right coracoid in dorsal view. Arrow points anteriorly. Scans courtesy of (c) The Trustees of the Natural History Museum, London. Red dashed lines indicate missing parts. Reconstruction of missing parts based on *Thalattosuchus superciliosus* GLAHM V1146 & *Gracilineustes leedsi* NHMUK PV R 3014.

4696 and *Thalattosuchus* (GLAHM V1005, GLAHM V1146, PMU 35988, NHMUK PV R 1530) is being strongly anteriorly shifted and hence not aligned with the long axis of the shaft of the coracoid.

The coracoid head of *G. leedsi* NHMUK PV R 3014 further differs from the other metriorhynchids with an open coracoid foramen in displaying a strong constriction at the base of the anterior expansion as well as a squat posterior portion. Indeed, the anteroposterior length of the posterior process at its base (taken from the coracoid foramen) is about three times larger than its mediolateral height (from its base to the tip). The exact shape of the anterior expansion of the coracoid of *G. leedsi* NHMUK PV R 3014 is unknown, but the marked constriction at its base hints at a either a relatively slender process or an intense lateral flaring.

In both *G. leedsi* NHMUK PV R 3014 and NHMUK PV R 3015, the scapulocoracoid synchondrosis surface of the coracoid forms a rough area which spreads over almost the entire anteroposterior length (about 98%) of the posterior portion of the coracoid head. In comparison, the scapulocoracoid synchondrosis surface constitutes about 95% of the entire posterior process of the coracoid head in *'Me.' brachyrhynchus* NHMUK PV R 4696 (although the value could be greater due to a missing fragment of the scapulocoracoid synchondrosis surface) and 91% in *Tyrannoneustes* GLAHM V1145, whereas this number reaches 78% and 82 % in *Thalattosuchus* GLAHM V1005 and GLAHM V1146 respectively. The scapulocoracoid synchondrosis surface of the coracoid of *G. leedsi* NHMUK PV R 3014 & NHMUK PV R 3015 has the outline of a scalene triangle with the hypotenuse located on the dorsal side as in *Tyrannoneustes* GLAHM V1145 and *Thalattosuchus* GLAHM V1146 & NHMUK PV R 1530, but unlike the almond-shaped surface of *'Me.' brachyrhynchus* NHMUK PV R 4696. Hence, the scapulocoracoid synchondrosis surface of *G. leedsi* increases in dorsoventral thickness posteriorly until it reaches a peak (*i.e.* the ventral apex of the scalene triangle), then gradually slims down afterwards. The peak in thickness of the scapulocoracoid synchondrosis surface is located at a little less than two–thirds (about 60%) of the length posteriorly, and also coincides with the anterior corner of the glenoid facet. The dorsoventral thickness of the coracoid head does not decline with that of the scapulocoracoid synchondrosis surface: it keeps increasing with the glenoid facet and reaches its max width at around 82% of the anteroposterior length. This phenomenon is due to both the posteroventral position of the glenoid facet as a whole as well as the extension of the scapulocoracoid synchondrosis surface dorsal to the glenoid facet, as in other metriorhynchids with an open coracoid foramen (*e.g. Tyrannoneustes* GLAHM V1145, *'Me.' brachyrhynchus* NHMUK PV R 4696 and *Thalattosuchus* GLAHM V1005, GLAHM V1146, PMU 35988 & NHMUK PV R 1530). In comparison, the glenoid facet of the coracoid of *D. maximus* SMNS 8203 and *Dakosaurus sp.* DMA-JP-2009/001 is positioned posteriorly and the scapulocoracoid synchondrosis surface does not appear to extend dorsally to it (it is possible that *Cricosaurus* species possess a similar architecture). In *G. leedsi* NHMUK PV R 3014 & NHMUK PV R 3015, the glenoid facet displays a semi-circular outline except on the side corresponding to its junction with the scapulocoracoid synchondrosis surface similar to *Turnersuchus* LRM 2021/45 and most metriorhynchoids (*e.g. Pelagosaurus* BRLSI M.1418, *Magyarosuchus* (Ősi et al., 2018), *C. albersdoerferi* BMMS-BK 1-2, *C. suevicus* SMNS 9808, *C. araucanensis* MLP 72-IV-7-1, *Dakosaurus sp.* Rygol specimen, *Tyrannoneustes* GLAHM V1145, etc.). As in other metriorhynchids, the posterior portion of the glenoid facet of the coracoid of *G. leedsi* NHMUK PV R 3014 & NHMUK PV R 3015 shows a slightly concave area whereas the surroundings and remaining parts form a smoothly convex surface. The posterior and ventral rims of the glenoid facet form a bulged margin, which emphasizes the widening of the glenoid process and give it an overall trumpet-shaped appearance. However, the overall surface covered by the glenoid facet of the coracoid of *G. leedsi* NHMUK PV R 3014 & NHMUK PV R 3015 is proportionally smaller than what is observed in other metriorhynchids with an open coracoid foramen (*e.g. Thalattosuchus* NHMUK PV R 1530 & GLAHM V1146, *'Me.' brachyrhynchus* NHMUK PV R 4696, *Tyrannoneustes* GLAHM V1145).

Similar to *Thalattosuchus* (GLAHM V1005, GLAHM V1146, PMU 35988, NHMUK PV R 1530), *'Me.' brachyrhynchus* NHMUK PV R 4696, *Tyrannoneustes* GLAHM V1145, the shaft of the coracoid

of *G. leedsi* NHMUK PV R 3014 & NHMUK PV R 3015 displays a slender shape as its mediolateral extension markedly exceeds (by one and a half) the minimal width of the shaft at the constriction (anteroposteriorly). This shape is notably induced by the anterior and posterior margins of the coracoid, which possess a similar degree of concavity for most of their length in *G. leedsi* NHMUK PV R 3014 & NHMUK PV R 3015 (but with the anterior margin being slightly more curved). In other metriorhynchids with an open coracoid foramen, the anterior and posterior margins are less similar than in what is observed on the coracoid of *G. leedsi* NHMUK PV R 3014 and NHMUK PV R 3015, and this asymmetry markedly ascends in metriorhynchids with a closed coracoid foramen (*e.g. C. albersdoerferi* BMMS-BK 1-2, *C. bambergensis* NKMB-P-Watt14/274, *C. suevicus* SMNS 9808, *C. lithographicus* MOZ-PV 5787, *C. araucanensis* MLP 72-IV-7-1, *D. maximus* SMNS 8203, *Dakosaurus sp.* DMA-JP-2009/001, *Dakosaurus sp.* Rygol specimen). A consequence of the similar concavity of the anterior and posterior margins of the coracoid of *G. leedsi* NHMUK PV R 3014 and NHMUK PV R 3015, is the anteroposterior symmetry of the coracoid blade. Indeed, the long axis of the shaft of the coracoid of *G. leedsi* NHMUK PV R 3014 & NHMUK PV R 3015 separates the coracoid blade into two similarly sized portion. In addition, the medial margin of the coracoid blade forms a convex dome-shaped edge whose apex also coincides with the long axis of the shaft of the coracoid. As such, the anterior and posterior corners of the coracoid blade are positioned on the same level and form two sharp corners with a slight lateral component in their orientation. In comparison, the coracoid blade of *Thalattosuchus* (GLAHM V1005, GLAHM V1146, PMU 35988, NHMUK PV R 1530),*'Me.' brachyrhynchus* NHMUK PV R 4696 and *Tyrannoneustes* GLAHM V1145 also display a symmetrical and dome-shaped medial margin but with its apex anteriorly shifted in relation to the long axis of the shaft of the coracoid. Hence, the posterior corner of the coracoid blade of those taxa (*e.g. Thalattosuchus* GLAHM V1005, GLAHM V1146, PMU 35988 & NHMUK PV R 1530,*'Me.' brachyrhynchus* NHMUK PV R 4696 and *Tyrannoneustes* GLAHM V1145) is less prominent in relation to the shaft of the coracoid than the anterior corner.

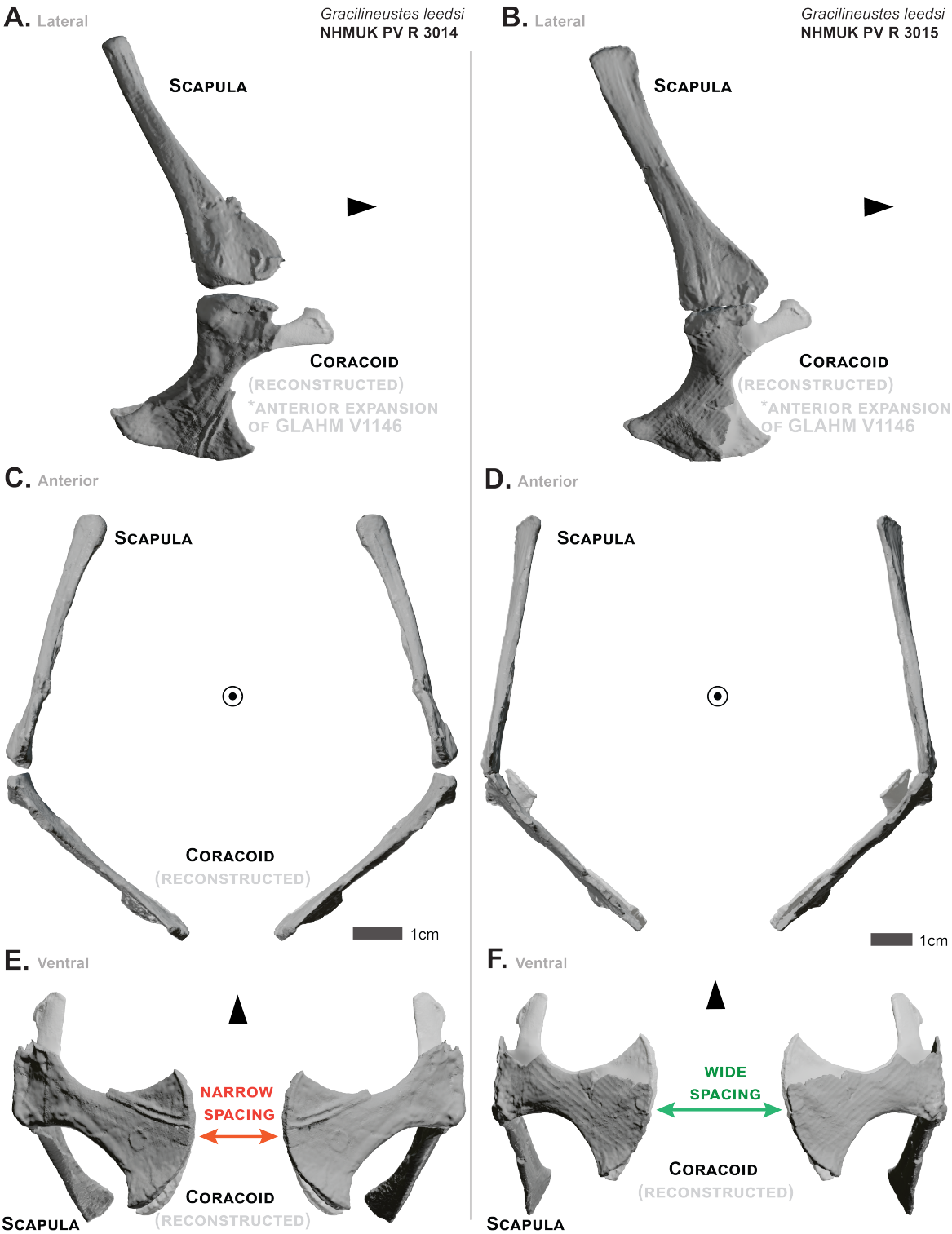


FIGURE 23. Reconstruction of the pectoral girdle of *Gracilineustes leedsi* NHMUK PV R 3014 (A, C & E) and *Gracilineustes leedsi* NHMUK PV R 3015 (B, D, & F) (3D models). **A.** Right lateral view NHMUK PV R 3014; **B.** Right lateral view NHMUK PV R 3015; **C.** Anterior view NHMUK PV R 3014; **D.** Anterior view NHMUK PV R 3015; **E.** Ventral view NHMUK PV R 3014; **F.** Ventral view NHMUK PV R 3015. Target indicates anterior. Arrow points anteriorly. The left scapula and coracoid of NHMUK PV R 3014 and NHMUK PV R 3015 are mirrored. The anterior expansion of the coracoid of *Thalattosuchus* GLAHM V1146 was used to reconstruction the coracoid of NHMUK PV R 3014 and NHMUK PV R 3015. The exact dimensions of the ventral spacing between the coracoids is uncertain so two reconstitutions are offered.

7.4. ***Rhacheosaurus gracilis* von Meyer, 1831.** For measurements, see table 7. This specimen is presumably a juvenile. No particular traits could be attributed to ontogenetic changes (Brochu, 1992).

7.4.1. *Coracoid.* The coracoid of *Rhacheosaurus gracilis* NHMUK PV R 3948 (see figs. 12 and 24) is fragmentary but bears the typically broad axe-head shaped coracoid blade found in other thalattosuchians.

The exact shape and extension of the coracoid head of *Rhacheosaurus* NHMUK PV R 3948 is unknown, but presumably mirrored the coracoid blade as in other thalattosuchians. Indeed, the coracoid head of *Rhacheosaurus* NHMUK PV R 3948 markedly flares out from the shaft of the coracoid as it can be seen on the preserved anterior portion – the anterior expansion. The latter also shows the rudiment of its lateral margin, which appears markedly convex. It is not clear if the coracoid head of *Rhacheosaurus* NHMUK PV R 3948 possessed an open coracoid foramen as in the coracoids of *Thalattosuchus*, *'Me.' brachyrhynchus* NHMUK PV R 4696, and *Tyrannoneustes*, but there is no trace of a coracoid foramen on the exposed surface of the head. In comparison, *C. araucanensis* MLP 72-IV-7-1, *C. albersdoerferi* BMMS-BK 1-2 and *C. bambergensis* NKMB-P-Watt14/274 display a coracoid foramen located near the base of the shaft of the coracoid, whereas its is placed slighting closer to the scapulocoracoid synchondrosis surface in *C. suevicus* SMNS 9808. In all *Cricosaurus* species, the coracoid foramen is in line with the long axis of the shaft of the coracoid.

The shaft of the coracoid of *Rhacheosaurus* NHMUK PV R 3948 displays a marked constriction at its junction with the coracoid head and hence appears relatively slender, which contrasts with the proportionally thicker shaft of most other rhacheosaurines (except *C. albersdoerferi* BMMS-BK 1-2). In comparison, other metriorhynchoid taxa like *Thalattosuchus* (all specimens), *'Me.' brachyrhynchus* NHMUK PV R 4696, *Dakosaurus sp.* Rygol specimen, and *Tyrannoneustes* GLAHM V1145 also possess relative sharp constriction of their shaft, however at varying degrees. In *Rhacheosaurus* NHMUK PV R 3948, the shaft of the coracoid forms a blunt right-angle corner with the anterior expansion of the coracoid head which is a smaller angular relation than observed in metriorhynchids with an open coracoid foramen such as *Thalattosuchus* (all specimens),*'Me.' brachyrhynchus* NHMUK PV R 4696 and *Tyrannoneustes* GLAHM V1145. In comparison, metriorhynchid taxa with a closed coracoid foramen (*e.g. C. araucanensis* MLP 72-IV-7-1, *C. albersdoerferi* BMMS-BK 1-2 and *C. bambergensis* NKMB-P-Watt14/274, *C. suevicus* SMNS 9808, *Dakosaurus sp.* DMA-JP-2009/001 and *Dakosaurus sp.* Rygol specimen) display a large and thick anterior expansion which extends closer to the coracoid shaft (*i.e.* the angle between the shaft and the anterior expansion of the coracoid head approaches to 90 °).

The coracoid blade of *Rhacheosaurus* NHMUK PV R 3948 is severed from the head, and hence the full extension of the shaft of the coracoid is not observable. However the anteroposterior width of the shaft at its junction with the coracoid blade is similar to that of the base of the shaft near the coracoid head. As in other metriorhynchoids, the anterior and posterior processes of the coracoid blade of *Rhacheosaurus* NHMUK PV R 3948 are dissimilar in size, with the anterior one being markedly larger. However, both the anterior and posterior tips of the coracoid blade of *Rhacheosaurus* NHMUK PV R 3948 form sharp and partially rounded-off corners. The shape and extension of the coracoid blade of *Rhacheosaurus* NHMUK PV R 3948 presumably mirrors the global anteroposterior expansion of the coracoid head, similar to other metriorhynchoids. In addition, the medial margin of the coracoid blade of *Rhacheosaurus* NHMUK PV R 3948 is markedly convex which gives an axe-head shape to the entire process, as in other thalattosuchians.

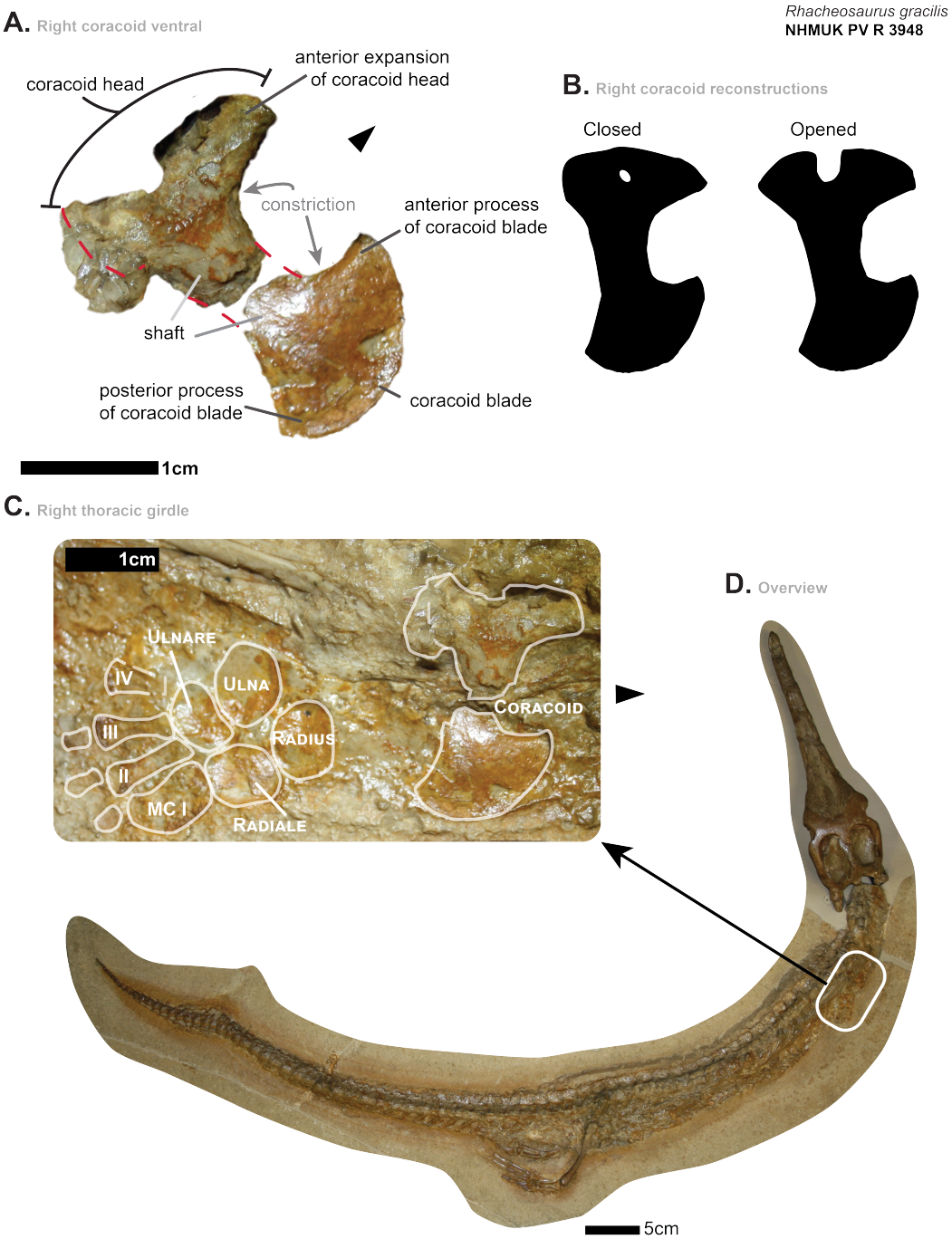


FIGURE 24. Pectoral girdle of *Rhacheosaurus gracilis* NHMUK PV R 3948 (photographs). **A.** Right coracoid in ventral view ; **B.** Right coracoid reconstructions with a closed (based on *Cricosaurus suevicus* SMNS 9808) and opened coracoid foramen (based on *Thalattosuchus superciliosus* GLAHM V1146) ; **C.** Overview of right pectoral girdle ; **D.** Overview of entire skeleton. Arrow points anteriorly. Red dashed lines indicate missing parts.

7.5. ***Cricosaurus albersdoerferi* Sachs et al., 2021.** For measurements, see tables 6 and 7.

7.5.1. *Scapula.* The anterior margin of the scapula is not clear, so that the exact shape of the shaft and the anterior expansion of the scapular blade are unknown.

The scapula of *Cricosaurus albersdoerferi* BMMS-BK 1-2 (see figs. 11 and 25) appears proportionally short but actually accounts for about 92% of the total length of the coracoid (this ratio reached 97% for *Thalattosuchus* GLAHM V1146). The impression of shortening of the scapula of *C. albersdoerferi* BMMS-BK 1-2 is given by its relative breadth, especially compared to the slenderer scapula of more basal metriorhynchoids (*e.g. Pelagosaurus* BRLSI M.1418 or *Thalattosuchus* GLAHM V1146). Indeed, the scapula of *C. albersdoerferi* BMMS-BK 1-2 does not display a major anteroposterior constriction of the shaft (unlike in *Pelagosaurus* BRLSI M.1418 and *Thalattosuchus* GLAHM V1146), and the anteroposterior length of its proximal extremity (from the acromion to the glenoid processes) corresponds to about half (48%) of the total proximodistal height of the bone.

The acromion process of the scapula of *C. albersdoerferi* BMMS-BK 1-2 shows a relatively limited expansion anteroposteriorly, whereas its dorsoventral height is at least three times greater. The anterior margin of the acromion process is subtly convex and culminates dorsally in a sharp corner. The latter appears to point strictly anteriorly. Comparatively, *C. suevicus* SMNS 9808 also shows an anteroposteriorly short but dorsoventrally wide acromion process, topped with a sharp and anteriorly oriented corner. However, in *C. albersdoerferi* BMMS-BK 1-2, the apex of the acromion process is much taller as it is located at about one–third of the total proximodistal height of the scapula. The overall shape of the acromion process of the scapula of *C. albersdoerferi* BMMS-BK 1-2, with the apex located further dorsally than the surface of the scapulocoracoid synchondrosis is also found in other metriorhynchids (*e.g. Thalattosuchus* GLAHM V1146, *Thalattosuchus* PMU 35988, *D. maximus* SMNS 8203, *To. carpenteri* BRSMG Cd7203, etc.).

The scapulocoracoid synchondrosis surface of the scapula lies posteriorly to the acromion process. In *C. albersdoerferi* BMMS-BK 1-2, due to a short acromion process, the scapulocoracoid synchrodrosis surface accounts for most of the anteroposterior length of the proximal portion of the scapula (see fig. 25), similarly to *C. suevicus* SMNS 9808. *Thalattosuchus* GLAHM V1146 and *Thalattosuchus* PMU 35988 also displayed a proportionally long scapulocoracoid synchondrosis surface.

The glenoid facet of the scapula of *C. albersdoerferi* BMMS-BK 1-2 is strongly tilted (about 70°) compared to the scapulocoracoid synchondrosis surface, as seen in *C. suevicus* SMNS 9808 and other metriorhynchoids (*e.g. Pelagosaurus* BRLSI M.1418, *Thalattosuchus* GLAHM V1146, *Ge. lapparenti* UJF-ID.11847j & UJF-ID.11852f, *D. maximus* SMNS 8203, *To. carpenteri* BRSMG Cd7203). The maximal height of the glenoid facet (proximodistally) is slightly lesser than the length of the anterior margin of the acromion process, which contrasts with *Pelagosaurus* BRLSI M.1418, *Thalattosuchus* GLAHM V1146, *Thalattosuchus* PMU 35988, *D. maximus* SMNS 8203, *To. carpenteri* BRSMG Cd7203.

7.5.2. *Coracoid.* The coracoid of *Cricosaurus albersdoerferi* BMMS-BK 1-2 (see figs. 12 and 25) possesses the following typical metriorhynchoid features: enlarged, similarly sized and convex coracoid head and coracoid blade, joined together by a proportionally short shaft. Furthermore, the coracoid head of *C. albersdoerferi* BMMS-BK 1-2 shows a short posterior protrusion and a large anterior one as in other *Cricosaurus* species.

As in *C. bambergensis* NKMB-P-Watt14/274 and *C. suevicus* SMNS 9808, the anterior expansion of the coracoid head of *C. albersdoerferi* BMMS-BK 1-2 displays a strongly convex lateral margin and a short and subtly concave medial margin. This contrasts with *C. araucanensis* MLP 72-IV-7-1 in which the anterior expansion possesses convex margins laterally and medially. As a result, the apex of the anterior expansion of the coracoid head of *C. albersdoerferi* BMMS-BK 1-2 is not centered but is positioned

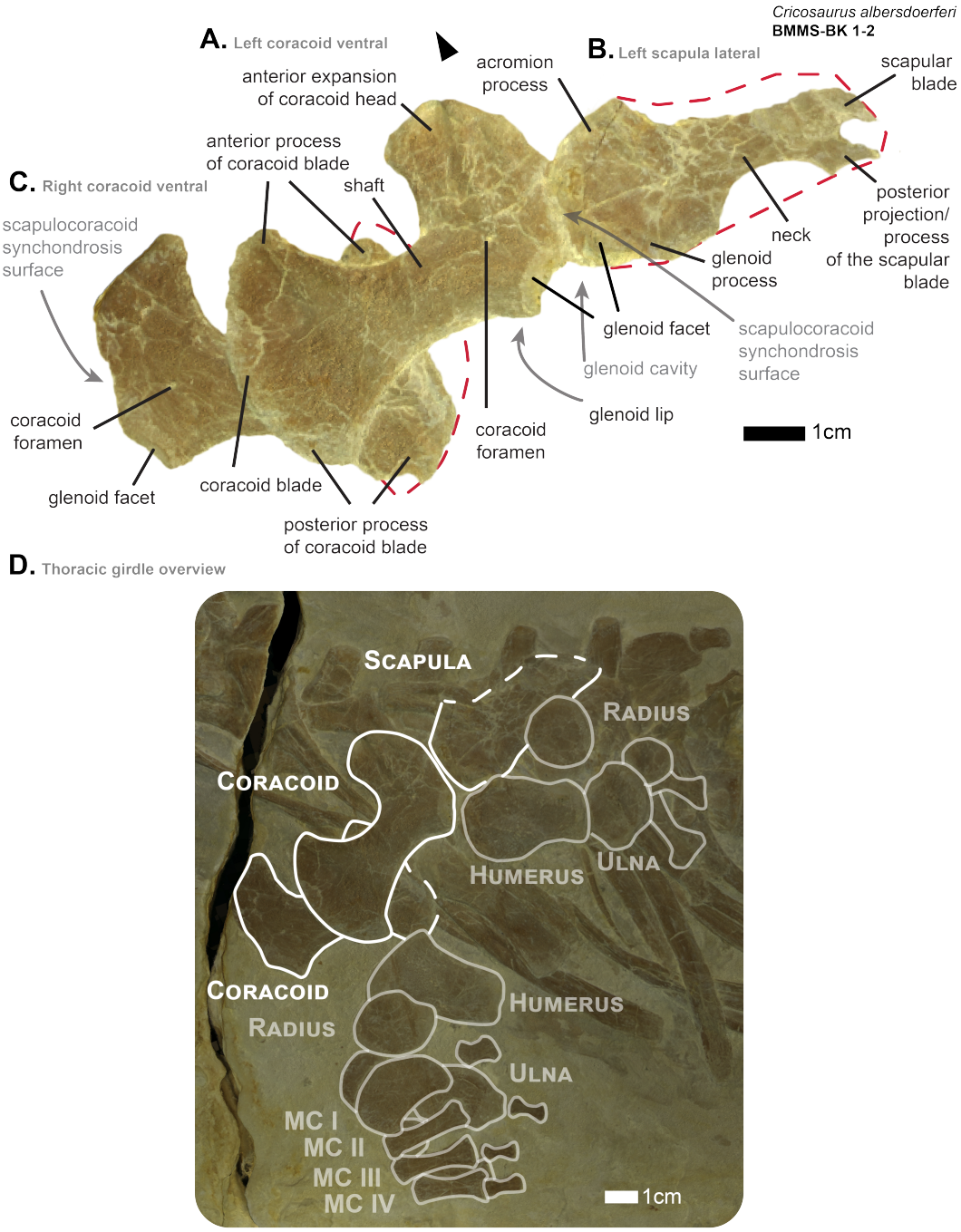


FIGURE 25. Pectoral girdle of *Cricosaurus albersdoerferi* BMMS-BK 1-2 (photographs). **A.** Left coracoid in ventral view ; **B.** Left scapula in lateral view ; **C.** Right coracoid in ventral view ; **D.** Overview of pectoral girdle. Arrow points anteriorly. Red dashed lines indicate missing parts. Reconstruction of missing parts based on *Cricosaurus suevicus* SMNS 9808.

along its medial margin and hence points anteromedially rather than strictly anteriorly as in *C. araucanensis* MLP 72-IV-7-1. Similar to other *Cricosaurus* species, the anterior expansion of the coracoid head of *C. albersdoerferi* BMMS-BK 1-2 is large as it accounts more than half of the total anteroposterior length of the coracoid head from its apex to the coracoid foramen (*e.g.* about 64% in *C. albersdoerferi* BMMS-BK 1-2, 57% in *C. bambergensis* NKMB-P-Watt14/274, 60% in *C. araucanensis* MLP 72-IV-7-1, and about 66% in *C. suevicus* SMNS 9808). In the *Dakosaurus sp.* Rygol specimen the relative size of the anterior expansion of the coracoid head is even greater as it accounts for about 66% of the total anteroposterior length of the coracoid head, whereas in the basal metriorhynchoid *Pelagosaurus* BRLSI M.1418 this number is slightly lower and reaches about 54%. In metriorhynchids with an open coracoid foramen, the length of the anterior expansions plummets (*e.g.* 43% in *Thalattosuchus* GLAHM V1146) as the coracoid foramen is enlarged.

In comparison, the posterior protrusion of the glenoid process of the coracoid head of *C. albersdoerferi* BMMS-BK 1-2 is proportionally short in relation to the shaft of the coracoid, which creates a strong unbalanced look for the coracoid head as in other *Cricosaurus* species, but also as in *Dakosaurus sp.* Rygol specimen. In parallel, the glenoid process is comparatively more prominent posteriorly in *D. maximus* SMNS 8203, and in the basal metriorhynchoids *Pelagosaurus typus* BRLSI M.1418 & BRLSI M.3578 and *Magyarosuchus* (Ősi et al., 2018). The protrusion of the glenoid process in relation to the shaft of the coracoid is greater in metriorhynchids with an open coracoid foramen (*e.g. Thalattosuchus* NHMUK PV R 1530, *Thalattosuchus* GLAHM V1146, *'Me.' brachyrhynchus* NHMUK PV R 4696, *Tyrannoneustes* GLAHM V1145) with the exception of *G. leedsi* (NHMUK PV R 3014 & NHMUK PV R 3015). In *C. albersdoerferi* BMMS-BK 1-2, the glenoid facet displays a rounded outline and is oriented posteroventrally, as in *C. suevicus* SMNS 9808 and *C. araucanensis* MLP 72-IV-7-1. In comparison, the glenoid facet of the coracoid of *C. bambergensis* NKMB-P-Watt14/274 draws a slight curved margin near the posterior border of the bone, and hence appears to possess a more posterior orientation. The glenoid facet of the coracoid of *C. albersdoerferi* BMMS-BK 1-2 is proportionally larger (mediolateral height accounts for around 33% of total anteroposterior length of coracoid head) than what is observed in the more basal metriorhynchine taxa *Thalattosuchus* (16% in GLAHM V1146) and *G. leedsi* (NHMUK PV R 3014 & NHMUK PV R 3015). As in other metriorhynchoids, the surface of the glenoid facet of the coracoid of *C. albersdoerferi* BMMS-BK 1-2 is also anteroposteriorly inclined, with the lateral margin of the facet (in contact with the scapulocaroid synchondrosis surface) being positioned more anteriorly than the medial margin.

As in other metriorhynchoids, the scapulocoracoid synchondrosis surface of the coracoid of *C. albersdoerferi* BMMS-BK 1-2 is short as it only accounts for about 41% of the total anteroposterior length of the coraroid head (it reaches around 44% for *C. suevicus* SMNS 9808 and *C. bambergensis* NKMB-P-Watt14/274). In *C. albersdoerferi* BMMS-BK 1-2, the scapulocoracoid synchondrosis surface appears to form almost a right angle with the long axis of the shaft of the coracoid, as in *C. suevicus* SMNS 9808 and *C. araucanensis* MLP 72-IV-7-1. In comparison, the relative length of the scapulocoracoid synchondrosis surface is very similar in *Thalattosuchus* GLAHM V1146 (42%) although both strongly differ in the shape of their scapula (which is broader and shorter in *C. albersdoerferi* BMMS-BK 1-2) and coracoid head. Indeed, the coracoid head of *C. albersdoerferi* BMMS-BK 1-2 has a closed coracoid foramen similar to other more derived rhacheosaurines, and only possesses a proportionally small and presumably sub-circular coracoid foramen as in *C. suevicus* SMNS 9808 and *C. bambergensis* NKMB-P-Watt14/274. The coracoid foramen of *C. albersdoerferi* BMMS-BK 1-2 is positioned on the same level as the medial (and posterior) extremity of the glenoid facet and is also relatively centered in relation to the long axis of the shaft of the coracoid. In comparison, the coracoid foramen of other *Cricosaurus* species is relatively more laterally positioned (*i.e.* it is closer to the scapulocoracoid synchondrosis surface), with that of *C.*

bambergensis NKMB-P-Watt14/274 also being slightly wider and that of *C. araucanensis* MLP 72-IV-7-1 bearing an elliptical outline.

The anterior and posterior margins of the coracoid of *C. albersdoerferi* BMMS-BK 1-2 are strongly dissimilar: the anterior margin is markedly concave and ovoid in shape whereas the posterior margin displays a more gently curved silhouette, similar to other *Cricosaurus* species. In comparison, other metriorhynchids also possess a strong asymmetry in the shapes of their anterior and posterior margins, with high degree of concavity equivalent to *Cricosaurus* species attained in other metriorhynchids with a closed coracoid foramen (*e.g. Dakosaurus sp.* DMA-JP-2009/001, *Dakosaurus sp.* Rygol specimen and presumably *D. maximus* SMNS 8203). The greater degree of concavity of the anterior margin of the coracoid of *C. albersdoerferi* BMMS-BK 1-2 brings the anterior expansion of the coracoid head closer to the coracoid blade, but also causes a rapid increase in anteroposterior width. As a result, the mediolateral height of the shaft of the coracoid of *C. albersdoerferi* BMMS-BK 1-2 is proportionally short as in other *Cricosaurus* species as it reaches about 26% of total mediolateral height of the coracoid, which is proportionally lesser than in most other metriorhynchoids (*e.g.* about 50% in *Pelagosaurus* BRLSI M.1418, 32% in *Thalattosuchus* NHMUK PV R 1530 and 31% in GLAHM V1146, about 31% in *Tyrannoneustes* GLAHM V1145, and presumably 26-28% in *G. leedsi* NHMUK PV R 3014). In *C. albersdoerferi* BMMS-BK 1-2, the shaft of the coracoid displays an overall rod-like appearance mainly caused by its abrupt junction with the coracoid head. Indeed, the anteroposterior width of the shaft of the coracoid remains relatively constant throughout and especially towards the coracoid head (*i.e.* in the lateral direction). As a result, the junction between the shaft of the coracoid of *C. albersdoerferi* BMMS-BK 1-2 and the coracoid head appears almost angular, as if it formed two relatively blunt and obtuse angles. A similar observation can be made in the taxa *C. suevicus* SMNS 9808 and presumably *C. lithographicus* MOZ-PV 5787.

Medially, differing from its transition with the coracoid head, the shaft of the coracoid of *C. albersdoerferi* BMMS-BK 1-2 gradually and smoothly flares out to form the coracoid blade. As in *C. araucanensis* MLP 72-IV-7-1, and possibly *C. suevicus* SMNS 9808, the coracoid blade of *C. albersdoerferi* BMMS-BK 1-2 displays a symmetrically convex shape with a centered apex. In comparison, the coracoid blade of *C. bambergensis* NKMB-P-Watt14/274 has its apex anterioly shifted, and displays a drastic change in degree of convexity on each side of the apex. Similar to other metriorhynchoids, the anterior protrusion of the coracoid blade of *C. albersdoerferi* BMMS-BK 1-2 in relation to the shaft of the coracoid is proportionally larger than posteriorly, which mirrors the coracoid head. Each extremity of the coracoid blade has a concave lateral margin and a convex medial margin, and displays a slight lateral component in their orientation.

7.6. ***Cricosaurus bambergensis* Sachs et al., 2019.** For measurements, see tables 6 and 7.

7.6.1. *Coracoid.* The coracoid of *Cricosaurus bambergensis* NKMB-P-Watt14/274 displays the typical hourglass shape found in other *Cricosaurus* species: the coracoid head and coracoid blade are both large and similarly sized, whereas the shaft of the coracoid is short and thick. In addition, the anterior expansion is enlarged and the coracoid head possesses a closed coracoid foramen.

As in *C. albersdoerferi* BMMS-BK 1-2, *C. suevicus* SMNS 9808, and *C. araucanensis* MLP 72-IV-7-1, the coracoid head of *C. bambergensis* NKMB-P-Watt14/274 (see figs. 12 and 26) markedly protrudes anteriorly but shows a more limited extension posteriorly. This uneven distribution of mass in relation to the shaft of the coracoid is usually mirrored on the coracoid blade in other *Cricosaurus* species (*e.g. C. albersdoerferi* BMMS-BK 1-2, *C. suevicus* SMNS 9808, *C. araucanensis* MLP 72-IV-7-1 and presumably *C. lithographicus* MOZ-PV 5787), but the difference is not as pronounced on the coracoid blade of *C. bambergensis* NKMB-P-Watt14/274. Indeed, the anterior and posterior processes of the coracoid blade display similar anteroposterior extensions from the shaft of the coracoid, whereas the posterior expansion of the coracoid blade is usually shorter in other *Cricosaurus* species (*e.g. C. araucanensis* MLP 72-IV-7-1 and *C. albersdoerferi* BMMS-BK 1-2). Also, the coracoid head of *C. bambergensis* NKMB-P-Watt14/274 displays an anteroposterior length which is around 11% shorter than that of the coracoid blade, which further contrasts with *C. albersdoerferi* BMMS-BK 1-2 (about 7% difference) and *C. araucanensis* MLP 72-IV-7-1 (about 4% difference). In *C. bambergensis* NKMB-P-Watt14/274, the coracoid head displays a distinctive pickaxe silhouette among *Cricosaurus* species: the entire lateral margin of the coracoid head is dome-shaped (*i.e.* convex and symmetrical) whereas the medial margin of the anterior expansion is markedly concave, resulting in a slim and hook-shaped anterior extremity. The shape of the anterior expansion of the coracoid head of *C. bambergensis* NKMB-P-Watt14/274 strongly contrasts with the more bulbous shape observed in *C. araucanensis* MLP 72-IV-7-1 (and possibly *C. lithographicus* MOZ-PV 5787). In comparison, the concave medial margin of the coracoid head of *C. albersdoerferi* BMMS-BK 1-2 also results in a curved and pointed anterior expansion but the overall shape of their lateral margin is more uneven than in *C. bambergensis* NKMB-P-Watt14/274, which gives them a broader appearance. In *C. suevicus* SMNS 9808, this margin is not entirely concave but is slightly sinuous. In addition, the apex of the anterior expansion of the coracoid head of *C. bambergensis* NKMB-P-Watt14/274 is located proportionally more laterally than in *C. albersdoerferi* BMMS-BK 1-2 and *C. suevicus* SMNS 9808. Indeed, it is located at the same level as the mid-height of the glenoid facet as in *C. araucanensis* MLP 72-IV-7-1.

The glenoid facet of the coracoid of *C. bambergensis* NKMB-P-Watt14/274 is borne by the glenoid process which is located on the posterior extremity of the coracoid head, as in other metriorhynchoids. In *C. bambergensis* NKMB-P-Watt14/274, the glenoid process is proportionally more prominent posteriorly than in *C. albersdoerferi* BMMS-BK 1-2 and *C. araucanensis* MLP 72-IV-7-1, which is similar to what is observed in *C. suevicus* SMNS 9808. This difference is induced by the greater degree of concavity of the posterior margin of the coracoid in *C. bambergensis* NKMB-P-Watt14/274 and *C. suevicus* SMNS 9808. However, the glenoid facet of the coracoid of *C. bambergensis* NKMB-P-Watt14/274 contrasts with that of *C. suevicus* SMNS 9808 in being proportionally more posteriorly oriented. Overall, the morphology of the glenoid facet of the coracoid of *C. bambergensis* NKMB-P-Watt14/274 is similar to what is observed in other *Cricosaurus* species: its outline is curved and its margin forms a thin rim. Yet, the glenoid facet of the coracoid of *C. bambergensis* NKMB-P-Watt14/274 is in line with the scapulocoracoid synchondrosis surface of the coracoid, which contrasts with other *Cricosaurus* species (*e.g. C. albersdoerferi* BMMS-BK 1-2, *C. suevicus* SMNS 9808, and *C. araucanensis* MLP 72-IV-7-1). The exact size of the

scapulocoracoid synchondrosis surface of the coracoid of *C. bambergensis* NKMB-P-Watt14/274 is unknown as it is unclear if a portion of the scapulocoracoid synchondrosis surface of the coracoid extends dorsally to the glenoid facet of the coracoid.

As in other *Cricosaurus* species, the coracoid head of *C. bambergensis* NKMB-P-Watt14/274 possesses a closed coracoid foramen, which forms a proportionally small and sub-circular aperture directly in line with the long axis of the shaft of the coracoid. The coracoid foramen of *C. bambergensis* NKMB-P-Watt14/274 displays a centered position on the ventral surface of the coracoid head as it is placed halfway between the base of the shaft of the coracoid and the lateral margin of the bone, similar to other *Cricosaurus* species (*e.g. C. albersdoerferi* BMMS-BK 1-2, *C. suevicus* SMNS 9808, *C. araucanensis* MLP 72-IV-7-1).

In *C. bambergensis* NKMB-P-Watt14/274, the shaft of the coracoid is short and broad similar to other *Cricosaurus* species, which emphasizes the hourglass shape of the coracoid. Indeed, both the maximum mediolateral extension and the minimal anteroposterior width (at the constriction) of the shaft of the coracoid of *C. bambergensis* NKMB-P-Watt14/274 display similar length, and hence account for about one–fourth of the total mediolateral height of the coracoid (as in other *Cricosaurus* species). The overall short extension of the shaft of the coracoid of *C. bambergensis* NKMB-P-Watt14/274 is notably induced by the high degree of concavity of the anterior margin of the coracoid – which is elliptical – similar to other *Cricosaurus* species but unlike other metriorhynchoids. Due to the intense curvature of the anterior margin of the coracoid of *C. bambergensis* NKMB-P-Watt14/274, the anteroposterior thickness of the bone rapidly increases in the mediolateral direction, and results in an overall short shaft. In comparison, the posterior margin of the coracoid of *C. bambergensis* NKMB-P-Watt14/274 is less elliptical than the anterior margin, but is still markedly concave. Compared to most *Cricosaurus* species the concavity of the posterior margin of the coracoid of *C. bambergensis* NKMB-P-Watt14/274 displays a greater intensity, which in turn produces a more posteriorly prominent apex for the coracoid blade (*e.g. C. araucanensis* MLP 72-IV-7-1, *C. lithographicus* MOZ-PV 5787, *C. albersdoerferi* BMMS-BK 1-2). It is possible that the coracoid of *C. suevicus* SMNS 9808 also possesses a markedly concave posterior margin.

The coracoid blade of *C. bambergensis* NKMB-P-Watt14/274 displays a strongly convex and yet asymmetrical medial margin, which contrasts with the smoother and/or more symmetrical shape observed in *C. albersdoerferi* BMMS-BK 1-2 and *C. araucanensis* MLP 72-IV-7-1. Indeed, the apex of the convexity of the medial margin of the coracoid blade of *C. bambergensis* NKMB-P-Watt14/274 is posteriorly shifted rather than being relatively centered as in other metriorhynchoids (*e.g. Pelagosaurus* BRLSI M.1418, *Thalattosuchus* GLAHM V1005 & PMU 35988, *G. leedsi* NHMUK PV R 3014 & NHMUK PV R 3015, *Rhacheosaurus* NHMUK PV R 3948, *C. albersdoerferi* BMMS-BK 1-2, *C. bambergensis* NKMB-P-Watt14/274, *C. araucanensis* MLP 72-IV-7-1, *'Me.' brachyrhynchus* NHMUK PV R 4696, *Dakosaurus sp.* Rygol specimen, *Tyrannoneustes* GLAHM V1145). A consequence of this asymmetry can be observed in the shape of the anterior and posterior extremities of the coracoid blade of *C. bambergensis* NKMB-P-Watt14/274, which are strongly dissimilar. Indeed, the anterior apex of the coracoid blade form a sharp and slender corner with a strong lateral component in its orientation, whereas the posterior apex constitutes a thicker and blunter tip with a proportionally less pronounced lateral component in its orientation. In comparison, the anterior and posterior extremities of the coracoid blade of other metriorhynchids also display differences in their shapes although less pronounced than in *C. bambergensis* NKMB-P-Watt14/274 (*e.g. Thalattosuchus* GLAHM V1005 & PMU 35988, *G. leedsi* NHMUK PV R 3014 & NHMUK PV R 3015, *Rhacheosaurus* NHMUK PV R 3948, *C. albersdoerferi* BMMS-BK 1-2, *C. bambergensis* NKMB-P-Watt14/274, *C. araucanensis* MLP 72-IV-7-1, *'Me.' brachyrhynchus* NHMUK PV R 4696, *Dakosaurus sp.* Rygol specimen, *Tyrannoneustes* GLAHM V1145).

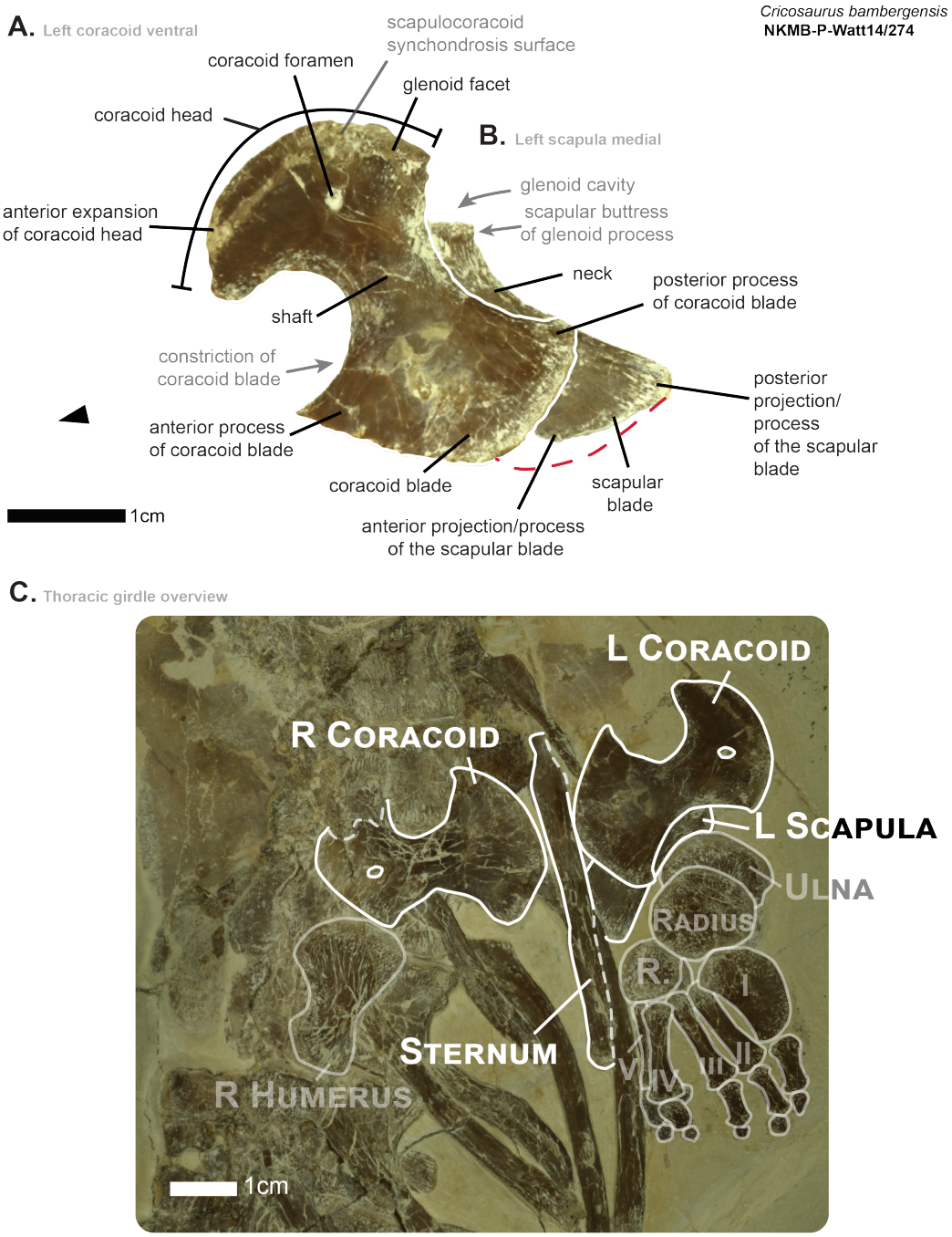


FIGURE 26. Pectoral girdle of *Cricosaurus bambergensis* NKMB-P-Watt14/274 (photographs). **A.** Left coracoid in ventral view ; **B.** Left scapula in medial view ; **C.** Overview of pectoral girdle. Arrow points anteriorly. Red dashed lines indicate missing parts. Reconstruction of missing parts based on *Cricosaurus suevicus* SMNS 9808.

7.7. ***Cricosaurus suevicus* Fraas, 1901.** For measurements, see tables 6 and 7.

7.7.1. *Scapula.* The scapula of *Cricosaurus suevicus* SMNS 9808 (see figs. 11 and 27) appears overall short and broad, like that of *C. albersdoerferi* BMMS-BK 1-2. Comparatively, the scapula of *C. suevicus* SMNS 9808 reaches about 80% of the total proximodistal length of its coracoid, which is lesser than *C. albersdoerferi* BMMS-BK 1-2. The shaft of the scapula, corresponding to the main anteroposterior constriction, is also relatively short in *C. suevicus* SMNS 9808 (accounts for about one–fifth of the total height of the scapula). In other metriorhynchoids, the scapular shaft is proportionally larger, mainly due to differences in the degree of concavity of both the anterior and posterior margins of the bone. Indeed, in *C. suevicus* SMNS 9808, the anterior and posterior margins display a relatively high concavity over a short distance, resulting in a shaft of proportionally limited expansion.

Dorsally, the shaft of the scapula rapidly flares out to form the scapular blade. The latter possesses a domed dorsal surface culminating in two slightly protruding corners anteriorly and posteriorly. The minor axis of the dome in congruent with the long axis of the shaft of the scapula, so that the concavity of the scapular blade is oriented strictly dorsally as in *Pelagosaurus* BRLSI M.1418, *Thalattosuchus* GLAHM V1146, *Thalattosuchus* PMU 35988, *Mycterosuchus* NHMUK PV R 2617, and *Lemmysuchus* NHMUK PV R 3168, and not anterodorsally as in *Platysuchus* SMNS 9930 & UMH-0005, *Macrospondylus* SMNS 54063, or *Neosteneosaurus* NHMUK PV R 3701 & PETMG R178. Another trait adding to the overall broad appearance of the scapula of *C. suevicus* SMNS 9808 is the relatively limited expansion of the scapular blade in the anteroposterior direction. Indeed, the scapular blade is only subtly larger than the proximal portion of the scapula anteroposteriorly, which contrasts with *Pelagosaurus* BRLSI M.1418 and *D. maximus* SMNS 8203 among metriorhynchoids.

As in most metriorhynchoids, the acromion process of the scapula of *C. suevicus* SMNS 9808 forms a relatively sharp corner at around its mid-height which is pointing strictly anteriorly (*e.g. Thalattosuchus* GLAHM V1146, *Thalattosuchus* PMU 35988, *C. albersdoerferi* BMMS-BK 1-2, *D. maximus* SMNS 8203, *To. carpenteri* BRSMG Cd7203). The dorsal and ventral margins of the acromion process both appear relatively straight to slightly concave. Similarly to *C. albersdoerferi* BMMS-BK 1-2,*D. maximus* SMNS 8203, *Thalattosuchus* GLAHM V1146, and *Thalattosuchus* PMU 35988, the acromion process of the scapula of *C. suevicus* SMNS 9808 faintly protrude anteriorly whereas being dorsoventrally elongated (about four times). This greatly contrasts with the prominent acromion process of the scapula of *To. carpenteri* BRSMG Cd7203.

The scapulocoracoid synchondrosis surface of *C. suevicus* SMNS 9808 (see fig. 27) accounts for most of the anteroposterior expansion of the proximal region of the scapula (about 54% for *C. suevicus* SMNS 9808, whereas this number reached 44% in *C. albersdoerferi* BMMS-BK 1-2). The scapular fossa is located on the lateral surface of the acromion process and above the scapulocoracoid synchondrosis, and forms a triangular area slightly in recess. The scapular fossa ends at the glenoid process, which usually protrudes mediolaterally to hold the articular facet of the glenoid. Dorsally, the scapular fossa seems bordered by a shallow ridge – the acromial crest.

Similarly to what is observed in *C. albersdoerferi* BMMS-BK 1-2, the glenoid process of the scapula of *C. suevicus* SMNS 9808 does not appear to protrude posteriorly. The glenoid facet is tilted of about 67° from the ventral surface of the scapula. Its height does not reach that of the corner of the acromion process, similarly to *C. albersdoerferi* BMMS-BK 1-2. In addition, in *C. suevicus* SMNS 9808, the glenoid facet of the scapula is proportionally smaller than that of the coracoid.

7.7.2. *Coracoid.* The coracoid of *Cricosaurus suevicus* SMNS 9808 displays the typical features of derived rhacheosaurines: the coracoid head is large with an extensive anterior expansion; the coracoid head possesses a closed coracoid foramen; the shaft of the coracoid is short due to strongly concave anterior

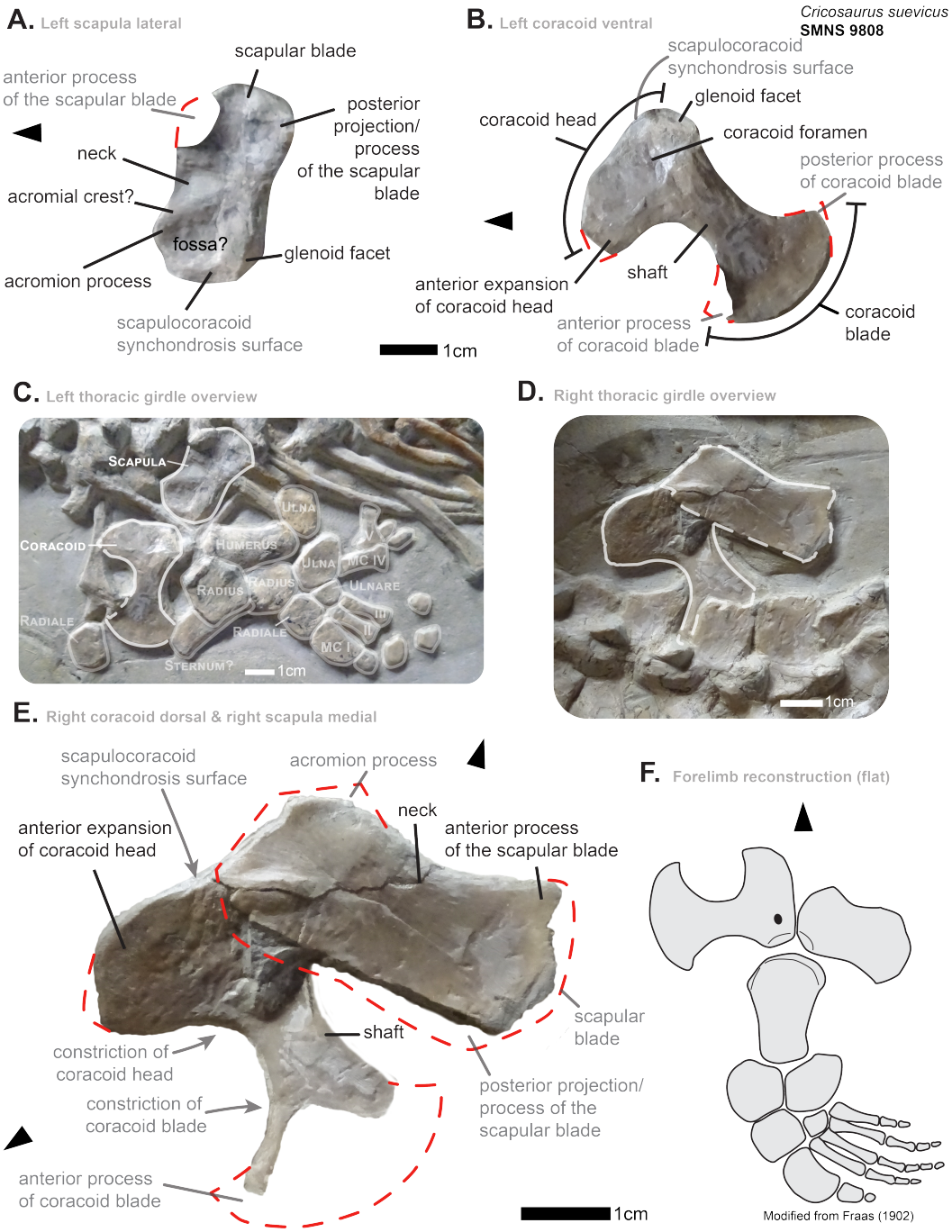


FIGURE 27. Pectoral girdle of *Cricosaurus suevicus* SMNS 9808 (photographs). **A.** Left scapula in lateral view ; **B.** Left coracoid in ventral view ; **C.** Overview of left pectoral girdle ; **D.** Overview of right pectoral girdle ; **E.** Right coracoid in dorsal view and right scapula in medial view ; **F.** Reconstruction of the left forelimb laying flat (forelimb modified from Fraas (1902)). Arrow points anteriorly. Red dashed lines indicate missing parts. Reconstruction of missing parts based on *Cricosaurus bambergensis* NKMB-P-Watt14/274.

and posterior margins.

The coracoid head of *C. suevicus* SMNS 9808 (see figs. 12 and 27) possesses a closed coracoid foramen, similar to other *Cricosaurus* species as well as *D. maximus* SMNS 8203 (and also *Dakosaurus sp.* DMA-JP-2009/001, *Dakosaurus sp.* Rygol specimen) among metriorhynchids. Hence, the coracoid foramen of *C. suevicus* SMNS 9808 forms a proportionally small and sub-circular aperture located near the base of shaft and centered in relation to the long axis of the shaft of the coracoid, as in most metriorhynchids with a closed coracoid foramen (*e.g. C. albersdoerferi* BMMS-BK 1-2, *C. araucanensis* MLP 72-IV-7-1, *D. maximus* SMNS 8203, *Dakosaurus sp.* DMA-JP-2009/001, and *Dakosaurus sp.* Rygol specimen). In *C. bambergensis* NKMB-P-Watt14/274, however, the coracoid foramen displays a proportionally larger size compared to *C. suevicus* SMNS 9808 and other *Cricosaurus* species. Also, the position of the coracoid foramen of *C. suevicus* SMNS 9808 on the ventral surface of the coracoid head is positioned around the mid-length of the glenoid facet, similar to other *Cricosaurus* species (*e.g. C. albersdoerferi* BMMS-BK 1-2, *C. bambergensis* NKMB-P-Watt14/274, *C. araucanensis* MLP 72-IV-7-1).

Similar to other *Cricosaurus* species, the coracoid head of *C. suevicus* SMNS 9808 presents a strongly unbalanced appearance: the anterior expansion markedly protrudes from the shaft of the coracoid whereas the posterior portion is less prominent. Indeed, the anteroposterior length of the anterior expansion of the coracoid head of *C. suevicus* SMNS 9808 is large and accounts for about 66% of the total anteroposterior length of the coracoid head (from the coracoid foramen to its apex anteriorly). In comparison, other *Cricosaurus* species also display large anterior expansions with a length reaching 64% in *C. albersdoerferi* BMMS-BK 1-2, 57% in *C. bambergensis* NKMB-P-Watt14/274, and 60% in *C. araucanensis* MLP 72-IV-7-1. Furthermore, the shape of the coracoid head of *C. suevicus* SMNS 9808 resembles the head of a pickaxe, which is a silhouette that can also be observed in other *Cricosaurus* species although different in each one. Indeed, the anterior expansion of the coracoid head of *C. suevicus* SMNS 9808 is anteriorly tapered and forms a slight hook shape, whereas the posterior extremity of the coracoid head is short (protrusion from the shaft) and bears an articular facet (the glenoid facet). The hooked silhouette of the anterior expansion is given by the shape of its margins: the lateral margin is smoothly convex anteriorly and becomes relatively straighter posteriorly, whereas the medial margin is slightly undulated (as in *C. araucanensis* MLP 72-IV-7-1 but to a lesser extent). As a result, the apex of the anterior expansion of the coracoid head of *C. suevicus* SMNS 9808 is not positioned on the medial margin as in *C. albersdoerferi* BMMS-BK 1-2 and *C. bambergensis* NKMB-P-Watt14/274, but appears more laterally positioned similar to *C. araucanensis* MLP 72-IV-7-1 but to a lesser extent. In comparison, the lateral margin of the coracoid head of *C. albersdoerferi* BMMS-BK 1-2 has a similar shape but with a greater degree of convexity, whereas in *C. araucanensis* MLP 72-IV-7-1 and *C. bambergensis* NKMB-P-Watt14/274 the lateral margin displays a more bulbous shape.

The posterior portion of the coracoid head of *C. suevicus* SMNS 9808 is mainly constituted by the glenoid process, which usually corresponds to the dorsoventrally thickest portion of the coracoid as it bears the glenoid facet. In *C. suevicus* SMNS 9808, the glenoid facet displays a sub-circular outline and is mainly oriented posteroventrally as in *C. araucanensis* MLP 72-IV-7-1 and *C. albersdoerferi* BMMS-BK 1-2. In *C. suevicus* SMNS 9808, the scapulocoracoid synchondrosis surface does not appear to extend dorsally to the glenoid facet, as in *C. albersdoerferi* BMMS-BK 1-2 and *C. araucanensis* MLP 72-IV-7-1. The scapulocoracoid synchondrosis surface of the coracoid of *C. suevicus* SMNS 9808 is positioned along the lateral margin of the coracoid, on the posterior side of the coracoid head. As in other metriorhynchoids, the scapulocoracoid synchondrosis surface of the coracoid of *C. suevicus* SMNS 9808 is also proportionally short: the observed length (correlated with the scapulocoracoid synchondrosis surface of the scapula) corresponds to about 44% of the total anteroposterior length of the coraroid head. In

C. bambergensis NKMB-P-Watt14/274 and *C. albersdoerferi* BMMS-BK 1-2, the scapulocoracoid synchondrosis surface displays similar lengths (44% and 41% respectively).

The anterior and posterior margins of the coracoid of *C. suevicus* SMNS 9808 are noticeably concave, with the anterior margin bearing the longest degree of concavity similar to other metriorhynchids. However, the anterior margin of the coracoid of *C. suevicus* SMNS 9808 appears elliptic in shape, which is more specifically observed in other metriorhynchids with a closed coracoid foramen (namely *Cricosaurus* species as well as *Dakosaurus sp.* Rygol specimen, and presumably *Dakosaurus sp.* DMA-JP-2009/001 and *D. maximus* SMNS 8203). Yet, the exact curvature of the anterior margin of the coracoid of *C. suevicus* SMNS 9808 is uncertain which impacts the exact extension of the shaft. However, the shaft of the coracoid of *C. suevicus* SMNS 9808 appears relatively slender as in *C. araucanensis* MLP 72-IV-7-1. Overall, the shaft of the coracoid of *C. suevicus* SMNS 9808 is proportionally short: its total mediolateral extension accounts for about one–fourth (26%) of the total mediolateral height of the bone. In parallel, the minimal anteroposterior width of the shaft of the coracoid at the constriction is slightly shorter (about 20%) than its mediolateral extension which gives the shaft a relatively slender appearance, as in *C. araucanensis* MLP 72-IV-7-1. In *C. albersdoerferi* BMMS-BK 1-2 and *C. bambergensis* NKMB-P-Watt14/274, the anteroposterior width of the shaft of the coracoid at the constriction and the mediolateral extension of the shaft of the coracoid display similar length, whereas the shaft of the coracoid of *C. lithographicus* MOZ-PV 5787 is markedly thicker anteroposteriorly than its mediolateral extension. The width of the minimal constriction of the shaft of the coracoid of *C. suevicus* SMNS 9808 accounts for about 34% of the total anteroposterior length of the coracoid head, which is closer to *C. araucanensis* MLP 72-IV-7-1 (36.6%) than *C. albersdoerferi* BMMS-BK 1-2 (39%) and*C. bambergensis* NKMB-P-Watt14/274 (39%).

Medially, the shaft of the coracoid of *C. suevicus* SMNS 9808 gradually flares out to form the coracoid blade. Similar to most *Cricosaurus* species, the coracoid blade of *C. suevicus* SMNS 9808 displays an overall symmetrical appearance: the medial margin of the process is markedly convex with its apex relatively centered. The anterior process of the coracoid blade of *C. suevicus* SMNS 9808 is not preserved but it is possible that it spread anteriorly as far as the tip of the anterior expansion of the coracoid head, similar to other *Cricosaurus* species and metriorhynchids. In parallel, the posterior corner of the coracoid blade of *C. suevicus* SMNS 9808 possibly extended slightly further posteriorly than the glenoid process as in *C. bambergensis* NKMB-P-Watt14/274.

7.8. ***Cricosaurus lithographicus* (Herrera et al., 2013b) Wagner, 1858.** For measurements, see table 7.

7.8.1. *Coracoid.* The coracoid of *Cricosaurus lithographicus* MOZ-PV 5787 (Herrera et al., 2013b) Wagner, 1858 (see figs. 12 and 28) is fragmentary, but still displays a short and broad shaft with a large axe-head coracoid blade as in other *Cricosaurus* species.

The preserved portion of the coracoid head of *C. lithographicus* MOZ-PV 5787 (see fig. 28) shows its junction with the base of the shaft of the coracoid, as well as a fraction of its dorsal surface. The position and shape of the coracoid foramen is unclear, but was possibly similar to that of other *Cricosaurus* species.

As in other *Cricosaurus* species, the anteroposterior widening of the coracoid head is asymmetrical, with the anterior expansion being presumably more prominent than the posterior portion of the coracoid head (*e.g. C. araucanensis* MLP 72-IV-7-1, *C. albersdoerferi* BMMS-BK 1-2, *C. bambergensis* NKMB-P-Watt14/274, *C. suevicus* SMNS 9808). Indeed, the anterior expansion of the coracoid head of *C. lithographicus* MOZ-PV 5787 forms a noticeable bend at its junction with the shaft of the coracoid indicating a strong anterior protrusion, whereas the posterior margin of the coracoid only shows a smooth curve in the corresponding area. Furthermore, the strong stoop observed at the anterior junction between the shaft of the coracoid and the coracoid head also implies a markedly convex medial margin of the anterior expansion of the coracoid head, as in *C. araucanensis* MLP 72-IV-7-1 among rhacheosaurines.

As in *C. araucanensis* MLP 72-IV-7-1, *C. albersdoerferi* BMMS-BK 1-2 and *C. bambergensis* NKMB-P-Watt14/274, the shaft of the coracoid of *C. lithographicus* MOZ-PV 5787 is short and broad with a subtly concave posterior margin and a markedly concave anterior margin. However, the anteroposterior width of the shaft of the coracoid of *C. lithographicus* MOZ-PV 5787 exceeds its mediolateral length, which contrasts with what is observed in *C. araucanensis* MLP 72-IV-7-1, *C. albersdoerferi* BMMS-BK 1-2 and *C. bambergensis* NKMB-P-Watt14/274. As in other *Cricosaurus* species, the strong degree of concavity of the anterior margin rapidly increases the anteroposterior width of the coracoid, and hence the shaft of the coracoid quickly transitions to the coracoid blade (which is partly responsible for the shortness of the shaft of the coracoid as well).

The coracoid blade of *C. lithographicus* MOZ-PV 5787 displays the typical axe-head outline found in other metriorhynchoids (and other thalattosuchians as a whole). However, the coracoid blade of *C. lithographicus* MOZ-PV 5787 appears to markedly differ from other *Cricosaurus* species in possessing a longer and sharper posterior apex (*e.g. C. albersdoerferi* BMMS-BK 1-2, *C. bambergensis* NKMB-P-Watt14/274, *C. suevicus* SMNS 9808, and *C. araucanensis* MLP 72-IV-7-1). Presumably, the anterior extension of the glenoid process of the coracoid of *C. lithographicus* MOZ-PV 5787 matched that of the coracoid blade.

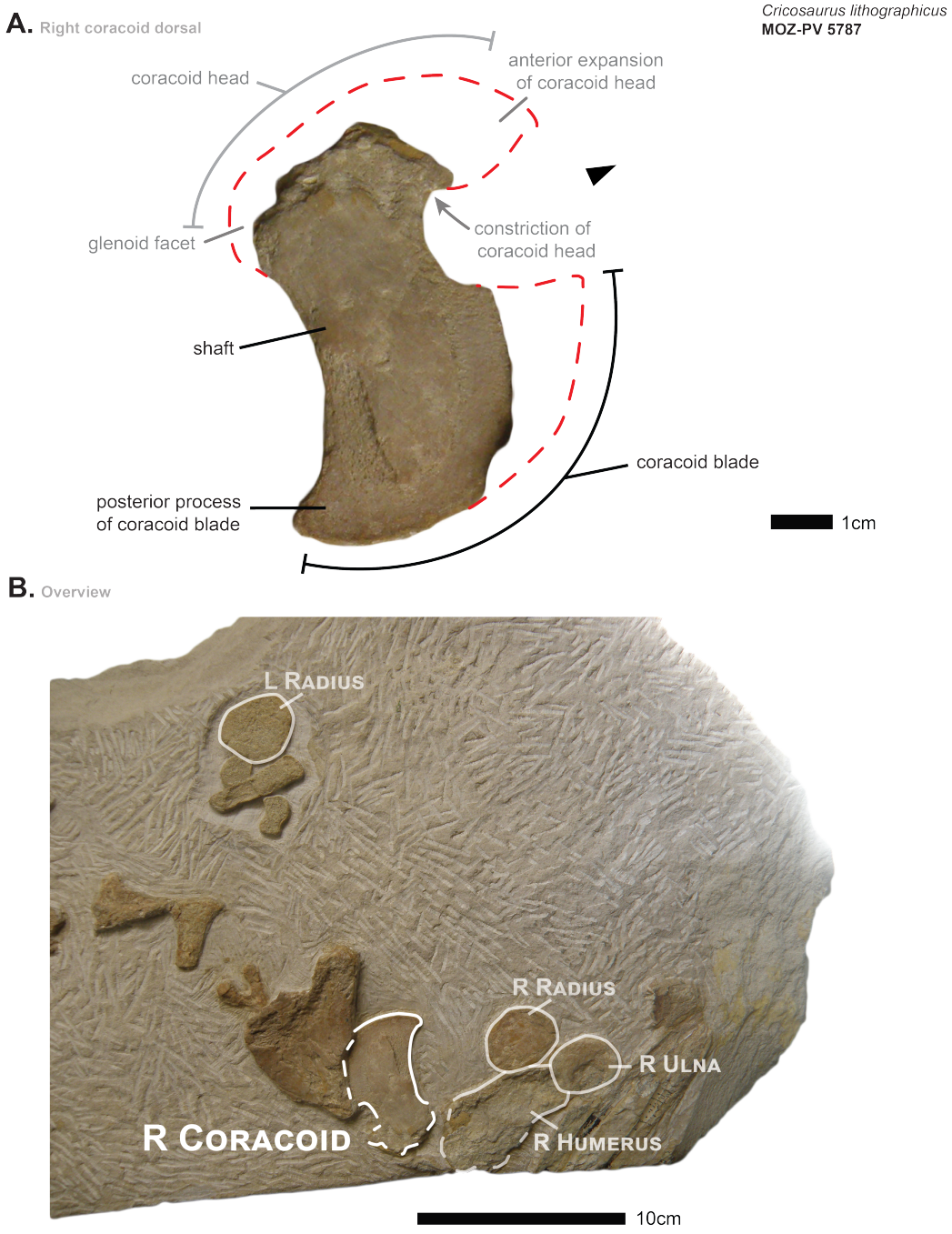


FIGURE 28. Pectoral girdle of *Cricosaurus lithographicus* MOZ-PV 5787 (Herrera et al., 2013b) Wagner, 1858 (photographs). **A.** Right coracoid in ventral view ; **B.** Overview of pectoral girdle. Arrow points anteriorly. Pictures courtesy of Dr. Yanina Herrera. Red dashed lines indicate missing parts. Reconstruction of missing parts based on *Cricosaurus araucanensis* MLP 72-IV-7-1.

7.9. ***Cricosaurus araucanensis* (Gasparini and Dellapé, 1976) Wagner, 1858.** For measurements, see table 7.

7.9.1. *Coracoid.* The shape of the coracoid of *Cricosaurus araucanensis* MLP 72-IV-7-1 (Gasparini and Dellapé, 1976) Wagner, 1858 (see figs. 12 and 29) bears the typical metriorhynchoid features: the shaft of the coracoid is short and the coracoid head and blade are anteroposteriorly large. The coracoid of *C. araucanensis* MLP 72-IV-7-1 also displays a broad outline, which is a common characteristics found in other rhacheosaurines. In addition, the coracoid head of *C. araucanensis* MLP 72-IV-7-1 possesses a closed coracoid foramen as in several basal and derived metriorhynchoids (*e.g. Pelagosaurus*, *Magyarosuchus* (Ősi et al., 2018), *C. albersdoerferi* BMMS-BK 1-2, *C. bambergensis* NKMB-P-Watt14/274, *C. suevicus* SMNS 9808, *D. maximus* SMNS 8203).

Similar to other metriorhynchoids, the coracoid of *C. araucanensis* MLP 72-IV-7-1 (see fig. 29) possesses an overall symmetrical outline in the mediolateral direction: its coracoid head and coracoid blade display a similar length, with a short anterior extension and a larger one posteriorly. In addition, the shaft of the coracoid of *C. araucanensis* MLP 72-IV-7-1 is not centered on the bone but slightly posteriorly shifted, and thus the coracoid head and coracoid blade appear markedly unbalanced in the anteroposterior direction as in other metriorhynchoids. However, the coracoid head of *C. araucanensis* MLP 72-IV-7-1 displays a strong asymmetrical shape with a strongly enlarged anterior expansion, which similar to other *Cricosaurus* species. Indeed, the anteroposterior length of the anterior expansion of the coracoid head of *C. araucanensis* MLP 72-IV-7-1 accounts for slightly more than half its total length, and hence it markedly protrudes from the shaft of the coracoid (as in other metriorhynchids). In parallel, the glenoid process of the coracoid of *C. araucanensis* MLP 72-IV-7-1 does not noticeably extend posteriorly which emphasizes the asymmetrical appearance of the coracoid head. This peculiarity is mainly observed in *C. albersdoerferi* BMMS-BK 1-2, *C. bambergensis* NKMB-P-Watt14/274, *C. suevicus* SMNS 9808, *D. maximus* SMNS 8203 (presumably) and *Dakosaurus sp.* Rygol specimen among metriorhynchids.

The anterior expansion of the coracoid head of *C. araucanensis* MLP 72-IV-7-1 possesses a distinctive outline unlike other *Cricosaurus* species: both margins are convex which creates a lancet arch appearance. However, each margin slightly differs as the lateral one is longer but shows a lesser degree of convexity than the medial margin (which is condensed due to the insertion of the shaft of the coracoid). A consequence of the convex shape of both margins is the relatively centered position of the apex of the anterior expansion of the coracoid head in *C. araucanensis* MLP 72-IV-7-1, differing from the medial location observed in *C. albersdoerferi* BMMS-BK 1-2, *C. bambergensis* NKMB-P-Watt14/274 and *C. suevicus* SMNS 9808. In addition, the median of the anterior expansion of the coracoid head of *C. araucanensis* MLP 72-IV-7-1 is overall perpendicular to the long axis of the shaft of the coracoid, and hence the apex of the anterior expansion appears strictly anteriorly oriented (which further contrasts with most *Cricosaurus* species). In *C. suevicus* SMNS 9808, the median of the anterior expansion of the coracoid head also appears overall perpendicular to the shaft of the coracoid.

The coracoid foramen of *C. araucanensis* MLP 72-IV-7-1 appears to form a rather elliptic aperture on the ventral surface of the coracoid head, which contrasts with the sub-circular aperture observed on the ventral surface of the coracoid head of *C. bambergensis* NKMB-P-Watt14/274. The exact outline of the coracoid foramen is uncertain, but seems sub-circular for *C. albersdoerferi* BMMS-BK 1-2 and *C. suevicus* SMNS 9808. As in other *Cricosaurus* species (and *D. maximus* SMNS 8203, *Dakosaurus sp.* DMA-JP-2009/001, *Dakosaurus sp.* Rygol specimen), the coracoid foramen of *C. araucanensis* MLP 72-IV-7-1 displays a relatively centered position on the coracoid head: it is located near the glenoid facet and is overall equidistant from the base of the shaft of the coracoid and the scapulocoracoid synchondrosis surface. In addition, the coracoid foramen is also relatively in line with the long axis of the shaft of the coracoid, similar to other metriorhynchoids.

As in *C. albersdoerferi* BMMS-BK 1-2 and *C. suevicus* SMNS 9808, the glenoid facet of the coracoid of *C. araucanensis* MLP 72-IV-7-1 forms a large sub-circular surface on the posterior corner of the coracoid head with a posteroventral orientation. In comparison, the glenoid facet of the coracoid of *C. bambergensis* NKMB-P-Watt14/274 is barely observable in ventral view and appears to be more strictly posteriorly oriented. The little posterior protrusion of the glenoid process of the coracoid of *C. araucanensis* MLP 72-IV-7-1 positions the glenoid facet closer to the centre of mass of the coracoid head, and directly in line with the coracoid shaft, as in *C. albersdoerferi* BMMS-BK 1-2, *C. suevicus* SMNS 9808, *D. maximus* SMNS 8203 (presumably) and *Dakosaurus sp.* Rygol specimen compared to other metriorhynchids.

The shaft of the coracoid of *C. araucanensis* MLP 72-IV-7-1 is both proportionally short and broad, similar to most *Cricosaurus* species and also *Dakosaurus sp.* Rygol specimen. Indeed, in *C. araucanensis* MLP 72-IV-7-1 the length of the shaft of the coracoid accounts for less than one–third of total mediolateral length of the coracoid, and also the minimum anteroposterior width of the shaft of the coracoid at constriction equals its total mediolateral length. Hence, it further contrasts with the proportionally more gracile shaft of the coracoid of other metriorhynchids (*e.g. Thalattosuchus* all specimens, *Rhacheosaurus* NHMUK PV R 3948, *'Me.' brachyrhynchus* NHMUK PV R 4696, *Tyrannoneustes* GLAHM V1145). In comparison, the shaft of the coracoid of *C. suevicus* SMNS 9808 appears to differ from that of *C. araucanensis* MLP 72-IV-7-1 as it displays a proportionally greater constriction anteroposteriorly. As mentioned above, the outline of the coracoid of *C. araucanensis* MLP 72-IV-7-1 shows a strong asymmetry when comparing its anterior and posterior margins: both are concave but the posterior one is shallower due to a lesser degree of concavity. Such a strong difference of intensity between the concavity of the anterior and posterior margins of the coracoid is a common feature of rhacheosaurines (*e.g. Rhacheosaurus* NHMUK PV R 3948, *C. lithographicus* MOZ-PV 5787, *C. albersdoerferi* BMMS-BK 1-2, *C. bambergensis* NKMB-P-Watt14/274, *C. suevicus* SMNS 9808) and *Dakosaurus sp.* Rygol specimen which possess a particularly enlarged anterior expansion of the coracoid head. The difference of concavity is also observed in other metriorhynchids but to lesser extent, presumably linked to their contrasting coracoid head shape and extension (*e.g. Thalattosuchus* all specimens, *'Me.' brachyrhynchus* NHMUK PV R 4696, *Tyrannoneustes* GLAHM V1145). In *C. araucanensis* MLP 72-IV-7-1 and other *Cricosaurus* species, the strong concavity of the anterior margin of the coracoid gives it a semi-circular appearance. As a consequence, the shaft of the coracoid displays a short mediolateral extension (due to rapid increase in thickness of the bone) and the coracoid head and blade are brought closer to one another than in most metriorhynchids. In parallel, the subtly concave posterior margin of the coracoid of *C. araucanensis* MLP 72-IV-7-1 ensures a slow increase in thickness over distance, which provokes an anteroposteriorly thicker shaft similar to most *Cricosaurus* species and *Dakosaurus sp.* Rygol specimen. This contrasts with *C. suevicus* SMNS 9808 and other metriorhynchoids which display a greater posterior concavity and a subsequently greater anteroposterior constriction of the shaft of the coracoid.

Medially, the shaft of the coracoid of *C. araucanensis* MLP 72-IV-7-1 drastically fans out to form the coracoid blade. As in other thalattosuchians, the coracoid blade of *C. araucanensis* MLP 72-IV-7-1 is broad mediolaterally and anteroposteriorly and possesses an axe-head outline. Despite the asymmetry in the length of the anterior and posterior extensions of the coracoid blade of *C. araucanensis* MLP 72-IV-7-1 (which are assessed in relation to the shaft of the coracoid), the convex medial margin of the blade displays a symmetrical shape due to a relatively centered apex. As a result, the coracoid blade of of *C. araucanensis* MLP 72-IV-7-1 displays a symmetrical shape as in other metriorhynchoids and teleosauroids.

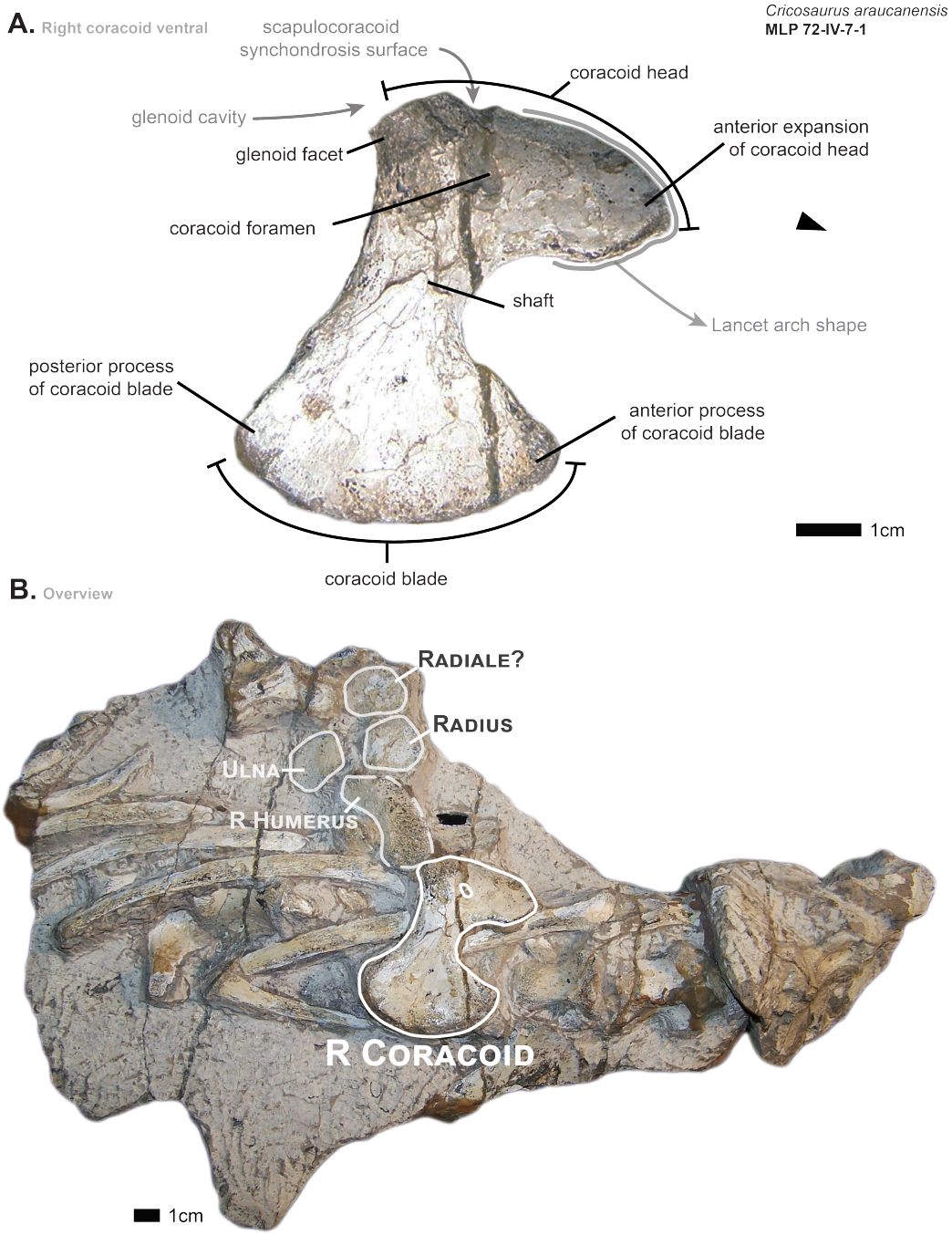


FIGURE 29. Pectoral girdle of *Cricosaurus araucanensis* MLP 72-IV-7-1 (Gasparini and Dellapé, 1976) Wagner, 1858 (photographs). **A.** Right coracoid in ventral view ; **B.** Overview of pectoral girdle. Arrow points anteriorly. Pictures courtesy of Dr. Yanina Herrera.

7.10. ***'Metriorhynchus' brachyrhynchus*** **Eudes-Deslongchamps, 1867.** For measurements, see table 7. This specimen is number NHMUK PV R 4696 but corresponds to the forelimb of NHMUK PV R 4763 (NHM, 2023).

7.10.1. *Coracoid.* The coracoid of *'Metriorhynchus' brachyrhynchus* Eudes-Deslongchamps, 1867 NHMUK PV R 4696 (see figs. 12, 30 and 31) differs from that of other metriorhynchoids in displaying the following distinct combination of traits: an open coracoid foramen, a seemingly partially obstructed coracoid foramen, a markedly flared posterior portion of the coracoid head, and an asymmetrical coracoid blade. Based on the shape of its preserved margins, it is possible that the anterior expansion of the coracoid displayed a wide anteroposterior flaring possibly larger than the posterior portion of the coracoid head. In comparison, in *Thalattosuchus* GLAHM V1146 the anterior expansion of the coracoid head displays a shorter anteroposterior length than the posterior counterpart.

The coracoid foramen of *'Me.' brachyrhynchus* NHMUK PV R 4696 (see fig. 30) forms a relatively deep but narrow indentation on the coracoid head, which contrasts with what is observed in metriorhynchids with an open coracoid foramen (*e.g. Tyrannoneustes* GLAHM V1145, *Thalattosuchus* GLAHM V1005, GLAHM V1146, PMU 35988, NHMUK PV R 1530, *G. leedsi* NHMUK PV R 3014, etc.). Indeed, the total depth of the perforation accounts for about 16% of the total mediolateral height of the coracoid, which is similar to *Thalattosuchus* GLAHM V1146 & NHMUK PV R 1530 but larger than in *Tyrannoneustes* GLAHM V1145 (12.5%) and *G. leedsi* NHMUK PV R 3014 (8.7%). However, in *'Me.' brachyrhynchus* NHMUK PV R 4696, the bottom of the coracoid foramen (medially) draws a much narrower elliptic shape than in the aforementioned metriorhynchids with an open coracoid foramen. Indeed, the preserved portion of the anterior expansion of the coracoid head forming the anterior wall of the coracoid foramen is already markedly recurved which indicates the beginning of the flaring out of the anterior expansion. It subsequently marks the coming of the inflexion point of the concavity of the anterior wall of the coracoid foramen, rather than a further anteroposterior widening of the perforation. Another feature distinct feature of *'Me.' brachyrhynchus* NHMUK PV R 4696 is the marked flaring of the posterior portion of the coracoid head, which shows a strong anterior protrusion partially covering the lateral opening of the coracoid foramen. In comparison, the anterior projection of the scapulocoracoid synchondrosis surface in other metriorhynchids with an open coracoid foramen does not meet with nor come close to the greater axis of the coracoid foramen (*e.g. Tyrannoneustes* GLAHM V1145, *Thalattosuchus* GLAHM V1146 & NHMUK PV R 1530, *G. leedsi* NHMUK PV R 3014, etc.). Similar to most metriorhynchids with an open coracoid foramen, the coracoid foramen of *'Me.' brachyrhynchus* NHMUK PV R 4696 is in line with the long axis of the shaft of the coracoid (*e.g. Tyrannoneustes* GLAHM V1145, *Thalattosuchus* GLAHM V1146 & NHMUK PV R 1530). This feature strongly contrasts with the anteriorly shifted coracoid foramen of *G. leedsi* NHMUK PV R 3014.

As in other metriorhynchids with an open coracoid foramen, the posterior portion of the coracoid head of *'Me.' brachyrhynchus* NHMUK PV R 4696 displays a proportionally shorter mediolateral extension than the anterior expansion (*e.g. Tyrannoneustes* GLAHM V1145, *Thalattosuchus* GLAHM V1146 & NHMUK PV R 1530). However, the posterior portion of the coracoid head of *'Me.' brachyrhynchus* NHMUK PV R 4696 markedly differs from that of *Thalattosuchus* GLAHM V1146 & PMU 35988 in showing a stronger anteroposterior flaring. Most of the anteroposterior length of the extremity of the posterior portion is constituted by the scapulocoracoid synchondrosis surface as it accounts for about 95% of the total length. In other metriorhynchids with an open coracoid foramen, the scapulocoracoid synchondrosis surface is also relatively extended as it reaches 98% in *G. leedsi* NHMUK PV R 3014, 91% in *Tyrannoneustes* GLAHM V1145 and 78% and 82% in *Thalattosuchus* GLAHM V1005 and GLAHM V1146 respectively. The scapulocoracoid synchondrosis surface of the coracoid of *'Me.' brachyrhynchus* NHMUK PV R 4696 is markedly scarred and possesses a prominent ridge along its anteroposterior axis

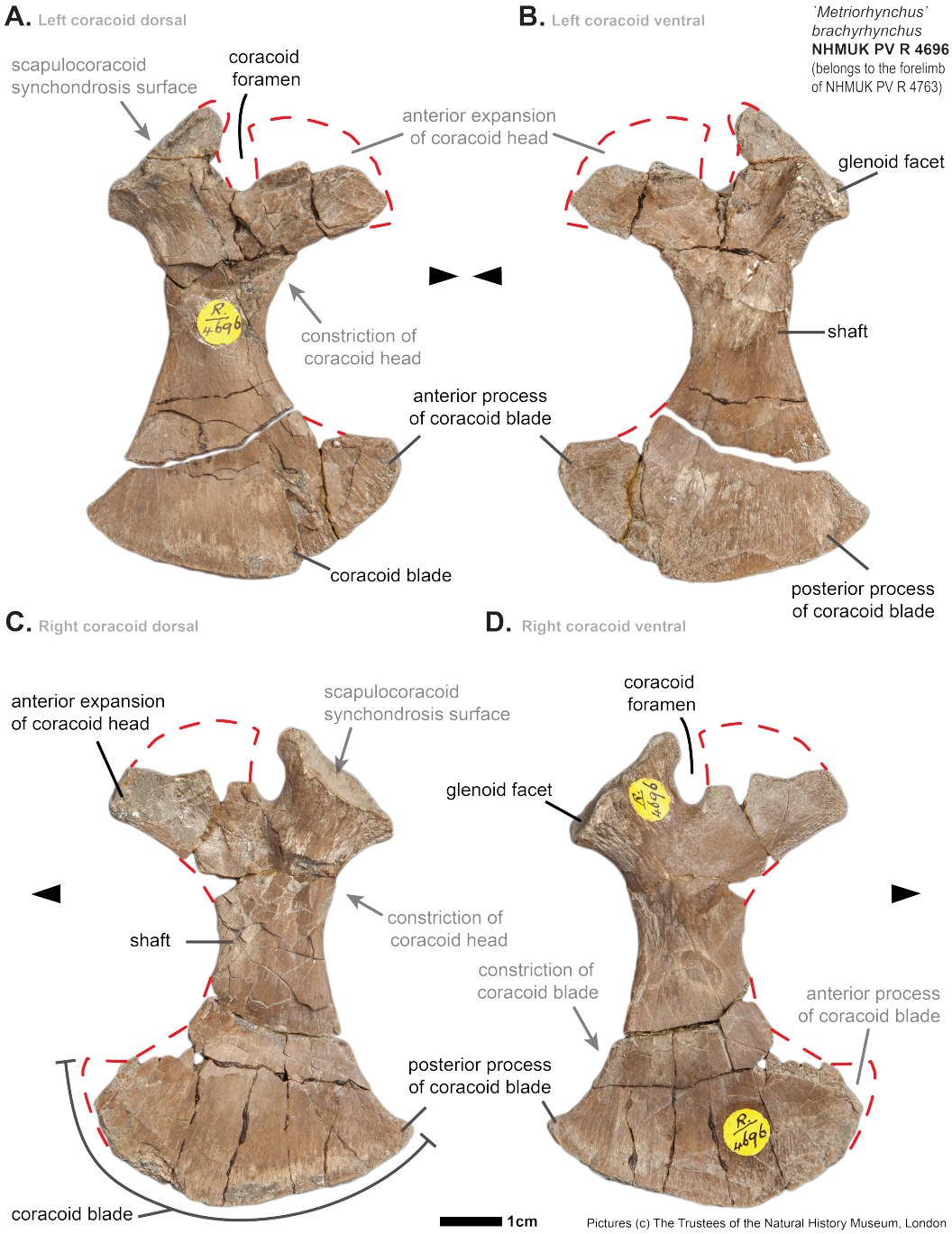


FIGURE 30. Pectoral girdle of *'Metriorhynchus'* NHMUK PV R 4696, forelimb of *'Metriorhynchus' brachyrhynchus* NHMUK PV R 4763 (photographs). **A.** Left coracoid in dorsal view ; **B.** Left coracoid in ventral view ; **C.** Right coracoid in dorsal view ; **D.** Right coracoid in ventral view. Arrow points anteriorly. Pictures (c) The Trustees of the Natural History Museum, London. Red dashed lines indicate missing parts. Reconstruction of missing parts based on *Thalattosuchus superciliosus* GLAHM V1146.

as in *Thalattosuchus*(GLAHM V1146 & NHMUK PV R 1530) and *G. leedsi* NHMUK PV R 3014. The ridge further divides the surface two sub-areas of differing orientation: the dorsal portion possesses a marked dorsal component in its orientation whereas the ventral one has a slight ventral orientation. In comparison, *Thalattosuchus* GLAHM V1146 & NHMUK PV R 1530 also have a similar configuration, although emphasized by their strong dorsoventral compaction. The overall outline of the scapulocoracoid synchondrosis surface of the coracoid of*'Me.' brachyrhynchus* NHMUK PV R 4696 is almond-shaped with convex dorsal and ventral margins and sharp anterior and posterior extremities. Hence it strongly differs from the triangular shape of the scapulocoracoid synchondrosis surface of the coracoid of other metriorhynchids with an open coracoid foramen (*e.g. Tyrannoneustes* GLAHM V1145, *G. leedsi* NHMUK PV R 3014, *Thalattosuchus* GLAHM V1146 & NHMUK PV R 1530).

Similar to other metriorhynchids with an open coracoid foramen, the glenoid facet of the coracoid of*'Me.' brachyrhynchus* NHMUK PV R 4696 is located posteroventrally with the scapulocoracoid synchondrosis surface lying dorsally to it (*e.g. Tyrannoneustes* GLAHM V1145, *G. leedsi* NHMUK PV R 3014, *Thalattosuchus* GLAHM V1146 & NHMUK PV R 1530). This contrasts with the more posteriorly positioned glenoid facet of metriorhynchids with a closed coracoid foramen (*e.g. D. maximus* SMNS 8203, *C. bambergensis* NKMB-P-Watt14/274, *C. suevicus* SMNS 9808, etc.). Overall, the glenoid facet of the coracoid of *'Me.' brachyrhynchus* NHMUK PV R 4696 is large as in most metriorhynchids with an open coracoid foramen except *G. leedsi* NHMUK PV R 3014, and displays a sub-circular outline as in most metriorhynchids with an open coracoid foramen except *Thalattosuchus* GLAHM V1146 & NHMUK PV R 1530 (in which it is more elliptic in shape). Most of the surface of the glenoid facet of the coracoid of*'Me.' brachyrhynchus* NHMUK PV R 4696 is concave, but becomes slightly convex over the anterior third. The junction between the glenoid facet and the scapulocoracoid synchondrosis surface of the coracoid of*'Me.' brachyrhynchus* NHMUK PV R 4696 only forms a subtle bulge as in *Tyrannoneustes* GLAHM V1145, whereas it forms a more prominent rim in *G. leedsi* NHMUK PV R 3014 and *Thalattosuchus* GLAHM V1146 & NHMUK PV R 1530. The outer margins of the glenoid facet of the coracoid of *'Me.' brachyrhynchus* NHMUK PV R 4696 form a thin rim as in most other metriorhynchids with an open coracoid foramen, but which contrasts with the thicker border observed in *G. leedsi* NHMUK PV R 3014. Due to singular shape of the scapulocoracoid synchondrosis surface of the coracoid of *'Me.' brachyrhynchus* NHMUK PV R 4696, the dorsoventrally thickest point of the coracoid does not exactly coincides with the longest axis of the glenoid facet, but is slightly shifted anteriorly. As in other metriorhynchids, the entire surface of the glenoid process of the coracoid of *'Me.' brachyrhynchus* NHMUK PV R 4696 is concave as it flares out to form the glenoid facet, which gives it a trumpet-shaped appearance.

The shaft of the coracoid of*'Me.' brachyrhynchus* NHMUK PV R 4696 is slender as the minimal anteroposterior width of the shaft at the constriction accounts for about 79% of the total mediolateral extension of the shaft. In comparison, this number reaches about 65-68% in *G. leedsi* NHMUK PVR R 3015 & NHMUK PV R 3014 respectively, about 74% in *Tyrannoneustes* GLAHM V1145, and about 88% in *Thalattosuchus* PMU 35988, GLAHM V1005, GLAHM V1146, & NHMUK PV R 1530. In addition, the mediolateral extension of the shaft of the coracoid of *'Me.' brachyrhynchus* NHMUK PV R 4696 accounts for 27% of the presumed total height of the coracoid. The slender appearance of the shaft of the coracoid of*'Me.' brachyrhynchus* NHMUK PV R 4696 is induced by the shape of its anterior and posterior margins: the anterior margin is markedly concave and almost semi-circular whereas the posterior margin displays a lesser degree of concavity. In addition, as in other metriorhynchids with an open coracoid foramen, the apex of each margin is aligned to one another which helps lengthen the extension of the shaft of the coracoid.

Medially, the shaft of the coracoid drastically flares out to form the coracoid blade. The latter strongly differs from the other metriorhynchids with an open coracoid foramen (*e.g. Tyrannoneustes* GLAHM

V1145, *G. leedsi* NHMUK PV R 3014, *Thalattosuchus* GLAHM V1146 & NHMUK PV R 1530) in displaying an asymmetrical silhouette. Indeed, the medial margin of the coracoid blade of '*Me.' brachyrhynchus* NHMUK PV R 4696 is markedly convex with its apex not centered but anteriorly shifted, which resembles what is observed in *C. bambergensis* NKMB-P-Watt14/274 among metriorhynchids. As a consequence, the degree of convexity of the anterior and posterior portions of the medial margin of the coracoid blade of '*Me.' brachyrhynchus* NHMUK PV R 4696 on each side of the apex is not similar, with the anterior portion displaying a proportionally greater degree of convexity. In parallel, the shape of the extremities of the coracoid blade are also dissimilar: the anterior corner is more prominent and thicker than the posterior corner. Furthermore, the anterior corner possesses a greater lateral component in its orientation than the posterior corner which appears to be mainly facing posteriorly. Overall, the anteroposterior extension of the coracoid blade mirrors that of the coracoid head, as in other metriorhynchids with an open coracoid foramen.

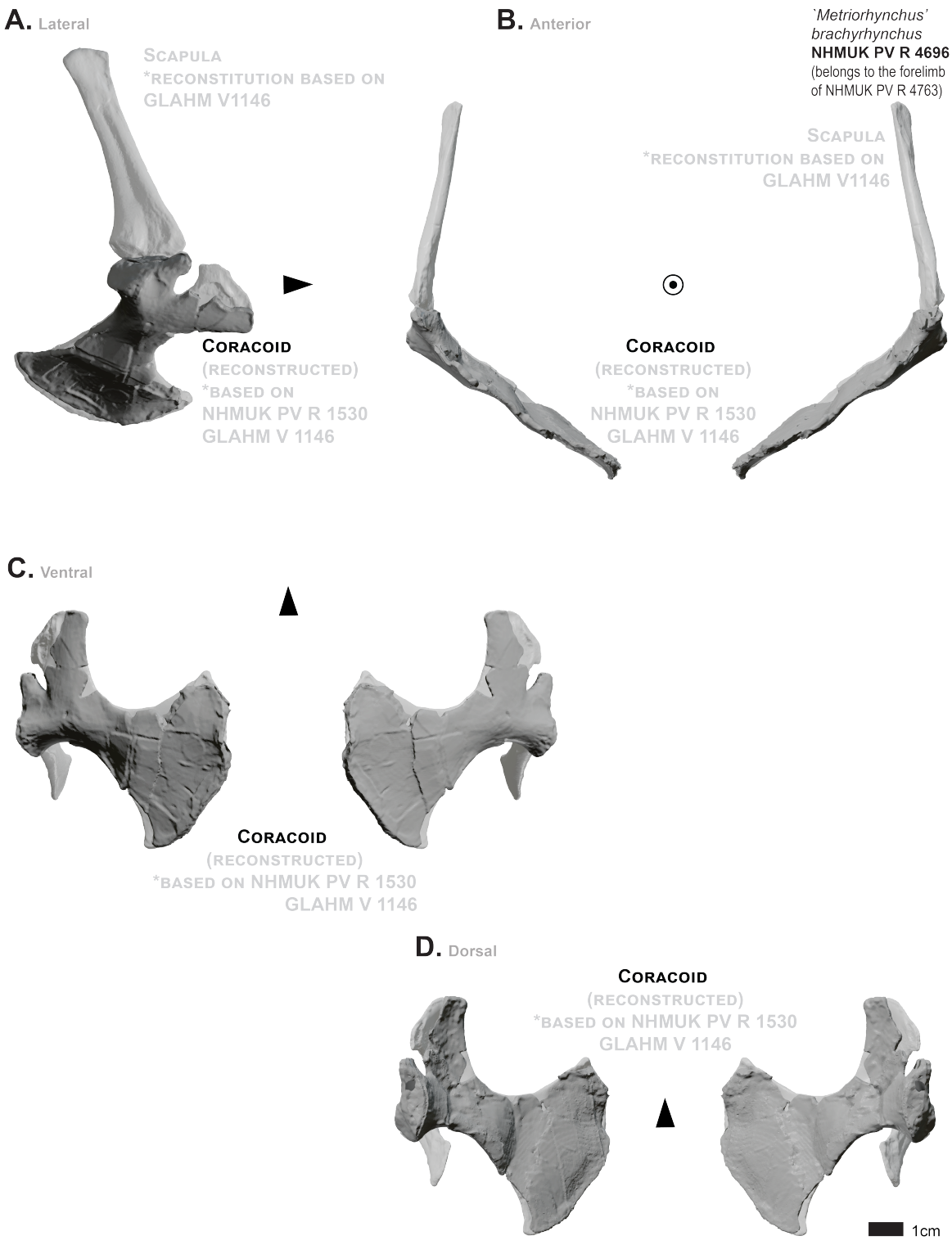


FIGURE 31. Reconstruction of the pectoral girdle of *'Metriorhynchus'* NHMUK PV R 4696 (3D models). **A.** Lateral view; **B.** Anterior view; **C.** Ventral view; **D.** Dorsal view. Arrow points anteriorly. Target indicates anterior. The right coracoid of *'Metriorhynchus'* NHMUK PV R 4696 is mirrored. The reconstitution of the scapula is based on *Thalattosuchus superciliosus* GLAHM V1146. Reconstruction of missing parts based on *Thalattosuchus superciliosus* GLAHM V1146.

7.11. ***Geosaurus lapparenti*** **Debelmas and Strannoloubsky, 1957.** For measurements, see table 6.

7.11.1. *Scapula.* The scapula of *Geosaurus lapparenti* UJF-ID.11847j & UJF-ID.11852f (see figs. 11, 32 and 33) displays a markedly concave posterior margin, as seen in other members of Geosaurini (*e.g. D. maximus* SMNS 8203, *To. carpenteri* BRSMG Cd7203, etc.). Indeed, both scapular remains still possess the apex of the posterior concavity, and can be overlapped to obtain the overall shape of the posterior margin (UJF-ID.11847j & UJF-ID.11852f, see fig. 32). Hence, the apex of the posterior margin – corresponding to the thinnest portion of the anteroposterior constriction of the shaft of the scapula – appears to be located at about 58% of the total proximodistal height of the scapula. This value contrasts with that of *D. maximus* SMNS 8203 (about 48%) and the rhacheosaurine *C. suevicus* SMNS 9808 (about 51%) which have their constriction more centered. Comparatively, the basal metriorhynchoid *Pelagosaurus* BRLSI M.1418 has the maximal constriction of the shaft of the scapula located even closer to its proximal head with around 41%.

The scapular blade of *Ge. lapparenti* UJF-ID.11852f appears to depart from that of other metriorhynchoids (*e.g. Pelagosaurus* BRLSI M.1418, *Thalattosuchus* GLAHM V1146, *C. suevicus* SMNS 9808, *D. maximus* SMNS 8203): its dorsal margin is not domed but is rather straight. Based on the preserved portion of & UJF-ID.11852f (about half of the scapular blade plus shaft width), the scapular blade reached about half of the total proximodistal height of the scapula. Comparatively, *Pelagosaurus* BRLSI M.1418 and *D. maximus* SMNS 8203 display similar values, whereas the scapular blade of *Thalattosuchus* GLAHM V1146 reaches about 21% and that of *C. suevicus* SMNS 9808 accounts for 62%. Posteriorly, the scapular blade of *Ge. lapparenti* UJF-ID.11852f appears to form a relatively blunt corner, not unlike what is observed in *D. maximus* SMNS 8203.

As in *D. maximus* SMNS 8203, the glenoid process of the scapula of *Ge. lapparenti* UJF-ID.11847j appears to protrude posteriorly, notably due to the high degree of concavity of the posterior margin as a whole. This strongly contrasts with the shorter glenoid process of rhacheosaurines (*e.g. C. albersdoerferi* BMMS-BK 1-2 and *C. suevicus* SMNS 9808), and the strongly prominent one of *Pelagosaurus* BRLSI M.1418. The glenoid facet of the scapula of *Ge. lapparenti* UJF-ID.11847j has an elliptic shape with the greater axis being anteroposteriorly oriented similarly to other metriorhynchoids (but differing from the more circular facet of teleosauroids). Hypothetically, the glenoid facet of the scapula of *Ge. lapparenti* UJF-ID.11847j reached at least 85% of the anteroposterior length of the scapulocoracoid synchondrosis surface, but its dorsal extremity is missing. The glenoid facet is tilted at an angle of about 60° from the ventral plane including the scapulocoracoid synchondrosis surface. The scapulocoracoid synchondrosis surface is located directly anteriorly to the glenoid facet. It displays a triangular outline as in other metriorhynchoids, and its anteroposterior length supposedly slightly exceeded the length of the glenoid facet. *D. maximus* SMNS 8203 and *To. carpenteri* BRSMG Cd7203 also show proportionally large glenoid facets, whereas it differs from the short glenoid facets of rhacheosaurines (*e.g. C. albersdoerferi* BMMS-BK 1-2 and *C. suevicus* SMNS 9808).

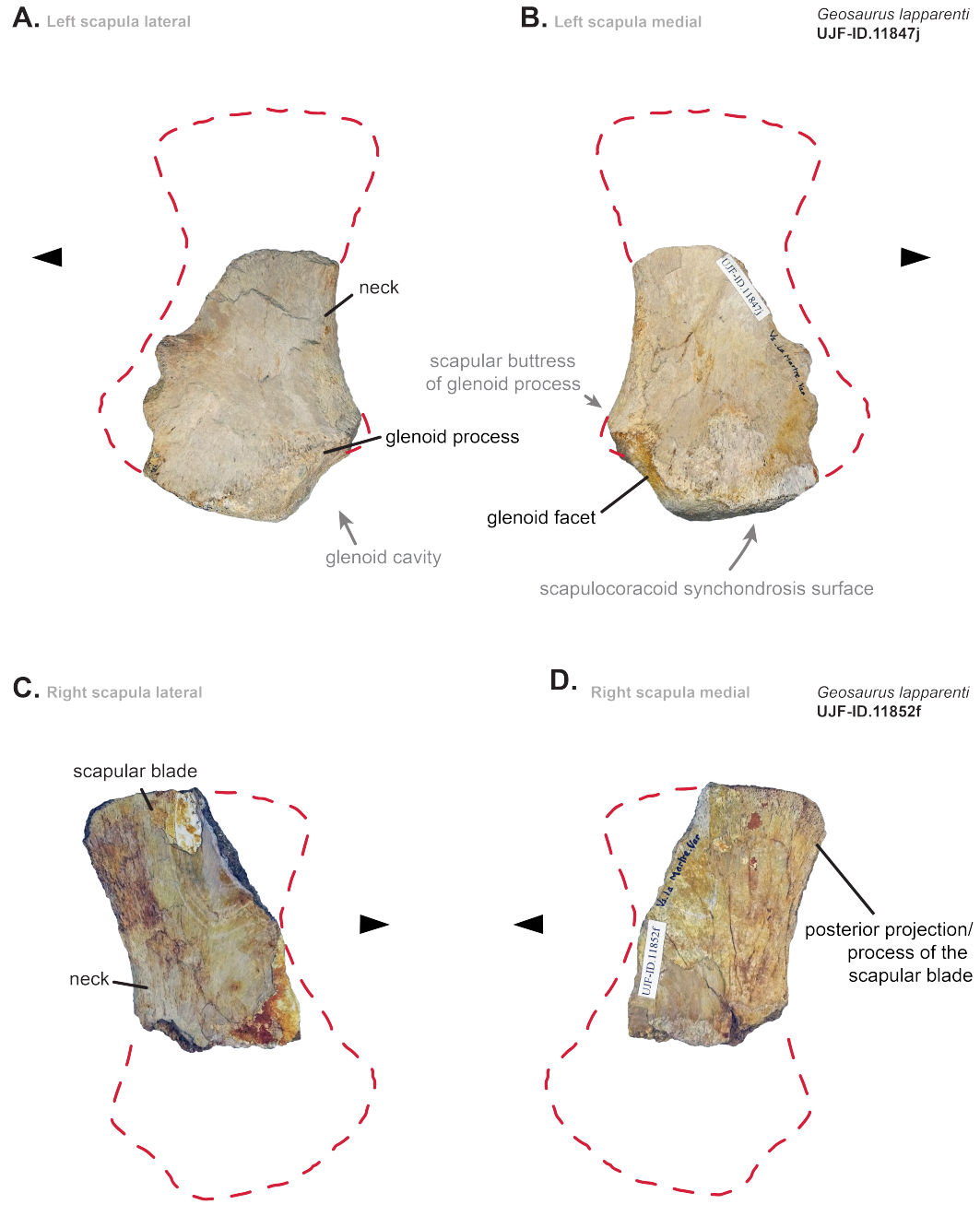


FIGURE 32. Pectoral girdle of *Geosaurus lapparenti* UJF-ID.11847j (A&B) and *Geosaurus lapparenti* UJF-ID.11852f (C&D) (photographs). **A.** Left scaoula in lateral view; **B.** Left scapula in medial view; **C.** Right scapula in lateral view; **D.** Right scapula in ledial view. Cross indicates posterior. Arrow points anteriorly. Red dashed lines indicate missing parts. Reconstruction of missing parts based on *Torvoneustes carpenteri* BRSMG Cd7203 and *Dakosaurus maximus* SMNS 8203.

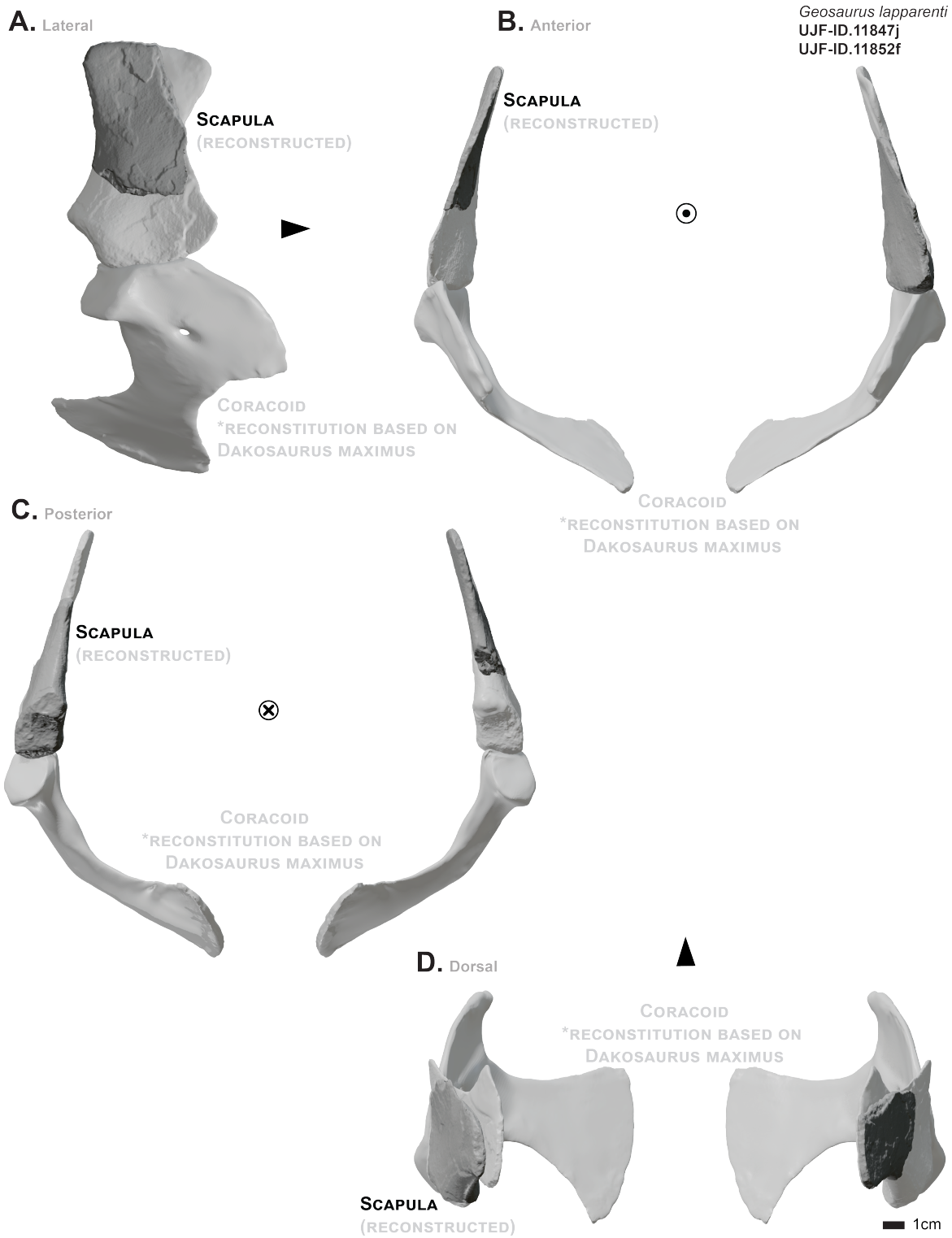


FIGURE 33. Reconstruction of the pectoral girdle of *Geosaurus lapparenti* UJF-ID.11847j & UJF-ID.11852f (3D models). **A.** Lateral view; **B.** Anterior view; **C.** Posterior view; **D.** Dorsal view. Arrow points anteriorly. Target indicates anterior. Cross indicates posterior. The reconstitution of the coracoid is putative and is based on *Torvoneustes carpenteri* BRSMG Cd7203 and *Dakosaurus maximus* SMNS 8203. Reconstruction of missing parts of the scapula is based on *Torvoneustes carpenteri* BRSMG Cd7203 and *Dakosaurus maximus* SMNS 8203.

7.12. ***Dakosaurus maximus* Plieninger, 1846.** For measurements, see tables 6 and 7.

7.12.1. *Scapula.* The scapula of *Dakosaurus maximus* SMNS 8203 (see figs. 11, 34 and 35) has an overall slender appearance, especially compared to rhacheosaurines (*e.g. C. albersdoerferi* BMMS-BK 1-2 and *C. suevicus* SMNS 9808) but also *Ge. lapparenti* (UJF-ID.11847j & UJF-ID.11852f) and *Dakosaurus sp.* DMA-JP-2009/001. Indeed, the anterior and posterior margins of the scapula of *D. maximus* SMNS 8203 are both markedly concave and strongly constrict the shaft of the scapula anteroposteriorly. However, the apexes of each margin are not aligned: the posterior margin has its apex located further ventrally than the anterior margin, resulting in the strong asymmetry of its concavity. In comparison, *To. carpenteri* BRSMG Cd7203 also appears to possess a relatively slender scapula, however, the degree of concavity of its posterior margin is lesser than that of *D. maximus* SMNS 8203.

The constriction of the shaft or neck of the scapula of *D. maximus* SMNS 8203 accounts for 57% of the total anteroposterior length of the proximal region of the bone (hence showing a reduction of almost half its length). The thinnest part of the constriction is located at around the mid proximodistal height of the scapula. Dorsally, the neck of the scapula strongly flares out to form the scapular blade. The latter appears to display uneven corners anteriorly and posteriorly, with the anterior corner appearing proportionally sharper. This difference is imputable to the positioning of the concavities of the anterior and posterior margins. The exact outline of the dorsal margin is unclear, but was presumably slightly domed as in other metriorhynchoids (*e.g. Pelagosaurus* BRLSI M.1418, *Thalattosuchus* GLAHM V1146, *C. suevicus* SMNS 9808, etc.). Presumably, the anteroposterior length of the scapular blade exceeded that of the proximal head, as both are equal with an incomplete scapular blade.

Ventrally, the neck of the scapula flares out (but less strongly than dorsally) to form the acromion process anteriorly and the glenoid process posteriorly. Both processes are not similar as the glenoid process is proportionally more prominent.

At about its mid-height, the acromion process of the scapula of *D. maximus* SMNS 8203 forms a sharp corner which points directly anteriorly. The acromion process is also about four times taller dorsoventrally than it is long anteroposteriorly. The dorsal margin of the acromion process (*i.e.* dorsal to the anterior corner) is slightly concave, whereas its ventral margin is subtly convex (unlike that of *To. carpenteri* BRSMG Cd7203). The overall pointed shape of the acromion process of the scapula of *D. maximus* SMNS 8203 is only found in other metriorhynchids within Thalattosuchia (*e.g. Thalattosuchus* GLAHM V1146, *Thalattosuchus* PMU 35988, *C. albersdoerferi* BMMS-BK 1-2, *C. suevicus* SMNS 9808, *To. carpenteri* BRSMG Cd7203). The acromion process does not bear an acromial crest laterally similarly to other more derived metriorhynchids. However, the acromion process of the scapula of *D. maximus* SMNS 8203 constitutes a blade-like process as it corresponds to the thinnest portion of the proximal head mediolaterally. Furthermore, the acromion process of the scapula of *D. maximus* SMNS 8203 is slightly curved outward (*i.e.* laterally), creating a shallow depression (as in *To. carpenteri* BRSMG Cd7203) which could be associated with the scapular fossa.

In *D. maximus* SMNS 8203, the total length of the ventral margin of the acromion process is similar to that of the scapulocoracoid synchondrosis surface, but both are shorter – they account for about 80% – than that of the glenoid facet. In rhacheosaurines (*e.g. C. albersdoerferi* BMMS-BK 1-2 and *C. suevicus* SMNS 9808), the scapulocoracoid synchondrosis surface is anteroposteriorly longer than the acromion process or glenoid facet. The articular facet of the glenoid process of the scapula of *D. maximus* SMNS 8203 forms an angle of about 45° with the ventral plane whereas the acromion process is tilted of about 60°. The dorsal corner of the glenoid process, marking the junction between the dorsal margin of the glenoid process and the glenoid facet, is sharp and forms an angle of about 107°. In addition, the glenoid process of the scapula of *D. maximus* SMNS 8203 is strongly prominent as in other geosaurines (*e.g. Ge. lapparenti* UJF-ID.11847j & UJF-ID.11852f and *To. carpenteri* BRSMG Cd7203 among metriorhynchoids).

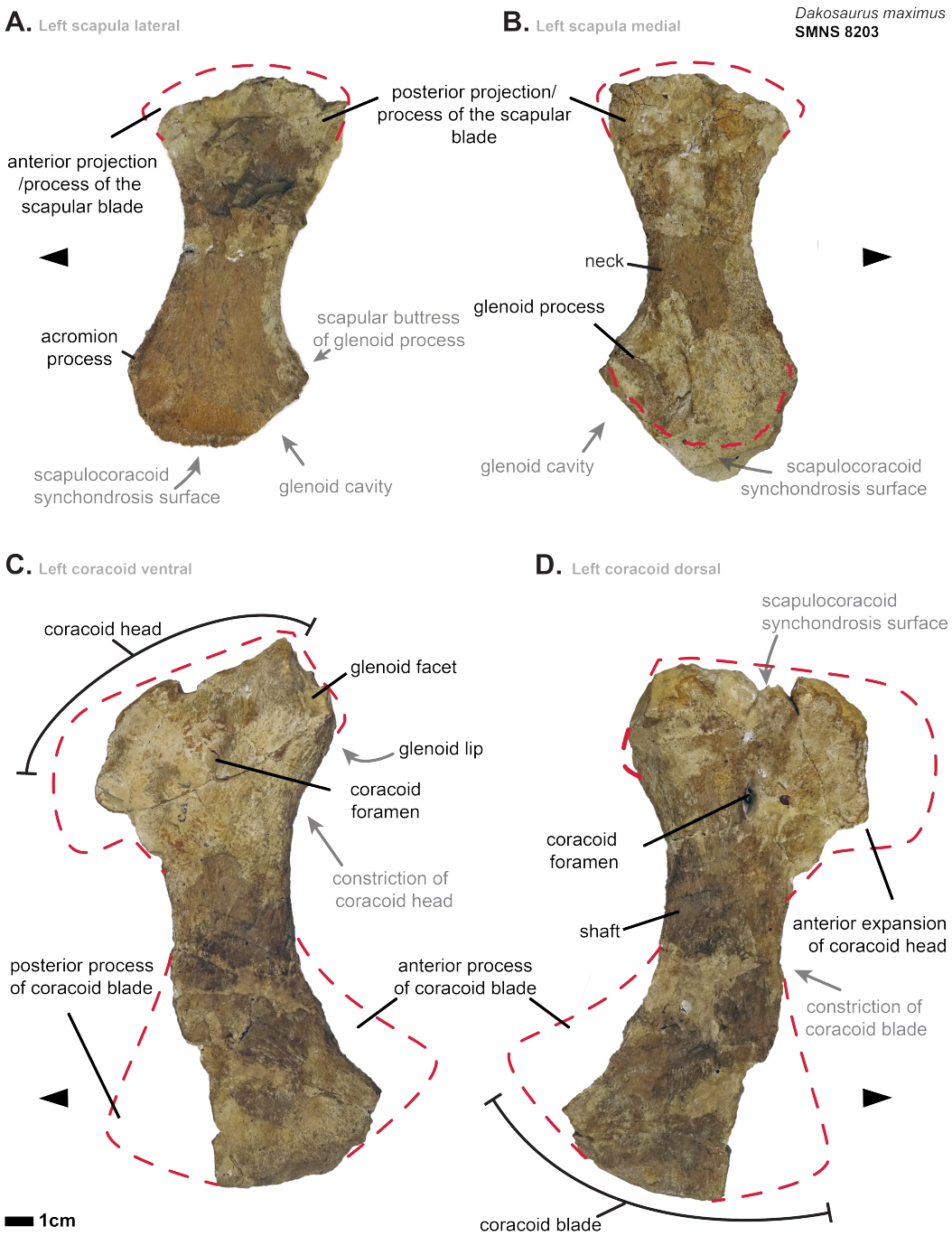


FIGURE 34. Pectoral girdle of *Dakosaurus maximus* SMNS 8203 (photographs). **A.** Left scapula in lateral view ; **B.** Left scapula in medial view ; **C.** Left coracoid in ventral view ; **D.** Left coracoid in dorsal view. Cross indicates posterior. Arrow points anteriorly. Red dashed lines indicate missing parts. Reconstruction of missing parts based on *Dakosaurus sp.* DMA-JP-2009/001.

7.12.2. *Coracoid.* The coracoid of *D. maximus* SMNS 8203 is fragmentary but possesses a closed coracoid foramen similar to rhacheosaurine taxa. Compared to *Dakosaurus sp.* DMA-JP-2009/001, the coracoid of *D. maximus* SMNS 8203 shows a greater mediolateral extension, due to a proportionally more elongated shaft.

The coracoid of *D. maximus* SMNS 8203 (see figs. 12 and 34) possesses a large head (as in *Dakosaurus sp.* DMA-JP-2009/001 and *Dakosaurus sp.* Rygol specimen) which contrasts with the other Geosaurinae taxa'*Me.' brachyrhynchus* NHMUK PV R 4696 and *Tyrannoneustes* GLAHM V1145. Indeed, the coracoid foramen of *D. maximus* SMNS 8203 is closed and forms a small elliptic aperture whose longest axis is overall oriented in the mediolateral direction. The coracoid foramen of *D. maximus* SMNS 8203 is overall located near the base of the shaft of the coracoid (as in *Cricosaurus* species), but its exact positions slightly differ on the ventral and dorsal surfaces as it forms a tilted canal. In comparison, *C. albersdoerferi* BMMS-BK 1-2 and *C. suevicus* SMNS 9808 also bear a small coracoid foramen but its shape appear proportionally more circular than in *D. maximus* SMNS 8203.

The posterior portion of the coracoid head of *D. maximus* SMNS 8203 – the glenoid process – corresponds to the dorsoventrally thickest area of the bone as it bears the glenoid facet. Indeed, it reaches about 6 times the thickness of the anterior expansion of the coracoid head, which markedly exceeds what is observed in metriorhynchids with an open coracoid foramen. The glenoid facet of the coracoid of *D. maximus* SMNS 8203 appears to form a large sub-circular surface positioned at the posterior extremity of the coracoid head. The orientation of the glenoid facet of the coracoid of *D. maximus* SMNS 8203 is mainly posterior as in *C. bambergensis* NKMB-P-Watt14/274, with a small ventral component as it can be observed on the ventral surface of the coracoid. It is possible that the glenoid facet of the coracoids of the different *Cricosaurus* species bore a similar orientation before the compaction. The anterior expansion of the coracoid head of *D. maximus* SMNS 8203, although not complete, forms a dorsoventrally thin blade. The latter corresponds to the dorsoventrally thinnest portion of the coracoid, and is even finer than the preserved portion of the coracoid blade (which is the apex of its convexity). The consequent dorsoventral widening of the coracoid blade to form the glenoid process also results in a large scapulocoracoid synchondrosis surface, which appears to display the approximative silhouette of an isosceles triangle (with the median oriented anteroposteriorly). However, the exact outline of the scapulocoracoid synchondrosis surface of the coracoid of *D. maximus* SMNS 8203 is not clearly observable due to rock matrix still being adherent.

Medially to the coracoid head, the shaft of the coracoid of *D. maximus* SMNS 8203 appears to be short and thin which is similar to what is observed on the coracoids of *C. albersdoerferi* BMMS-BK 1-2, *C. araucanensis* MLP 72-IV-7-1 and also *C. suevicus* SMNS 9808. Yet, the exact extent of the shaft of the coracoid of *D. maximus* SMNS 8203 is unknown due to poorly preserved anterior and posterior margins. Likewise, the exact shape and extension of the coracoid blade of *D. maximus* SMNS 8203 cannot be assessed. However, as in other thalattosuchians, the coracoid markedly slims down dorsoventrally from the coracoid head towards the coracoid blade.

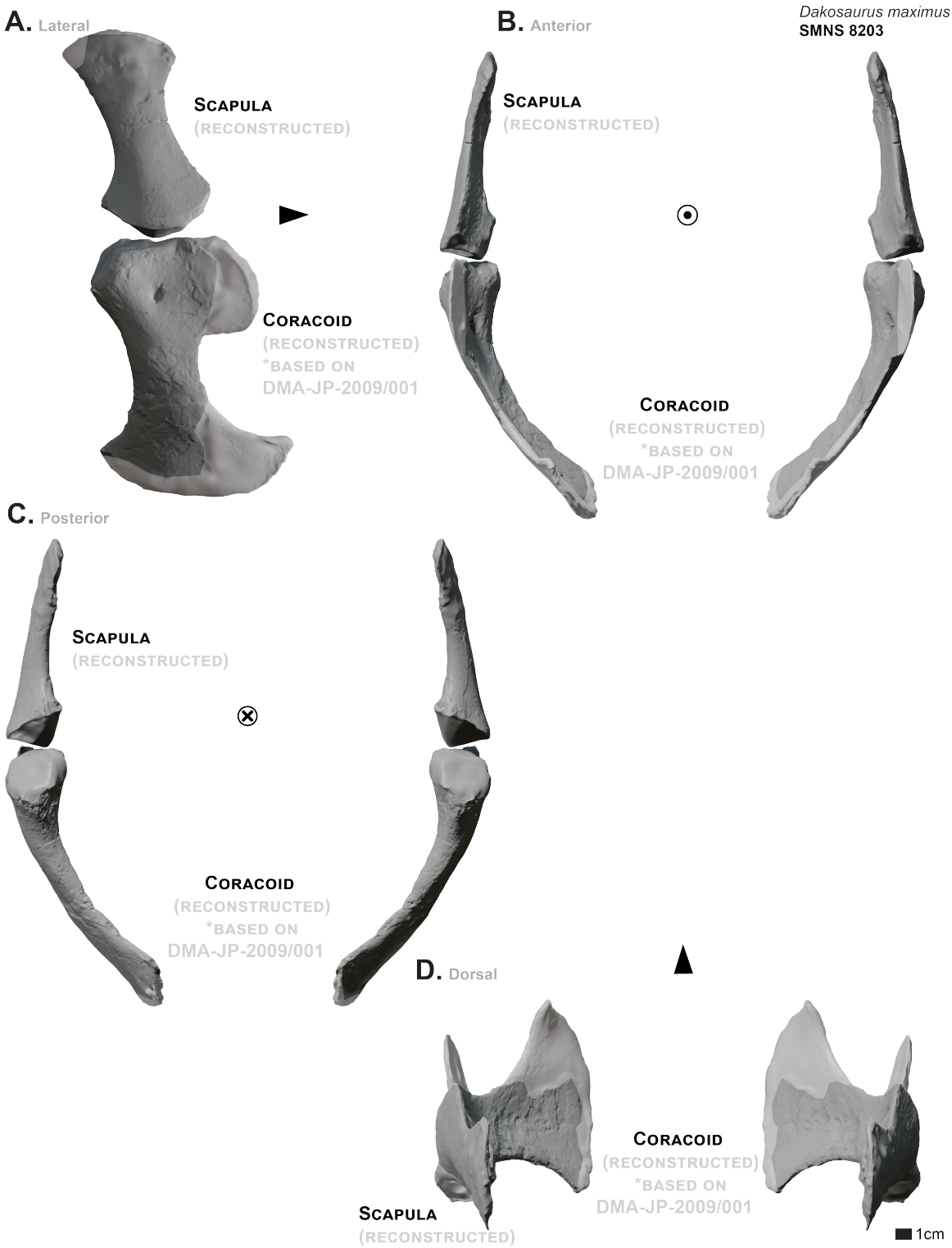


FIGURE 35. Reconstruction of the pectoral girdle of *Dakosaurus maximus* SMNS 8203 (3D models). **A.** Lateral view; **B.** Anterior view; **C.** Posterior view; **D.** Dorsal view. Arrow points anteriorly. Target indicates anterior. Cross indicates posterior. The reconstitution of the coracoid is putative and is based on *Dakosaurus sp.* DMA-JP-2009/001.

7.13. ***Tyrannoneustes lythrodectikos*** **Young et al., 2012.** For measurements, see table 7.

7.13.1. *Coracoid.* The coracoid of *Tyrannoneustes lythrodectikos* GLAHM V1145 Young et al., 2012 (see figs. 12, 36 and 37) possesses the following distinct combination of features: an open and wide coracoid foramen, a slender shaft with a narrow constriction, a sub-circular glenoid facet, and a relatively symmetrical coracoid blade. The exact extension and shape of the anterior expansion of the coracoid head is not observable.

The coracoid head of *Tyrannoneustes* GLAHM V1145 (see fig. 36) displays a laterally open coracoid foramen which participates in the lateral outline of the bone, similar to several metriorhynchids (*e.g. Thalattosuchus* GLAHM V1005, GLAHM V1146, PMU 35988, & NHMUK PV R 1530, *G. leedsi* NHMUK PV R 3014, and *'Me.' brachyrhynchus* NHMUK PV R 4696). In *Tyrannoneustes* GLAHM V1145, the coracoid foramen forms an anteroposteriorly wide and mediolaterally deep perforation which resembles that of *Thalattosuchus* (GLAHM V1005, GLAHM V1146, PMU 35988, & NHMUK PV R 1530) the most among metriorhynchids with an open coracoid foramen. Indeed, the mediolateral depth of the aperture of the coracoid foramen of *Tyrannoneustes* GLAHM V1145 reaches about 14% of the total mediolateral extension of the coracoid, which is similar to what is observed in *Thalattosuchus* (14.5–16% in NHMUK PV R 1530, GLAHM V1005 and GLAHM V1146) but contrasts with the lower value of *'Me.' brachyrhynchus* NHMUK PV R 4696 (10.6%) and *G. leedsi* NHMUK PV R 3014 (8.37%). The large perforation formed by the coracoid foramen divides the coracoid head into two distinct areas: the posterior portion of the coracoid head bears the scapulocoracoid synchondrosis surface an glenoid process, whereas the anterior expansion forms a proportionally large blade. Similar to other metriorhynchids with an open coracoid foramen, the scapulocoracoid synchondrosis surface of the coracoid of *Tyrannoneustes* GLAHM V1145 constitutes the majority of the anteroposterior length of the posterior portion of the coracoid head as it accounts for about 91% of the total. In comparison, this value reaches 95% in *'Me.' brachyrhynchus* NHMUK PV R 4696, 98% in *G. leedsi* NHMUK PV R 3014, and ranges from 78% to 82 % in *Thalattosuchus* (GLAHM V1005 and GLAHM V1146 respectively). As in *G. leedsi* NHMUK PV R 3014 and *Thalattosuchus* GLAHM V1005 & GLAHM V114, the scapulocoracoid synchondrosis surface of the coracoid of *Tyrannoneustes* GLAHM V1145 displays the outline of a scalene triangle, whose hypotenuse lies along the dorsal side of the bone. The scapulocoracoid synchondrosis surface of the coracoid met with that of the scapula *in vivo* and hence was presumably covered in cartilaginous structures. Consequently, the entire surface of the scapulocoracoid syncondrosis is uneven and scarred. In *Tyrannoneustes* GLAHM V1145, the scapulocoracoid synchondrosis surface shows a slight ridge along its main axis (anteroposterior), which divides the area into two sub-portions. The dorsal sub-portion of the scapulocoracoid synchondrosis surface shows deeper scars and hence bears an overall more concave surface than the ventral sub-portion. Such a difference in relief over the scapulocoracoid synchondrosis surface is also observed on *Thalattosuchus* GLAHM V1146 & NHMUK PV R 1530, *G. leedsi* NHMUK PV R 3014, and *'Me.' brachyrhynchus* NHMUK PV R 4696. However, as in *Thalattosuchus* GLAHM V1005, there is no major differences in the orientation of both sub-portions of the scapulocoracoid synchondrosis surface of the coracoid of *Tyrannoneustes* GLAHM V1145 as both appear relatively planar, except for the smooth ridge along the greater axis. In *Tyrannoneustes* GLAHM V1145, the junction between the scapulocoracoid synchondrosis surface and the glenoid facet forms a well-defined but rather blunt corner without any prominent ridge. In this way, it departs from the smooth bulged transition observed in *Thalattosuchus* GLAHM V1005 & NHMUK PV R 1530, *G. leedsi* NHMUK PV R 3014 and *'Me.' brachyrhynchus* NHMUK PV R 4696.

The glenoid facet of the coracoid of *Tyrannoneustes* GLAHM V1145 possesses a sub-circular shape as well as a smoothly concave surface, as in *'Me.' brachyrhynchus* NHMUK PV R 4696 and *G. leedsi* NHMUK PV R 3014. Ventrally, the glenoid facet of the coracoid of *Tyrannoneustes* GLAHM V1145 is

bordered by a thin margin similar to *Thalattosuchus* (GLAHM V1005, GLAHM V1146, PMU 35988, and NHMUK PV R 1530) and *'Me.' brachyrhynchus* NHMUK PV R 4696, but differing from *G. leedsi* NHMUK PV R 3014. The glenoid facet of the coracoid of *Tyrannoneustes* GLAHM V1145 is positioned posteroventrally on the coracoid head, and the scapulocoracoid synchondrosis surface noticeably extends dorsally to it, which is similar to other metriorhynchids with an open coracoid foramen but seemingly contrasts with metriorhynchids with a closed coracoid foramen . Indeed, *Cricosaurus* species (*e.g. C. albersdoerferi* BMMS-BK 1-2, *C. bambergensis* NKMB-P-Watt14/274, *C. suevicus* SMNS 9808, *C. araucanensis* MLP 72-IV-7-1) and *D. maximus* SMNS 8203 (plus *Dakosaurus sp.* DMA-JP-2009/001 and Rygol specimen) possess a more posteriorly positioned and oriented glenoid facet which presumably hampers a lengthy extension of the scapulocoracoid synchondrosis surface dorsally to it (as in *Pelagosaurus* BRLSI M.1418 and *Turnersuchus* LRM 2021/45. In *Tyrannoneustes* GLAHM V1145, the glenoid facet faces mainly posteriorly with a small ventral and lateral components as well, which is similar to other metriorhynchids with an open coracoid foramen. As in other metriorhynchoids, the glenoid facet of the coracoid of *Tyrannoneustes* GLAHM V1145 corresponds to the dorsoventrally thickest point of the coracoid. Indeed, the coracoid head markedly increases in dorsoventral thickness posteriorly to form the glenoid facet; this portion of the coracoid head constitutes the glenoid process. As in other metriorhynchids with an open coracoid foramen, the entire ventral surface of glenoid process is concave and hence displays trumpet-like appearance as it flares out laterally to form the glenoid facet.

Similar to other metriorhynchids, the anterior and posterior margins of the coracoid of *Tyrannoneustes* GLAHM V1145 are strongly concave with the anterior margin displays a greater degree of curvature. Yet, the degree of concavity of the anterior margin of the coracoid of *Tyrannoneustes* GLAHM V1145 do not reach the levels observed in metriorhynchids with a closed coracoid foramen (*e.g. C. albersdoerferi* BMMS-BK 1-2, *C. bambergensis* NKMB-P-Watt14/274, *C. suevicus* SMNS 9808, *C. araucanensis* MLP 72-IV-7-1, and *D. maximus* SMNS 8203, plus *Dakosaurus sp.* DMA-JP-2009/001 and Rygol specimen). In *Tyrannoneustes* GLAHM V1145, the apex of the concavity of the anterior and posterior margins are aligned, which enables relatively slender shaft: the minimal anteroposterior width of the shaft of the coracoid at the constriction accounts for about 74% of total mediolateral extension of coracoid shaft. In comparison, this number reaches about 79% in *'Me.' brachyrhynchus* NHMUK PV R 4696, 65–68% in *G. leedsi* NHMUK PV R 3014 & NHMUK PV R 3015, and about 88% in *Thalattosuchus* GLAHM V1005, GLAHM V1146, PMU 35988, and NHMUK PV R 1530. Also, in *Tyrannoneustes* GLAHM V1145, the mediolateral extension of the shaft of the coracoid accounts for around one–fourth of total height of coracoid similar to *Thalattosuchus* GLAHM V1005, GLAHM V1146, & NHMUK PV R 1530 and *G. leedsi* NHMUK PV R 3014, but slightly lesser than in *'Me.' brachyrhynchus* NHMUK PV R 4696 (about 27.6%). Despite being dorsoventrally flattened, the coracoid of *Tyrannoneustes* GLAHM V1145 stills displays signs of its original shape: it appears ventrally curved with slight twisting of the coracoid head in relation to the shaft of the coracoid. It is possible that the coracoid blade also presented a relative dorsoventral inclination.

Medially, the shaft of the coracoid of *Tyrannoneustes* GLAHM V1145 gradually flares out to form the coracoid blade, with a more pronounced anterior expansion due to the marked concavity of this margin. However, the coracoid blade of *Tyrannoneustes* GLAHM V1145 possesses a strongly balanced silhouette mainly due to the symmetrically convex shape of the medial margin. Indeed, the apex of the convexity, which corresponds to the inflexion point, is centered on the midpoint of the margin and both sides display a similar curvature. As a consequence, the anterior and posterior extremities of the coracoid blade appear enantiomorphic: their outline is analogous with a convex medial margin and a concave lateral one, and both display an almost identical interior angle. Furthermore, both corners possess a similar inclination with a marked lateral component in their orientation. In this way, the outline of the coracoid blade of

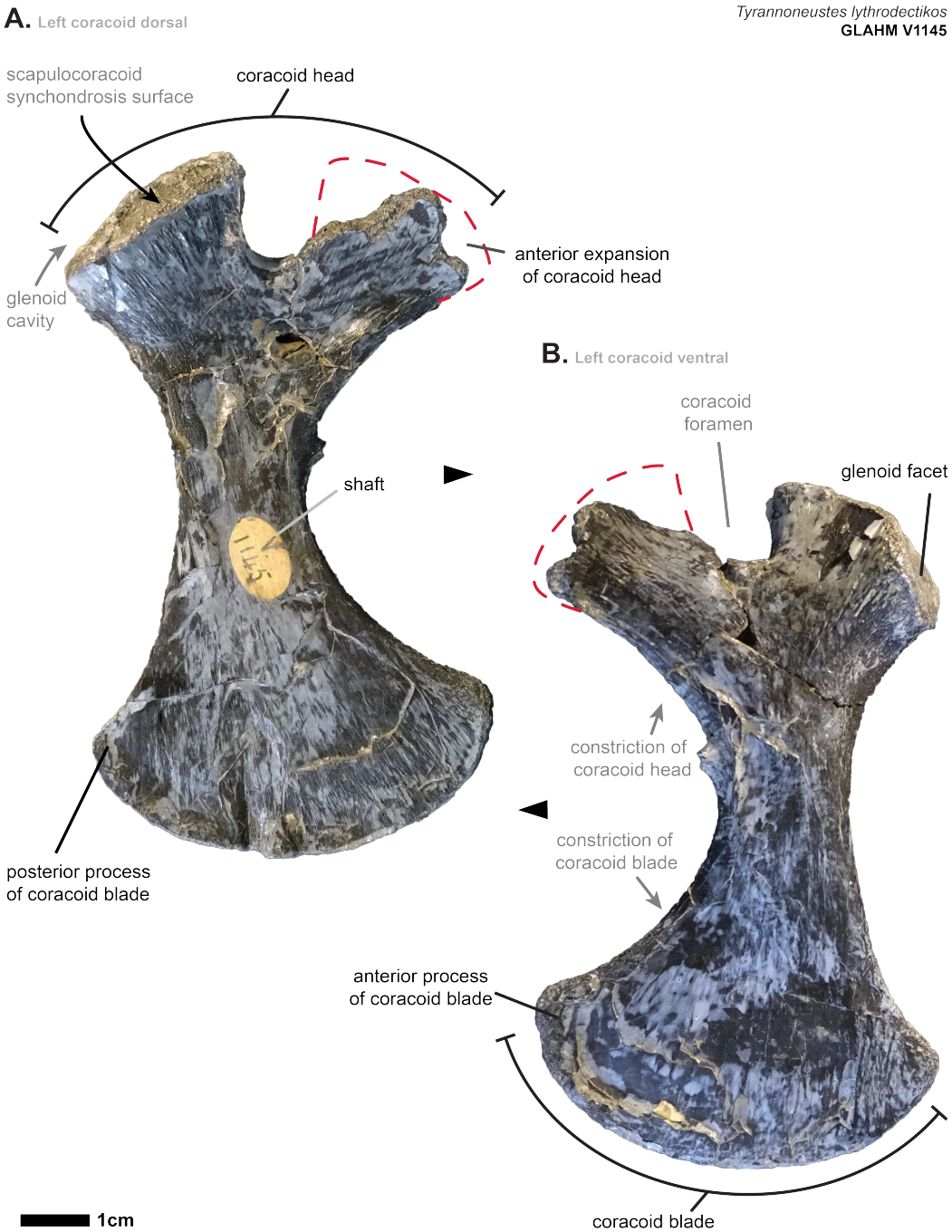


FIGURE 36. Pectoral girdle of *Tyrannoneustes lythrodectikos* GLAHM V1145 (photographs). **A.** Left coracoid in dorsal view ; **B.** Left coracoid in ventral view. Arrow points anteriorly. Red dashed lines indicate missing parts. Reconstruction of missing parts based on *Thalattosuchus superciliosus* GLAHM V1146.

Tyrannoneustes GLAHM V1145 mildly differs from *Thalattosuchus* PMU 35988 and *G. leedsi* NHMUK PV R 3014, but strongly opposes *'Me.' brachyrhynchus* NHMUK PV R 4696.

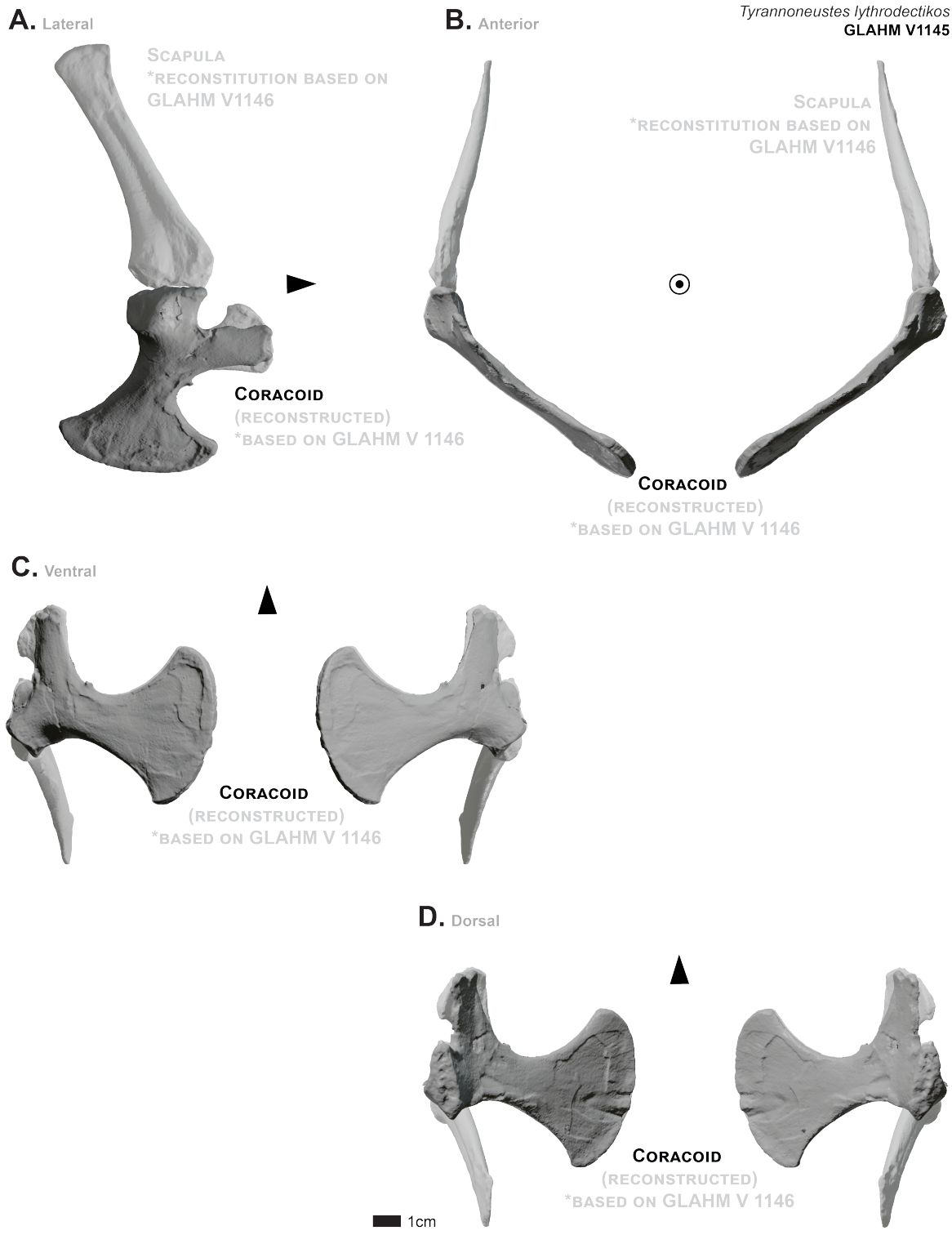


FIGURE 37. Reconstruction of the pectoral girdle of *Tyrannoneustes lythrodectikos* GLAHM V1145 (3D models). **A.** Lateral view; **B.** Anterior view; **C.** Ventral view; **D.** Dorsal view. Arrow points anteriorly. Target indicates anterior. The right coracoid of *Tyrannoneustes* GLAHM V1145 is mirrored. The reconstitution of the scapula is based on *Thalattosuchus superciliosus* GLAHM V1146. Reconstruction of missing parts based on *Thalattosuchus superciliosus* GLAHM V1146.

7.14. ***Torvoneustes carpenteri* Wilkinson et al., 2008.** For measurements, see table 6.

7.14.1. *Scapula.* The scapula of *Torvoneustes carpenteri* BRSMG Cd7203 (see figs. 11, 38 and 39) appears to be relatively slender with a gently concave posterior margin. The latter also seems to be overall symmetrical with its apex located somewhere around the potential mid-height of the bone. Among metriorhynchoids, *Thalattosuchus* GLAHM V1146 and *D. maximus* SMNS 8203 also displayed relatively slender scapulae.

Ventrally, the posterior margin of the scapula of *To. carpenteri* BRSMG Cd7203 gently flares out to form the glenoid process. Indeed, the glenoid process of scapula of *To. carpenteri* BRSMG Cd7203 does not appear to markedly protrude posteriorly due to the low degree of concavity of the posterior margin, as in *C. suevicus* SMNS 9808 and *Ge. lapparenti* UJF-ID.11847j. The articular facet of the glenoid process of the scapula of *To. carpenteri* BRSMG Cd7203 is set at an angle of about 45° with the plane defined by the scapulocoracoid synchondrosis surface, as in *D. maximus* SMNS 8203 among metriorhynchoids. The outline of the glenoid facet of the scapula of *To. carpenteri* BRSMG Cd7203 appears bulged, mainly due to a recessed area surrounding the border of the facet on the dorsal side. Along the posterior margin of the glenoid process, and dorsal to the recess, is a small bump. The latter is not pronounced enough to be defined as a tubercle. The glenoid facet is overall elliptic and presents a slightly concave surface as in other metiorhynchoids.

The scapulocoracoid synchondrosis surface is adjacent to and positioned posteriorly the glenoid facet. Its shape is triangular as it strongly thins down mediolaterally towards the blade-like acromion process. In *To. carpenteri* BRSMG Cd7203, the scapulocoracoid synchondrosis surface reaches around 40% of the total anteroposterior length of the proximal region of the scapula, which is similar to the value found in *D. maximus* SMNS 8203, but shorter than in *Thalattosuchus* GLAHM V1146, *Thalattosuchus* PMU 35988, *C. albersdoerferi* BMMS-BK 1-2, and *C. suevicus* SMNS 9808. This effect is presumably imputable to the proportionally more developed acromion process of the scapula of *D. maximus* SMNS 8203 and *To. carpenteri* BRSMG Cd7203. Similarly to other metriorhynchids, the acromion process of the scapula of *To. carpenteri* BRSMG Cd7203 is devoid of an acromial crest on its lateral surface. As for *D. maximus* SMNS 8203, the acromion process of the scapula of *To. carpenteri* BRSMG Cd7203 is mediolaterally thin like a blade, and is slightly curved towards the lateral side. This also results in a shallow recessed area on the lateral surface of the acromion process which ends at the base of the glenoid process (where the mediolateral thickening of the scapula is the longest). This recessed area could be associated with the scapular fossa.

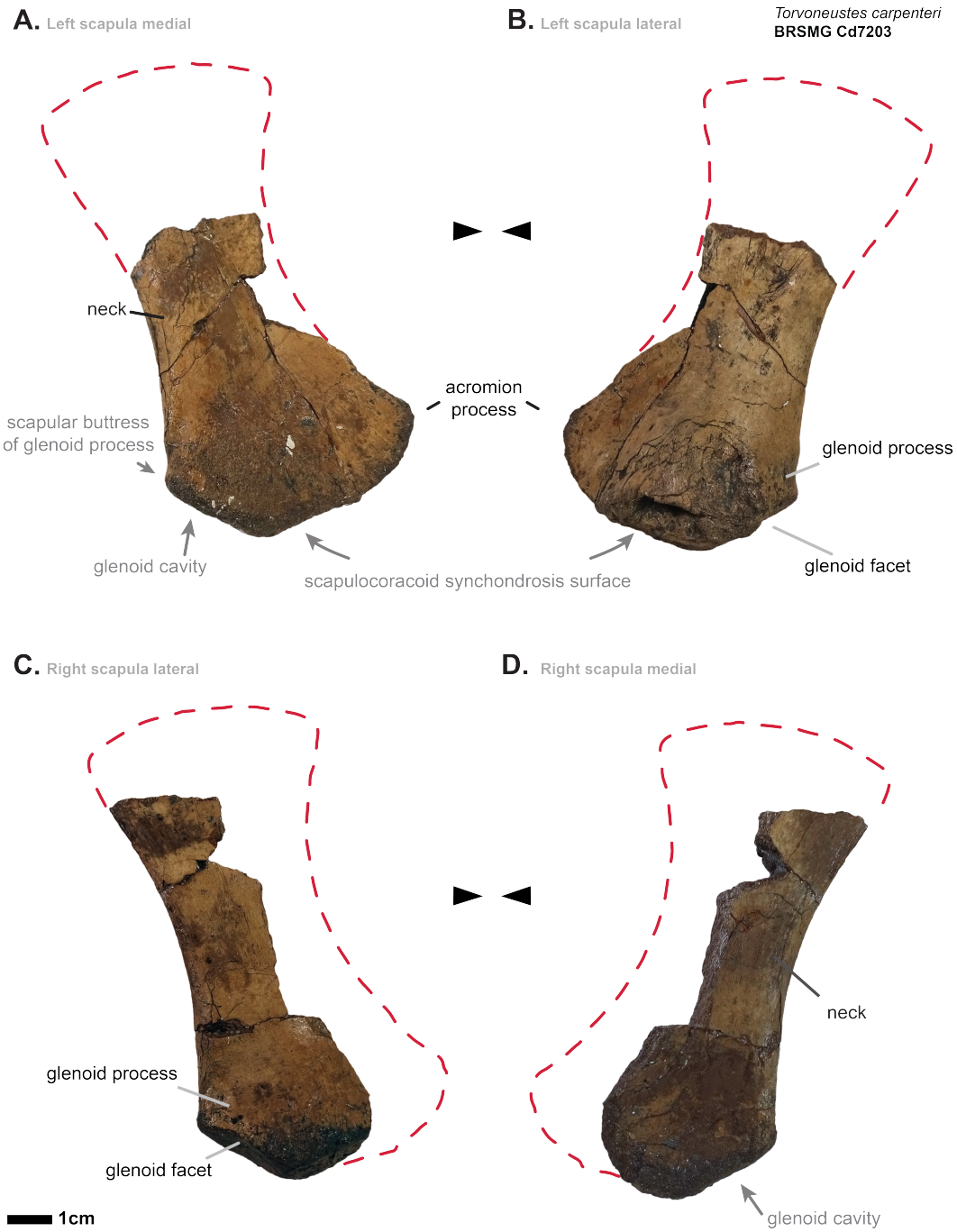


FIGURE 38. Pectoral girdle of *Torvoneustes carpenteri* BRSMG Cd7203 (photographs). **A.** Left scapula in medial view ; **B.** Left scapula in lateral view ; **C.** Right scapula in lateral view ; **D.** Right scapula in medial view. Arrow points anteriorly. Red dashed lines indicate missing parts. Reconstruction of missing parts based on *Dakosaurus maximus* SMNS 8203.

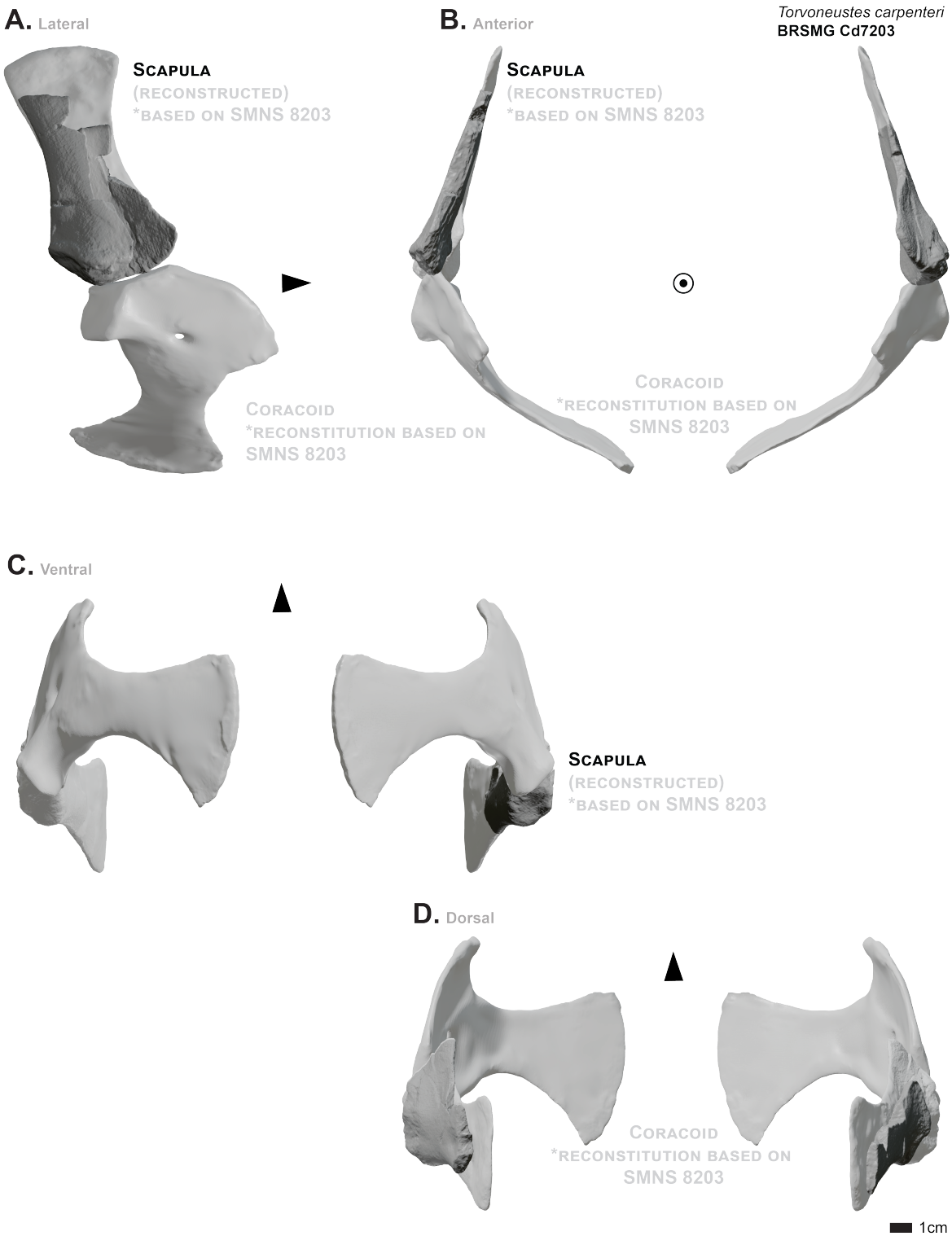


FIGURE 39. Reconstruction of the pectoral girdle of *Torvoneustes carpenteri* BRSMG Cd7203 (3D models). **A.** Lateral view; **B.** Anterior view; **C.** Ventral view; **D.** Dorsal view. Arrow points anteriorly. Target indicates anterior. Both the right and left fragments of the scapula of *To. carpenteri* BRSMG Cd7203 were combined to build the reconstructed version. The reconstitution of the coracoid is putative and is based on *Dakosaurus maximus* SMNS 8203. Reconstruction of missing parts based on *Dakosaurus maximus* SMNS 8203.

8. THE APPENDICULAR SKELETON OF THALATTOSUCHIANS: TELEOSAUROIDS

8.1. ***Mycterosuchus nasutus* Andrews, 1913.** For measurements, see tables 6 and 7.

8.1.1. *Scapula.* The scapula of *Mycterosuchus nasutus* NHMUK PV R 2617 (see figs. 40 and 41) strongly contrasts with that of metriorhynchoids in showing a laterally positioned glenoid facet and subsequently elongated scapulocoracoid synchondrosis surface running medially to the glenoid facet of the scapula. The scapula of *Mycterosuchus* NHMUK PV R 2617 has an overall slender appearance due to its proportionally elongated neck, and anteroposteriorly limited scapular blade and proximal head, as in *Thalattosuchus* GLAHM V1146, *Charitomenosuchus* NHMUK PV R 3806, *Neosteneosaurus* NHMUK PV R 3701 & PETMG R178 and *Lemmysuchus* NHMUK PV R 3168.

The anterior margin of the scapula of *Mycterosuchus* NHMUK PV R 2617 is s-shaped, with the dorsal portion being markedly concave before switching to a convex shape ventrally as it forms the acromion process. In comparison, the posterior margin appears gently concave throughout its length. However, both of the margins share the relative displacement of their apex in relation to the mid-height of the bone (*i.e.* dorsal displacement for the anterior concavity and ventral displacement for the posterior concavity), which results in the strong asymmetrical look of either margin. The position and greater degree of concavity of the anterior margin also places the maximal constriction of the neck relatively dorsally, as in *Charitomenosuchus* NHMUK PV R 3806, *Neosteneosaurus* NHMUK PV R 3701 and *Lemmysuchus* NHMUK PV R 3168. Furthermore, the greater degree of concavity of the anterior margin results in a more pronounced flaring for the anterior portion of the scapular blade compared to the posterior one. As a result, the scapular blade is relatively asymmetrical as the posterior corner of the scapular blade forms a more acute angle than the anterior corner, as for other teleosauroids (*e.g. Ind. potamosiamensis* PRC-24, *Macrospondylus* SMNS 9428, *Charitomenosuchus* NHMUK PV R 3806, *Neosteneosaurus* NHMUK PV R 3701, and *Lemmysuchus* NHMUK PV R 3168). In *Mycterosuchus* NHMUK PV R 2617, the dorsal margin of the scapular blade is gently domed as in *Charitomenosuchus* NHMUK PV R 3806, *Neosteneosaurus* NHMUK PV R 3701, and *Lemmysuchus* NHMUK PV R 3168.

Ventrally, the neck of the scapula of *Mycterosuchus* NHMUK PV R 2617 widens as it gradually transitions to the proximal region. As mentioned above, the anterior margin forms a strong bulge anteroventrally which corresponds to the acromion process. The latter constitutes one of the thinnest portions of the bone mediolaterally (along with the scapular blade). The lateral surface of the acromion process does not display any laterally protruding ridge as in extant crocodylians, or *Pelagosaurus* BRLSI M.1418 and *Turnersuchus* LRM 2021/45 (Wilberg et al., 2023) within Thalattosuchia. Instead, similarly to other teleosauroids (*e.g. Platysuchus* SMNS 9930 & UMH-0005, *Macrospondylus* SMNS 9428, *Charitomenosuchus* NHMUK PV R 3806, *Neosteneosaurus* NHMUK PV R 3701, *Lemmysuchus* NHMUK PV R 3168, etc.), the anterior margin of the acromion process of the scapula of *Mycterosuchus* NHMUK PV R 2617 shows a relatively greater width mediolaterally which presumably corresponded to the lateral deltoid/acromial crest of extant crocodylians and basal thalattosuchians. This thickened anterior border of the acromion process is even more emphasized by the underlying scapular fossa, which lies directly underneath the anterior border of the acromion process and extends posteriorly up until the glenoid process (about the anteroposterior mid-length of the proximal region). The tip of the acromion process is missing, but it was potentially located on the same level as the scapulocoracoid synchondrosis surface as in other teleosauroids.

Unlike in other teleosauroids, the posterior margin of the neck of the scapula of *Mycterosuchus* NHMUK PV R 2617 does not directly transitions to that of the glenoid process. Instead, it twists medially forming a curled ridge. In lateral view, the medial disappearance of the posterior margin of the neck creates a unique bend look of the posterior edge of the scapula around the transition between the neck

and the glenoid process. Hence, in *Mycterosuchus* NHMUK PV R 2617, the glenoid process seems to gradually rise from the lateral surface of the scapula. As in most teleosauroids, the glenoid process of the scapula of *Mycterosuchus* NHMUK PV R 2617 culminates in a laterally oriented glenoid facet. The latter is strongly concave and possesses a prominent overhanging ridge dorsally – the scapular buttress of the glenoid process – as seen in *Macrospondylus* SMNS 9428 and *Charitomenosuchus* NHMUK PV R 3806, and *Neosteneosaurus* NHMUK PV R 3701 but to a lesser extent. In all these cases, the scapular buttress of the glenoid process is only present dorsal to the glenoid facet and does not extend on the anterior and posterior sides of the facet.

In *Mycterosuchus* NHMUK PV R 2617 and other teleosauroids with a laterally positioned glenoid facet (*e.g. Macrospondylus* SMNS 9428, *Charitomenosuchus* NHMUK PV R 3806, *Lemmysuchus* NHMUK PV R 3168), the latter appears proportionally large in relation to the entire proximal region of the scapula. However, the largest structure corresponds to the scapulocoracoid synchondrosis surface, which takes up the entire anteroposterior length of the scapula proximally as it extends medially to the glenoid facet. In *Mycterosuchus* NHMUK PV R 2617, the scapulocoracoid synchondrosis surface was presumably triangular in shape due to the mediolateral thinning of the acromion process.

8.1.2. *Coracoid.* The coracoid of *Mycterosuchus* NHMUK PV R 2617 (see figs. 40 and 43) displays the typical teleosauroid features: similarly sized proximal head and coracoid blade, triangular anterior expansion, marked shaft constriction, large glenoid facet, ventroposteriorly positioned glenoid facet and parallelepiped scapulocoracoid synchondrosis surface, and a marked projected rim along the ventroposterior margin of the glenoid facet (with is not found in metriorhynchids). In parallel *Mycterosuchus* NHMUK PV R 2617 stands out with its short shaft and its triangular cross-section.

The coracoid head of *Mycterosuchus* NHMUK PV R 2617 (see fig. 40) stands out from most teleosauroids with its almost flawless diamond-shaped silhouette (*e.g. Aeolodon* NHMUK PV R 1086 & MNHN.F.CNJ 78, *Platysuchus* SMNS 9930, *Macrospondylus* SMNS 54063, SMNS 9428 & PMU 35980, *Charitomenosuchus* NHMUK PV R 3806, *Neosteneosaurus* NHMUK PV R 3701, *Lemmysuchus* NHMUK PV R 3169, *Machimosaurus* spp.). Indeed, the anterior and posterior extremities – the apex of the anterior expansion and the posterior tip of the glenoid facet – of the coracoid head of *Mycterosuchus* NHMUK PV R 2617 are aligned as the anteroposterior axis joining them is overall perpendicular to the long axis of the shaft of the coracoid. In addition, the junction between the lateral margin of the anterior expansion and the scapulocoracoid synchondrosis surface appears to have been located around the mid length of the anteroposterior axis of the coracoid head, which results in similar anteroposterior extensions for each side of the coracoid head (*i.e.* the anterior expansion and posterior part) and further emphasizes the diamond-shaped silhouette of the coracoid head. Set side by side, the shape of the coracoid head of *Aeolodon* NHMUK PV R 1086 strongly resembles that of *Mycterosuchus* NHMUK PV R 2617. Compared to other teleosauroids, the shape of the coracoid head of the more derived taxon *Neosteneosaurus* NHMUK PV R 3701 comes the closest to that of *Mycterosuchus* NHMUK PV R 2617, but differs in having misaligned anterior and posterior extremities (in relation to the long axis of the shaft of the coracoid) as well as a proportionally more elongated anterior expansion. The tip of the anterior expansion of the coracoid of *Mycterosuchus* NHMUK PV R 2617 forms a sharp and acute corner as in most teleosauroids (*e.g. Macrospondylus* SMNS 54063, SMNS 942 & PMU 35980, *Charitomenosuchus* NHMUK PV R 3806, *Neosteneosaurus* NHMUK PV R 3701, *Machimosaurus* spp. see C on fig. 61). In comparison, *Aeolodon* NHMUK PV R 1086 shows a shorter anterior expansion with a relatively wider and more right-angled anterior apex.In addition, the lateral and medial margins of the anterior expansion of the coracoid of *Mycterosuchus* NHMUK PV R 2617 are straight throughout their length, which is also observed in several teleosauroids (*e.g. Macrospondylus* SMNS 54063, SMNS 9428 & PMU 35980, *Charitomenosuchus* NHMUK PV R 3806, *Neosteneosaurus* NHMUK PV R 3701, *Lemmysuchus* NHMUK PV R

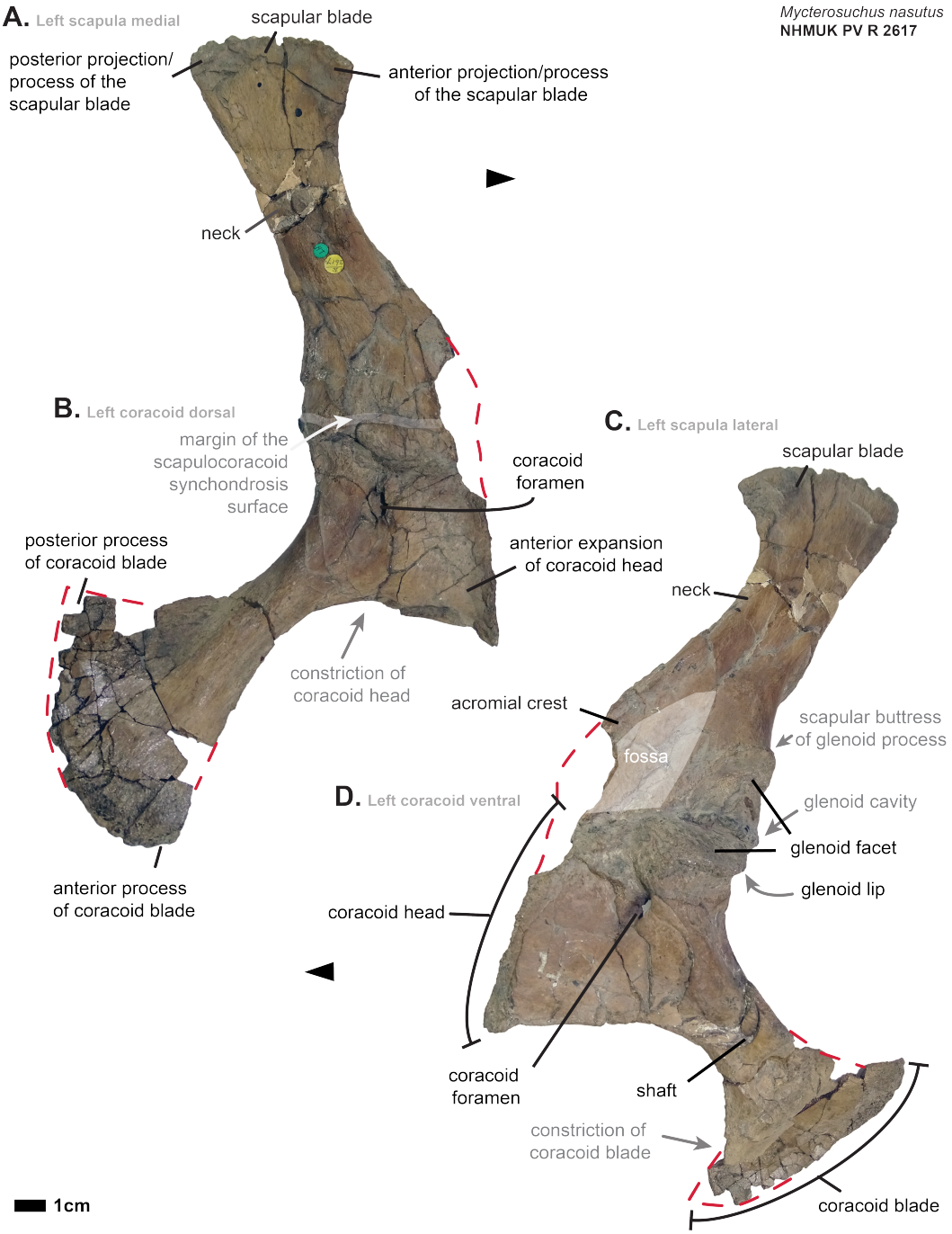


FIGURE 40. Pectoral girdle of *Mycterosuchus nasutus* NHMUK PV R 2617 (photographs). **A.** Left scapula in medial view ; **B.** Left coracoid in dorsal view ; **C.** Left scapula in lateral view ; **D.** Left coracoid in ventral view. Arrow points anteriorly. Red dashed lines indicate missing parts. Reconstruction of missing parts based on *Macrospondylus bollensis* SMNS 54063.



FIGURE 41. Comparative figure of teleosauroid scapulae. **A.** Aeolodontinae (3D model); **B.** Teleosauridae (3D model); **C.** Teleosaurinae (photographs); **D.** Machimosauridae (photograph and 3D model); **E.** Machimosaurinae (photographs); **F.** Machimosaurini (photograph). Arrow points anteriorly. Scale bars represent 1cm. Red dashed lines indicate missing parts.

3169, *Machimosaurus* spp.). In contrasts, in *Aeolodon* NHMUK PV R 1086 & MNHN.F.CNJ 78 and *Platysuchus* SMNS 9930 the lateral margin of the anterior expansion bears a strongly convex appearance.

The scapulocoracoid synchondrosis surface of the coracoid of *Mycterosuchus* NHMUK PV R 2617 is proportionally elongated yet is missing its anterior extremity. Indeed, its anteroposterior extension presumably reached about half of the total anteroposterior length of the coracoid head. The proportionate length of the scapulocoracoid synchondrosis surface of the coracoid mirrors the relative sturdy appearance of the scapula, as in other thalattosuchians. Particularly, the scapula of *Mycterosuchus* NHMUK PV R 2617 displays a bulky appearance due to a marked anteroposterior breadth throughout its length, despite an elongated build. This contrasts with the relatively more reduced scapulocoracoid syncondrosis surface of the coracoid of *Charitomenosuchus* NHMUK PV R 3806, *Neosteneosaurus* NHMUK PV R 3701 and presumably *Lemmysuchus* NHMUK PV R 3169, which possess a more slender scapula. However, the anteroposterior length of the scapulocoracoid synchondrosis surface of the coracoid of *Mycterosuchus* NHMUK PV R 2617 does not reach the extended levels found in *Macrospondylus* SMNS 54063, SMNS 9428 & PMU 35980 and *Platysuchus* SMNS 9930. The exact outline of the scapulocoracoid synchondrosis surface of the coracoid of *Mycterosuchus* NHMUK PV R 2617 is not observable but appears to display a tapered anterior tip and a sub-quadrangular posterior extremity, similar to *Charitomenosuchus* NHMUK PV R 3806, *Neosteneosaurus* NHMUK PV R 3701 & PETMG R178 and *Lemmysuchus* NHMUK PV R 3169. This sub-quadrangular posterior extremity of the scapulocoracoid synchondrosis surface contrasts with the triangular shape found in metriorhynchids with an open coracoid foramen, and the difference is primarily linked to the position of the glenoid facet which is more ventral in teleosauroids.

Posteriorly, the coracoid head of *Mycterosuchus* NHMUK PV R 2617 gradually widens dorsoventrally to form the glenoid facet. This widening, which corresponds to the glenoid process, is mainly concentrated on the ventral surface of the coracoid head as in other teleosauroids. Most of the surface of the glenoid process of the coracoid of *Mycterosuchus* NHMUK PV R 2617 is concave with the only exception being the slightly convex anteroventral portion of the glenoid process, which is similar to *Macrospondylus* SMNS 9428 and *Neosteneosaurus* NHMUK PV R 3701. On the dorsal side of the coracoid head of *Mycterosuchus* NHMUK PV R 2617, the posterior portion of the bone is also concave which emphasizes the trumpet-shape of the glenoid process, as in *Charitomenosuchus* NHMUK PV R 3806, *Macrospondylus* SMNS 54063 & PMU 35980, and *Lemmysuchus* NHMUK PV R 3169. The posterior margin of the coracoid head of *Mycterosuchus* NHMUK PV R 2617 possesses a noticeable ridge which marks the junction between the concave ventral and dorsal surfaces of the coracoid head, similar to *Macrospondylus* SMNS 54063 & PMU 35980, *Charitomenosuchus* NHMUK PV R 3806, and possibly *Lemmysuchus* NHMUK PV R 3169. In *Mycterosuchus* NHMUK PV R 2617, the glenoid facet is proportionally large and displays a hemispherical outline. As in other teleosauroids, the main orientation of the glenoid facet of the coracoid of *Mycterosuchus* NHMUK PV R 2617 is posteroventral and its surface becomes slightly concave near its posterior border. As in *Macrospondylus* SMNS 9428 and possibly *Aeolodon* NHMUK PV R 1086, the posteroventral margin of the glenoid facet of the coracoid of *Mycterosuchus* NHMUK PV R 2617 forms a thin and prominent rim, whereas it transitions to a smooth and blunt corner anteriorly. This contrasts with the marked and protruding margin surrounding the entirety of the ventral rim of the glenoid facet of the coracoids of *Platysuchus* SMNS 9930, *Charitomenosuchus* NHMUK PV R 3806, *Neosteneosaurus* NHMUK PV R 3701, *Lemmysuchus* NHMUK PV R 3169. In *Machimosaurus* spp. (see C on fig. 61), the glenoid facet appears surrounded by a thick bulge throughout. Despite a thick shaft, the posterior portion of the coracoid head hosting the glenoid facet and scapulocoracoid synchondrosis surface corresponds to the dorsoventrally thickest portion of the bone, as in other teleosauroids.

The coracoid foramen of *Mycterosuchus* NHMUK PV R 2617 forms an oval aperture on both sides of the coracoid head, whose longest axis is oriented anteroposteriorly as in *Platysuchus* SMNS 9930 but

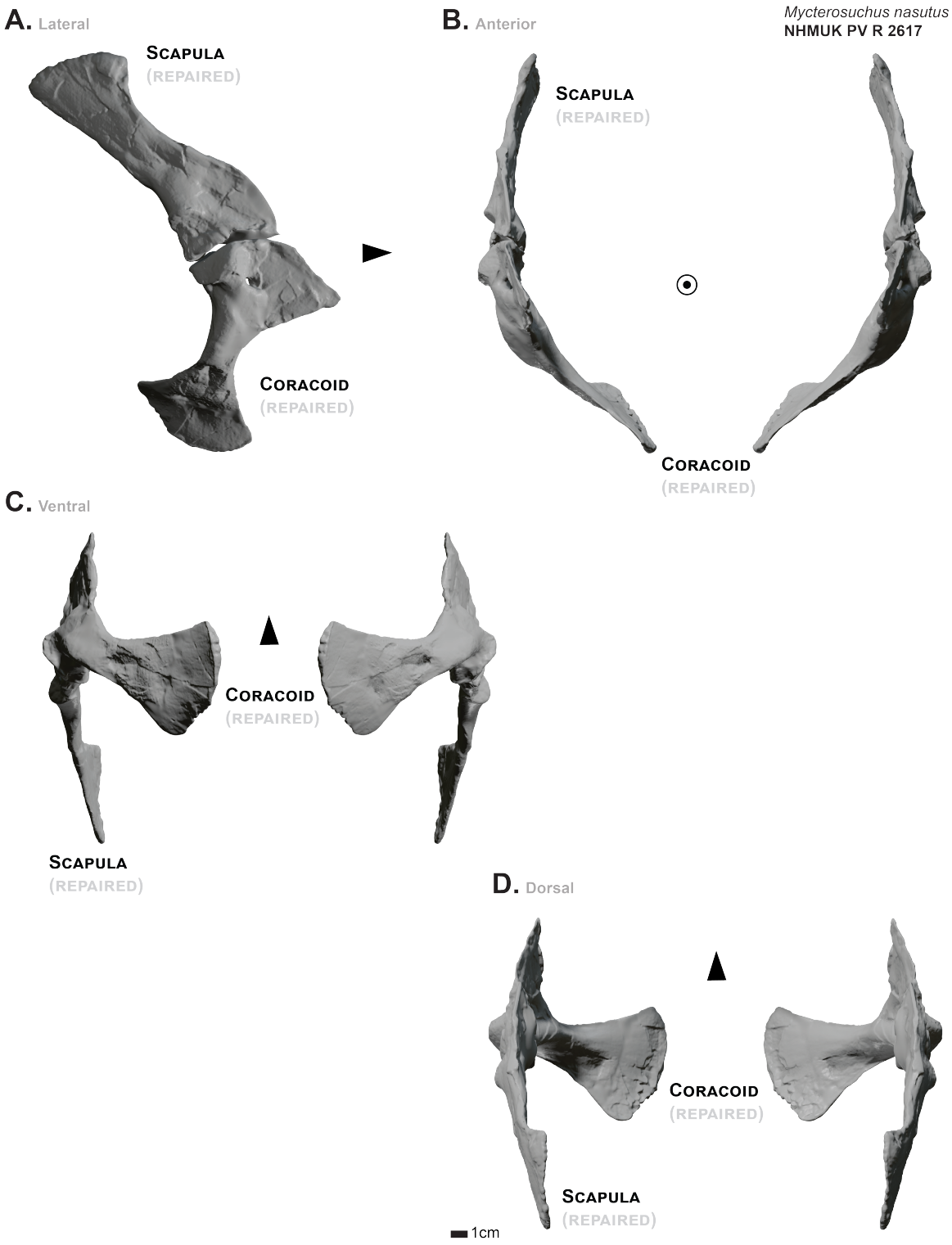


FIGURE 42. Reconstruction of the pectoral girdle of *Mycterosuchus nasutus* NHMUK PV R 2617 (3D models). **A.** Lateral view; **B.** Anterior view; **C.** Ventral view; **D.** Dorsal view. Arrow points anteriorly. Target indicates anterior. The right scapula and coracoid are mirrored. Scapula and coracoid have been slightly repaired based on *Macrospondylus* SMNS 54063, SMNS 9428 & PMU 35980.

unlike other teleosauroids (*e.g.* *Aeolodon* NHMUK PV R 1086 & MNHN.F.CNJ 78, *Macrospondylus* SMNS 54063, SMNS 9428 & PMU 35980, *Charitomenosuchus* NHMUK PV R 3806, *Neosteneosaurus* NHMUK PV R 3701, *Lemmysuchus* NHMUK PV R 3169, *Machimosaurus* spp.). In addition, the coracoid foramen of *Mycterosuchus* NHMUK PV R 2617 forms a mainly mediolaterally tilted canal which also slightly shifts the orifice posteriorly on the dorsal side of the coracoid head. On the ventral surface, the coracoid foramen of *Mycterosuchus* NHMUK PV R 2617 is positioned near the glenoid facet and also lies on the anteroposterior (main) axis of the coracoid head (which joins each extremity), similar to *Aeolodon* NHMUK PV R 1086 & MNHN.F.CNJ 78, *Macrospondylus* SMNS 54063, SMNS 9428 & PMU 35980, *Neosteneosaurus* NHMUK PV R 3701, *Machimosaurus* spp. and possibly *Platysuchus* SMNS 9930 as well as *Lemmysuchus* NHMUK PV R 3169. In *Charitomenosuchus* NHMUK PV R 3806, the coracoid foramen is also located near the glenoid facet on the ventral surface of the coracoid head but is lying slightly underneath the anteroposterior axis of the coracoid head.

The shaft of the coracoid of *Mycterosuchus* NHMUK PV R 2617 displays a proportionally short extension mediolaterally as it accounts for about 29% of the total length of the coracoid, and hence it contrasts with the slender shaft of the coracoid of other teleosauroids (*e.g.* *Aeolodon* NHMUK PV R 1086, *Platysuchus* SMNS 9930, *Macrospondylus* SMNS 54063, SMNS 9428 & PMU 35980, *Charitomenosuchus* NHMUK PV R 3806, *Neosteneosaurus* NHMUK PV R 3701, *Lemmysuchus* NHMUK PV R 3169, *Machimosaurus* spp.). In *Mycterosuchus* NHMUK PV R 2617, the minimal anteroposterior thickness of the shaft of the coracoid at the constriction reaches 47% of the total mediolateral extension of the shaft of the coracoid. In comparison, the shaft of the coracoid of *Mycterosuchus* NHMUK PV R 2617 displays a marked dorsoventral thickness (58% of total mediolateral extension of the shaft of the coracoid), not equally distributed but gathered along its anterior side which gives the shaft an overall triangular cross-section. This contrasts with the more regular distribution of thickness observed in *Charitomenosuchus* NHMUK PV R 3806, *Neosteneosaurus* NHMUK PV R 3701 & PETMG R178 and *Lemmysuchus* NHMUK PV R 3169 whose cross-section is more elliptic. The dorsoventral thickening of the coracoid of *Mycterosuchus* NHMUK PV R 2617 starts near the coracoid foramen and increases towards the base of the shaft of the coracoid where it reaches its maximum. Furthermore, the shaft of the coracoid of *Mycterosuchus* NHMUK PV R 2617 corresponds to the dorsoventrally widest portion of the coracoid, differing from *Charitomenosuchus* NHMUK PV R 3806, *Neosteneosaurus* NHMUK PV R 3701 and *Lemmysuchus* NHMUK PV R 3169 in which the glenoid facet fills this role. The dorsoventral thickening of the coracoid of *Mycterosuchus* NHMUK PV R 2617 then slightly thins down medially until it reaches the anteroposterior constriction of the shaft of the coracoid. At this point, the coracoid starts to rapidly decrease in dorsoventral thickness, and reaches a plate-like appearance around the midway of the medial flaring out corresponding to the coracoid blade. A similar configuration with a rapid decrease in dorsoventral thickness starting from the shaft constriction is observed in *Neosteneosaurus* NHMUK PV R 3701 and *Lemmysuchus* NHMUK PV R 3169 which however possess distinct shaft shapes. In comparison, the dosoventral flattening of the coracoid starts more laterally in *Charitomenosuchus* NHMUK PV R 3806 near the proximal base of the shaft of the coracoid, and shows a gradual decline medially. As in other teleosauroids and metriorhynchoids, the shaft of the coracoid of *Mycterosuchus* NHMUK PV R 2617 is dorsoventrally arched, and its coracoid blade is posteroventrally twisted which overall mirrors the relative inclination of the scapulocoracoid synchondrosis surface.

The coracoid blade of *Mycterosuchus* NHMUK PV R 2617 is fragmentary but its overall shape appears anteroposteriorly asymmetrical as in *Aeolodon* NHMUK PV R 1086, *Neosteneosaurus* NHMUK PV R 3701, and *Machimosaurus* spp. (see A on fig. 61, presumably). Indeed, the anterior corner of the coracoid blade is (presumably) located more medially than the posterior one. Furthermore, although the distal margin is convex and its apex – which is the inflexion point – is centered in relation to the long axis of the shaft of the coracoid, each side of the blade displays a different curvature, with the posterior one

being more drastically inclined. Additionally, the dorsoventral thickness of the coracoid blade is variable throughout its length, with the posterior extremity being the thinnest.

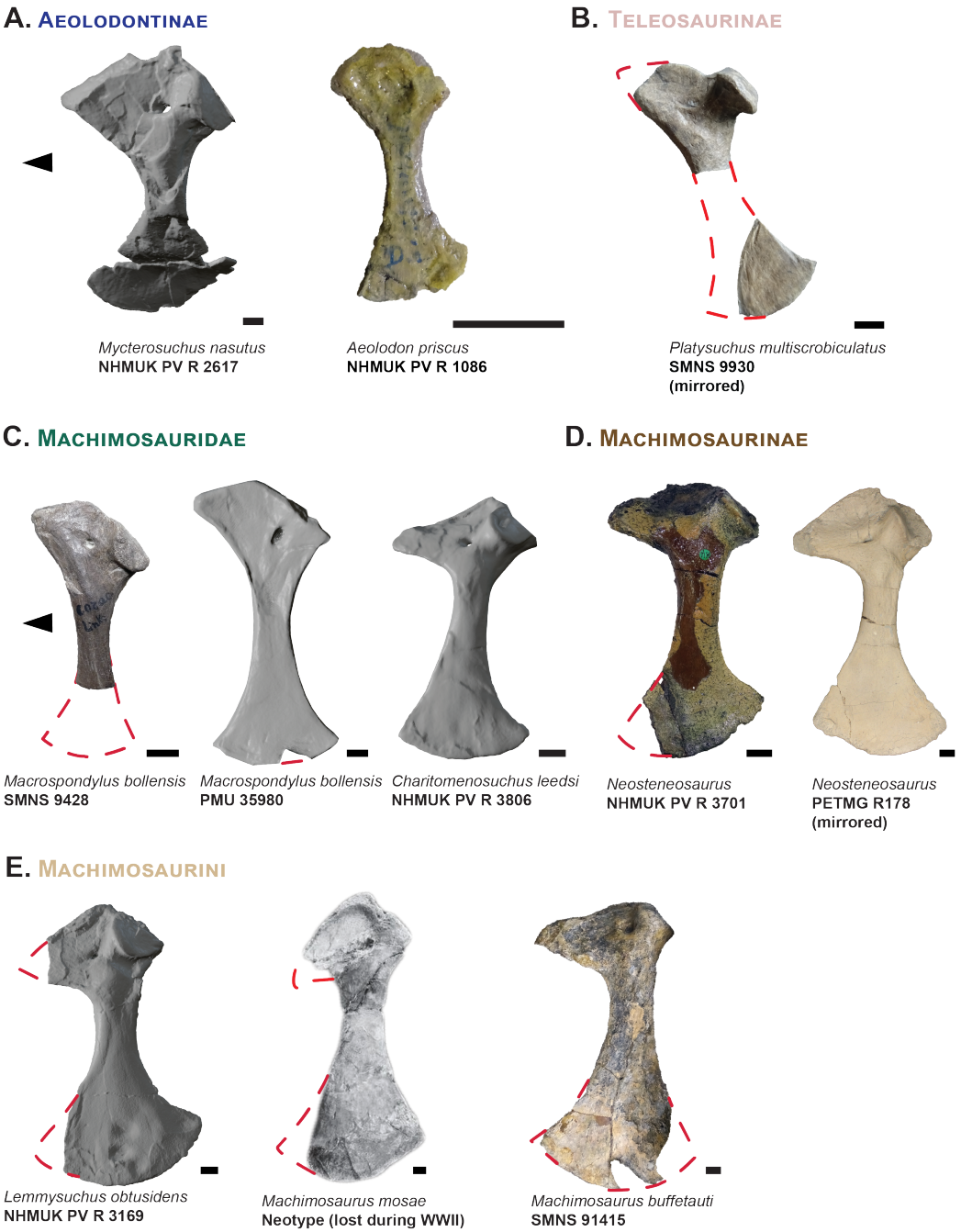


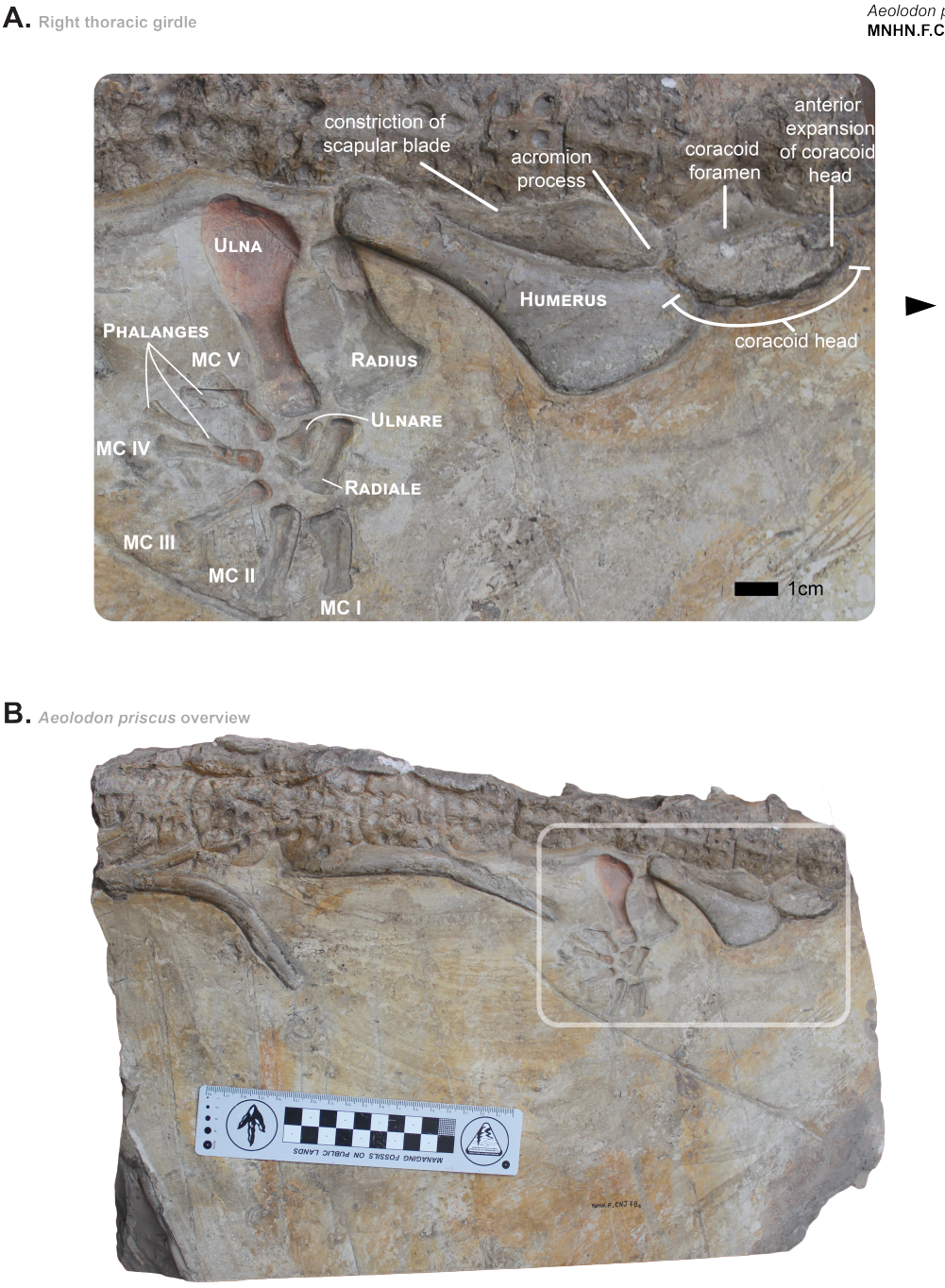
FIGURE 43. Comparative figure of teleosauroid coracoids. **A.** Aeolodontinae (3D model and photograph); **B.** Teleosaurinae (photograph); **C.** Machimosauridae (photograph and 3D models); **D.** Machimosaurinae (photographs); **E.** Machimosaurini (3D model and photographs). Arrow points anteriorly. Scale bars represent 1cm. Red dashed lines indicate missing parts.

8.2. ***Aeolodon priscus* von Sömmerring, 1814.** For measurements, see table 7. The specimen MNHN.F.CNJ 78 (see fig. 44) corresponds to a more mature individual, whereas NHMUK PV R 1086 is a juvenile (see fig. 45). No particular traits could be attributed to ontogenetic changes (Brochu, 1992).

8.2.1. *Scapula.* The scapula of *Aeolodon priscus* MNHN.F.CNJ 78 (see fig. 44) is obstructed in parts by the humerus and the osteoderms. However, it presents portions of the anterior margin of the scapula, which shows a sinusoid curve as in most teleosauroids (*e.g.* *Macrospondylus* SMNS 54063, SMNS 9428 & PMU 35980, *Charitomenosuchus* NHMUK PV R 3806, *Neosteneosaurus* NHMUK PV R 3701, *Lemmysuchus* NHMUK PV R 3168, etc.). Furthermore, the anterior margin of the scapula of *Aeolodon* MNHN.F.CNJ 78, appears to be strongly undulated, with a marked concave shape dorsally and a prominent bulged shape ventrally, which is more similar to *Macrospondylus* SMNS 54063, SMNS 9428 & PMU 35980, *Lemmysuchus* NHMUK PV R 3168 and *Mycterosuchus* (presumably). Ventrally, the scapula of *Aeolodon* MNHN.F.CNJ 78 culminates in a rounded apex corresponding to the acromion process. The latter seems located on the same level as the scapulocoracoid synchondrosis surface, as in other teleosauroids (*e.g.* *Macrospondylus* SMNS 54063, SMNS 9428 & PMU 35980, *Charitomenosuchus* NHMUK PV R 3806,*Neosteneosaurus* NHMUK PV R 3701, *Lemmysuchus* NHMUK PV R 3168, etc.).

8.2.2. *Coracoid.* The coracoid of *Aeolodon priscus* MNHN.F.CNJ 78 (see fig. 44) and NHMUK PV R 1086 (see figs. 43, 45 and 46) possesses the following common teleosauroid features: similarly sized lateral and medial extremities, a slender shaft, a tapered and triangular anterior expansion, an anteroposteriorly asymmetrical coracoid blade. The coracoid of *Aeolodon* differs from other teleosauroids mainly in displaying a strongly convex lateral margin, as well as a relatively broad anterior expansion.

The coracoid head of *Aeolodon* MNHN.F.CNJ 78 and NHMUK PV R 1086 (see figs. 44 and 45 respectively) strongly differs from that of other teleosauroids due to both a broad appearance and a dome-shaped lateral margin (*e.g.* *Mycterosuchus* NHMUK PV R 2617, *Platysuchus* SMNS 9930, *Macrospondylus* SMNS 54063, SMNS 9428 & PMU 35980, *Charitomenosuchus* NHMUK PV R 3806, *Neosteneosaurus* NHMUK PV R 3701, *Lemmysuchus* NHMUK PV R 3169, *Machimosaurus* spp.). Proportionally, in *Aeolodon* MNHN.F.CNJ 78 and NHMUK PV R 1086, the anteroposterior length of the anterior expansion accounts for about 55% of the total length of the coracoid head, which is most similar to *Mycterosuchus* NHMUK PV R 2617 (58%), and *Neosteneosaurus* NHMUK PV R 3701 (54.6%) but slightly differs from other teleosauroids (*e.g.* this number reaches 43.8% in *Macrospondylus* SMNS 9428, and 63% in *Charitomenosuchus* NHMUK PV R 3806 and *Machimosaurus* spp. see C on fig. 61). However, the anterior expansion of the coracoid of *Aeolodon* MNHN.F.CNJ 78 and NHMUK PV R 1086 displays a marked mediolateral thickness at its base which exceeds its total anteroposterior length and emphasizes its broad appearance. Compared to other teleosauroids, only *Mycterosuchus* NHMUK PV R 2617 possesses a similarly dimensioned anterior expansion (presumably since a portion is missing). Nevertheless, besides the relatively straight area defined by the scapulocoracoid synchondrosis surface of the coracoid, the rest of the coracoid head of *Aeolodon* MNHN.F.CNJ 78 and NHMUK PV R 1086 displays a strongly arched margin laterally which markedly departs from the angular appearance of the coracoid head of other teleosauroids (*e.g.* *Mycterosuchus* NHMUK PV R 2617, *Platysuchus* SMNS 9930, *Macrospondylus* SMNS 54063, SMNS 9428 & PMU 35980, *Charitomenosuchus* NHMUK PV R 3806, *Neosteneosaurus* NHMUK PV R 3701, *Lemmysuchus* NHMUK PV R 3169, *Machimosaurus* spp.). Presumably, the length of the scapulocoracoid synchondrosis surface of the coracoid of *Aeolodon* NHMUK PV R 1086 accounts for about 42% of the total anteroposterior length of the coracoid head, which is slightly lesser than the presumed length of *Mycterosuchus* NHMUK PV R 2617. This hints at a possibly more slender scapula for *Aeolodon* than that of *Mycterosuchus*. As in the latter, the scapulocoracoid synchondrosis surface of the coracoid of *Aeolodon* NHMUK PV R 1086 forms an acute angle with the long axis of the shaft of the coracoid of around 40°, whereas this value is proportionally greater in other teleosauroids.



(c) Pictures courtesy of Dr. Michela Johnson

FIGURE 44. Pectoral girdle of *Aeolodon priscus* MNHN.F.CNJ 78 (photographs). **A.** Right pectoral girdle with the scapula mainly in anterior view and the coracoid in dorsal view; **B.** Overview of right pectoral girdle. Arrow points anteriorly.

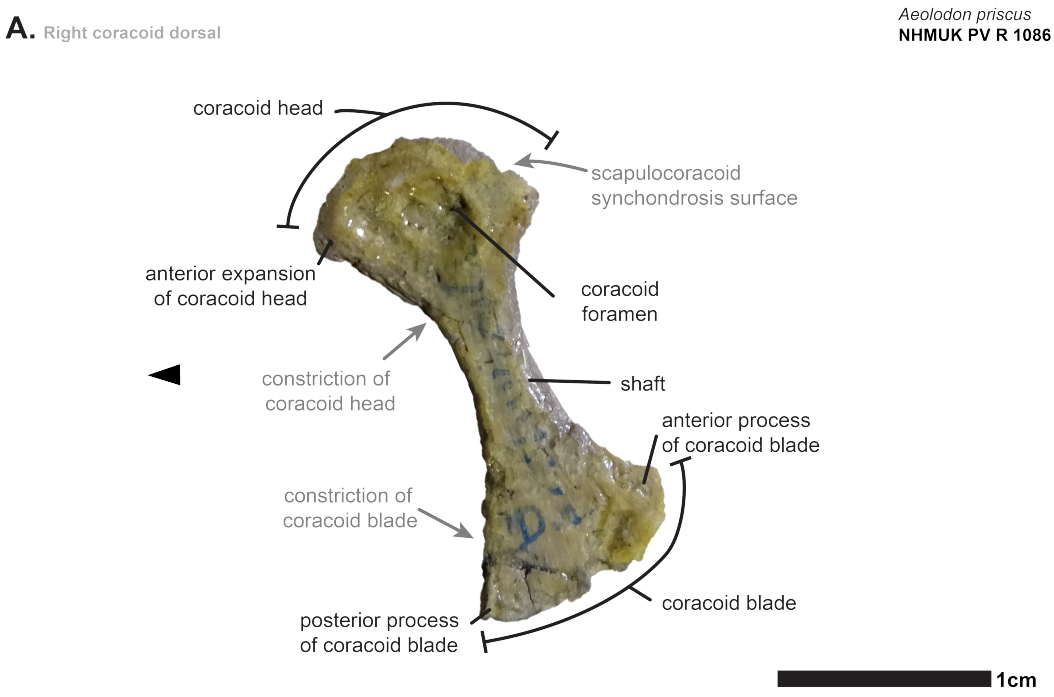


FIGURE 45. Pectoral girdle of *Aeolodon priscus* NHMUK PV R 1086 (photographs). **A.** Right coracoid in dorsal view ; **B.** Overview of the pectoral girdle. Arrow points anteriorly.

The coracoid foramen of *Aeolodon* MNHN.F.CNJ 78 and NHMUK PV R 1086 forms a sub-circular aperture on the dorsal surface of the coracoid, similar to *Macrospondylus* SMNS 54063, SMNS 9428 & PMU 35980, *Charitomenosuchus* NHMUK PV R 3806 and *Neosteneosaurus* NHMUK PV R 3701. In *Aeolodon* MNHN.F.CNJ 78 and NHMUK PV R 1086, the coracoid foramen is positioned relatively in line with the long axis of the shaft of the coracoid and the anterior extremity of the scapulocoracoid synchondris surface (*i.e.* the junction with the anterior expansion), which resembles what it observed in most teleosauroids (*e.g. Mycterosuchus* NHMUK PV R 2617, *Macrospondylus* SMNS 54063, SMNS 9428 & PMU 35980, *Neosteneosaurus* NHMUK PV R 3701, and *Machimosaurus* spp. see C on fig. 61) but contrast with the anteriorly shifted foramen of the coracoid of *Charitomenosuchus* NHMUK PV R 3806. In addition, the coracoid foramen of *Aeolodon* MNHN.F.CNJ 78 and NHMUK PV R 1086 lies along the anteroposterior axis of the coracoid head, as in *Mycterosuchus* NHMUK PV R 2617,*Macrospondylus* SMNS 54063, SMNS 9428 & PMU 35980, *Neosteneosaurus* NHMUK PV R 3701 & PETMG R178 and *Machimosaurus* spp. (see C on fig. 61).

The anterior and posterior margins of the coracoid of *Aeolodon* NHMUK PV R 1086 are both concave within a similar range of curvature, and with their apex aligned. Yet, the posterior margin of the coracoid is relatively more recurved towards its medial and lateral extremities. However, the relative geometry of the anterior and posterior margins of the coracoid (*i.e.* gentle degree of curvature of both margins plus alignment of their apex) results in a slender and rod-like shaft for *Aeolodon* NHMUK PV R 1086 (see fig. 45). The latter strongly contrasts with the short shaft of the coracoid of *Mycterosuchus* NHMUK PV R 2617, but most teleosauroids also display an elongated shaft (*e.g. Macrospondylus* SMNS 54063, SMNS 9428 & PMU 35980, *Charitomenosuchus* NHMUK PV R 3806, *Neosteneosaurus* NHMUK PV R 3701, *Lemmysuchus* NHMUK PV R 3169, and possibly *Platysuchus* SMNS 9930). Hence, the shaft of the coracoid of *Aeolodon* NHMUK PV R 1086 slowly flares out medially to form the coracoid blade.

As in other teleosauroids, the extension of the coracoid blade of *Aeolodon* NHMUK PV R 1086 mirrors that of the coracoid head. Hence, the anteroposterior length of the coracoid blade is proportionally short, and only accounts for about half of the total mediolateral extension of the coracoid as a whole. Such a reduced coracoid blade is similar to what is observed in *Macrospondylus* PMU 35980 and possibly *Neosteneosaurus* NHMUK PV R 3701, but strongly contrasts with *Mycterosuchus* NHMUK PV R 2617 and most other teleosauroids. The coracoid blade of *Aeolodon* NHMUK PV R 1086 also displays a strongly anteroposteriorly asymmetrical appearance which is similar to *Mycterosuchus* NHMUK PV R 2617 (presumably), *Charitomenosuchus* NHMUK PV R 3806 and *Neosteneosaurus* NHMUK PV R 3701. Indeed, the posterior corner of the coracoid blade is positioned proportionally more laterally and also points posterolaterally whereas the anterior corner is relatively more slender and is strictly anteriorly oriented. This asymmetry affects the shape of the medial margin, which displays different degrees of convexity on each side of its apex (*i.e.* inflexion point) similar to *Mycterosuchus* NHMUK PV R 2617 (presumably), *Charitomenosuchus* NHMUK PV R 3806 and *Neosteneosaurus* NHMUK PV R 3701.

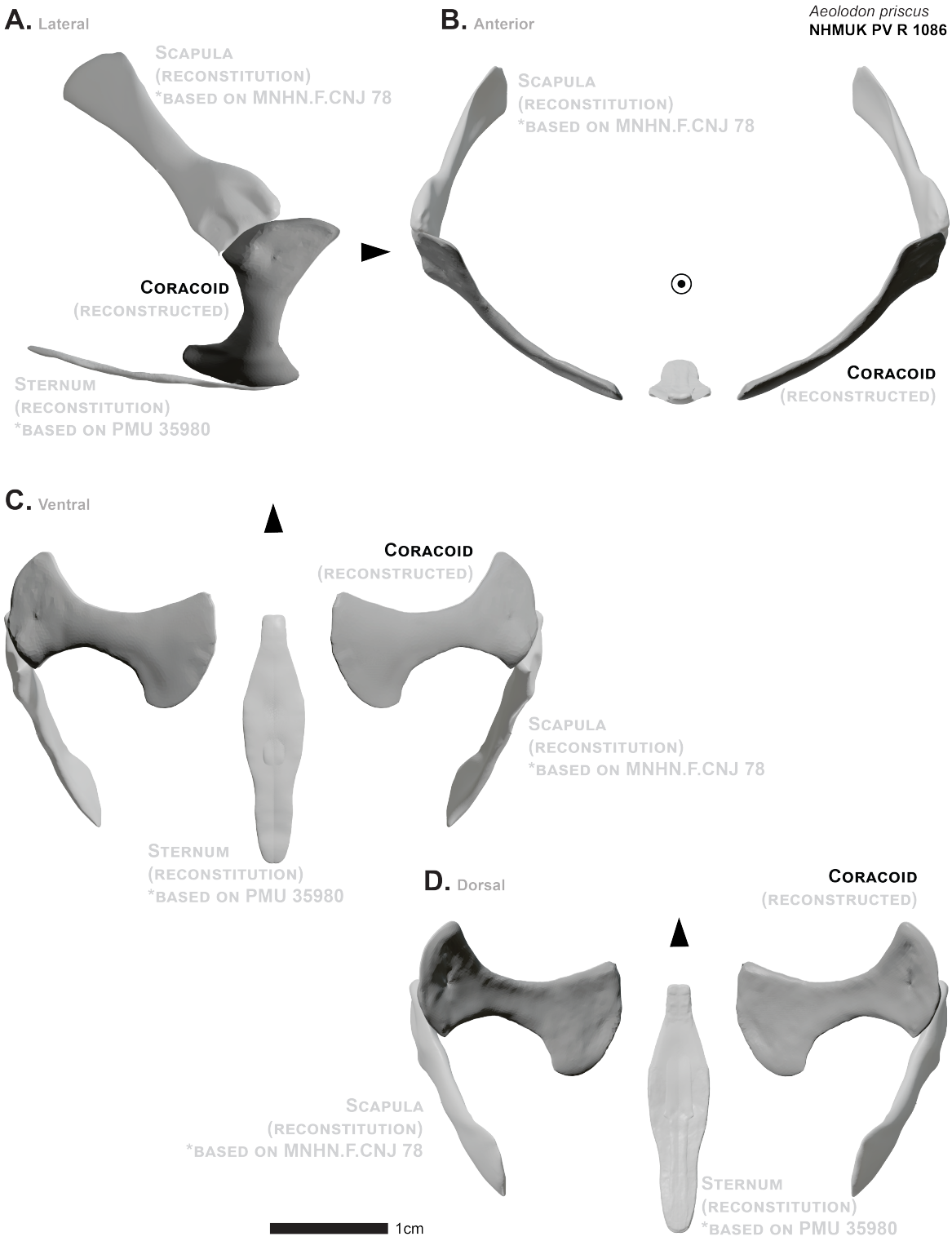


FIGURE 46. Reconstruction of the pectoral girdle of *Aeolodon priscus* NHMUK PV R 1086 (3D models). **A.** Lateral view; **B.** Anterior view; **C.** Ventral view; **D.** Dorsal view. Arrow points anteriorly. Target indicates anterior. The left coracoid is mirrored. The scapula has been putatively reconstituted based on *Aeolodon* MNHN.F.CNJ 78 and *Te. cadomensis* NHMUK PV OR 31836. The ventral surface of the coracoid has been reconstructed.

8.3. ***Indosinosuchus potamosiamensis* Martin et al., 2019b.** For measurements, see table 6.

8.3.1. *Scapula.* The scapula of *Indosinosuchus potamosiamensis* PRC-24 Martin et al., 2019b (see figs. 41 and 47) bears an overall slender appearance, which is encountered in several other teleosauroids (*e.g.* *Mycterosuchus* NHMUK PV R 2617, *Te. cadomensis* NHMUK PV OR 31836, *Charitomenosuchus* NHMUK PV R 3806 *Neosteneosaurus* NHMUK PV R 3701, and *Lemmysuchus* NHMUK PV R 3168). The scapula of *Ind. potamosiamensis* also displays the combination of a marked anteroposterior constriction of the shaft of the scapula and flaring of the scapular blade which is overall similar to *Mycterosuchus* NHMUK PV R 2617, *Neosteneosaurus* NHMUK PV R 3701 and *Lemmysuchus* NHMUK PV R 3168. This however contrasts with the rod-like scapula of *Te. cadomensis* NHMUK PV OR 31836 and *Charitomenosuchus* NHMUK PV R 3806, and the large fan-like scapular blade of *Platysuchus* SMNS 9930 & UMH-0005 and *Macrospondylus* SMNS 54063, SMNS 9428 & PMU 35980.

The slender appearance of the scapula of *Ind. potamosiamensis* PRC-24 (see fig. 47) is given by the overall constant thickness of its shaft throughout its length. Indeed, the anterior and posterior margins of the scapula of *Ind. potamosiamensis* PRC-24 form relatively straight surfaces for most of their length which helps maintain a constant thickness. The anterior and posterior margins of the scapula gradually become concave directly after the neck constriction, although in opposite directions (*i.e.* ventrally for the posterior margin and dorsally for the anterior margin). The constriction of the neck of the scapula of *Ind. potamosiamensis* PRC-24 is located around the mid-height of the bone as in *Te. cadomensis* NHMUK PV OR 31836, *Neosteneosaurus* NHMUK PV R 3701 and *Lemmysuchus* NHMUK PV R 3168. Also, the anteroposterior width of the neck constriction of the scapula of *Ind. potamosiamensis* PRC-24 accounts for about 14% of the total dorsoventral extension of the scapula, which is similar to what is observed in *Charitomenosuchus* NHMUK PV R 3806 and *Neosteneosaurus* NHMUK PV R 3701. In *Ind. potamosiamensis* PRC-24, the shaft of the scapula shows a moderate extension as it accounts for about 40% of the total height of the bone, similar to what is observed in *Mycterosuchus* NHMUK PV R 2617. This contrasts with the proportionally shorter shaft of taxa bearing a large scapular blade (*e.g.* *Macrospondylus* SMNS 54063, SMNS 9428 & PMU 35980 and *Platysuchus* SMNS 9930 & UMH-0005), and further differs from the relatively longer shafts of the scapulae of *Te. cadomensis* NHMUK PV OR 31836, *Charitomenosuchus* NHMUK PV R 3806 *Neosteneosaurus* NHMUK PV R 3701, and *Lemmysuchus* NHMUK PV R 3168.

Dorsally, the scapula of *Ind. potamosiamensis* PRC-24 gradually flares out to form the scapular blade, which is moderately large as it accounts for about 37% of the total dorsoventral height of the bone. In comparison, this value reaches about 62% in *Platysuchus* UMH-0005, and 50–56% in *Macrospondylus* SMNS 54063 & PMU 35980, and lower amounts in *Mycterosuchus* NHMUK PV R 2617 (12%), *Te. cadomensis* NHMUK PV OR 31836 (19.5%), *Charitomenosuchus* NHMUK PV R 3806 (22%), *Neosteneosaurus* NHMUK PV R 3701 (31%), and *Lemmysuchus* NHMUK PV R 3168 (30%). In *Ind. potamosiamensis* PRC-24, the scapular blade displays a strongly convex distal margin with its apex being posteriorly shifted rather than centered which gives it an ovoid appearance. As a result, the anterior and posterior extremities of the scapular blade are positioned markedly more ventrally than the apex of the convexity, similar to what is observed in *Te. cadomensis* NHMUK PV OR 31836, *Platysuchus* SMNS 9930 & UMH-0005, and *Macrospondylus* SMNS 54063, SMNS 9428 & PMU 35980. In comparison, the distal margin of the scapular blade of *Mycterosuchus* NHMUK PV R 2617, *Charitomenosuchus* NHMUK PV R 3806, *Neosteneosaurus* NHMUK PV R 3701 & PETMG R178 and *Lemmysuchus* NHMUK PV R 3168 is proportionally less bulged. In *Ind. potamosiamensis* PRC-24, the relative position of each corner of the scapular blade is different: the anterior corner is positioned more ventrally than the posterior one, as in *Platysuchus* SMNS 9930 & UMH-0005, *Macrospondylus* SMNS 54063, SMNS 9428 & PMU 35980,

Neosteneosaurus NHMUK PV R 3701, and *Lemmysuchus* NHMUK PV R 3168 (but to a lesser extent).

Ventrally, the shaft of the scapula expands both anteroposteriorly and mediolaterally to form the proximal region of the scapula, which bears the glenoid process posteriorly and the acromion process anteriorly. In *Ind. potamosiamensis* PRC-24, the anteroposterior length of the proximal region is slightly lesser than that of the scapular blade (about 93%) which is similar to *Mycterosuchus* NHMUK PV R 2617. In other teleosaurids, the scapular blade of *Te. cadomensis* NHMUK PV OR 31836 only accounts for half of the total anteroposterior length of the proximal region, whereas in *Platysuchus* UMH-0005 the proximal region reaches three–quarters of the total anteroposterior extension of the scapular blade. As in *Platysuchus* SMNS 9930 & UMH-0005 and *Te. cadomensis* NHMUK PV OR 31836, the glenoid process of the scapula of *Ind. potamosiamensis* PRC-24 forms a posteriorly prominent protuberance as it markedly emerges from the neck constriction. In this way, it contrasts with machimosaurid taxa in which the glenoid process displays a more limited expansion (*e.g. Macrospondylus* SMNS 54063, SMNS 9428 & PMU 35980, *Charitomenosuchus* NHMUK PV R 3806, *Neosteneosaurus* NHMUK PV R 3701, *Lemmysuchus* NHMUK PV R 3168). As in other teleosauroids, the glenoid facet of the scapula of *Ind. potamosiamensis* PRC-24 forms a concave surface with a semioval outline, which is bordered dorsally by a slightly prominent bulge. Yet, the glenoid facet of the scapula of *Ind. potamosiamensis* PRC-24 contrasts with most teleosauroids as it is mainly posteriorly facing, which is similar to *Platysuchus* SMNS 9930, *Platysuchus* Kloster Banz unnumbered specimen & UMH-0005, and *Neosteneosaurus* NHMUK PV R 3701 among teleosauroids. As such, the glenoid facet of the scapula of *Ind. potamosiamensis* PRC-24 is positioned relatively posteriorly in relation to the scapulocoracoid synchondrosis surface (rather than more laterally as in post teleosauroids). In *Ind. potamosiamensis* PRC-24, the anterior extremity of the glenoid facet corresponds to the mediolaterallly widest point of the scapulocoracoid synchondrosis surface and the scapula as a whole, which is similar to other teleosauroids. Anteriorly to the glenoid facet, the scapulocoracoid synchondrosis surface of the scapula of *Ind. potamosiamensis* PRC-24 displays a triangular outline, whereas the remainder portion bears the shape of a truncated hemicycle due to the disposition of the glenoid facet on its lateral border, like other teleosauroids. The surface of the scapulocoracoid synchondrosis is slightly convex anteriorly and lightly concave posteromedially, and is also scarred throughout.

The acromion process of the scapula of *Ind. potamosiamensis* PRC-24 contrasts with that of most teleosauroids in displaying a prominent and strictly anteriorly facing apex (*e.g. Te. cadomensis* NHMUK PV OR 31836, *Platysuchus* SMNS 9930, UMH-0005 and *Platysuchus* Kloster Banz unnumbered specimen, *Macrospondylus* SMNS 54063, SMNS 9428 & PMU 35980, *Charitomenosuchus* NHMUK PV R 3806, *Neosteneosaurus* NHMUK PV R 3701, *Lemmysuchus* NHMUK PV R 3168). Indeed, the anterior extremity of the acromion process forms a relatively blunt corner which is more dorsally positioned than the scapulocoracoid synchondrosis surface. This shape is often encountered in metriorhynchoids. In addition, the apex of the acromion process of the scapula of *Ind. potamosiamensis* PRC-24 forms a thin blade mediolaterally, with differs from the bulkier acromion processes of machimosaurids (*e.g. Charitomenosuchus* NHMUK PV R 3806, *Neosteneosaurus* NHMUK PV R 3701 & PETMG R178, *Lemmysuchus* NHMUK PV R 3168). The thin appearance of the acromion process of the scapula of *Ind. potamosiamensis* PRC-24 is furthers accentuated by the presence of a shallow recess –the scapular fossa – on the lateral surface of the scapula. The scapular fossa lies along the dorsal/anterior margin of the acromion process and extends further dorsally than the glenoid facet, similar to other teleosauroids. hence, the dorsal/anterior margin of the acromion process of the scapula of *Ind. potamosiamensis* PRC-24 appears slightly in relief and forms a fine ridge, which can be associated to a reduced acromial crest. Compared to other teleosauroids, the scapular fossa of *Ind. potamosiamensis* PRC-24 appears to displays a proportionally more limited extension anteroposteriorly due to the smoothly bulged surface of the scapula directly anteriorly to the glenoid facet.

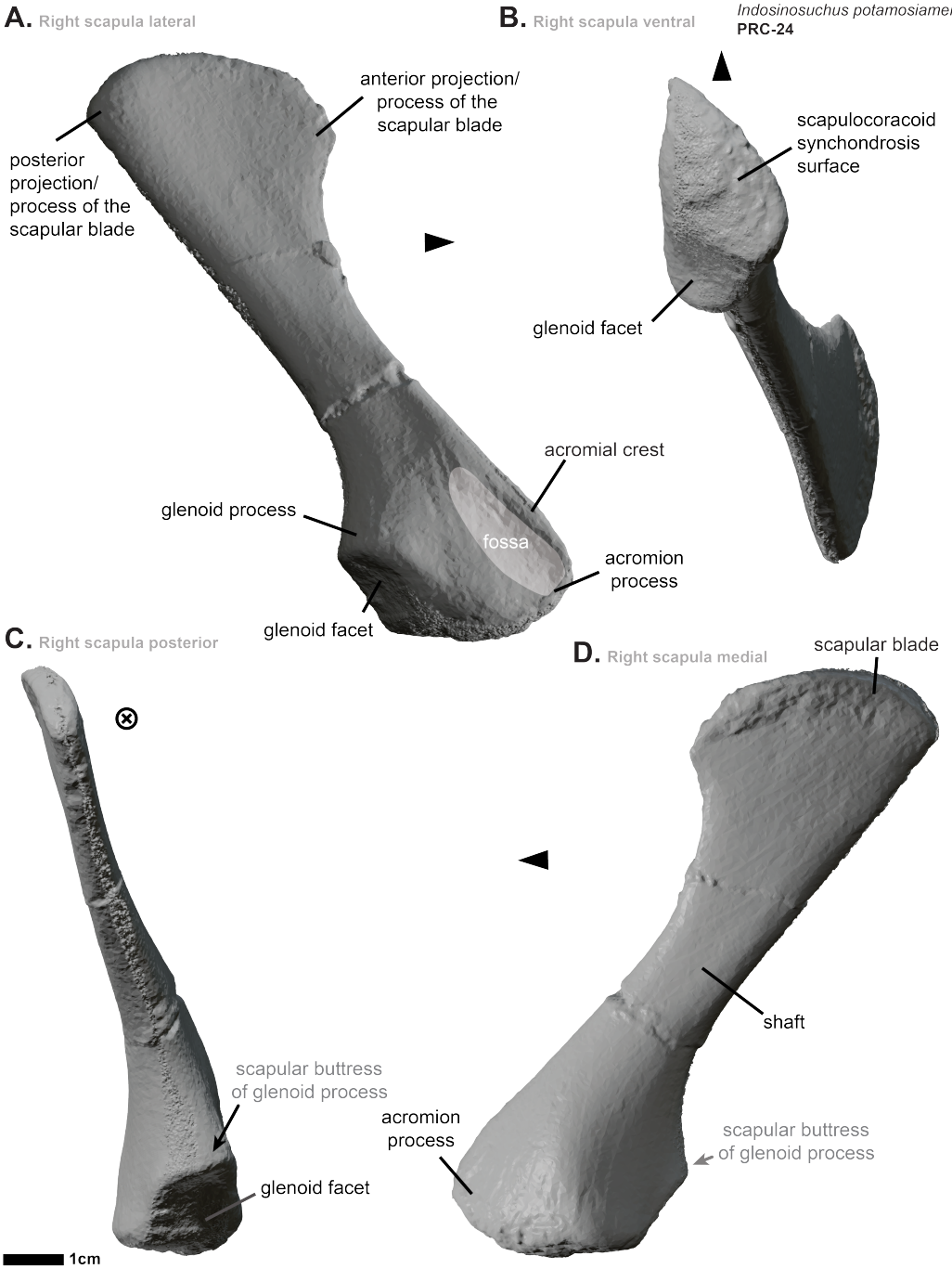


FIGURE 47. Pectoral girdle of *Indosinosuchus potamosiamensis* PRC-24 (3D models). **A.** Right scapula in lateral view ; **B.** Right scapula in ventral view ; **C.** Right scapula in posterior view ; **D.** Right scapula in medial view. Arrow points anteriorly. Cross indicates posterior view. 3D model courtesy of Suravech Suteethorn.

8.4. ***Teleosaurus cadomensis* Lamouroux, 1820.** For measurements, see table 6.

8.4.1. *Scapula.* The scapula of *Teleosaurus cadomensis* NHMUK PV OR 31836 (see figs. 41 and 48) strongly differs from that of basal teleosauroids in displaying the combination of a slender shaft and confined scapular blade (*e.g. Mycterosuchus* NHMUK PV R 2617, *Ind. potamosiamensis*, *Platysuchus* SMNS 9930, UMH-0005 and *Platysuchus* Kloster Banz unnumbered specimen, *Macrospondylus* SMNS 54063, SMNS 9428 & PMU 35980, *Charitomenosuchus* NHMUK PV R 3806, *Neosteneosaurus* NHMUK PV R 3701, *Lemmysuchus* NHMUK PV R 3168). Indeed, the neck of the scapula of *Te. cadomensis* NHMUK PV OR 31836 displays an overall constant anteroposterior thickness throughout its height. This is due to the anterior and posterior margins of the scapula of *Te. cadomensis* NHMUK PV OR 31836 being parallel: the anterior margin is concave whereas the posterior margin is convex with a similar degree of curvature. In comparison, only the scapula *Charitomenosuchus* NHMUK PV R 3806 shows parallel anterior and posterior margins, as the posterior margin is most often concave in other teleosauroids (*e.g. Mycterosuchus* NHMUK PV R 2617, *Platysuchus* SMNS 9930, UMH-0005 and *Platysuchus* Kloster Banz unnumbered specimen, *Macrospondylus* SMNS 54063, SMNS 9428 & PMU 35980, *Charitomenosuchus* NHMUK PV R 3806, *Neosteneosaurus* NHMUK PV R 3701, *Lemmysuchus* NHMUK PV R 3168). In *Te. cadomensis* NHMUK PV OR 31836, the anteroposterior constriction of the shaft of the scapula is located around the mid-height of the bone, which is most similar to *Ind. potamosiamensis* PRC-24 and *Neosteneosaurus* NHMUK PV R 3701.

Another trait adding to the slenderness appearance of the scapula of *Te. cadomensis* NHMUK PV OR 31836 is the confined scapular blade. Indeed, the anteroposterior length of the scapular blade of *Te. cadomensis* NHMUK PV OR 31836 is only slightly larger than the constriction of the shaft of the scapula, unlike in most teleosauroids (*e.g. Platysuchus* SMNS 9930, UMH-0005 and *Platysuchus* Kloster Banz unnumbered specimen, *Ind. potamosiamensis* PRC-24, *Mycterosuchus* NHMUK PV R 2617, *Macrospondylus* SMNS 54063, SMNS 9428 & PMU 35980, *Neosteneosaurus* NHMUK PV R 3701, *Lemmysuchus* NHMUK PV R 3168). In comparison, *Charitomenosuchus* NHMUK PV R 3806 also presents a short scapular blade, but the latter still flares out and exceeds the shaft's anteroposterior thickness. In *Te. cadomensis* NHMUK PV OR 31836, the anterior and posterior corners of the scapular blade are located on the same level dorsally as in *Mycterosuchus* NHMUK PV R 2617, *Charitomenosuchus* NHMUK PV R 3806 and *Lemmysuchus* NHMUK PV R 3168. However, the dorsal margin of the scapular blade of *Te. cadomensis* NHMUK PV OR 31836 is markedly convex, with the apex of the concavity only slightly shifted anteriorly so that it appears almost centered. Other teleosauroids with a markedly convex scapular blade include *Ind. potamosiamensis* PRC-24, *Macrospondylus* SMNS 54063 & PMU 35980, and also *Platysuchus* which is the only of the three not presenting a hemispherical shape (*i.e.* the apex of the concavity is not centered but posteriorly shifted). In comparison, the scapular blade of *Mycterosuchus* NHMUK PV R 2617, *Charitomenosuchus* NHMUK PV R 3806, *Neosteneosaurus* NHMUK PV R 3701 and *Lemmysuchus* NHMUK PV R 3168 is relatively flat to slightly convex. The scapular blade of *Te. cadomensis* NHMUK PV OR 31836 further differs from other teleosauroids in displaying smooth and rounded anterior and posterior corners, which emphasize the rounded appearance of the scapular blade. In *Ind. potamosiamensis* PRC-24, the extremities of the scapular blade form obtuse angles with relatively pointed apexes. In other teleosauroids, one of the corner is usually sharper than the other (*e.g. Mycterosuchus* NHMUK PV R 2617, *Charitomenosuchus* NHMUK PV R 3806, *Lemmysuchus* NHMUK PV R 3168, *Macrospondylus* SMNS 54063), but in *Platysuchus* UMH-0005 both extremities are relatively sharp. The scapular blade of *Neosteneosaurus* NHMUK PV R 3701 seems to present smooth anterior and posterior corners, not unlike *Te. cadomensis* NHMUK PV OR 31836. The medial surface of the scapula of *Te. cadomensis* NHMUK PV OR 31836 presents a series a long ridges dorsoventrally oriented (so parallel to the longest axis of the bone) which start near the dorsal margin of the scapular blade. The ridges reach a little less than one-third of the total dorsoventral height of the

scapula.

Ventrally, the shaft of the scapula of *Te. cadomensis* NHMUK PV OR 31836 flares out to form the proximal region of the scapula. The latter is proportionally well-developed as it accounts for twice the anteroposterior length of the scapular blade, which greatly exceeds what is observed in other teleosauroids (*e.g. Platysuchus* SMNS 9930, UMH-0005 and *Platysuchus* Kloster Banz unnumbered specimen, *Ind. potamosiamensis* PRC-24, *Mycterosuchus* NHMUK PV R 2617, *Macrospondylus* SMNS 54063 & PMU 35980, *Neosteneosaurus* NHMUK PV R 3701, *Lemmysuchus* NHMUK PV R 3168, *Charitomenosuchus* NHMUK PV R 3806). The anterior margin of the scapula of *Te. cadomensis* NHMUK PV OR 31836 appears concave throughout its entire length, but there is a slight change in shape as the scapula widens to form the proximal area. Ventrally, the anterior margin of the scapula culminates to form a blunt and rounded corner anteroventrally oriented corresponding to the apex of the acromion process. Similar to other teleosauroids, the apex of the acromion process of the scapula of *Te. cadomensis* NHMUK PV OR 31836 is located on the same level as the scapulocoracoid synchondrosis surface. The extent of the latter is not clearly observable, but it is possible that it ranged from the apex of the acromion process until the first ventral bump. Likewise, since the lateral side of the scapula of *Te. cadomensis* NHMUK PV OR 31836 is obstructed, the shape and exact extent of the glenoid process are not observable. Yet, due to the relative small difference in height between the tip of the scapular buttress of the glenoid process and the ventral margin of the scapula, it is possible that the glenoid process was mainly posteriorly oriented as in *Platysuchus* SMNS 9930, UMH-0005 and *Platysuchus* Kloster Banz unnumbered specimen and *Ind. potamosiamensis* PRC-24 and also *Neosteneosaurus* NHMUK PV R 3701. The posterior half of the ventral margin of the scapula presumably corresponding to the area of the glenoid process is strongly undulated: it forms two marked bumps ventrally separated by a strong indentation (which could be a broken artefact). In *Te. cadomensis* NHMUK PV OR 31836, the scapular buttress of the glenoid process forms a protruding corner posteriorly, as in *Platysuchus* SMNS 9930, UMH-0005 and *Platysuchus* Kloster Banz unnumbered specimen and *Ind. potamosiamensis* PRC-24. In comparison, the scapular buttress of *Neosteneosaurus* NHMUK PV R 3701 is less prominent posteriorly. Dorsally to the scapular buttress, the posterior margin of the scapula of *Te. cadomensis* NHMUK PV OR 31836 forms a concave curve as in *Platysuchus* SMNS 9930, UMH-0005 and *Platysuchus* Kloster Banz unnumbered specimen and *Ind. potamosiamensis* PRC-24. In *Te. cadomensis* NHMUK PV OR 31836, it accounts for about one-third of the total height of the scapula. The switch in the concavity of the posterior margin of the scapula of *Te. cadomensis* NHMUK PV OR 31836 marks the junction between the neck of the scapula and the beginning of the proximal widening.

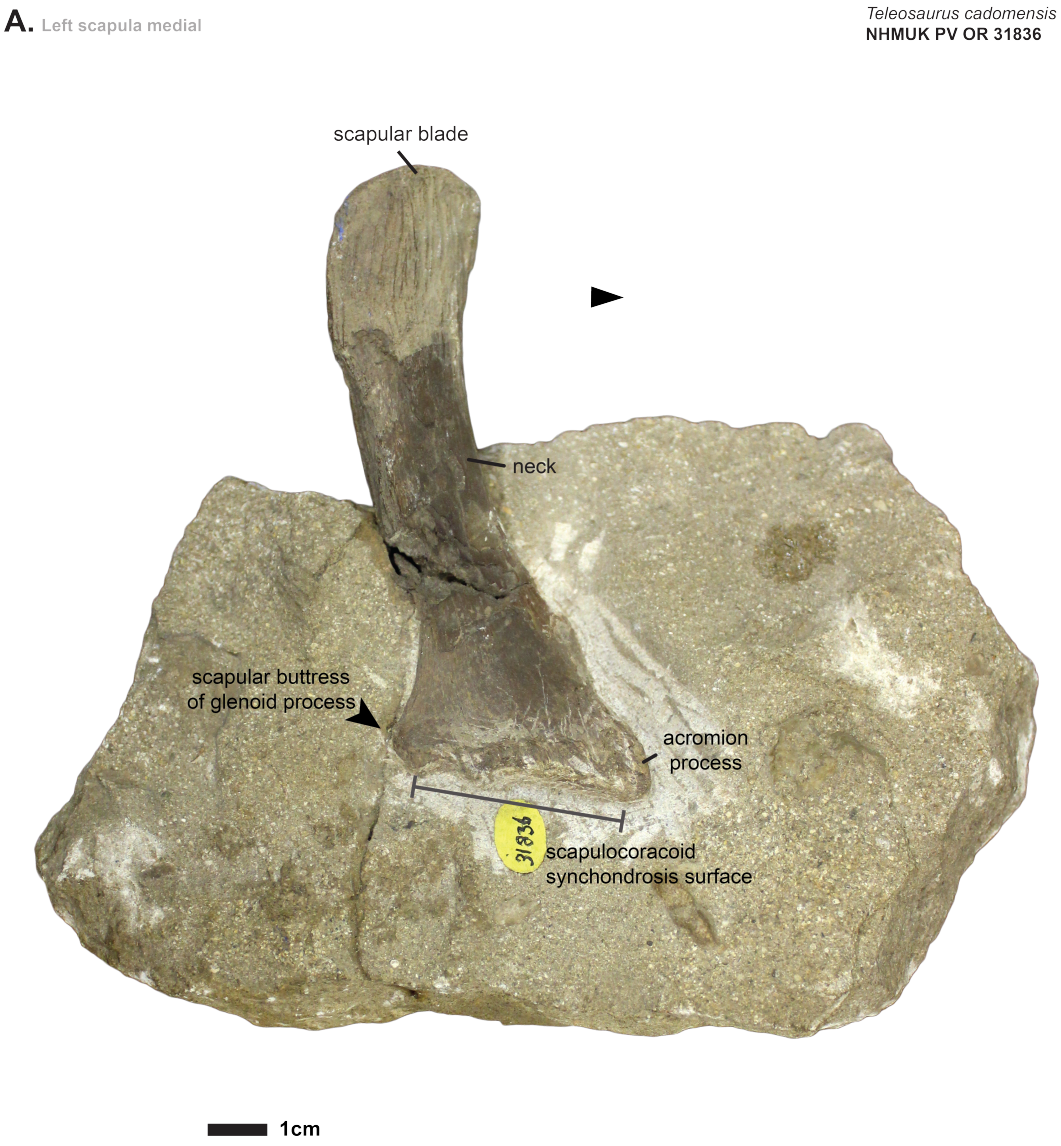


FIGURE 48. Pectoral girdle of *Teleosaurus cadomensis* NHMUK PV OR 31836 (photograph). **A.** Left scapula in medial view. Arrow points anteriorly.

8.5. ***Platysuchus multiscrobiculatus* Berckhemer, 1929.** For measurements, see tables 6 and 7. The unnumbered specimen labelled *Platysuchus multiscrobiculatus* from the Kloster Banz see (see fig. 50) is currently referred to *Platysuchus multiscrobiculatus* in our study based on the similarity of their pelvic and pectoral girdles but will require a thorough re-examination in the future.

8.5.1. *Scapula.* The scapula of *Platysuchus multiscrobiculatus* SMNS 9930 & UMH-0005 (see figs. 41, 49 and 51), and *Platysuchus* Kloster Banz unnumbered specimen see (see fig. 50) displays a uniquely enlarged scapular blade and proximal head within Teleosauroidea. In addition, the scapula of *Platysuchus* SMNS 9930, UMH-0005 and *Platysuchus* Kloster Banz unnumbered specimen shows a proportionally strong neck constriction in relation to both its total height and to the extension of the scapular blade and proximal region. Overall, the maximal constriction of the neck of the scapula of *Platysuchus* SMNS 9930 reaches around 16% of its total dorsoventral height, which is a value similar to those of *Mycterosuchus* NHMUK PV R 2617, *Macrospondylus* SMNS 54063, SMNS 9428 & PMU 35980 and *Pelagosaurus* (BRLSI M.1418, BRLSI M.3578). In *Neosteneosaurus* NHMUK PV R 3701, *Lemmysuchus* NHMUK PV R 3168 and *Charitomenosuchus* NHMUK PV R 3806, the relative value of the constriction is even less than 15%. In *Platysuchus* SMNS 9930, the neck constriction is located around the two-fifth of the height of the bone as in *Macrospondylus* SMNS 54063, SMNS 9428 & PMU 35980.

The anterior and posterior margins of the scapula of *Platysuchus* SMNS 9930, UMH-0005 and *Platysuchus* Kloster Banz unnumbered specimen are strongly concave unlike any other teleosauroid. Presumably, the anterior margin of the scapula presented a sinusoidal shape with the ventral portion becoming slightly convex as it forms the acromion process (see fig. 49 C). In contrast, the posterior margin appears concave throughout, with its apex being slightly shifted towards the proximal end of the bone. In comparison, *Mycterosuchus* NHMUK PV R 2617 and *Macrospondylus* SMNS 54063, PMU 35980 also display a deeply concave anterior margin but a straighter posterior one. Another distinct feature of *Platysuchus* SMNS 9930, UMH-0005 and *Platysuchus* Kloster Banz unnumbered specimen corresponds to the overall shape of its scapular blade: its anterior and posterior corners are not aligned and its dorsal margin is asymmetrical and strongly arched. Indeed, the anterior corner of the scapular blade of *Platysuchus* SMNS 9930 is located further ventrally than the posterior one so that the line drawn between the corners is strongly tilted in relation to the ventral surface of the proximal region. Within Teleosauroidea, only *Macrospondylus* SMNS 54063, SMNS 9428 & PMU 35980, *Neosteneosaurus* NHMUK PV R 3701 and *Ind. potamosiamensis* (PRC-24; Martin et al. (2019b)) share a similar configuration. In parallel, the dorsal margin of the scapular blade of *Platysuchus* SMNS 9930 forms a strongly convex dome whose apex is posteriorly shifted in relation to the mid-length of the process, giving a unique hunched appearance to the bone. Most teleosauroids have a lightly domed scapular blade, and amongst those bearing a strongly arched scapular blade (*e.g. Macrospondylus* SMNS 54063, SMNS 9428, PMU 35980 and *Ind. potamosiamensis* PRC-24 Martin et al. (2019b)), the dorsal margin forms a relatively symmetrical dome with a more centered apex.

Proximally, the neck of the scapula of *Platysuchus* SMNS 9930, UMH-0005 and *Platysuchus* Kloster Banz unnumbered specimen markedly widens as it forms the glenoid and acromion processes. Hence, the glenoid process appears posteriorly prominent which strongly contrasts with most teleosauroids, but is similar to what is observed in *Ind. potamosiamensis* PRC-24. This phenomenon is imputable to both the shape of the posterior margin and the position of the glenoid facet. Indeed, in *Platysuchus* SMNS 9930 and *Ind. potamosiamensis* PRC-24, the glenoid facet is oriented posteroventrally rather than laterally as in most teleosauroids. In *Neosteneosaurus* NHMUK PV R 3701, the glenoid facet is also oriented mainly posteroventrally, but the glenoid process is less prominent than in *Platysuchus* SMNS 9930 and *Ind. potamosiamensis* PRC-24. The glenoid facet of the scapula of *Platysuchus* SMNS 9930 is tilted an angle of 45° with the plane which coincides with the scapulocoracoid synchondrosis surface. The latter

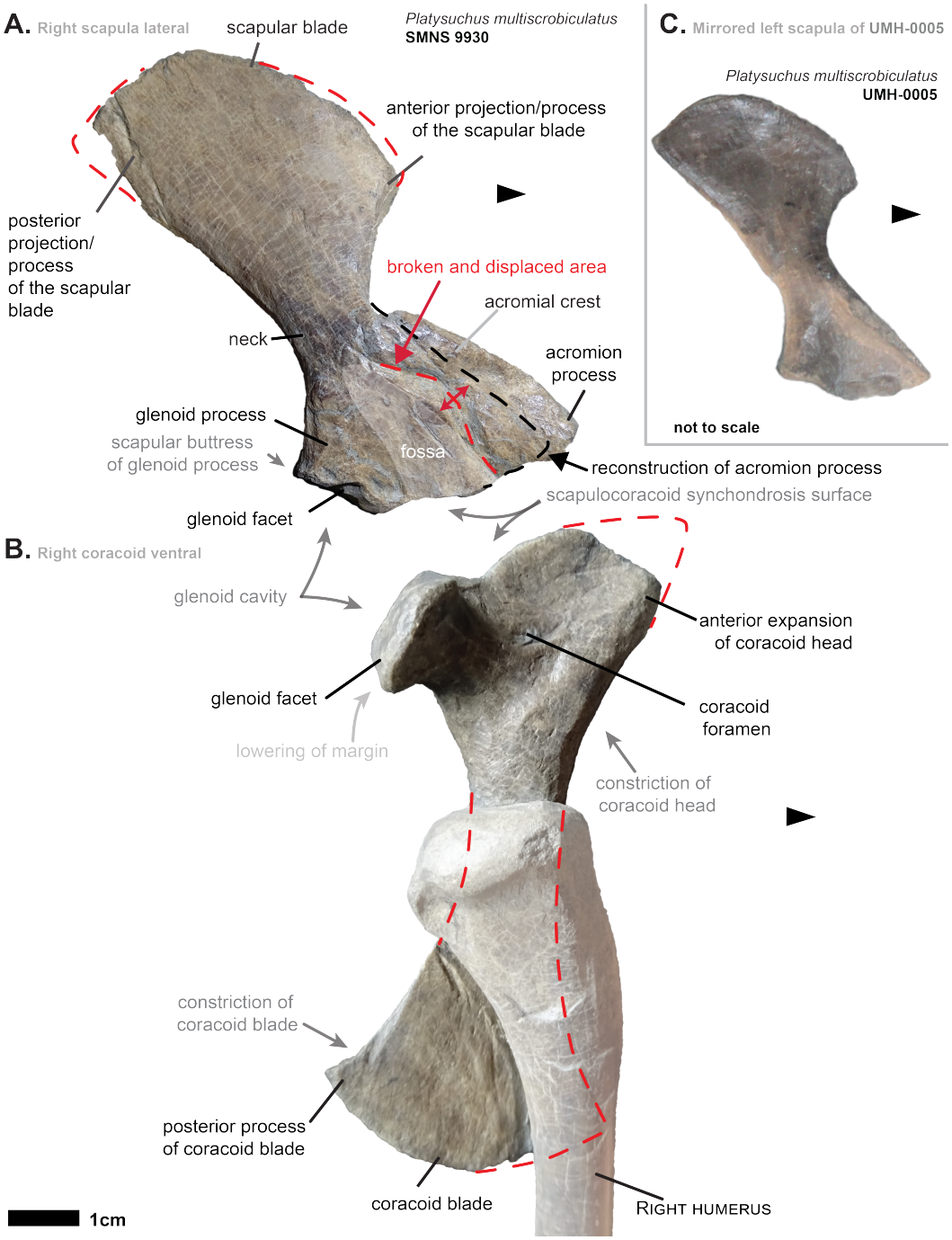


FIGURE 49. Pectoral girdle of *Platysuchus multiscrobiculatus* SMNS 9930 (**A** and **B**) & UMH-0005 (**C**) (photographs). **A.** Right scapula in lateral view; **B.** Right coracoid in ventral view; **C.** Left scapula of UMH-0005 mirrored not to scale. Arrow points anteriorly. Red dashed lines indicate missing parts. Reconstruction of missing parts of the scapula of SMNS 9930 based on UMH-0005. Reconstruction of missing parts of the coracoid based on *Macrospondylus bollensis* SMNS 54063.

seems to account for most of the anteroposterior length of the proximal region of the scapula, even with the posterior position of the glenoid facet.

The lateral surface of the scapula between the glenoid and acromion processes appears slightly shallow as in other teleosauroids, and could correspond to the scapular fossa of extant crocodylians. Similarly to other teleosauroids, in *Platysuchus* SMNS 9930, the tip of the acromion process is positioned relatively ventrally, and appears to almost coincide with the same plane as the scapulocoracoid synchondrosis surface. The dorsal margin of the acromion process is slightly convex throughout, which gives the anterior margin of the scapula its undulated appearance. In comparison, the dorsal margin of the acromion process of the scapula of *Macrospondylus* SMNS 54063, SMNS 9428 & PMU 35980 also forms a bulge but shows a greater intensity. As in other teleosauroids, the lateral surface of the acromion process does not display a protruding ridge in *Platysuchus* SMNS 9930, UMH-0005 and *Platysuchus* Kloster Banz unnumbered specimen. However, the dorsal margin of the acromion process appears proportionally thickened and could have corresponded to the acromial crest of extant crocodylians.

8.5.2. *Coracoid.* The coracoid of *Platysuchus multiscrobiculatus* SMNS 9930 (see figs. 43, 49 and 51) and *Platysuchus* Kloster Banz unnumbered specimen (see fig. 50) possesses the typical teleosauroids features: hourglass outline, enclosed coracoid foramen, large glenoid facet, and indications of a tapering anterior expansion for the coracoid head. The coracoid head of *Platysuchus* SMNS 9930 differs from that of other teleosauroids based on the following combination of traits: the anterior expansion has convex medial and lateral margin, the anterior expansion also shows a strong lateral inclination (in relation to the long axis of the shaft of the coracoid), the glenoid facet is strongly prominent, the coracoid blade displays a marked anteroposterior symmetry.

The coracoid of *Platysuchus* SMNS 9930 (see fig. 49) and *Platysuchus* Kloster Banz unnumbered specimen (see fig. 50) appears to displays a relatively slender silhouette, with smoothly concave anterior and posterior margins as in most teleosauroids (*e.g. Aeolodon* NHMUK PV R 1086, *Macrospondylus* PMU 35980, *Charitomenosuchus* NHMUK PV R 3806, *Neosteneosaurus* NHMUK PV R 3701, *Lemmysuchus* NHMUK PV R 3169). Yet, the coracoid head of *Platysuchus* strongly differs from what is observed in other teleosauroids, due to the shape of both its anterior expansion as well as its glenoid facet. Indeed, the anterior expansion of the coracoid head of *Platysuchus* SMNS 9930 and *Platysuchus* Kloster Banz unnumbered specimen is strongly inclined laterally and forms an angle of about 130° with the long axis of the shaft of the coracoid whereas this value is closer to a right-angle in most teleosauroids (*e.g. Aeolodon* NHMUK PV R 1086, *Mycterosuchus* NHMUK PV R 2617, *Charitomenosuchus* NHMUK PV R 3806, *Neosteneosaurus* NHMUK PV R 3701, *Lemmysuchus* NHMUK PV R 3169). In addition, the anterior expansion of the coracoid of *Platysuchus* SMNS 9930 and *Platysuchus* Kloster Banz unnumbered specimen displays an overall lancet arch shape: both its margins are convex and presumably met anteriorly to form a sharp apex. The lancet arch appearance of the anterior expansion of the coracoid head of *Platysuchus* SMNS 9930 is emphasized by the presence of a marked notch at the junction between the glenoid facet and the lateral margin of the anterior expansion. The latter forms a triangular indentation which also accentuates the prominent appearance of the glenoid facet. Indeed, the glenoid facet of the coracoid of *Platysuchus* SMNS 9930 is strongly protruding from the coracoid head, particularly as its underlying base – the glenoid process – is narrower and entirely concave giving it a pinched neck appearance. As a consequence, the margin surrounding the glenoid facet appears even more salient. The surface of the glenoid facet of the coracoid of *Platysuchus* SMNS 9930 is almost entirely concave with its ventral and anterior sides being slightly bulged. The concavity of the glenoid facet is prolonged towards the posteroventral side of the facet which results in the lowering of the margin along that border, as in most teleosauroids (*e.g. Mycterosuchus* NHMUK PV R 2617, *Macrospondylus* SMNS 9428, *Neosteneosaurus* NHMUK PV R 3701, *Lemmysuchus* NHMUK PV R 3169, *Machimosaurus* spp. see C on fig. 61). Yet,

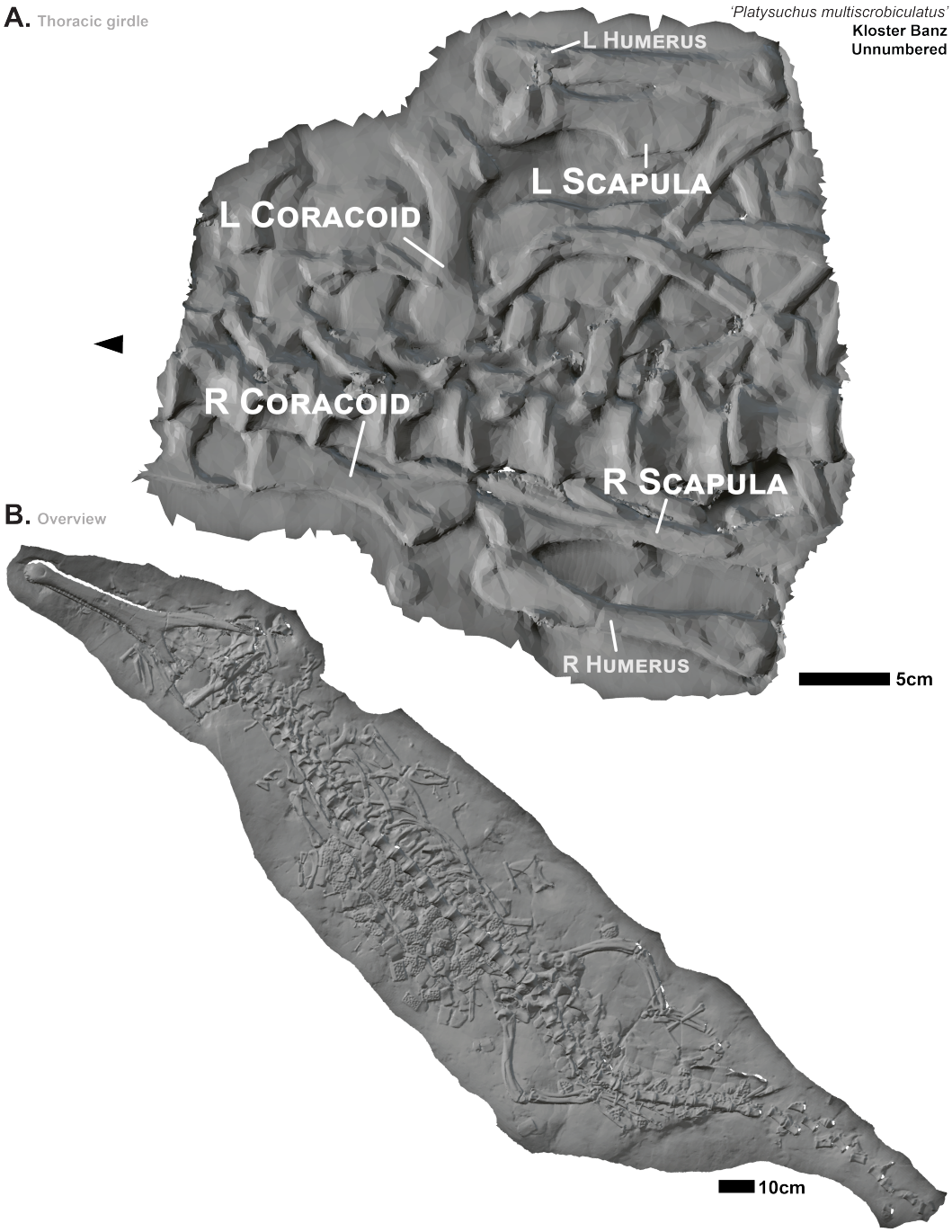


FIGURE 50. Pectoral girdle of *Platysuchus multiscrobiculatus* from Kloster Banz (unnumbered) (3D models). **A.** Pectoral girdle; **B.** Overview of the entire skeleton. Arrow points anteriorly.

this lowering of the posteroventral margin of the glenoid facet does not form a recurved rim as in extant crocodylians and dyrosaurids (*i.e.* the glenoid lip).

The exact shape of the shaft of the coracoid of *Platysuchus* SMNS 9930 is not recovered, but is relatively elongated and broad on the Kloster Banz specimen (see fig. 50). As in other teleosauroids, the coracoid of *Platysuchus* SMNS 9930 and *Platysuchus* Kloster Banz unnumbered specimen appears to gradually flare out to form the coracoid blade. The latter is relatively symmetrical as in *Macrospondylus* PMU 35980 and presumably *Lemmysuchus* NHMUK PV R 3169. In *Platysuchus* SMNS 9930, the preserved posterior portion of the coracoid blade displays a mainly posteriorly facing corner as well as a smoothly convex medial margin. In the *Platysuchus* Kloster Banz unnumbered specimen, the coracoid blade is preserved in its entirely and shows its overall dome-shaped and anteroposteriorly symmetrical medial margin. As a result, the extremities of the coracoid blade of the *Platysuchus* Kloster Banz unnumbered specimen form very similarly shaped sharp corners, whose main orientation is in the anteroposterior direction with little lateral component.

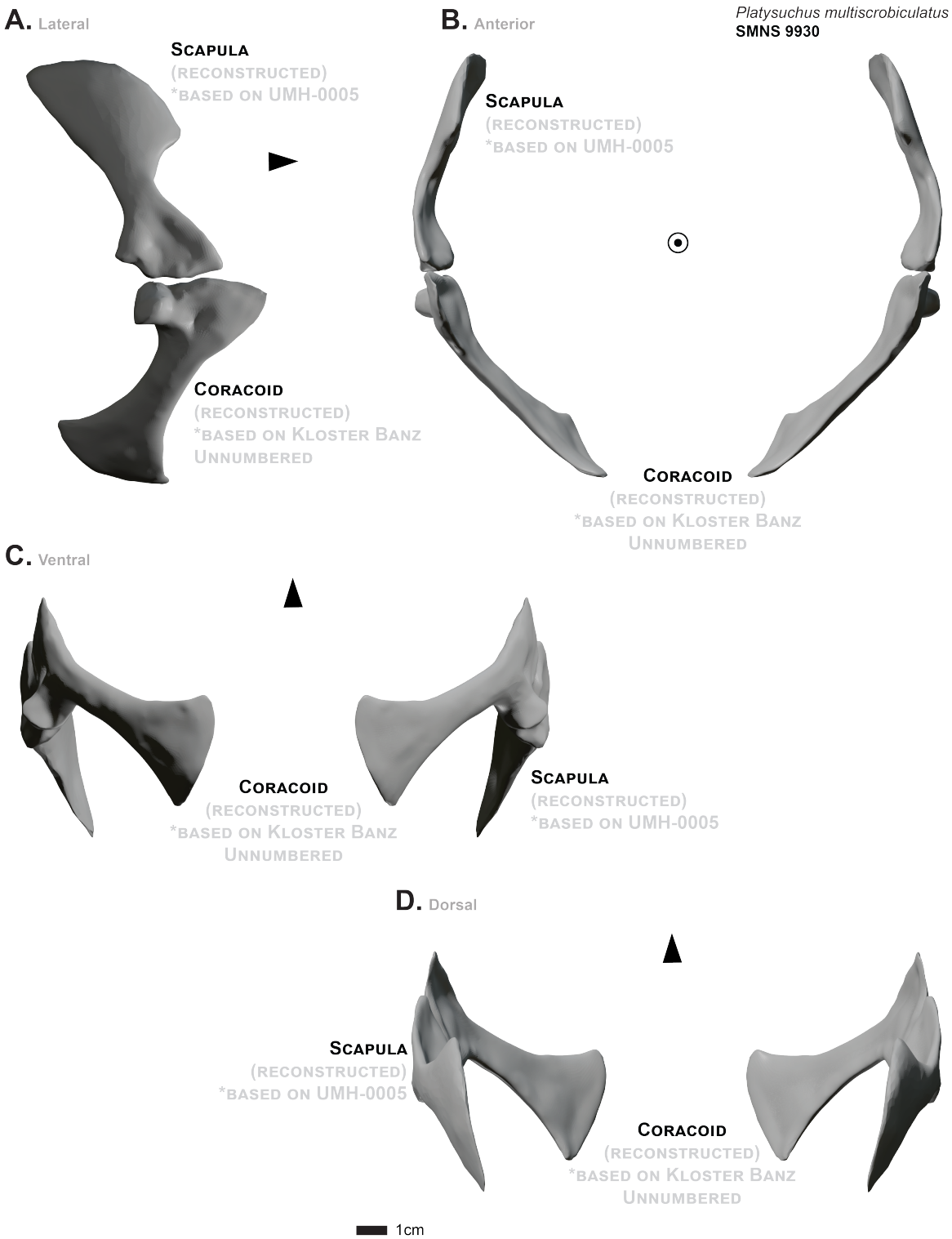


FIGURE 51. Reconstruction of the pectoral girdle of *Platysuchus multiscrobiculatus* SMNS 9930 (3D models). **A.** Lateral view; **B.** Anterior view; **C.** Ventral view; **D.** Dorsal view. Arrow points anteriorly. Target indicates anterior. The left scapula and coracoid are mirrored. The scapula has been reconstructed based on *Platysuchus multiscrobiculatus* UMH-0005, and the coracoid based on *Platysuchus multiscrobiculatus* Kloster Banz unnumbered specimen.

8.6. ***Macrospondylus bollensis* Jäger, 1828.** For measurements, see tables 6 and 7. The SMNS 9428 specimen is a juvenile; the presence of a saddle-like glenoid facet on the scapula can be attributed to an acquired ontogenetic change (Brochu, 1992).

8.6.1. *Scapula.* The scapula of *Macrospondylus bollensis* SMNS 54063, SMNS 9428 & PMU 35980 (see figs. 41, 52 and 53) shares several similarities with that of *Platysuchus* SMNS 9930, UMH-0005 and *Platysuchus* Kloster Banz unnumbered specimen within Teleosauroidea: the scapular blade and proximal region are similarly enlarged, the acromion process is convex, and the neck shows a strong anteroposterior constriction. Comparatively, the scapula of *Mycterosuchus* NHMUK PV R 2617 appears overall similar to that of *Macrospondylus* SMNS 54063, SMNS 9428 & PMU 35980, but shows a shorter distal blade and proximal region resulting in a proportionally lesser neck constriction.

The anterior margin of the scapula of *Macrospondylus* SMNS 54063, SMNS 9428 & PMU 35980 is strongly undulated: the acromion process forms a markedly convex bulge ventrally whereas the neck region is strongly concave. In addition, the degree of concavity is uneven between the acromion process and the neck. Indeed, the acromion process shows a lower degree of convexity than the following concavity of the neck, which results in a widely spread but proportionally slightly protruding acromion process. In comparison, the concavity of the neck shows a shorter base arc with a proportionally stronger protrusion of its apex – a.k.a the neck shows a stronger recess anteriorly. The posterior margin of the scapula of *Macrospondylus* SMNS 54063, SMNS 9428 & PMU 35980 is slightly concave throughout, but shows some minor waving dorsal to the maximal constriction of the neck (*i.e.* the area flaring out to form the scapular blade). The dorsoventral position (at about two–fifth) and intensity of the neck constriction of the scapula of *Macrospondylus* SMNS 54063, SMNS 9428 & PMU 35980 is most similar to what is observed in *Platysuchus* SMNS 9930 within Teleosauroidea.

The scapular blade of *Macrospondylus* SMNS 54063, SMNS 9428 & PMU 35980 takes the shape of a widened fan with a markedly convex dorsal margin. The apex of the dorsal concavity appears to be positioned around the mid length of the scapular blade anteroposteriorly, which contrasts with the strongly asymmetrical appearance of the scapula of *Platysuchus* SMNS 9930, UMH-0005 and *Platysuchus* Kloster Banz unnumbered specimen. In *Macrospondylus* SMNS 54063, SMNS 9428 & PMU 35980, the corners of the scapular blade are not aligned in the coronal plane as the anterior corner is located more ventrally than the posterior one as in *Platysuchus* SMNS 9930, UMH-0005 and *Platysuchus* Kloster Banz unnumbered specimen. This asymmetry of the corners of the scapular blade of *Macrospondylus* SMNS 54063, SMNS 9428 & PMU 35980 concurrently results in an anteroposteriorly enlarged scapular blade (which is also observed in *Platysuchus* SMNS 9930, UMH-0005 and *Platysuchus* Kloster Banz unnumbered specimen within Teleosauroidea). Indeed, the scapular blade of *Macrospondylus* SMNS 54063, SMNS 9428 & PMU 35980 is about 1.4–1.6 times longer anteroposteriorly than the proximal region of the bone (encompassing the acromion and glenoid processes). However, this value exceeds that of *Platysuchus* SMNS 9930, UMH-0005 and *Platysuchus* Kloster Banz unnumbered specimen as both its dorsal and ventral extremities are similarly sized.

The proximal region of the scapula directly starts underneath the maximal constriction of the neck. As mentioned earlier, the acromion process forms a convex bulge throughout and culminates ventrally into a rounded apex. The presence of an anteriorly oriented apex is a characteristic shared among teleosauroids, but is also found in *Turnersuchus* LRM 2021/45, *Pelagosaurus* BRLSI M.1418, and in extant crocodylians. The anterior region of the scapula of *Macrospondylus* SMNS 54063, SMNS 9428 & PMU 35980 (see fig. 52) strongly departs from that of *Platysuchus* SMNS 9930, UMH-0005 and *Platysuchus* Kloster Banz unnumbered specimen in being anteroposteriorly less expanded. However, the proximal region of the scapula of *Macrospondylus* SMNS 54063, SMNS 9428 & PMU 35980 is larger

than what is observed in more derived teleosauroids. The lateral surface of the acromion process of the scapula of *Macrospondylus* SMNS 9428 displays a shallow recessed area – the scapular fossa – which extends posteriorly until the glenoid facet as in other teleosauroids. In addition, the lateral surface of the acromion process of the scapula of *Macrospondylus* SMNS 9428 (and other teleosauroids) does not display a laterally protruding ridge as in extant crocodylians or dyrosaurids. As in other teleosauroids, the scapular fossa of *Macrospondylus* SMNS 9428 does not extend anteriorly until the margin of the bone, which emphasizes the anteriormost margin of the acromion process. For this reason, the anterodorsal margin of the acromion process appears like a 'crest' (see fig. 52 C).

The glenoid facet of the scapula of *Macrospondylus* SMNS 9428 is located on the lateral surface of the bone, cornered in the posterior extremity of the proximal region. As a result, the scapulocoracoid synchondrosis surface extends medially to the glenoid facet and accounts for the entire anteroposterior length of the proximal region. This positioning of the glenoid facet is found in other teleosauroids except *Ind. potamosiamensis* PRC-24, *Platysuchus* SMNS 9930, UMH-0005 and *Platysuchus* Kloster Banz unnumbered specimen and *Neosteneosaurus* NHMUK PV R 3701 for which it is located more posteriorly. In *Macrospondylus* SMNS 9428, the glenoid facet is lightly concave with a semioval shape and is dorsally bordered by a slightly prominent ridge, as in *Mycterosuchus* NHMUK PV R 2617, *Charitomenosuchus* NHMUK PV R 3806, and *Neosteneosaurus* NHMUK PV R 3701. The ridge progressively fades on the anterior and posterior sides of the glenoid facet. The glenoid process of the scapula of *Macrospondylus* SMNS 9428 corresponds to the mediolaterally thicker area encompassing the glenoid facet. This process is tenuous as it does not significantly protrude from the main body of the scapula, similarly to most teleosauroids (except for *Platysuchus Macrospondylus* SMNS 54063, SMNS 9428 & PMU 35980).

8.6.2. *Coracoid.* The coracoid of *Macrospondylus bollensis* SMNS 54063, SMNS 9428 & PMU 35980 (see figs. 43, 52 and 53) displays several common teleosauroid features: a hourglass silhouette, a long and slender shaft, a triangular anterior expansion, a large glenoid facet, an enclosed coracoid foramen. It also possesses an anteroposteriorly symmetrical coracoid blade which is possibly also present in *Lemmysuchus* NHMUK PV R 3169 and *Platysuchus* SMNS 9930 and *Platysuchus* Kloster Banz unnumbered specimen. The coracoid of *Macrospondylus* SMNS 54063, SMNS 9428 & PMU 35980 differs from that of other teleosauroids in prepossessing the combination of: a proportionally short anterior expansion and large scapulocoracoid synchondrosis surface, a more laterally tilted anterior expansion (in relation to the long axis of the shaft of the coracoid), similarly concave anterior and posterior margins leading to a markedly (anteroposteriorly) symmetrical coracoid blade.

As in several teleosauroids, the coracoid of *Macrospondylus* SMNS 54063, SMNS 9428 & PMU 35980 (see fig. 52) displays an overall slender silhouette due to the low degree of curvature of both its anterior and posterior margins plus the relative alignment of their apex (*e.g. Aeolodon* NHMUK PV R 1086, *Charitomenosuchus* NHMUK PV R 3806, *Neosteneosaurus* NHMUK PV R 3701). The coracoid of *Macrospondylus* SMNS 54063, SMNS 9428 & PMU 35980 also appears ventrally curved due to the lightly concave appearance of the dorsal side of the coracoid head and slightly convex ventral surface. In *Macrospondylus* SMNS 54063, SMNS 9428 & PMU 35980, the slender appearance of the bone is accentuated by the proportionally long shaft which accounts for about 40% of the total mediolateral extension of the coracoid. In comparison, *Aeolodon* NHMUK PV R 1086, *Charitomenosuchus* NHMUK PV R 3806 and *Neosteneosaurus* NHMUK PV R 3701 also possess comparatively long shafts (about 39–43% of total length) whereas *Mycterosuchus* NHMUK PV R 2617, *Lemmysuchus* NHMUK PV R 3169 and *Machimosaurus* spp. (see C on fig. 61) display lower values (*i.e.* 30–35%). Furthermore, the shaft of the coracoid *Macrospondylus* SMNS 54063, SMNS 9428 & PMU 35980 displays a relatively thin width anteroposteriorly which remains relatively constant throughout its length. As such, the shaft of the coracoid of *Macrospondylus* SMNS 54063, SMNS 9428 & PMU 35980 presents an overall rod-like

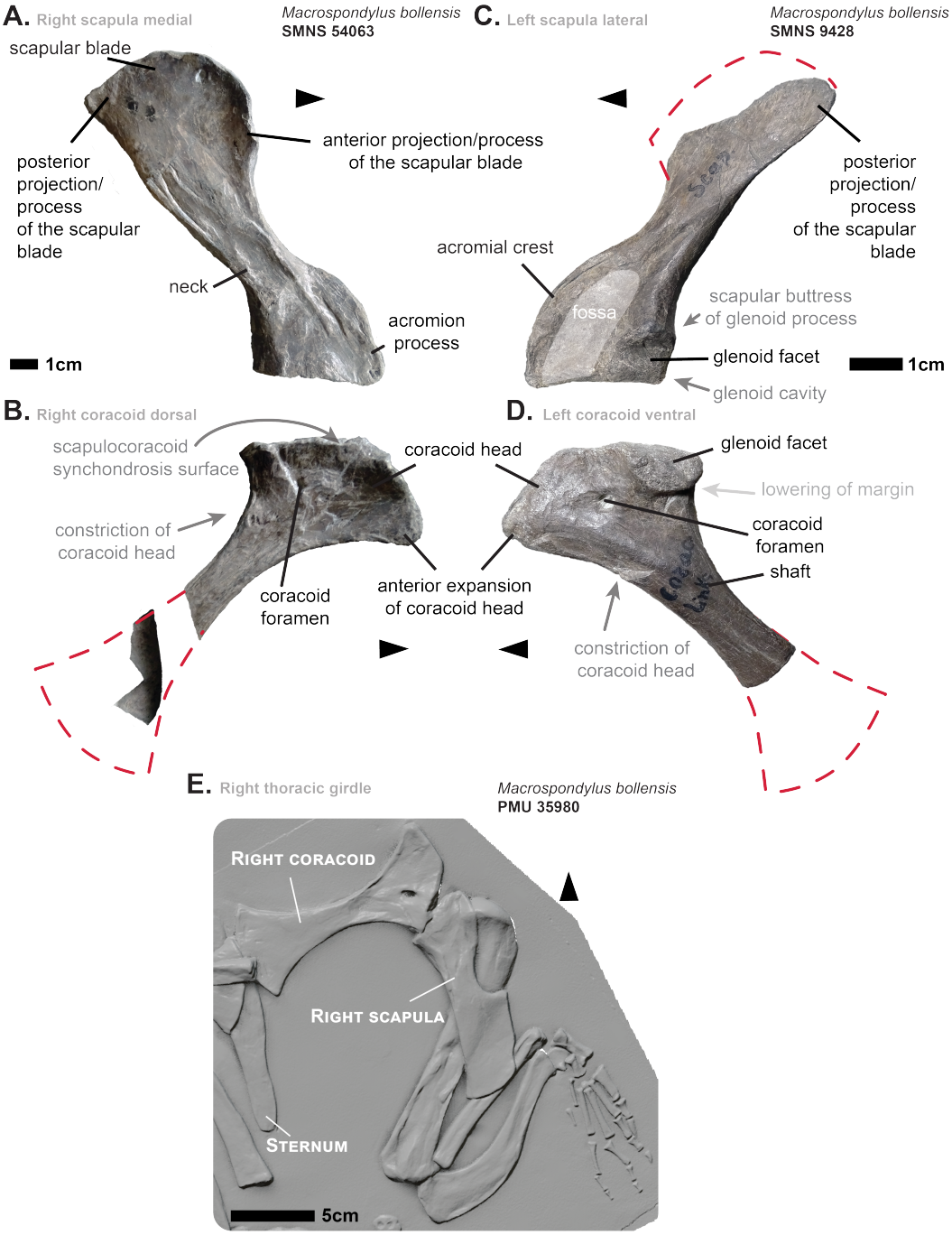


FIGURE 52. Pectoral girdle of *Macrospondylus bollensis* SMNS 54063 (A&B; photographs), *Macrospondylus bollensis* SMNS 9428 (C&D; photographs) and *Macrospondylus bollensis* PMU 35980 (E; 3D model). **A.** Right scapula in medial view; **B.** Right coracoid in dorsal view; **C.** Left scapula in lateral view; **D.** Left coracoid in ventral view; **E.** Overview of right pectoral girdle. Arrow points anteriorly. Red dashed lines indicate missing parts. Reconstruction of missing parts of the scapula of *Macrospondylus bollensis* SMNS 9428 based on *Macrospondylus bollensis* SMNS 54063 and *Macrospondylus bollensis* PMU 35980. Reconstruction of missing parts of the coracoids of *Macrospondylus bollensis* SMNS 54063 and *Macrospondylus bollensis* SMNS 9428 based on *Macrospondylus bollensis* PMU 35980.

shape without any marked anteroposterior constriction, similar to *Charitomenosuchus* NHMUK PV R 3806 and *Neosteneosaurus* NHMUK PV R 3701.

In *Macrospondylus* PMU 35980 the relative size of coracoid head accounts for about half of the total mediolateral height of the coracoid, which is similar to what is observed in *Charitomenosuchus* NHMUK PV R 3806. In comparison, other teleosauroids show either proportionally shorter (*e.g. Aeolodon* NHMUK PV R 1086, *Machimosaurus* spp. see C on fig. 61) or larger coracoid heads (*e.g. Mycterosuchus* NHMUK PV R 2617, *Neosteneosaurus* NHMUK PV R 3701). However, the coracoid head of *Macrospondylus* SMNS 54063, SMNS 9428 & PMU 35980 departs from that of most teleosauroids in displaying a proportionally shorter anterior expansion and subsequently longer scapulocoracoid synchondrosis surface, as in *Platysuchus* SMNS 9930 and *Platysuchus* Kloster Banz unnumbered specimen but to a lesser extent. The relative size of the scapulocoracoid synchondrosis surface of the coracoid of *Macrospondylus* mirrors the enlarged proximal region of its scapula (which is almost entirely constituted by the scapulocoracoid synchondrosis surface). Overall, the shape of the anterior expansion of the coracoid of *Macrospondylus* SMNS 54063, SMNS 9428 & PMU 35980 is strongly similar to what is observed in most teleosauroids (except *Aeolodon* NHMUK PV R 1086 & MNHN.F.CNJ 78 and *Platysuchus* SMNS 9930 and *Platysuchus* Kloster Banz unnumbered specimen): the lateral and medial margins are rather straight and converge anteriorly into a relatively sharp apex, giving a triangular outline to the process. Yet, the anterior expansion of the coracoid head of *Macrospondylus* SMNS 54063, SMNS 9428 & PMU 35980 further differs from that of other teleosauroids in forming a slightly obtuse angle with the shaft of the coracoid (both medians are set at about 105–110°), whereas this angular relation is closer to 90° in *Aeolodon* NHMUK PV R 1086, *Mycterosuchus* NHMUK PV R 2617, *Charitomenosuchus* NHMUK PV R 3806, *Neosteneosaurus* NHMUK PV R 3701, and *Lemmysuchus* NHMUK PV R 3169.

As in most teleosauroids, the scapulocoracoid synchondrosis surface of the coracoid of *Macrospondylus* SMNS 54063, SMNS 9428 & PMU 35980 forms a relatively straight margin on the lateral side of the coracoid head and extends dorsally to the glenoid facet. The latter is found exclusively on the ventral surface of the coracoid head and is located along its posterior-most corner, as in other teleosauroids. As in *Mycterosuchus* NHMUK PV R 2617 and *Neosteneosaurus* NHMUK PV R 3701, the glenoid facet of the coracoid of *Macrospondylus* SMNS 9428 is bordered with a thin protruding rim over its posterior and ventral margins, which then becomes a rougher bulge along its anterior side. Similar to most teleosauroids, the glenoid facet displays an overall hemispherical shape with its surface being overall concave, especially towards its posteroventral side where the margin of the facet is actually slightly lowered. Subsequently, the anteriormost side of the glenoid facet of the coracoid of *Macrospondylus* SMNS 54063, SMNS 9428 & PMU 35980 is lightly convex. Hence, as in *Mycterosuchus* NHMUK PV R 2617 and *Neosteneosaurus* NHMUK PV R 3701, the glenoid process displays a concave surface over its posterior and ventral sides, but switches to slight convex anteriorly.

The coracoid foramen of *Macrospondylus* forms a small and sub-circular aperture on the ventral surface of the coracoid head SMNS 9428 but becomes larger and more elliptic on the dorsal surface SMNS 54063 & PMU 35980, which resembles what is observed in *Lemmysuchus* NHMUK PV R 3169. The elliptic dorsal aperture of the coracoid foramen of *Macrospondylus* SMNS 54063, SMNS 9428 & PMU 35980 has its longest axis oriented in the direction perpendicular to the scapulocoracoid synchondrosis surface similar to *Lemmysuchus* NHMUK PV R 3169. As in other teleosauroids, the coracoid foramen of *Macrospondylus* also constitutes a tilted canal: the dorsal aperture SMNS 54063 & PMU 35980 is proportionally closer to the lateral and posterior margins of the coracoid head than the ventral one SMNS 9428. In addition, the dorsal aperture is set along the anteroposterior axis of the coracoid head whereas the ventral aperture is set slightly underneath it. As in most teleosauroids, the coracoid foramen of *Macrospondylus* SMNS 54063, SMNS 9428 & PMU 35980 is relatively in line with the long axis of the

shaft of the coracoid, although the dorsal aperture shows a slight posterior deflection.

In *Macrospondylus* PMU 35980, the anteroposterior extension of the coracoid blade is slightly lesser than that of the coracoid head. The coracoid blade of *Macrospondylus* PMU 35980 strongly differs from that of most teleosauroids in displaying a marked anteroposterior symmetry due to the relative similarly in the curvature of the anterior and posterior margins of the coracoid (*e.g.* *Mycterosuchus* NHMUK PV R 2617, *Aeolodon* NHMUK PV R 1086, *Charitomenosuchus* NHMUK PV R 3806, *Neosteneosaurus* NHMUK PV R 3701). Indeed, the medial margin of the coracoid blade is equally convex on both sides of its apex, which is relatively centered in relation to the long axis of the shaft of the coracoid. As a consequence, the anterior and posterior extremities of the coracoid blade of *Macrospondylus* PMU 35980 are strongly similar in shape and orientation, as both form sharp and acute corners strictly oriented along the anteroposterior direction. Hence, the great axis of the coracoid blade (joining both corners) is overall perpendicular to the long axis of the shaft of the coracoid. In this way, the overall architecture of the coracoid blade of *Macrospondylus* PMU 35980 resembles that of *Platysuchus* (Kloster Banz unnumbered specimen).

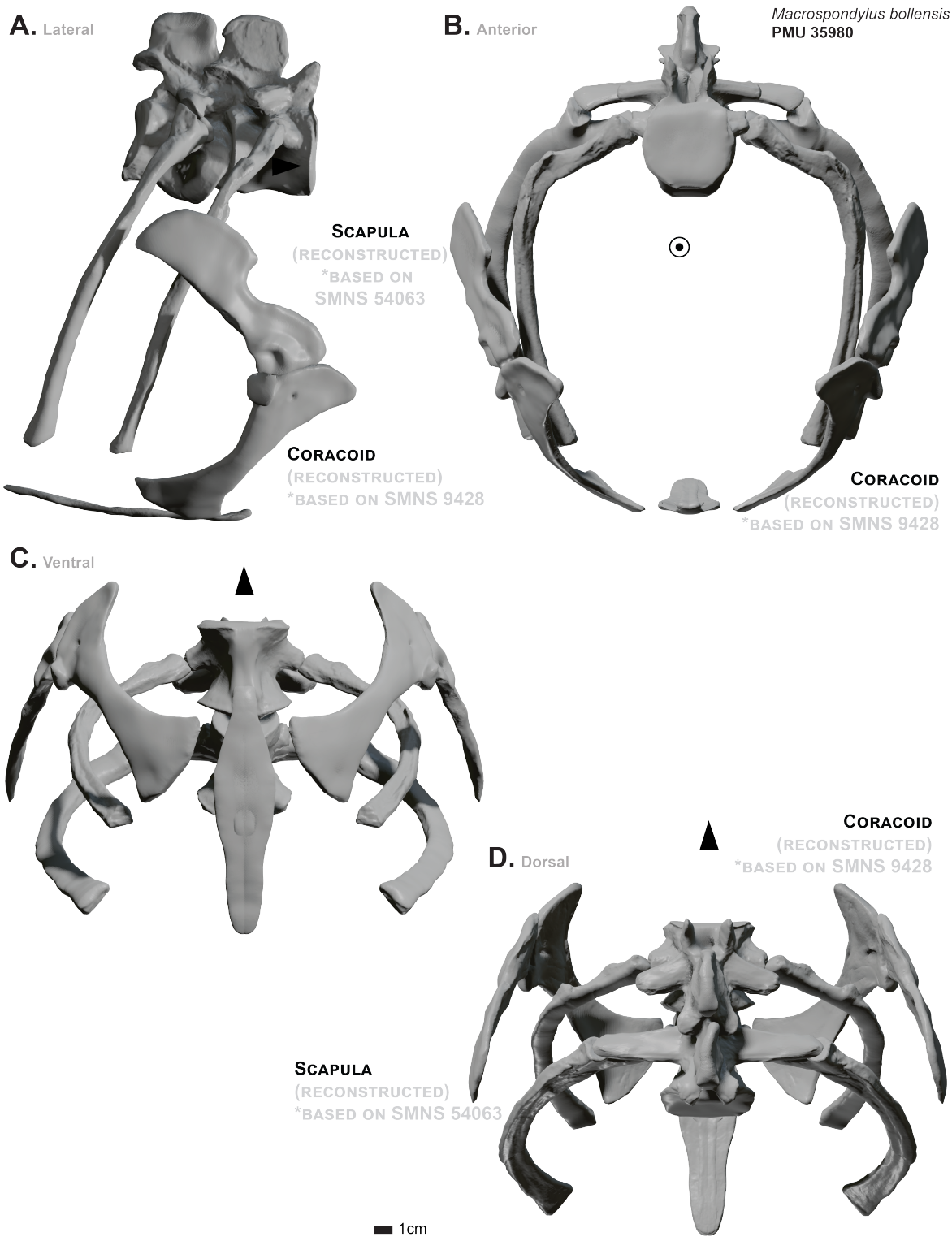


FIGURE 53. Reconstruction of the pectoral girdle of *Macrospondylus bollensis* PMU 35980 (3D models). **A.** Lateral view; **B.** Anterior view; **C.** Ventral view; **D.** Dorsal view. Arrow points anteriorly. Target indicates anterior. The left scapula and coracoid are mirrored. The scapula has been reconstructed based on *Macrospondylus bollensis* SMNS 54063, and the coracoid based on *Macrospondylus bollensis* SMNS 9428.

8.7. ***Charitomenosuchus leedsi* Andrews, 1909.** For measurements, see tables 6 and 7.

8.7.1. *Scapula.* The scapula of *Charitomenosuchus leedsi* NHMUK PV R 3806 (see figs. 41, 54 and 55) markedly departs from that of *Mycterosuchus* NHMUK PV R 2617, *Platysuchus* SMNS 9930, UMH-0005 and *Platysuchus* Kloster Banz unnumbered specimen, *Macrospondylus* SMNS 54063, SMNS 9428 & PMU 35980 in displaying an overall rod-like slender shape. The scapula and coracoid of *Charitomenosuchus* NHMUK PV R 3806 are overall similarly sized as in other thalattosuchians, showing that the scapula is not dorsoventrally elongated but actually anteroposteriorly shortened. Indeed, the anteroposterior length of both the scapular blade and anterior region each accounts for less than one–third of the total dorsoventral height of the scapula. In comparison, within Thalattosuchia, only *Neosteneosaurus* NHMUK PV R 3701 & PETMG R178, *Lemmysuchus* NHMUK PV R 3168, and *Thalattosuchus* PMU 35988 & GLAHM V1146 exhibit similarly shortened scapular blade and anterior region.

The anterior and posterior margins of the scapula of *Charitomenosuchus* NHMUK PV R 3806 are strongly dissimilar: the anterior margin is undulated whereas the posterior margin is relatively straight to subtly convex. In addition, the posterior margin of the scapula of *Charitomenosuchus* NHMUK PV R 3806 presents a brief concave episode directly underneath the posterior corner of the scapular blade which emphasizes it. The overall shape of the posterior margin of the scapula of *Charitomenosuchus* NHMUK PV R 3806 is not found in other thalattosuchians with a slender scapula (*e.g. Neosteneosaurus* NHMUK PV R 3701, *Lemmysuchus* NHMUK PV R 3168, and *Thalattosuchus* PMU 35988), but can be observed on *Macrospondylus* SMNS 54063 (however it could be a preservation bias).

The short anteroposterior extensions of the scapular blade and proximal region of the scapula of *Charitomenosuchus* NHMUK PV R 3806 subsequently lead to a less pronounced neck constriction. However, the anteroposterior constriction of the neck accounts for about 14% of the total dorsoventral extension of the bone, which is similar to what is observed in *Ind. potamosiamensis* PRC-24 and *Neosteneosaurus* NHMUK PV R 3701. Yet, in *Charitomenosuchus* NHMUK PV R 3806, the neck constriction is positioned relatively dorsally, just above three–fifth of the dorsoventral height of the bone. This contrasts with the other taxa bearing a relatively slender scapula (*e.g. Neosteneosaurus* NHMUK PV R 3701, *Lemmysuchus* NHMUK PV R 3168, and *Te. cadomensis* NHMUK PV OR 31836) in which the neck constriction is found more ventrally, around the mid-height of the bone.

The anterior and posterior margin of the scapula of *Charitomenosuchus* NHMUK PV R 3806 in the area of the neck appear to display opposing shapes (*i.e.* concave and convex respectively) of similar intensity, as if both margins could be perfectly imbricated. Ventrally, at around two–fifth of the dorsoventral height of the scapula, the anterior margin meets an inflexion point where it become convex. The degree of concavity of the anterior margin at the neck constriction is larger than the degree of convexity observed on its more ventral portion forming the acromion process, as in *Neosteneosaurus* NHMUK PV R 3701 and *Lemmysuchus* NHMUK PV R 3168. Comparatively, the inflexion point of the posterior margin of the scapula of *Charitomenosuchus* NHMUK PV R 3806 is located proportionally slightly more ventrally than for the anterior margin which further extends the imbricated appearance of the margins.

The scapular blade of *Charitomenosuchus* NHMUK PV R 3806 is strongly reduced compared to that of other teleosauroids. Indeed, in *Charitomenosuchus* NHMUK PV R 3806 the anteroposterior length of the scapular blade accounts for 22% of the total dorsoventral height of the bone, whereas this number is reaches 30–35% in *Neosteneosaurus* NHMUK PV R 3701, *Lemmysuchus* NHMUK PV R 3168, and *Ind. potamosiamensis* PRC-24. In comparison, the scapular blade of *Thalattosuchus* PMU 35988 & GLAHM V1146 also reached 21–22% of the total dorsoventral height of the scapula. The overall shape of the scapular blade of *Charitomenosuchus* NHMUK PV R 3806 is very similar to those of *Neosteneosaurus* NHMUK PV R 3701 and *Lemmysuchus* NHMUK PV R 3168, with only a difference of inclination in

Neosteneosaurus NHMUK PV R 3701 & PETMG R178. Indeed, in all three taxa, the dorsal margin of the scapular blade is lightly domed or flat, and culminates anteriorly in a blunt and rounded corner whereas the posterior corner is more acute and sharp. In both *Charitomenosuchus* NHMUK PV R 3806 and *Lemmysuchus* NHMUK PV R 3168, the dorsal margin of the scapular blade is overall parallel to the ventral surface of the scapulocoracoid synchondrosis surface.

Ventrally to the neck, the scapula of *Charitomenosuchus* NHMUK PV R 3806 only slightly widens anteroposteriorly to form the proximal region of the scapula. Posteriorly, the margin of the scapula almost forms a re-entrant angle at its junction with dorsal margin of the glenoid facet. Indeed, the scapular buttress of the glenoid process of the scapula of *Charitomenosuchus* NHMUK PV R 3806 markedly protrudes laterally and posteriorly, as in *Mycterosuchus* NHMUK PV R 2617. This shape contrasts with the more diffuse and smooth transitions observed in *Neosteneosaurus* NHMUK PV R 3701 and *Lemmysuchus* NHMUK PV R 3168. As in other teleosauroids, the glenoid facet of the scapula of *Charitomenosuchus* NHMUK PV R 3806 is concave with a semi-oval shape, and its dorsal margin is more pronounced laterally than the anterior and posterior ones.

As in *Macrospondylus* SMNS 54063 and *Lemmysuchus* NHMUK PV R 3168, the glenoid facet of the scapula of *Charitomenosuchus* NHMUK PV R 3806 is positioned on the lateral side of the scapula and is mainly oriented lateroposteriorly. Consequently, the scapulocoracoid synchondrosis surface of the scapula of *Charitomenosuchus* NHMUK PV R 3806 extends medially to the glenoid facet and makes the totality of the anteroposterior length of the proximal region of the scapula. The outline of the scapulocoracoid synchondrosis surface of the scapula of *Charitomenosuchus* NHMUK PV R 3806 is triangular due to the anterior thinning of the scapula as it forms the acromion process. The acromion process of the scapula of *Charitomenosuchus* NHMUK PV R 3806 bears the typical shape observed in other teleosauroids as well as *Turnersuchus* LRM 2021/45 and *Pelagosaurus* BRLSI M.1418: its dorsal margin is convex, and its apex is located on the same level as the scapulocoracoid synchondrosis surface. However, the dorsal margin of the acromion process is more lightly convex than in *Mycterosuchus* NHMUK PV R 2617, *Platysuchus* SMNS 9930, UMH-0005 and *Platysuchus* Kloster Banz unnumbered specimen, and *Macrospondylus* SMNS 54063, SMNS 9428 & PMU 35980. The lateral surface of the acromion process of the scapula of *Charitomenosuchus* NHMUK PV R 3806 up until the glenoid process is hollow. This recessed area is connected dorsally to another hollowed ridge which runs almost on the entirety of the scapula (but ends before the scapular blade). A similar ridge can be found on the lateral surface of the scapula of *Thalattosuchus* GLAHM V1146, PMU 35988 (but to a lesser extent), *Mycterosuchus* NHMUK PV R 2617, *Macrospondylus* SMNS 9428, *Neosteneosaurus* NHMUK PV R 3701, and *Lemmysuchus* NHMUK PV R 3168. The anterior margin of the acromion process of the scapula of *Charitomenosuchus* NHMUK PV R 3806 is mediolaterally thickened and overhangs over the underlying scapular fossa, as in other teleosauroids. This structure hypothetically served as the deltoid or acromial crest of extant crocodylians.

8.7.2. *Coracoid.* The coracoid of *Charitomenosuchus leedsi* NHMUK PV R 3806 (see figs. 43, 54 and 55) displays the following features typical of teleosauroids: large coracoid head and coracoid blade, proportionally elongated shaft with marked anteroposterior constriction, triangular anterior expansion, large glenoid facet, ventrally positioned glenoid facet with scapulocoracoid synchondrosis surface extending posteriorly to it, small enclosed coracoid foramen. The coracoid of *Charitomenosuchus* NHMUK PV R 3806 differs from other teleosauroids in possessing the combination of a slender anterior expansion of the coracoid head, an anteriorly shifted coracoid foramen, a more laterally positioned constriction of the shaft of the coracoid, and asymmetrical coracoid blade corners.

Similar to other teleosauroids, the coracoid of *Charitomenosuchus* NHMUK PV R 3806 (see fig. 54) displays an overall hourglass shape: its coracoid head and blade are large and the shaft of the coracoid

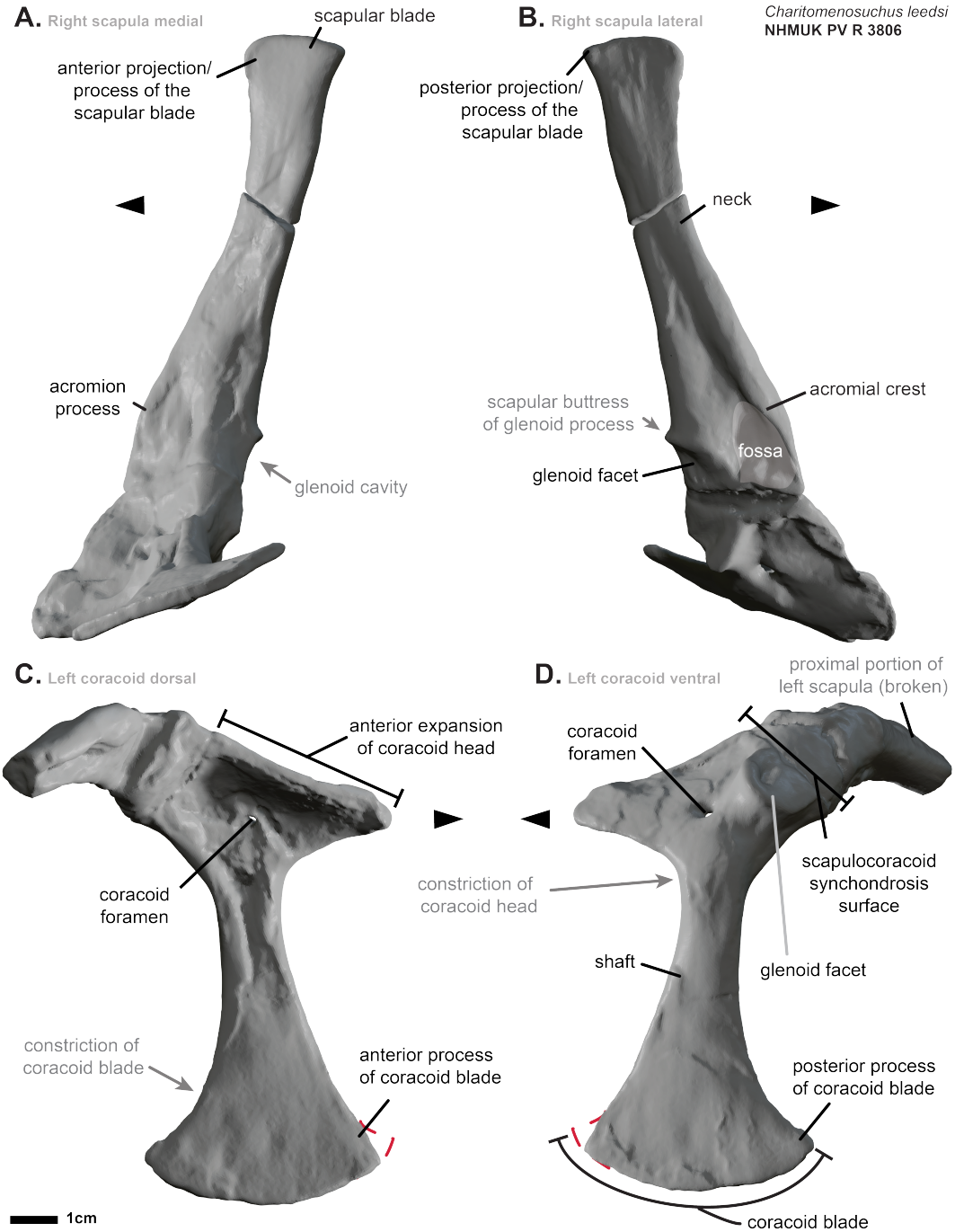


FIGURE 54. Pectoral girdle of *Charitomenosuchus leedsi* NHMUK PV R 3806 (3D models). **A.** Right scapula in medial view ; **B.** Right scapula in lateral view ; **C.** Left coracoid in dorsal view ; **D.** Left coracoid in ventral view. Arrow points anteriorly. Red dashed lines indicate missing parts.

connecting them shows a pronounced anteroposterior constriction. Indeed, the anteroposterior length of both the coracoid head and blade each accounts for about 50% total mediolateral extension of the bone. However, the anteroposterior extent of the coracoid blade of *Charitomenosuchus* NHMUK PV R 3806 is slightly lesser that of the coracoid head, as in other teleosauroids. Overall, the silhouette of the anterior expansion of the coracoid head of *Charitomenosuchus* NHMUK PV R 3806 superficially resembles that of other teleosauroids as it is triangular in shape: both its lateral and medial margins are relatively straight and converge anteriorly to form a sharp apex. Yet the coracoid head of *Charitomenosuchus* NHMUK PV R 3806 strongly departs from that of most teleosauroids in notably displaying a proportionally long and slender anterior expansion. Indeed, the overall anteroposterior length of the anterior expansion accounts for about 63% of the total extension of the coracoid head, whereas this number reaches about 55% in *Aeolodon* NHMUK PV R 1086 and *Neosteneosaurus* NHMUK PV R 3701, 58% in *Mycterosuchus* NHMUK PV R 2617, and 44% in *Macrospondylus* PMU 35980. In comparison, only *Machimosaurus* spp. (see C on fig. 61) appears to display a similarly slender and elongated anterior expansion as it reaches 63% of the total anteroposterior length of the coracoid head. In *Charitomenosuchus* NHMUK PV R 3806, the relatively large extension of the anterior expansion of the coracoid head is emphasized by the shortness of the scapulocoracoid synchondrosis surface. Compared to *Macrospondylus* SMNS 54063, SMNS 9428 & PMU 35980, *Charitomenosuchus* NHMUK PV R 3806 shows a markedly more slender and rod-like scapula with anteroposteriorly reduced proximal and distal extremities. In addition, the orientation of the anterior expansion of the coracoid head of *Charitomenosuchus* NHMUK PV R 3806 is more erect than in *Macrospondylus* SMNS 54063, SMNS 9428 & PMU 35980, as it forms an angle of about 90° with the long axis of the shaft of the coracoid similar to that of *Neosteneosaurus* NHMUK PV R 3701 (and possibly *Lemmysuchus* NHMUK PV R 3169). In the teleosaurid taxa, *Aeolodon* NHMUK PV R 1086 also shows a right-angle angular relation whereas *Mycterosuchus* NHMUK PV R 2617 and *Platysuchus* Kloster Banz unnumbered specimen have a more wider opening (about 125–130°). For *Machimosaurus* spp. the value of the angular relation between the anterior expansion of the coracoid head and the shaft of the coracoid drops to 50–70°.

The coracoid head of *Charitomenosuchus* NHMUK PV R 3806 further departs from other teleosauroids in displaying a small and offset coracoid foramen. The latter forms a circular aperture on both sides of the coracoid head with only a minor displacement between them (*i.e.* it does not form a majorly tilted canal through the bone). The position of the coracoid foramen of *Charitomenosuchus* NHMUK PV R 3806 is anteriorly shifted as in *Lemmysuchus* NHMUK PV R 3169 rather than being in line with the long axis of the shaft of the coracoid like most teleosauroids. In addition, the coracoid foramen of *Charitomenosuchus* NHMUK PV R 3806 is located slightly underneath the longest axis of the coracoid head (*i.e* connecting the anterior and posterior extremities) which further differs from other teleosauroids (*e.g. Aeolodon* NHMUK PV R 1086, *Mycterosuchus* NHMUK PV R 2617, *Macrospondylus* SMNS 54063, SMNS 9428 & PMU 35980, *Neosteneosaurus* NHMUK PV R 3701, *Machimosaurus* spp. see C on fig. 61). Instead, the ventral aperture of the coracoid foramen of *Charitomenosuchus* NHMUK PV R 3806 is found on the same level as the ventral tip of glenoid facet and the apex of anterior expansion.

Similar to other teleosauroids, the glenoid facet of the coracoid of *Charitomenosuchus* NHMUK PV R 3806 is located exclusively on the ventral side of the coracoid head and displays a large and hemispherical outline. As in other teleosauroids with the exception of *Mycterosuchus* NHMUK PV R 2617, the dorsoventral thickness of the coracoid of *Charitomenosuchus* NHMUK PV R 3806 is the longest in the area incorporating the glenoid facet. The glenoid facet of the coracoid of *Charitomenosuchus* NHMUK PV R 3806 is also strongly prominent ventrally due to an elongated glenoid process. In addition, the entire surface of the glenoid process is concave which gives it a trumpet-like shape and emphasises the prominent appearance of the glenoid facet. The glenoid process of the coracoid of *Neosteneosaurus* NHMUK PV R 3701 appears similarly salient, yet the strong dorsoventral compactness appearance of

most teleosauroids hampers clear observation of the relative size of the glenoid process. The glenoid facet of the coracoid of *Charitomenosuchus* NHMUK PV R 3806 presents a thick and bulged rim surrounding its entire outline. This contrasts with *Macrospondylus* SMNS 9428, *Neosteneosaurus* NHMUK PV R 3701 and also *Mycterosuchus* NHMUK PV R 2617 in which the margin of the glenoid facet only becomes salient along its ventral and posterior sides. Similar to other teleosauroids, the surface of the glenoid facet of the coracoid of *Charitomenosuchus* NHMUK PV R 3806 is entirely concave. However, the lowering of the margin of the glenoid facet of the coracoid of *Charitomenosuchus* NHMUK PV R 3806 is located along its posterior side, rather than being more posteroventral as in most teleosauroids.

The scapulocoracoid synchondrosis surface of the coracoid of *Charitomenosuchus* NHMUK PV R 3806 possesses an irregular parallelepiped shape: the anterior portion of the surface displays a triangular outline which then becomes sub-quadrangular starting from the glenoid facet. Similarly shaped scapulocoracoid synchondrosis surfaces are encountered in other teleosauroid coracoids, although the relative extension of the triangular is variable among the taxa and depends on the proportionate size of the glenoid facet in relation to the anteroposterior extension of the scapulocoracoid synchondrosis surface. In *Charitomenosuchus* NHMUK PV R 3806, the scapulocoracoid synchondrosis surface almost forms right-angle corners with the lateral and posterior margins of the coracoid head which gives an angular appearance to the posterior portion of the coracoid head. Furthermore, the anteroposterior extension of the scapulocoracoid synchondrosis surface of the coracoid of *Charitomenosuchus* NHMUK PV R 3806 is sub-equal to the length of the posterior margin of the coracoid head (from the base of the shaft of the coracoid) which accentuates the squared looked of the posterior portion of the coracoid head. In comparison, the machimosaurid taxa *Neosteneosaurus* NHMUK PV R 3701, *Lemmysuchus* NHMUK PV R 3169 and *Machimosaurus* spp. (see A on fig. 61) also display relatively right-angle corners between the scapulocoracoid synchondrosis surface and the lateral and posterior margins of the coracoid head. This configuration also gives a sub-quadrangular silhouette to the posterior portion of their coracoid head. Yet, the length of the posterior margin of the coracoid head of *Neosteneosaurus* NHMUK PV R 3701 and *Lemmysuchus* NHMUK PV R 3169 is lesser than what is observed in *Charitomenosuchus* NHMUK PV R 3806 and *Machimosaurus* spp. (see A on fig. 61).

The coracoid of *Charitomenosuchus* NHMUK PV R 3806 further differs from that of other teleosauroids in displaying an abrupt anteroposterior narrowing marking the junction between the shaft of the coracoid and the coracoid head. Furthermore, the maximal anteroposterior constriction of the shaft of the coracoid is located close to the narrowing, at around one–fourth of the total mediolateral extension of the shaft of the coracoid. In other teleosauroids, the junction between the shaft of the coracoid and the coracoid head forms a smoother and more gradual transition, and the maximal anteroposterior constriction of the shaft of the coracoid is located relatively more medially (*e.g.* *Mycterosuchus* NHMUK PV R 2617, *Aeolodon* NHMUK PV R 1086, *Platysuchus* SMNS 9930, UMH-0005 and *Platysuchus* Kloster Banz unnumbered specimen, *Platysuchus* Kloster Banz unnumbered specimen, *Macrospondylus* SMNS 54063, SMNS 9428 & PMU 35980, *Neosteneosaurus* NHMUK PV R 3701, *Lemmysuchus* NHMUK PV R 3169, *Machimosaurus* spp.). In *Charitomenosuchus* NHMUK PV R 3806, the junction between the shaft of the coracoid and the coracoid head also corresponds to the dorsoventrally thickest portion of the shaft of the coracoid, which then gradually decreases in thickness medially from there as in *Neosteneosaurus* NHMUK PV R 3701 and *Lemmysuchus* NHMUK PV R 3169. In *Charitomenosuchus* NHMUK PV R 3806 the anterior and posterior margins of the coracoid are both strongly concave as in other teleosauroids. However, the shape of the anterior margin is markedly irregular: it displays a relatively narrow lancet arch outline and its apex is located at the junction between the shaft and the coracoid head rather than being in line with the apex of the posterior concavity. This irregularity creates the abrupt narrowing at the junction between the shaft of the coracoid and the coracoid head but also creates an elongated and rod-like shaft of the coracoid. Indeed, the anterior and posterior margins of the shaft of the coracoid both show a low

degree of curvature and hence appear almost parallel. In comparison, other machimosaurid taxa also display an elongated and rod-like shaft of the coracoid as well as a lancet arch-shaped anterior margin but with a proportionally larger opening than in *Charitomenosuchus* NHMUK PV R 3806.

Similar to most teleosauroids, the shaft of the coracoid of *Charitomenosuchus* NHMUK PV R 3806 gradually flares out to form the coracoid blade. The latter displays a rather symmetrical outline in *Charitomenosuchus* NHMUK PV R 3806 which contrasts with the markedly asymmetrical coracoid blade of *Mycterosuchus* NHMUK PV R 2617, *Neosteneosaurus* NHMUK PV R 3701, and *Machimosaurus* spp. (see A on fig. 61). Indeed, the medial margin of the coracoid blade of *Charitomenosuchus* NHMUK PV R 3806 is relatively symmetrical as it displays a smoothly convex shape with its apex centered in relation to the long axis of the shaft of the coracoid which is similar to *Macrospondylus* PMU 35980 and *Platysuchus* Kloster Banz unnumbered specimen. The posterior extremity of the coracoid blade of *Charitomenosuchus* NHMUK PV R 3806 forms a sharp and acute corner with a concave lateral margin and convex medial one. It is mainly posteriorly facing but possesses a minor lateral component in its orientation. However, the anterior corner of the coracoid blade of *Charitomenosuchus* NHMUK PV R 3806 is relatively blunt and thick with both its margins being convex. It is mainly anteriorly facing without any lateral component in its orientation. The marked dissimilarity between the extremities of the coracoid blade of *Charitomenosuchus* NHMUK PV R 3806 lowers its symmetrical appearance. The dorsoventral thickness of the coracoid blade of *Charitomenosuchus* NHMUK PV R 3806 is constant throughout.

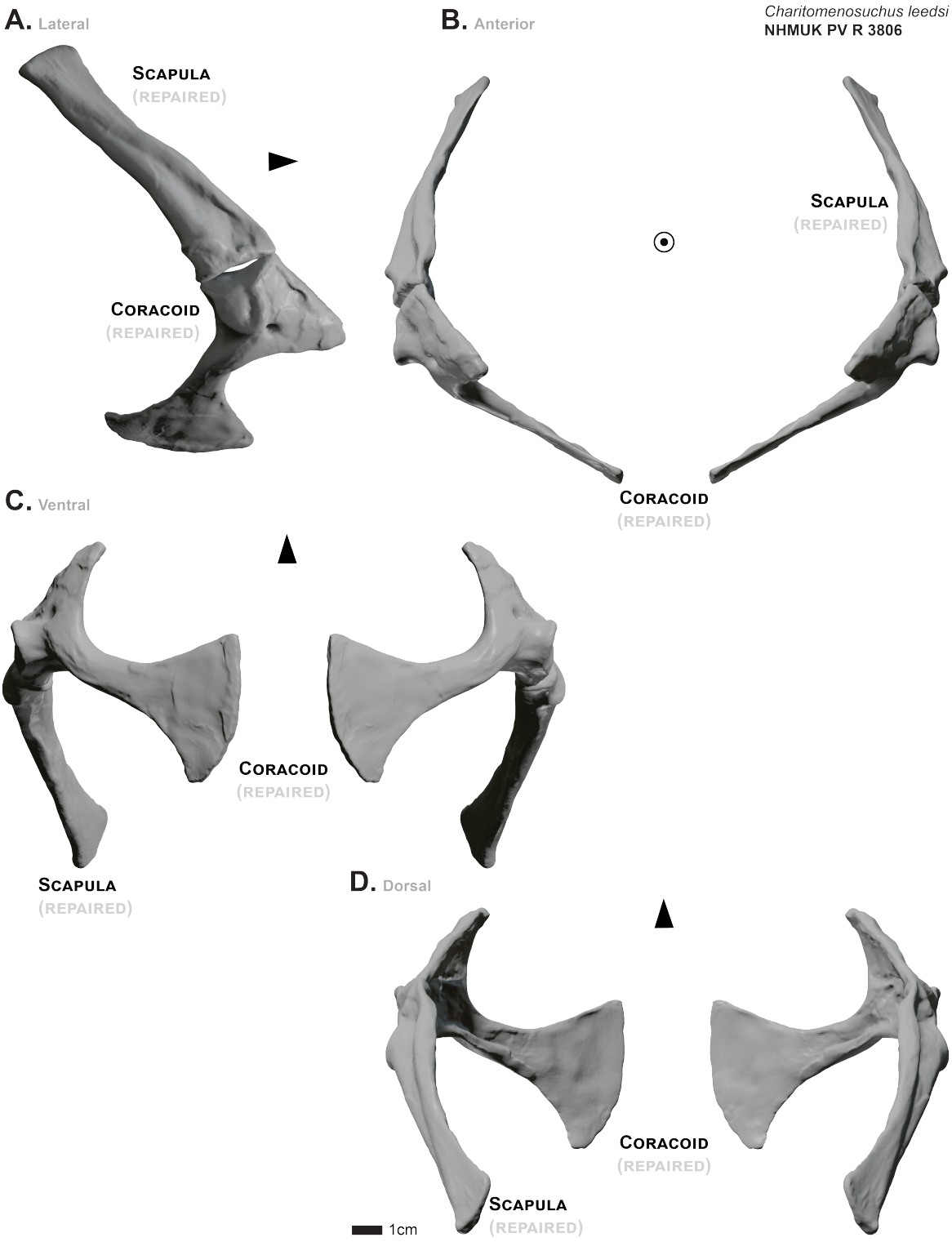


FIGURE 55. Reconstruction of the pectoral girdle of *Charitomenosuchus leedsi* NHMUK PV R 3806 (3D models). **A.** Lateral view; **B.** Anterior view; **C.** Ventral view; **D.** Dorsal view. Arrow points anteriorly. Target indicates anterior. The left scapula and coracoid are mirrored. Reconstruction of missing parts of the right girdle based on the left one (NHMUK PV R 3806).

8.8. ***Neosteneosaurus edwardsi* Eudes-Deslongchamps, 1868.** For measurements, see tables 6 and 7.

8.8.1. *Scapula.* The scapula of *Neosteneosaurus edwardsi* (NHMUK PV R 3701 see figs. 41, 56 and 58 and PETMG R178 see figs. 41 and 57) displays an overall slender shape like those of *Charitomenosuchus* NHMUK PV R 3806, *Lemmysuchus* NHMUK PV R 3168, but also *Mycterosuchus* NHMUK PV R 2617 and *Ind. potamosiamensis* PRC-24 within Teleosauroidea. Indeed, in *Neosteneosaurus* the scapular blade and proximal region are similarly sized, and also display an anteroposterior length only slightly larger than the neck constriction. The latter is located around the mid-height of the bone in *Neosteneosaurus*, as in *Ind. potamosiamensis* PRC-24. Comparatively, the position of the neck constriction of the scapula of *Lemmysuchus* NHMUK PV R 3168 and *Mycterosuchus* NHMUK PV R 2617 is overall similar but slightly more dorsally shifted compared to *Neosteneosaurus* NHMUK PV R 3701.

The anterior and posterior margins of the scapula of *Neosteneosaurus* NHMUK PV R 3701 are strongly dissimilar leading to a non-symmetrical scapula, as in other teleosauroids. This contrasts with the slender scapula of basal metriorhynchids (*e.g. Thalattosuchus* GLAHM V1146 or PMU 35988; *G. leedsi* NHMUK PV R 3014 & NHMUK PV R 3015) which displays an overall symmetrical look due to the similar shape of its anterior and posterior margins. In *Neosteneosaurus* NHMUK PV R 3701 and PETMG R178, the posterior margin is subtly concave shape throughout whereas the anterior margin is more sinusoidal in shape. The undulation of the anterior margin – ventrally convex and dorsally concave – is a trait observed in other teleosauroids (*e.g. Mycterosuchus* NHMUK PV R 2617, *Platysuchus* SMNS 9930 & UMH-0005, *Macrospondylus* SMNS 54063, *Charitomenosuchus* NHMUK PV R 3806, *Lemmysuchus* NHMUK PV R 3168). This is mainly due to the shape of the acromion process whose apex is positioned more ventrally (in line with the scapulocoracoid synchondrosis surface) in teleosauroids compared to metriorhynchoids. In *Neosteneosaurus* NHMUK PV R 3701, the posterior margin extends further dorsally than the anterior margin, leading to an anteriorly tilted scapular blade. Hence the anterior corner of the scapular blade is positioned more ventrally than the posterior one. As in *Mycterosuchus* NHMUK PV R 2617, *Charitomenosuchus* NHMUK PV R 3806, and *Lemmysuchus* NHMUK PV R 3168, the anterior corner of the scapular blade of *Neosteneosaurus* NHMUK PV R 3701 and PETMG R178 forms a broad and rounded angle, which contrasts with the more slender posterior corner. Similarly to *Mycterosuchus* NHMUK PV R 2617 and *Ind. potamosiamensis* PRC-24, the posterior corner of the scapular blade of *Neosteneosaurus* NHMUK PV R 3701 displays a relatively convex or straight posterior margin rather than concave as in *Charitomenosuchus* NHMUK PV R 3806 and *Lemmysuchus* NHMUK PV R 3168. The dorsal margin of the scapular blade of *Neosteneosaurus* NHMUK PV R 3701 is relatively flat to lightly domed, as in *Mycterosuchus* NHMUK PV R 2617, *Charitomenosuchus* NHMUK PV R 3806, and *Lemmysuchus* NHMUK PV R 3168. However, the anterior inclination of the scapular blade of *Neosteneosaurus* NHMUK PV R 3701 differs from the aforementioned teleosauroids. On this appearance, the scapular blade of *Ind. potamosiamensis* PRC-24 is also tilted anteriorly, but the effect appears lesser due to its strongly arched dorsal margin.

Ventrally, the neck of the scapula of *Neosteneosaurus* NHMUK PV R 3701 gradually widens to form the proximal region of the scapula. The latter is composed of the acromion process anteriorly and the glenoid process posteriorly. The acromion process of the scapula of *Neosteneosaurus* NHMUK PV R 3701 is not prominent as it does not form an anterior bulge differing from *Mycterosuchus* NHMUK PV R 2617 and *Macrospondylus* SMNS 9428, or even *Lemmysuchus* NHMUK PV R 3168 but to a lesser extent. In PETMG R178, the anterodorsal margin of the acromion process forms a slight bulge as in *Lemmysuchus* NHMUK PV R 3168. The apex of the acromion process of the scapula of *Neosteneosaurus* NHMUK PV R 3701 and PETMG R178 forms a blunt corner and is located anteroventrally, on the same level as the scapulocoracoid synchondrosis surface (which is a condition found in other teleosauroids).

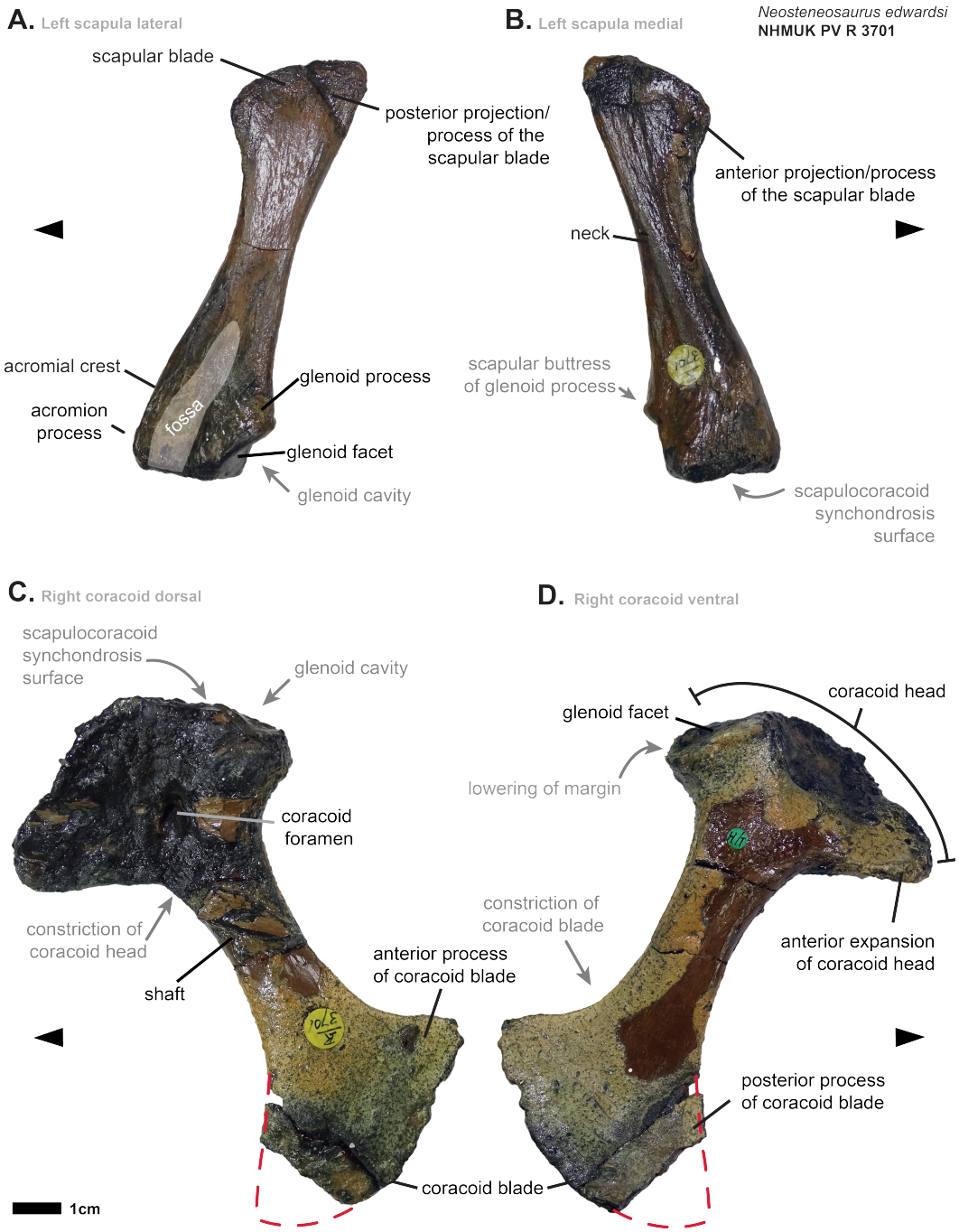


FIGURE 56. Pectoral girdle of *Neosteneosaurus edwardsi* NHMUK PV R 3701 (photographs). **A.** Left scapula in lateral view ; **B.** Left scapula in medial view ; **C.** Right coracoid in dorsal view ; **D.** Right coracoid in ventral view. Arrow points anteriorly. Red dashed lines indicate missing parts. Reconstruction of missing parts based on *Neosteneosaurus edwardsi* PETMG R178.

Laterally, the surface of the acromion process only shows a shallow depression which extends posteriorly until the glenoid process. This depression – or scapular fossa – has a shorter extension and appears shallower than in *Mycterosuchus* NHMUK PV R 2617, *Platysuchus* SMNS 9930 & UMH-0005, or *Macrospondylus* SMNS 9428. Comparatively, *Charitomenosuchus* NHMUK PV R 3806 and *Lemmysuchus* NHMUK PV R 3168 also display smaller scapular fossae similarly to what is observed in *Neosteneosaurus* NHMUK PV R 3701 and PETMG R178, but appear slightly deeper. As in other teleosauroids, there is a hollow running directly dorsally to the scapular fossa of *Neosteneosaurus* NHMUK PV R 3701 and PETMG R178 which extends up until the neck constriction. In *Neosteneosaurus* NHMUK PV R 3701, the anterior margin of the acromion process forms a subtle ridge overhanging the shallow scapular fossa, and could have corresponded to the acromial crest of extant crocodylians.

The shape of the glenoid facet of the scapula of *Neosteneosaurus* NHMUK PV R 3701 and PETMG R178 is overall similar to that of other teleosauroids in being oval and showing a proportionally more prominent dorsal ridge than the side ones (lateral and medial in this case). However, all the margins of the glenoid facet of the scapulae of *Neosteneosaurus* NHMUK PV R 3701 and PETMG R178 are relatively subtle, which results in a faint scapular buttress of the glenoid process unlike in *Mycterosuchus* NHMUK PV R 2617 or *Charitomenosuchus* NHMUK PV R 3806. The glenoid facet of the scapulae of *Neosteneosaurus* NHMUK PV R 3701 and PETMG R178 is also concave as in other teleosauroids, in which the apex of the concavity is not centered but medially shifted (posteriorly shifted in the case of other teleosauroids). Indeed, in *Neosteneosaurus* NHMUK PV R 3701, the glenoid facet is located posteriorly rather than laterally, differing from *Mycterosuchus* NHMUK PV R 2617, *Macrospondylus* SMNS 9428, *Charitomenosuchus* NHMUK PV R 3806 and *Lemmysuchus* NHMUK PV R 3168, but as in *Platysuchus* SMNS 9930, UMH-0005 and *Platysuchus* Kloster Banz unnumbered specimen, *Ind. potamosiamensis* PRC-24 and *Te. cadomensis* NHMUK PV OR 31836. As a consequence, the scapulocoracoid synchondrosis surface of the scapulae of *Neosteneosaurus* NHMUK PV R 3701 and PETMG R178 lies almost completely anteriorly to the glenoid facet and is also shorter than in taxa whose glenoid facet laterally positioned. Indeed, the anteroposterior length of the scapulocoracoid surface of the scapula of *Neosteneosaurus* NHMUK PV R 3701 accounts for about 71% of the total anteroposterior length of the proximal region of the scapula, whereas this number reaches more than 90% for *Mycterosuchus* NHMUK PV R 2617 and *Charitomenosuchus* NHMUK PV R 3806, and more than 80% for *Macrospondylus* SMNS 9428 and *Lemmysuchus* NHMUK PV R 3168. Overall, the shape of the scapulocoracoid synchondrosis surface of the scapula of *Neosteneosaurus* NHMUK PV R 3701 is triangular as in other teleosauroids due to the anterior thinning of the acromion process.

8.8.2. *Coracoid.* The coracoid of *Neosteneosaurus edwardsi* (NHMUK PV R 3701 see figs. 43, 56 and 58 and PETMG R178 see fig. 57) displays the following features typical of machimosaurids: large coracoid head and coracoid blade, strong anteroposterior constriction of the shaft of the coracoid, slender and rod-like shaft of the coracoid, large glenoid facet, triangular anterior expansion of the coracoid head, and small coracoid foramen. The coracoid of *Neosteneosaurus* NHMUK PV R 3701 and PETMG R178 differs from other teleosauroids in displaying the following combination of traits: a proportionally short and broad anterior expansion, a more posteriorly positioned glenoid facet (outflanking the posterior margin of the coracoid head), and an asymmetrical coracoid blade.

Similar to most teleosauroids, the coracoid of *Neosteneosaurus* NHMUK PV R 3701 (see fig. 56) and PETMG R178 (see fig. 57) possesses a parallelepiped outline with straight margins and angular corners (*e.g. Mycterosuchus* NHMUK PV R 2617, *Macrospondylus* SMNS 54063, SMNS 9428 & PMU 35980, *Charitomenosuchus* NHMUK PV R 3806, *Lemmysuchus* NHMUK PV R 3169, *Machimosaurus* spp.). Yet, in *Neosteneosaurus* NHMUK PV R 3701 and PETMG R178, the glenoid facet slightly outflanks the

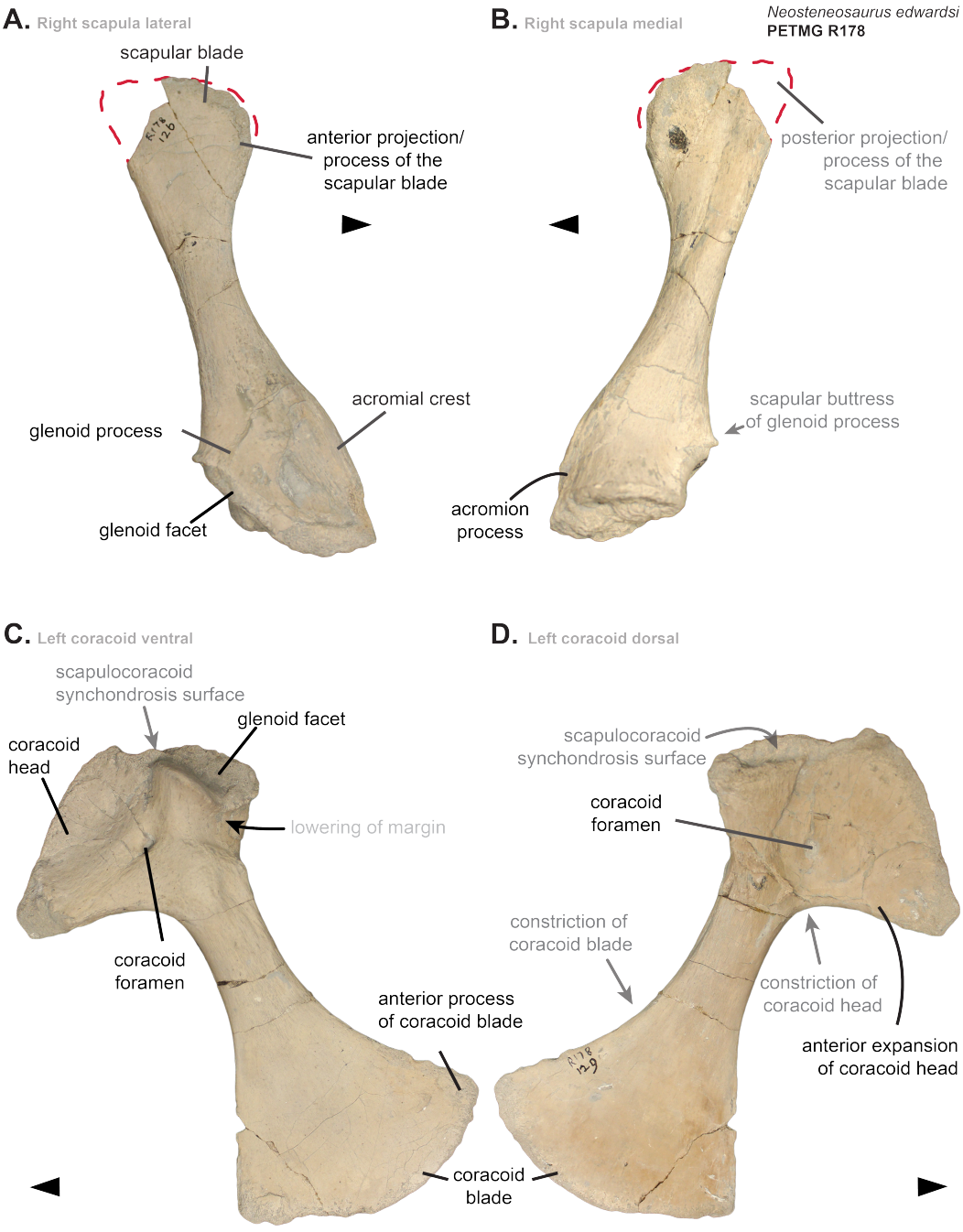


FIGURE 57. Pectoral girdle of *Neosteneosaurus edwardsi* PETMG R178 (photographs). **A.** Right scapula in lateral view ; **B.** Right scapula in medial view ; **C.** Left coracoid in ventral view ; **D.** Left coracoid in dorsal view. Arrow points anteriorly. Red dashed lines indicate missing parts. Reconstruction of missing parts based on *Neosteneosaurus edwardsi* NHMUK PV R 3701.

posterior margin of the coracoid which partly conceals it. The anteriorly converging margins of the coracoid head of *Neosteneosaurus* NHMUK PV R 3701 result in a triangular anterior expansion which is a common teleosauroid feature (*e.g. Mycterosuchus* NHMUK PV R 2617, *Macrospondylus* SMNS 54063, SMNS 9428 & PMU 35980, *Charitomenosuchus* NHMUK PV R 3806, *Lemmysuchus* NHMUK PV R 3169, *Machimosaurus* spp.). In *Neosteneosaurus* NHMUK PV R 3701 and PETMG R178, the anterior expansion of the coracoid is set at a relatively right-angle with the long axis of the shaft of the coracoid, which is similar to that of *Charitomenosuchus* NHMUK PV R 3806 (and possibly *Lemmysuchus* NHMUK PV R 3169), but which contrasts with the more obtuse angle encountered in the coracoids of *Macrospondylus* SMNS 54063, SMNS 9428 & PMU 35980 and the more acute angles of the coracoid of *Machimosaurus* spp. among machimosaurids. Compared to *Macrospondylus* SMNS 54063, SMNS 9428 & PMU 35980 and *Charitomenosuchus* NHMUK PV R 3806, the anterior expansion of the coracoids of *Neosteneosaurus* NHMUK PV R 3701 and PETMG R178 forms a relatively broader and blunter apex, notably due to a larger mediolateral height of the coracoid head at the base of the anterior expansion. In parallel, the relative length of the anterior expansion of the coracoid of *Neosteneosaurus* NHMUK PV R 3701 accounts for about 54% of the total anteroposterior length of the coracoid head which is similar to what is observed in *Aeolodon* NHMUK PV R 1086. In comparison, most teleosauroids display a proportionally longer anterior expansion (*e.g. Mycterosuchus* NHMUK PV R 2617 58%, *Charitomenosuchus* NHMUK PV R 3806 63%, *Machimosaurus* spp. 63%), except for taxa with a relatively extended scapulocoracoid synchondrosis surface like *Macrospondylus* SMNS 54063, SMNS 9428 & PMU 35980 (44%), and possibly *Platysuchus* SMNS 9930 and in the *Platysuchus* Kloster Banz unnumbered specimen. In *Neosteneosaurus* NHMUK PV R 3701 and PETMG R178, the junction between the anterior expansion of the coracoid head and the scapulocoracoid synchondrosis surface forms a slightly obtuse angle of about 110°, as in *Lemmysuchus* NHMUK PV R 3169. In addition, this corner is located directly in line with the long axis of the shaft of the coracoid, which is similar to what is observed in *Lemmysuchus* NHMUK PV R 3169 and *Machimosaurus* spp. but which contrasts with *Charitomenosuchus* NHMUK PV R 3806 and *Macrospondylus* SMNS 54063, SMNS 9428 & PMU 35980.

The glenoid process of the coracoids of *Neosteneosaurus* NHMUK PV R 3701 and PETMG R178 forms a prominent structure on the ventral margin of the bone and corresponds to the dorsoventrally thickest area of the coracoid, as in most teleosauroids (except *Mycterosuchus* NHMUK PV R 2617). Similar to *Charitomenosuchus* NHMUK PV R 3806, the glenoid process of the coracoid of *Neosteneosaurus* NHMUK PV R 3701 is particularly salient and markedly protrudes (especially in relation to the overall size of the glenoid facet and coracoid head) from the surface of the coracoid. In *Neosteneosaurus* NHMUK PV R 3701 and PETMG R178, the surface of the glenoid process of the coracoid is concave ventrally and posteriorly but it becomes straight anteriorly, as in *Mycterosuchus* NHMUK PV R 2617 and *Macrospondylus* SMNS 54063, SMNS 9428 & PMU 35980. As a result, the ventral and posterior edges of the glenoid facet of the coracoids of *Neosteneosaurus* NHMUK PV R 3701 and PETMG R178 show a thin bulged rim, which then becomes less visible along the anterior edge of the facet. This strongly contrasts with *Lemmysuchus* NHMUK PV R 3169 in which the glenoid process of the coracoid is entirely concave and the edge of the glenoid facet forms a broad and bulged rim throughout.

The shape of the glenoid facet of the coracoids of *Neosteneosaurus* NHMUK PV R 3701 and PETMG R178 also slightly differs from what is observed in other teleosauroids: it is large, but displays an oblong shape rather than a relatively hemispherical one. In addition, the glenoid facet of the coracoids of *Neosteneosaurus* NHMUK PV R 3701 and PETMG R178 slightly outflanks and conceals the posterior margin of the coracoid head. However, the glenoid facet of the coracoids of *Neosteneosaurus* NHMUK PV R 3701 and PETMG R178 is positioned on the ventral surface of the coracoid and along the posterior margin of the coracoid head as in other teleosauroids. The posteroventral margin of the glenoid facet of the coracoids of *Neosteneosaurus* NHMUK PV R 3701 and PETMG R178 is concave and displays a lowering of the posterior edge of the facet as in several teleosauroids (*e.g. Charitomenosuchus* NHMUK

PV R 3806, *Lemmysuchus* NHMUK PV R 3169. This lowering of the margin of the glenoid facet is strongly marked in *Neosteneosaurus* PETMG R178.

As in other teleosauroids, the scapulocoracoid synchondrosis surface of the coracoids of *Neosteneosaurus* NHMUK PV R 3701 and PETMG R178 forms a scarred area which lies dorsal to the glenoid facet and exceeds its width. The portion of the scapulocoracoid synchondrosis surface of the coracoids of *Neosteneosaurus* NHMUK PV R 3701 and PETMG R178 extending anteriorly to the glenoid facet displays a triangular outline as in other teleosauroids. However, the scapulocoracoid synchondrosis surface of the coracoid of *Neosteneosaurus* slightly differs from what is observed in other teleosauroids: instead of having an oblong posterior portion, this area is parallelepiped in shape. Indeed, the glenoid facet of the coracoids of *Neosteneosaurus* NHMUK PV R 3701 and PETMG R178 is positioned relatively more posteriorly than in other teleosauroids, and outflanks the posterior margin of the coracoid head. As a result, the ventral margin of the scapulocoracoid synchondrosis surface (which is adjacent to the glenoid facet) is slightly posteriorly sheared which creates the parallelepiped shape. In *Neosteneosaurus* NHMUK PV R 3701, the relative extension of the scapulocoracoid synchondrosis surface accounts for about 30% of the total mediolateral height of the coracoid, which is similar to what is observed in *Macrospondylus* SMNS 9428. In comparison, this value is slightly lesser (about 27%) in the machimosaurids *Charitomenosuchus* NHMUK PV R 3806 and *Lemmysuchus* NHMUK PV R 3169. In PETMG R178, the scapulocoracoid synchondrosis surface forms a hollowed area with salient margins.

The coracoid foramen of *Neosteneosaurus* NHMUK PV R 3701 and PETMG R178 forms a proportionally small aperture similar to other teleosauroids. Similar to *Mycterosuchus* NHMUK PV R 2617, *Aeolodon* NHMUK PV R 1086, *Macrospondylus* SMNS 54063, SMNS 9428 & PMU 35980 and *Machimosaurus* spp., the coracoid foramen of *Neosteneosaurus* NHMUK PV R 3701 is centered in relation to the long axis of the shaft of the coracoid. The overall shape of the coracoid foramen of *Neosteneosaurus* NHMUK PV R 3701 and PETMG R178 resembles *Lemmysuchus* NHMUK PV R 3169 and *Macrospondylus* SMNS 54063, SMNS 9428 & PMU 35980. On the ventral side of the coracoid head the coracoid foramen of *Neosteneosaurus* has a sub-circular shape. Dorsally, the coracoid foramen draws an elliptic aperture whose longest axis is perpendicular to the scapulocoracoid synchondrosis surface. Also, the coracoid foramen of *Neosteneosaurus* NHMUK PV R 3701 and PETMG R178 forms a mediolaterally tilted canal through the bone, as in *Lemmysuchus* NHMUK PV R 3169 and *Mycterosuchus* NHMUK PV R 2617. In addition, the coracoid foramen lies along the longest axis of the coracoid head (*i.e.* which joins the anterior and posterior extremities), which is similar to *Mycterosuchus* NHMUK PV R 2617, *Aeolodon* NHMUK PV R 1086, *Macrospondylus* SMNS 54063, SMNS 9428 & PMU 35980, and *Machimosaurus* spp. (see C on fig. 61).

The shaft of the coracoid of *Neosteneosaurus* NHMUK PV R 3701 and PETMG R178 is relatively elongated as its height accounts for about 43% of the total mediolateral extension of the coracoid, similar to *Aeolodon* NHMUK PV R 1086 and *Charitomenosuchus* NHMUK PV R 3806. In comparison, this value reaches proportionally lower values (i.e. 30 – 35%) in *Mycterosuchus* NHMUK PV R 2617, *Lemmysuchus* NHMUK PV R 3169, and *Machimosaurus* spp. (see C on fig. 61). In *Neosteneosaurus* NHMUK PV R 3701 and PETMG R178, the shaft of the coracoid displays a rod-like appearance due to its short overall width throughout its length, as in several teleosauroids (*e.g. Aeolodon* NHMUK PV R 1086, *Platysuchus* Kloster Banz unnumbered specimen, *Macrospondylus* PMU 35980, *Charitomenosuchus* NHMUK PV R 3806, *Lemmysuchus* NHMUK PV R 3169). This effect is mainly caused by the low degree of curvature of the anterior and posterior margins of the coracoid in the area corresponding to the shaft of the coracoid. Indeed, as in other machimosaurids, the shape of the anterior and posterior margins of the coracoid of *Neosteneosaurus* NHMUK PV R 3701 and PETMG R178 are strongly irregular: the posterior margin is relatively dome-shaped but with a flat top, whereas the anterior margin

displays the shape of a lancet arch. In addition, the apexes of these concavities are not aligned: for the posterior margin it is relatively centered (located around the mid-height of the shaft of the coracoid), but for the anterior margin it is situated at the junction between the shaft of the coracoid and the coracoid head. Similar to *Charitomenosuchus* NHMUK PV R 3806 and *Lemmysuchus* NHMUK PV R 3169, the dorsoventral thickness of the shaft of the coracoid of *Neosteneosaurus* NHMUK PV R 3701 and PETMG R178 is the longest near its lateral base, but gradually declines medially.

Compared to *Lemmysuchus* NHMUK PV R 3169, the shaft of the coracoid of *Neosteneosaurus* NHMUK PV R 3701 and PETMG R178 displays a milder flaring medially to form the coracoid blade. As in *Mycterosuchus* NHMUK PV R 2617, *Aeolodon* NHMUK PV R 1086 and *Machimosaurus* spp., the coracoid blade of *Neosteneosaurus* NHMUK PV R 3701 and PETMG R178 displays a markedly asymmetrical shape anteroposteriorly. Indeed, the degree of curvature of the coracoid blade of *Neosteneosaurus* NHMUK PV R 3701 and PETMG R178 differs on each side of its apex, and hence shows a greater inclination posteriorly. In addition, the apex of the medial margin of the coracoid blade of *Neosteneosaurus* NHMUK PV R 3701 and PETMG R178 is not exactly in line with the long axis of the shaft of the coracoid but is slightly shifted anteriorly. The posterior extremity of the coracoid blade of *Neosteneosaurus* NHMUK PV R 3701 and PETMG R178 forms a relatively sharp corner which points posterolaterally.

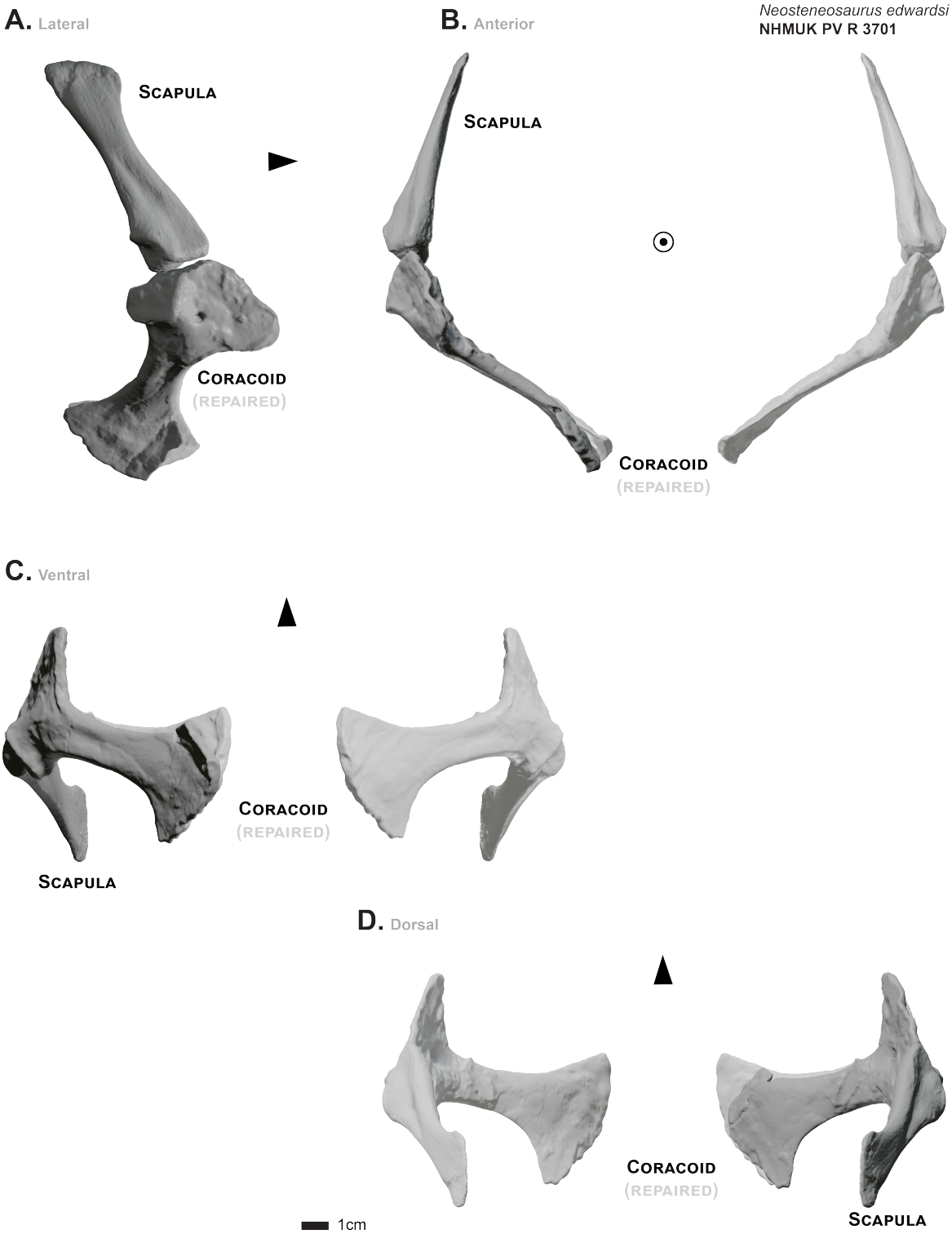


FIGURE 58. Reconstruction of the pectoral girdle of *Neosteneosaurus edwardsi* NHMUK PV R 3701 (3D models). **A.** Lateral view; **B.** Anterior view; **C.** Ventral view; **D.** Dorsal view. Arrow points anteriorly. Target indicates anterior. The left scapula and coracoid are mirrored. Reconstruction of missing parts based on *Neosteneosaurus edwardsi* PETMG R178.

8.9. ***Lemmysuchus obtusidens*** **Andrews, 1909 Johnson et al., 2017.** For measurements, see tables 6 and 7.

The coracoid labelled *Lemmysuchus obtusidens* NHMUK PV R 3169 presumably belongs to *Lemmysuchus obtusidens* NHMUK PV R 3168. This conjecture is based on the overall size of the coracoid (and notably the scapulocoracoid synchondrosis surface) which matches that of the scapula of *Lemmysuchus obtusidens* NHMUK PV R 3168, and is also based on the presence of bite marks on the coracoid blade which is also found on the holotype of *Lemmysuchus obtusidens* NHMUK PV R 3168 (Johnson et al., 2017).

8.9.1. *Scapula.* The scapula of *Lemmysuchus obtusidens* NHMUK PV R 3168 (see figs. 41, 59 and 60) displays a slender shape like those of most teleosauroids (except *Platysuchus* SMNS 9930, UMH-0005 and *Platysuchus* Kloster Banz unnumbered specimen and *Macrospondylus* SMNS 54063, SMNS 9428 & PMU 35980). However, the scapula of *Lemmysuchus* NHMUK PV R 3168 stands out with its combination of a marked neck constriction and well-developed scapular blade. Indeed, in *Lemmysuchus* NHMUK PV R 3168 the anteroposterior length of the scapular blade is almost equal to that of proximal region (*i.e.* reaches around 98%) like what is observed in *Ind. potamosiamensis* PRC-24. Compared to the other teleosauroids with slender scapulae, the scapular blades of *Charitomenosuchus* NHMUK PV R 3806 and *Neosteneosaurus* NHMUK PV R 3701 are proportionally shorter (about 83% and 95% respectively) whereas that of *Mycterosuchus* NHMUK PV R 2617 is slightly larger (about 109%). Similarly to other teleosauroids with slender scapulae, the scapular blade of *Lemmysuchus* NHMUK PV R 3168 also displays a rather lightly domed shape culminating anteriorly in a blunt corner and posteriorly in a sharper corner (*e.g. Mycterosuchus* NHMUK PV R 2617, *Charitomenosuchus* NHMUK PV R 3806 and *Neosteneosaurus* NHMUK PV R 3701). The overall shape of the dorsal margin of the scapular blade of *Lemmysuchus* NHMUK PV R 3168 resembles that of *Charitomenosuchus* NHMUK PV R 3806 the most, even though the latter is much smaller. Indeed, the dorsal margin of the scapular blade of *Lemmysuchus* NHMUK PV R 3168 is slightly undulated: anteriorly the margin is convex up until two-thirds of the length then the concavity switches (but shows a lower degree of intensity). As a consequence, the posterior corner of the scapular blade appears to show a slight dorsal component differing from the anterior corner which is strictly anteriorly oriented.

Ventrally, the scapular blade of *Lemmysuchus* NHMUK PV R 3168 narrows to form the neck constriction, whose thinnest thickness anteroposteriorly reaches about 13% of the total dorsoventral height of the bone. Similar values of the neck constriction are found in the metriorhynchoid *Thalattosuchus* GLAHM V1146 & PMU 35988. In comparison, teleosauroids display a proportionally thicker neck constriction; *Charitomenosuchus* NHMUK PV R 3806 and *Neosteneosaurus* NHMUK PV R 3701 show the proportionally thinnest neck constriction among teleosauroids following *Lemmysuchus* NHMUK PV R 3168, with their constriction accounting for about 14% of their total dorsoventral height. *Macrospondylus* PMU 35980 & SMNS 54063, *Mycterosuchus* NHMUK PV R 2617, and *Platysuchus* SMNS 9930 show relatively larger values with about 17-18%, 20% and 16% respectively. The marked neck constriction of the scapula of *Lemmysuchus* NHMUK PV R 3168 make it stand out from the rest of Telesauroidea, especially since it emphasizes the dorsal flaring of the scapular blade. Comparatively, *Ind. potamosiamensis* PRC-24 also shows a proportionally strong neck constriction and dorsal flaring of the scapular blade, but the global appearance is different since the scapular blade of *Ind. potamosiamensis* PRC-24 is proportionally larger than in *Lemmysuchus* NHMUK PV R 3168.

In *Lemmysuchus* NHMUK PV R 3168, the neck constriction is located around the mid-height of the scapula at 56% of the total dorsoventral height, which also corresponds to the apex of the anterior concavity. Similar values are found in *Mycterosuchus* NHMUK PV R 2617 (about 56%), *Ind. potamosiamensis* PRC-24 (about 53%) and *Neosteneosaurus* NHMUK PV R 3701 (about 53%). As in most

teleosauroids displaying a relatively slender scapula (*e.g.* *Mycterosuchus* NHMUK PV R 2617, *Neosteneosaurus* NHMUK PV R 3701, and *Ind. potamosiamensis* PRC-24), the anterior margin of the scapula of *Lemmysuchus* NHMUK PV R 3168 is strongly undulated whereas the posterior one is lightly concave (and appears almost straight). In comparison, *Charitomenosuchus* NHMUK PV R 3806 markedly differs from the other slender teleosauroid scapulae with its slightly convex posterior margin. In *Lemmysuchus* NHMUK PV R 3168, the concavity of the anterior margin switches to slightly convex at around one-third of the dorsoventral height of the scapula towards the ventral border. This change in concavity marks the start of the acromion process of the scapula, whose anterior margin is slightly convex throughout.

As mentioned, the acromion process of the scapula of *Lemmysuchus* NHMUK PV R 3168 forms a slightly convex bulge anteriorly, which stands out from the more gentle shape of the acromion process of the scapulae of *Charitomenosuchus* NHMUK PV R 3806, *Neosteneosaurus* NHMUK PV R 3701, and *Platysuchus* SMNS 9930. Yet, the acromion process of the scapula of *Lemmysuchus* NHMUK PV R 3168 does not reach the strongly convex shapes of *Macrospondylus* SMNS 54063 (and possibly *Mycterosuchus* NHMUK PV R 2617). The anterior bulge of the acromion process of the scapula of *Lemmysuchus* NHMUK PV R 3168 does not extend until the ventral margin of the bone as in *Platysuchus* SMNS 9930, *Charitomenosuchus* NHMUK PV R 3806 or *Neosteneosaurus* NHMUK PV R 3701, but rather ends around the same level as the mid-height of the glenoid facet similarly to *Macrospondylus* SMNS 54063 & SMNS 9428. The remainder portion of the acromion process forms a convex and rounded anterior corner whose apex is anteroventrally facing similarly to *Macrospondylus* (*e.g.* SMNS 54063) and *Neosteneosaurus* NHMUK PV R 3701. In *Macrospondylus* SMNS 54063 & SMNS 9428 and *Lemmysuchus* NHMUK PV R 3168, the difference of convexity between the dorsal portion of the acromion process and the ventral apex results in an apparent notch along the anterior margin of the scapula. However, it is not an indentation but merely the successive superimposition of two convex arcs (*i.e.* that of the anteroventral apex which is topped with that of the dorsal portion of the acromion process) which creates a gap in the global outline. The dorsal portion of the acromion process of the scapula of *Lemmysuchus* NHMUK PV R 3168 (*i.e.* the convex portion above the 'notch') is mediolaterally thickened as in other teleosauroids, and thus could correspond to the acromial crest of extant crocodylians. In addition, there is a hollowed area (*i.e.* the scapular fossa) extending from the acromial thickening anteriorly to the glenoid process posteriorly, which emphasizes the overhanging mediolateral thickening. The scapular fossa is overall bilobate in shape due to an anteroposterior pinching around its mid-height. Furthermore, the area of the pinching is slightly thicker mediolaterally so that each lobe of the scapular fossa also forms two separate cavities. As in other teleosauroids, the scapular fossa is long as it is almost twice as high dorsoventrally as the glenoid facet (*e.g.* *Mycterosuchus* NHMUK PV R 2617, *Platysuchus* UMH-0005, *Macrospondylus* SMNS 9428, *Charitomenosuchus* NHMUK PV R 3806, *Neosteneosaurus* NHMUK PV R 3701). In addition, there is a shallow groove connecting and extending dorsally to the scapular fossa, which runs in the middle of the neck of the scapula. Similarly to other teleosauroids, the groove ends when the neck starts to flare out to form the scapular blade.

In *Lemmysuchus* NHMUK PV R 3168, the glenoid facet of the scapula is slightly concave with a semi-oval shape and is located on the lateral side of the scapula as in *Charitomenosuchus* NHMUK PV R 3806, *Macrospondylus* SMNS 9428, and *Mycterosuchus* NHMUK PV R 2617. Hence, the surface of the glenoid facet is mainly laterally facing, rather than mainly posteriorly facing as in *Platysuchus* SMNS 9930 & UMH-0005 and *Neosteneosaurus* NHMUK PV R 3701. Posteriorly, similarly to other teleosauroids, the margin of the glenoid facet does not display a protruding ridge and smoothly transitions to the medial side of the scapula. Due to the concavity of the glenoid facet and the laterally emerging anterior and dorsal sides of the glenoid process, it is possible that the anterior and dorsal margins of the glenoid facet were slightly protruding laterally but this area is not preserved in *Lemmysuchus* NHMUK

PV R 3168. Despite the laterally positioned glenoid facet, the shape of the scapulocoracoid synchondrosis of the scapula of *Lemmysuchus* NHMUK PV R 3168 drastically differ from the triangular ones of *Charitomenosuchus* NHMUK PV R 3806, *Macrospondylus* SMNS 9428, and *Mycterosuchus* NHMUK PV R 2617. Indeed, the scapulocoracoid synchondrosis of the scapula of *Lemmysuchus* NHMUK PV R 3168 display a parallelepiped shape due to the mediolateral thickening of the scapula at the level of the anterior border of the glenoid facet. This thickening along with the anterior and posterior mediolateral thinning of the scapula gives the scapulocoracoid synchondrosis surface an overall diamond shape. In other teleosauroids, the scapulocoracoid synchondrosis surface takes the shape of an almost isosceles triangle with the greater axis oriented anteroposteriorly. Comparatively, the scapulocoracoid synchondrosis surface of the scapula of *Neosteneosaurus* NHMUK PV R 3701 is also quadrangular but still displays an overall triangular shape due to the main posterior orientation of the glenoid facet, which places the fourth corner strictly posteriorly along the base of the isosceles triangle.

8.9.2. *Coracoid.* The coracoid of *Lemmysuchus obtusidens* NHMUK PV R 3169 (see figs. 43, 59 and 60) displays the following features commonly found in machimosaurids: large lateral and medial extremities, rod-like shaft, seemingly triangular anterior expansion, exclusively ventral glenoid facet, small coracoid foramen. The coracoid of *Lemmysuchus* NHMUK PV R 3169 differs from other teleosauroids in displaying the combination of a proportionally large coracoid blade and a relatively narrow coracoid head. In addition, the glenoid facet of the coracoid of *Lemmysuchus* NHMUK PV R 3169 possesses a thick rim surrounding its entire edge, and the coracoid foramen is anteriorly shifted.

The coracoid of *Lemmysuchus* NHMUK PV R 3169 (see fig. 59) markedly stands out due to its unbalanced appearance: it displays a proportionally small coracoid head in relation to the large size of the coracoid blade. This configuration overall resembles what is observed in *Machimosaurus* spp. (see fig. 61). The unbalanced appearance of the coracoid of *Lemmysuchus* NHMUK PV R 3169 is caused by the general narrowness of the coracoid head: its maximal mediolateral height is proportionally short as it only accounts for about two–thirds of that of the coracoid blade. In addition, the anterior and posterior extremities of the coracoid head both significantly taper off whereas the coracoid blade shows a wide medial flaring. In comparison, the overall dimensions of the coracoid blade and coracoid head (*i.e.* their general anteroposterior length and mediolateral height) of most teleosauroids are similar in size and no preponderant widening is observed (*e.g.* *Mycterosuchus* NHMUK PV R 2617, *Aeolodon* NHMUK PV R 1086, *Platysuchus* Kloster Banz unnumbered specimen, *Macrospondylus* PMU 35980, *Charitomenosuchus* NHMUK PV R 3806). However, this relation seems inverted in *Neosteneosaurus* NHMUK PV R 3701 as it shows a shorter mediolateral height of the coracoid blade compared to the coracoid head.

Similar to most teleosauroids (except *Aeolodon* NHMUK PV R 1086 and *Platysuchus* SMNS 9930) the margins of the coracoid head of *Lemmysuchus* NHMUK PV R 3169 form relatively straight surfaces connected through angular corners. Furthermore, as in most machimosaurid taxa, the coracoid head of *Lemmysuchus* NHMUK PV R 3169 shows an uneven sub-quadrangular outline: both its anterior and posterior extremities form triangular shapes, with the anterior expansion being markedly more anteroposteriorly elongated (*e.g.* *Charitomenosuchus* NHMUK PV R 3806, *Neosteneosaurus* NHMUK PV R 3701, *Machimosaurus* spp.). However, the machimosaurid *Macrospondylus* SMNS 54063, SMNS 9428 & PMU 35980 differs from the latter due to a proportionally large scapulocoracoid synchondrosis surface. The anterior expansion of the coracoid of *Lemmysuchus* NHMUK PV R 3169 appears to be set at a relatively right-angle corner with the long axis of the shaft of the coracoid (although the apex of the anterior expansion is not preserved), which is similar to what is observed in *Charitomenosuchus* NHMUK PV R 3806, *Neosteneosaurus* NHMUK PV R 3701, but also *Aeolodon* NHMUK PV R 1086. In *Machimosaurus* spp., this angular relation is even more acute and ranges between 50 to 70 °. The narrower angle between the anterior expansion of the coracoid head and the long axis of the shaft of the

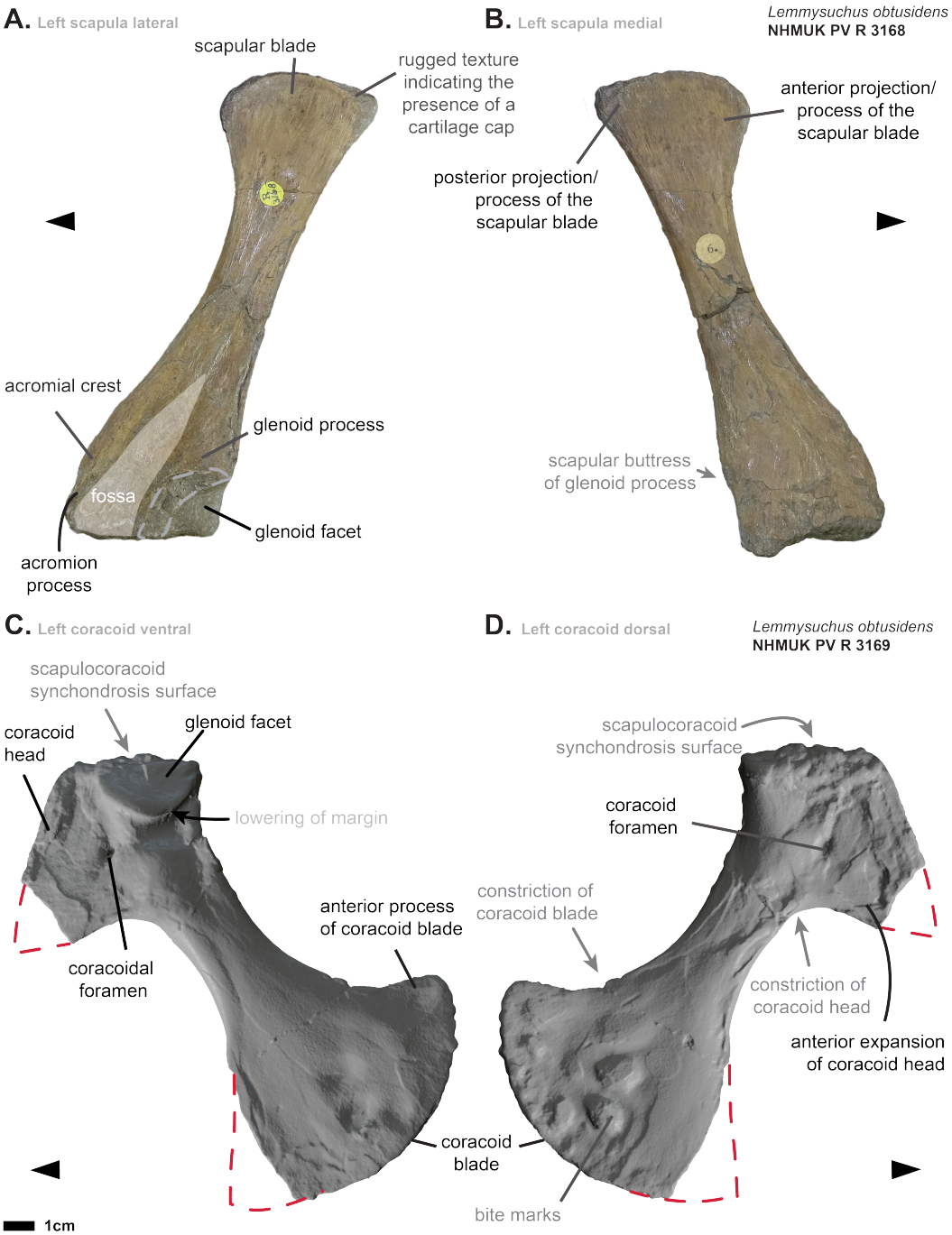


FIGURE 59. Pectoral girdle of *Lemmysuchus obtusidens* NHMUK PV R 3168 (A & B; photographs) and *Lemmysuchus* NHMUK PV R 3169 (C & D; 3D models). **A.** Left scapula in lateral view ; **B.** left scapula in medial view; **C.** Left coracoid in ventral view ; **D.** Left coracoid in dorsal view. Arrow points anteriorly. Red dashed lines indicate missing parts. Reconstruction of missing parts based on *Neosteneosaurus edwardsi* PETMG R178.

coracoid of *Lemmysuchus* NHMUK PV R 3169 lowers the symmetrical shape of the anterior margin of the coracoid, as in *Charitomenosuchus* NHMUK PV R 3806, *Neosteneosaurus* NHMUK PV R 3701 and *Machimosaurus* spp.

In *Lemmysuchus* NHMUK PV R 3169, the junction between the lateral margin of the anterior expansion and the scapulocoracoid synchondrosis surface forms a slightly obtuse angle of about 111°, as in *Neosteneosaurus* NHMUK PV R 3701. In comparison, this junction forms a right-angle corner in the machimosaurid taxa *Charitomenosuchus* NHMUK PV R 3806 and *Machimosaurus* spp., and forms an even greater angular relation in *Macrospondylus* SMNS 54063, SMNS 9428 & PMU 35980. In addition, the corner joining the lateral margin of the anterior expansion and the scapulocoracoid synchondrosis surface of the coracoid of *Lemmysuchus* NHMUK PV R 3169 is in line with the long axis of the shaft of the coracoid, which is similar to *Machimosaurus* spp. (see A on fig. 61), *Neosteneosaurus* NHMUK PV R 3701 but which contrasts with *Charitomenosuchus* NHMUK PV R 3806 and *Macrospondylus* SMNS 54063, SMNS 9428 & PMU 35980 among machimosaurids. Posteriorly, the scapulocoracoid synchondrosis surface of the coracoid of *Lemmysuchus* NHMUK PV R 3169 forms a more right angle corner with the posterior margin of the coracoid head, similar to *Charitomenosuchus* NHMUK PV R 3806 and *Machimosaurus* spp. (see A on fig. 61) whereas in *Macrospondylus* SMNS 54063, SMNS 9428 & PMU 35980 this corner is slightly more acute. In *Neosteneosaurus* NHMUK PV R 3701 the glenoid facet outflanks the posterior margin of the coracoid head and slightly conceals it, but its scapulocoracoid synchondrosis surface still lies at about 90° of it. As in other teleosauroids, the scapulocoracoid synchondrosis surface of the coracoid of *Lemmysuchus* NHMUK PV R 3169 displays a hybrid outline: most of its silhouette draws an oblong shape, which becomes triangular anteriorly to the glenoid facet. The posterior oblong shape of the scapulocoracoid synchondrosis surface of the coracoid of *Lemmysuchus* NHMUK PV R 3169 is possible thanks to the strictly ventrally positioned glenoid facet, as in other teleosauroids (but differing from meteriorhynchoids). The relative extension of the triangular portion of the scapulocoracoid synchondrosis surface depends on the relative size of the glenoid facet and proximal shape of the scapula. The surface of the scapulocoracoid synchondrosis of the coracoid of *Lemmysuchus* NHMUK PV R 3169 is markedly scarred indicating the presence of a cartilage cap *in vivo*: its centre displays several irregular portions in relief which give an overall dome-like shape to the surface of the scapulocoracoid synchondrosis.

As in other teleosauroids, the glenoid facet of the coracoid of *Lemmysuchus* NHMUK PV R 3169 is wide and hemispherical in shape, and is located exclusively on ventral side of the coracoid head. The orientation of the facet is posteroventral and its surface is almost entirely concave save most of the surrounding edges, as in other teleosauroids. Indeed, the concave appearance of the glenoid facet is slightly posteriorly offset, and induces a lowering of the posteroventral side of the surrounding margin as in most teleosauroids except *Charitomenosuchus* NHMUK PV R 3806 (in which it is more posterior). Yet, similar to *Charitomenosuchus* NHMUK PV R 3806, the glenoid facet of the coracoid of *Lemmysuchus* NHMUK PV R 3169 appears salient as its edge forms a thick and bulged rim, and also as its underlying surface – belonging to the glenoid process – is entirely concave.

As in other machimosaurid taxa, the coracoid foramen of *Lemmysuchus* NHMUK PV R 3169 is proportionally small in relation to the size of the coracoid head. In *Lemmysuchus* NHMUK PV R 3169, the coracoid foramen lies on the same level as the ventral-most margin of the glenoid facet but is slightly shifted anteriorly and hence is not in line with the long axis of the shaft of the coracoid, which resembles what is observed in *Charitomenosuchus* NHMUK PV R 3806. Similar to *Neosteneosaurus* NHMUK PV R 3701, *Macrospondylus* SMNS 54063, SMNS 9428 & PMU 35980, the coracoid foramen of *Lemmysuchus* NHMUK PV R 3169 forms a sub-circular aperture on the ventral side of the coracoid head but takes a more elliptic shape on the dorsal surface of the bone (with its longest axis being perpendicular to the scapulocoracoid synchondrosis surface). In addition, the coracoid foramen of *Lemmysuchus* NHMUK

PV R 3169 forms a tilted canal markedly inclined mediolaterally as in *Neosteneosaurus* NHMUK PV R 3701 and *Mycterosuchus* NHMUK PV R 2617.

The shaft of the coracoid of *Lemmysuchus* NHMUK PV R 3169 displays a rod-like appearance as in most teleosauroids (except *Mycterosuchus* NHMUK PV R 2617). Indeed, the anteroposterior width of the shaft of the coracoid of *Lemmysuchus* NHMUK PV R 3169 remains relatively constant throughout most of its height due to the low degree of curvature of the anterior and posterior margins of the coracoid in this portion of the bone, similar to *Neosteneosaurus* NHMUK PV R 3701. Yet, beyond the vicinity of the shaft of the coracoid, the degree of curvature of the margins of the coracoid of *Lemmysuchus* NHMUK PV R 3169 increases rapidly to form the coracoid head and coracoid blade. As in *Charitomenosuchus* NHMUK PV R 3806, *Neosteneosaurus* NHMUK PV R 3701 and *Machimosaurus* spp., this effect is predominantly caused by the lancet arch shape of the anterior margin of the coracoid of *Lemmysuchus* NHMUK PV R 3169, whose apex is located at the junction between the anterior expansion of the coracoid head and the shaft of the coracoid. In comparison, the shape of the concavity of the posterior margin of the coracoid of *Lemmysuchus* NHMUK PV R 3169 is hemispherical, with its apex being relatively centered (and located near the constriction of the shaft of the coracoid). Similar to *Charitomenosuchus* NHMUK PV R 3806 and *Neosteneosaurus* NHMUK PV R 3701, the dorsoventral thickness of the shaft of the coracoid of *Lemmysuchus* NHMUK PV R 3169 is the longest near the junction between the shaft of the coracoid and the coracoid head, then drastically decreases medially.

Medially, the shaft of the coracoid of *Lemmysuchus* NHMUK PV R 3169 markedly flares out to form the coracoid blade, which presumably exceeded the anteroposterior length of the coracoid head. Indeed, the posterior corner of the coracoid blade of *Lemmysuchus* NHMUK PV R 3169 is proportionally more prominent posteriorly in relation to the shaft of the coracoid than the posterior corner of the coracoid head is. Overall, the shape of the coracoid blade of *Lemmysuchus* NHMUK PV R 3169 appears relatively anteroposteriorly symmetrical similar to *Charitomenosuchus* NHMUK PV R 3806, but which contrasts with *Mycterosuchus* NHMUK PV R 2617, *Neosteneosaurus* NHMUK PV R 3701 and *Machimosaurus* spp. (see A on fig. 61). Indeed, the medial margin of the coracoid blade of *Lemmysuchus* NHMUK PV R 3169 is smoothly convex and dome-shaped with its apex centered in relation to the long axis of the shaft of the coracoid. In addition, it does not appear to displays any drastic change in the degree of curvature on either side of its apex. The posterior extremity of the coracoid blade of *Lemmysuchus* NHMUK PV R 3169 forms a relatively sharp and prominent corner which points posterolaterally, similar to *Neosteneosaurus* NHMUK PV R 3701 and *Charitomenosuchus* NHMUK PV R 3806 but differing from *Machimosaurus* spp. (see A on fig. 61). The dorsoventral thickness of the coracoid blade also remains relatively constant throughout, as in *Neosteneosaurus* NHMUK PV R 3701 and *Charitomenosuchus* NHMUK PV R 3806. The ventral surface of the coracoid blade of *Lemmysuchus* NHMUK PV R 3169 presents a series of impressions near its posterior corner: these impressions form six distinguishable ovoid shapes, several of which appear to be the mirrored reflection of another through an evident axis of symmetry. As a consequence, these impressions appear to be related to bite marks. In addition, these imprints are all located on the same side of the coracoid – the ventral surface – and bear the same orientation and as such would correspond to a portion (presumably the dentary) of the mandible.

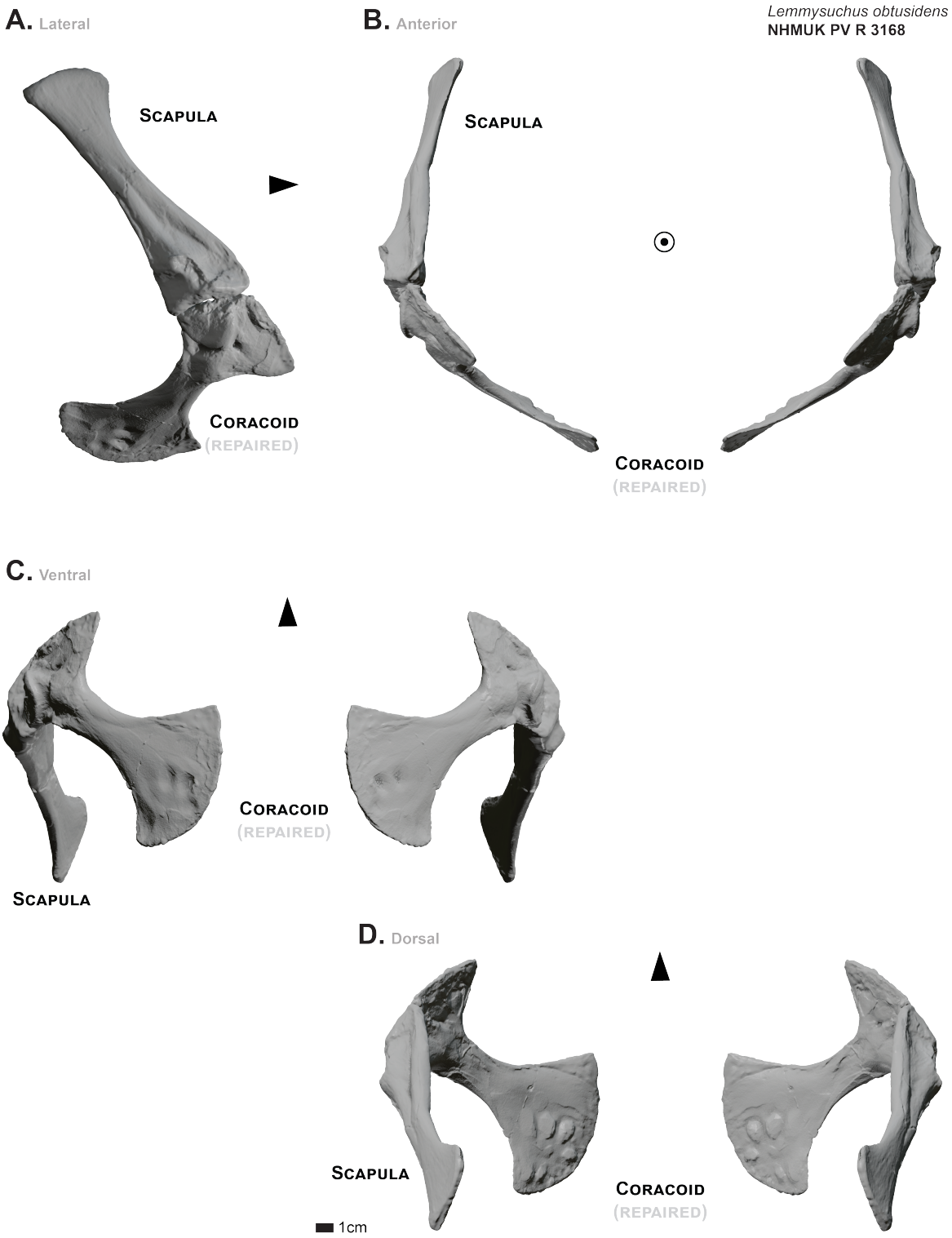


FIGURE 60. Reconstruction of the pectoral girdle of *Lemmysuchus obtusidens* (3D models). Scapula from *Lemmysuchus obtusidens* NHMUK PV R 3168 & coracoid from *Lemmysuchus obtusidens* NHMUK PV R 3169. **A.** Lateral view; **B.** Anterior view; **C.** Ventral view; **D.** Dorsal view. Arrow points anteriorly. Target indicates anterior. The left scapula and coracoid are mirrored. Reconstruction of missing parts based on *Neosteneosaurus edwardsi* PETMG R178 and *Neosteneosaurus edwardsi* NHMUK PV R 3701.

8.10. ***Machimosaurus hugii* von Meyer, 1837.** For measurements, see table 7.

The genus *Machimosaurus* is currently considered as possessing two single valid species: *Machimosaurus hugii* von Meyer, 1837 (Martin et al., 2015) and *Machimosaurus rex* Fanti et al., 2015 (Fanti et al., 2015). In the coracoid subsection, we describe the remains of the lost neotype of *Machimosaurus mosae* Sauvage and Liénard, 1879 from Hua et al. (1993); Hua (1999) and *Machimosaurus buffetauti* SMNS 91415 Young et al., 2014, which belong to *Machimosaurus hugii* (Martin et al., 2015). The bone referred to the pubis of *Machimosaurus mosae* in Hua et al. (1993); Hua (1999); Young et al. (2014) displays all the characteristics of a derived teleosauroid humerus: shortening of humeral shaft; posterior deflection of the articular proximal head; distal torsion of the condyles in relation to the coronal plane; continuous surface between the deltopectoral crest and the proximal articular head.

8.10.1. *Coracoid.* The coracoid of *Machimosaurus* spp. (see figs. 43 and 61) possesses several characteristics typical of other teleosauroids: large coracoid head and blade, triangular anterior expansion, small enclosed coracoid foramen, large glenoid facet, and slender shaft with marked anteroposterior constriction. Yet, the coracoid of *Machimosaurus* spp. differs from other teleosauroids in displaying the combination of a more posteriorly positioned glenoid facet, a more medially inclined anterior expansion which is also proportionally expanded. Compared to other machimosaurids, the coracoid of *Machimosaurus* spp. possesses a shaft proportionally shorter.

Similar to other teleosauroids, the coracoid of *Machimosaurus* spp. (see fig. 61) displays a relatively hourglass silhouette: the coracoid head and blade are both large and the shaft of the coracoid connecting them shows a marked constriction. In addition, the anterior expansion of the coracoid head of *Machimosaurus* spp. possesses a triangular outline with relatively straight margins converging into a sharp apex anteriorly, which is typically encountered in teleosauroids. However, in *Machimosaurus* spp. the anterior expansion of the coracoid head is proportionally more medially tilted as it forms an acute angle with the long axis of the shaft of the coracoid (55° and 73° see A and C on fig. 61 respectively). Also, the anterior expansion of the coracoid head of *Machimosaurus* spp. (see C on fig. 61) is proportionally larger than in most teleosauroids as it accounts for about 63% of the total anteroposterior length of the coracoid head (which is similar to what is observed in *Charitomenosuchus* NHMUK PV R 3806).

In contrast, the posterior portion of the coracoid head of *Machimosaurus* spp. – encompassing the scapulocoracoid synchondrosis surface and glenoid process – shows a more sub-quadrangular shape, similar to *Charitomenosuchus* NHMUK PV R 3806, *Neosteneosaurus* NHMUK PV R 3701 and *Lemmysuchus* NHMUK PV R 3169. Indeed, the posterior apex of the coracoid head of both *Machimosaurus* spp. specimens – the junction between the glenoid facet and the posterior margin of the coracoid head – forms a right-angle corner. Furthermore, the overall extension of the posterior margin of the coracoid head of *Machimosaurus* spp. (both specimens) is similar to the length of the glenoid facet which emphasizes the squared appearance of the posterior portion of the coracoid head. In one of the *Machimosaurus* spp. specimen (see A on fig. 61), the junction between the lateral margin of the anterior expansion and the scapulocoracoid synchondrosis surface even forms a clear right-angle corner which further accentuates the square-shaped appearance.

The exact shape and extension of the scapulocoracoid synchondrosis surface of the coracoid of *Machimosaurus* spp. is not observable. As in *Neosteneosaurus* NHMUK PV R 3701, the glenoid facet of the coracoid of SMNS 91415 appears relatively more posteriorly positioned than in most machimosaurids since the edge of the glenoid facet also participates in the silhouette of the coracoid head. In the other specimen (see A on fig. 61), the glenoid facet is not observable, but the proportionally short and posterolaterally facing area is interpreted as the scapulocoracoid synchondrosis surface. Hence, it is presumed that the glenoid facet of the coracoid of *Machimosaurus* spp. is mainly positioned on the ventral surface

of the coracoid head, with a certain degree of posterior shift in its placement. As such, the scapulocoracoid synchondrosis surface of the coracoid of *Machimosaurus* spp. mainly extends dorsally to the glenoid facet.

In *Machimosaurus* spp., the coracoid foramen forms a relatively small and sub-circular aperture which is located along the longest axis of the coracoid head as in *Macrospondylus* SMNS 9428, *Neosteneosaurus* NHMUK PV R 3701, *Lemmysuchus* NHMUK PV R 3169, and also *Aeolodon* NHMUK PV R 1086. In *Charitomenosuchus* NHMUK PV R 3806, the coracoid foramen is also relatively rounded in shape, but is found lying slightly underneath the longest axis of the coracoid head. Similar to most teleosauroids (except *Charitomenosuchus* NHMUK PV R 3806 and *Lemmysuchus* NHMUK PV R 3169), the coracoid foramen of *Machimosaurus* spp. is directly in line with the long axis of the shaft of the coracoid.

The shaft of the coracoid of *Machimosaurus* spp. forms a proportionally short structure as it accounts for about 31–35% of the total mediolateral extension of the bone, which is similar to what is observed in the machimosaurid *Lemmysuchus* NHMUK PV R 3169 and aeolodontid *Mycterosuchus* NHMUK PV R 2617. In comparison, the shaft of the coracoid reaches relatively larger values in other teleosauroids (*e.g.* about 43% in *Aeolodon* NHMUK PV R 1086, 40% in *Macrospondylus* PMU 35980, 38% in *Charitomenosuchus* NHMUK PV R 3806, 43% in *Neosteneosaurus* NHMUK PV R 3701). Such a short shaft in *Machimosaurus* spp. is mainly induced by the shape of the anterior and posterior margins of the coracoid, and particularly by the greater degree of curvature of the anterior margin. Indeed, the posterior margin of the coracoid of *Machimosaurus* spp. displays a smoothly concave outline with its apex being relatively centered, whereas the anterior margin shows a more asymmetrical appearance. As in other machimosaurids, the anterior margin of the coracoid of *Machimosaurus* spp. displays a lancet arch shape, with its apex being positioned at the junction between the coracoid head and the shaft of the coracoid. In *Machimosaurus* spp., the maximum anteroposterior constriction of the shaft of the coracoid is found around its mid-height, which is similar to most teleosauroids (except *Charitomenosuchus* NHMUK PV R 3806).

Medially, the shaft of the coracoid of *Machimosaurus* spp. rapidly flares out to form the coracoid blade. Similar to other teleosauroids with a proportionally short shaft (*e.g. Lemmysuchus* NHMUK PV R 3169 and *Mycterosuchus* NHMUK PV R 2617), the coracoid blade of *Machimosaurus* spp. displays a considerable mediolateral height which gives it a broad appearance. The medial margin of the coracoid blade of *Machimosaurus* spp. shows a convex outline, but the relative symmetry of its appearance is unknown. In SMNS 91415, the anterior apex of the coracoid blade appears to form a relatively sharp and acute corner, mainly anteriorly facing as in *Macrospondylus* PMU 35980 among machimosaurids.

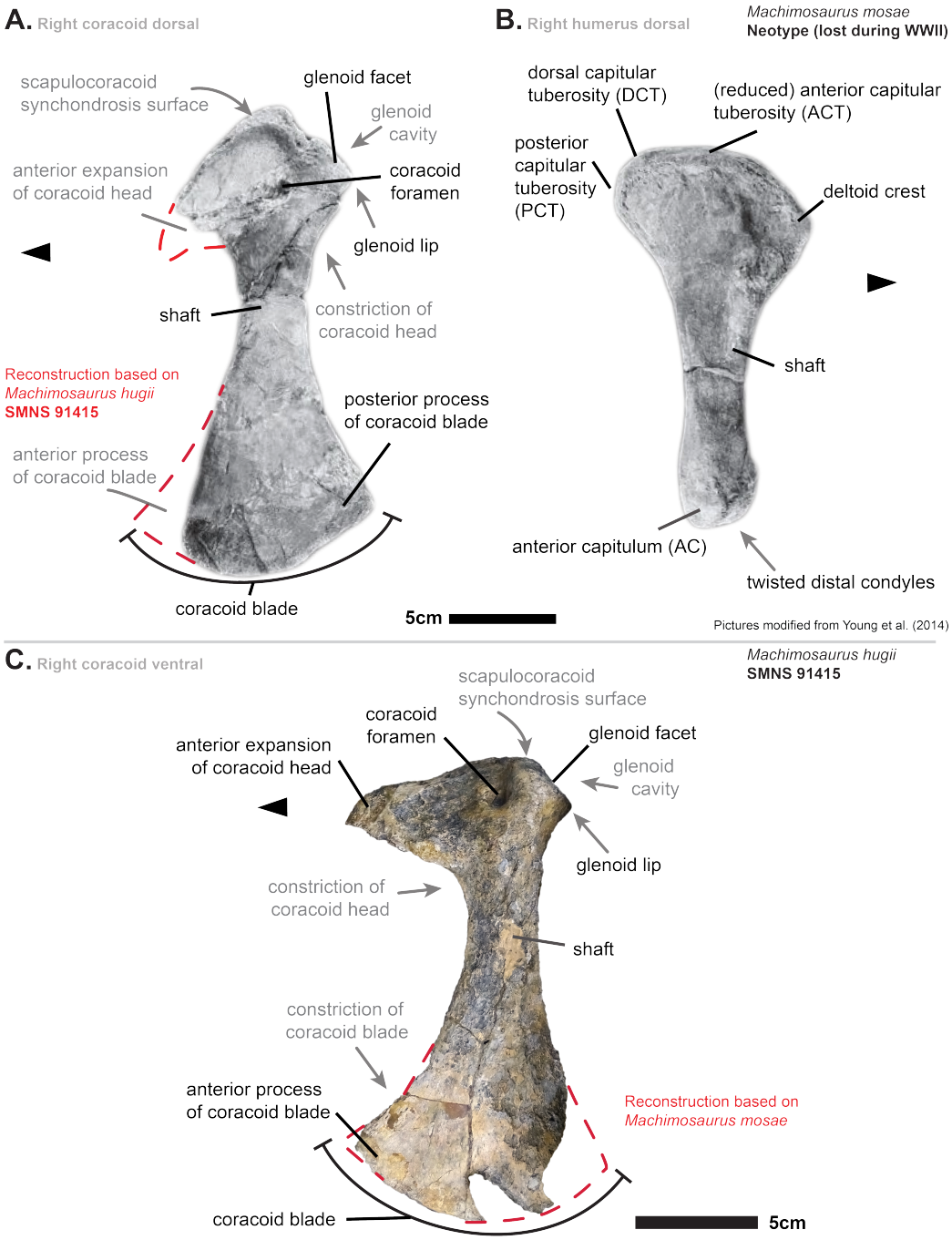


FIGURE 61. Pectoral girdle of *Machimosaurus* spp.: *Machimosaurus mosae* Neotype (lost during WWII) (A&B) and *Machimosaurus buffetauti* SMNS 91415 (C) (photographs). **A.** Right coracoid in dorsal view ; **B.** Right humerus in dorsal view ; **C.** Left coracoid in ventral view. Arrow points anteriorly. Red dashed lines indicate missing parts. Reconstruction of missing parts based on *Lemmysuchus obtusidens* NHMUK PV R 3168.

9. THE APPENDICULAR SKELETON OF DYROSAURIDS

9.1. ***Anthracosuchus balrogus*** **Hastings et al., 2014.** For measurements, see table 6.

9.1.1. *Scapula.* The scapula of *Anthracosuchus balrogus* Hastings et al., 2014 UF/IGM 68 (see figs. 62 and 63) displays a proportionally large proximal region and a marked neck constriction like in other dyrosaurids. Yet, the scapula of *Anthracosuchus* is distinct from that of other dyrosaurids in possessing a proportionally less expanded scapular blade.

The scapula of *Anthracosuchus* UF/IGM 68 displays the typical wide scapular blade flare of dyrosaurids, which greatly contrasts with most thalattosuchians (with *Macrospondylus* SMNS 54063, SMNS 9428 & PMU 35980 and *Platysuchus* SMNS 9930 & UMH-0005 and *Platysuchus* Kloster Banz unnumbered specimen as exceptions in this case). Although not entirely preserved, the anteroposterior length of the scapular blade of *Anthracosuchus* UF/IGM 68 appears to be more than half of the total dorsoventral height of the scapula (possibly reached around 70%) . In comparison, this value reaches at least 61% in *Dy. maghribensis* OCP DEK-GE 254 (incomplete), 104% in *H. natator* NJSM 23368, and would have also presumably reached around 100% in *Co. bequaerti* MRAC 1809 (also incomplete). The relatively low degree of concavity of the anterior margin of the scapula of *Anthracosuchus*, especially in the surroundings of the neck constriction, conveys the presence of a markedly less arched anterior margin of the scapula for *Anthracosuchus* compared to what is observed in *H. natator* NJSM 23368, *Dy. maghribensis* OCP DEK-GE 254 and *Co. bequaerti* MRAC 1809. As such, the scapula of *Anthracosuchus* appears to have been relatively anteroposteriorly symmetrical dorsally to the constriction of the neck, despite its state of preservation. In addition, the shape of the dorsal margin of the scapular blade of *Anthracosuchus* was possibly strongly convex which contrasts with the more subtle curvature of derived dyrosaurids (*e.g. H. natator*, *Dy. maghribensis*, *Co. bequaerti*).

The anterior and posterior margins of the scapula of *Anthracosuchus* are both concave, with the anterior one displaying a slightly greater degree of curvature than the posterior one. A similar relation is observed in other dyrosaurids, in which the anterior margin of the scapula is always more arched than the posterior one. However, the concavity of the anterior margin of the scapula of *Anthracosuchus* strongly differs from the hemispherical one of derived dyrosaurids as it is more parabolic in shape. As in other dyrosaurids, the constriction of the scapula of *Anthracosuchus* is located relatively ventrally at around one-fourth of the total dorsoventral height of the bone. In comparison, in *Co. bequaerti* and *H. natator*, the constriction is located at around 30% of the dorsoventral height of the scapula, and this number reaches 40% for *Dy. maghribensis*. In *Anthracosuchus*, the width of the constriction accounts for about 27% of the total dorsoventral height of the bone, which is a proportionally lesser narrowing than in derived dyrosaurids (with 23% for *Co. bequaerti*, and around 19% for *H. natator* and *Dy. maghribensis*).

Another great distinctive feature of the scapula of *Anthracosuchus* compared to other dyrosaurids is the overall orientation of its shaft and scapular blade. Indeed, in *Anthracosuchus*, the shaft of the scapula and scapular blade are posteriorly projected as the long axis of the shaft of the scapula forms an angle of about 124° with the plane of the scapulocoracoid synchondrosis surface, whereas it forms an angle of about 101° in *Co. bequaerti*, 109° in *Dy. maghribensis* OCP DEK-GE 252 & OCP DEK-GE 254, and about 95° in *H. natator* NJSM 23368. The marked difference in inclination between *Anthracosuchus* and derived dyrosaurids is not an artefact of its shorter scapular blade; the posterior margin of the scapula of *Anthracosuchus* forms a greater angle with the plane of the scapulocoracoid synchondrosis surface (about 143°) than in derived dyrosaurids (about 120-125°). The angular difference between *Anthracosuchus* and *Dy. maghribensis* (15°) is as pronounced as the difference between *Dy. maghribensis* and *H. natator* (14°).

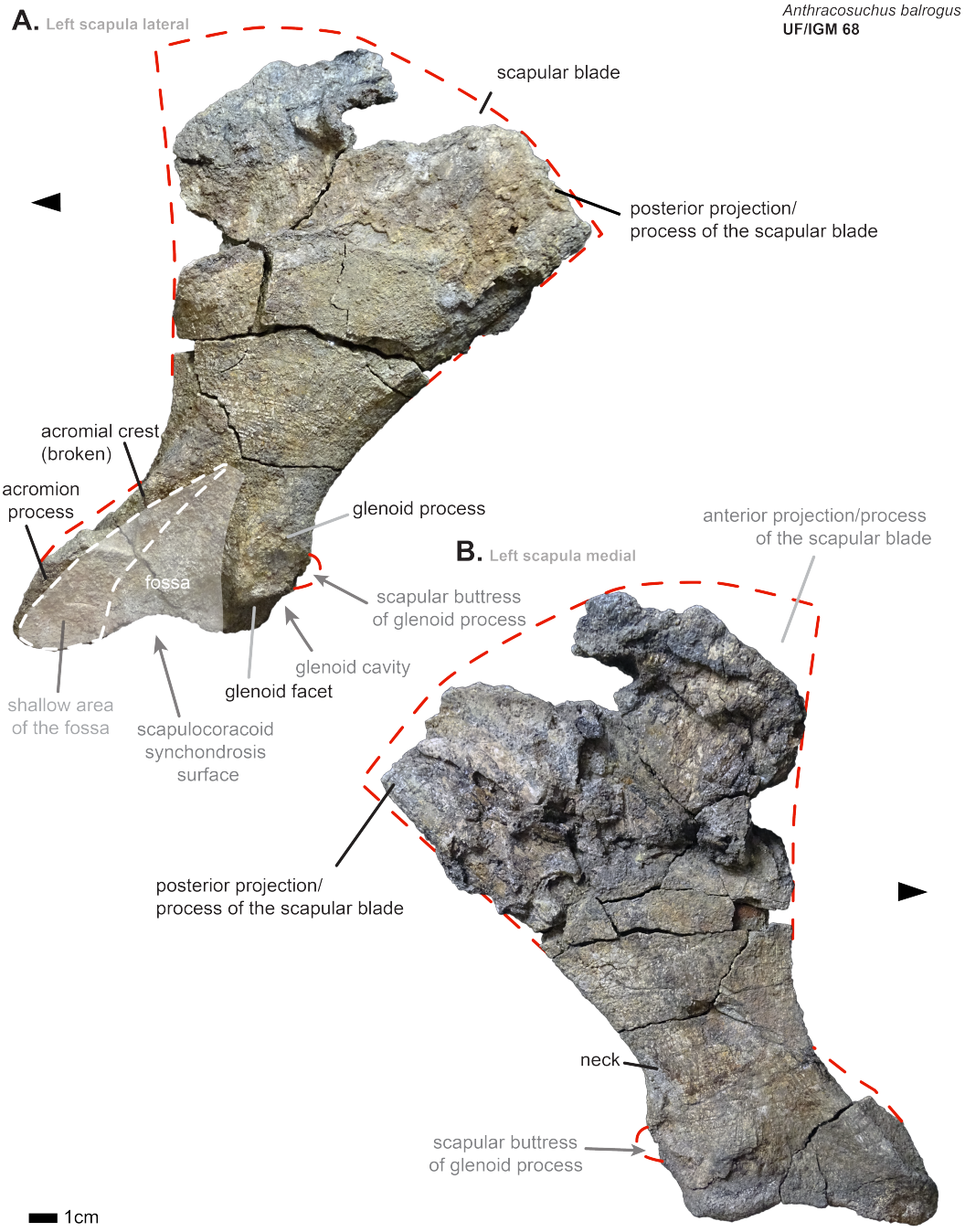


FIGURE 62. Pectoral girdle of *Anthracosuchus balrogus* UF/IGM 68 (photographs). **A.** Left scapula in lateral view ; **B.** Left scapula in medial view. Arrow points anteriorly. Red dashed lines indicate missing parts. Reconstruction of missing parts based on *Hyposaurus natator* NJSM 23368.

Similar to other dyrosaurids, the scapula of *Anthracosuchus* asymmetrically flares out ventrally to the constriction to constitute the proximal region. Anteriorly, the latter forms a prominent bulge corresponding to the acromion process. In *Anthracosuchus* the acromion process has an elliptic outline, whereas it displays a more complex shape in derived dyrosaurids (*i.e.* dorsally flat, ventrally semicircular, apex pointing dorsally). The apex of the acromion process of the scapula of *Anthracosuchus* is mediolaterally thick and points anteroventrally. It is also directly in line with the scapulocoracoid synchondrosis surface. The latter is well-developed as in other dyrosaurids as it accounts for three-quarters of the total anteroposterior length of the proximal region. Ventrally, the outline of the scapulocoracoid synchondrosis surface of the scapula of *Anthracosuchus* is similar to what is observed in derived dyrosaurids: the anterior two-thirds of the surface form a blade-like and mediolaterally thin shape, whereas the remainder portion is wider and subcircular. The latter is also slightly convex and finely pitted, whereas the blade-like portion is slightly concave and relatively smoother but with some deeper ridges anteriorly. The blade-like anterior portion of the scapulocoracoid synchondrosis surface has a slightly concave rim medially whereas the lateral rim shows the succession of two bulges as in *H. natator* (unlike *Co. bequaerti* which is slightly convex throughout). In *Anthracosuchus*, however, the anterior bulge is larger than the posterior one differing from *H. natator*. The entire ventral surface of the scapulocoracoid synchondrosis of the scapula of the scapula of *Anthracosuchus* is also concave, with its deepest point positioned at the junction between the blade-like anterior portion and the posterior sub-circular one (as in *H. natator* and *Dy. maghribensis*). In comparison, the ventral surface of the scapulocoracoid synchondrosis surface of the scapula of *Co. bequaerti* is more undulated.

The glenoid facet is directly attached to the posterolateral extremity of the sub-circular portion of the scapulocoracoid synchondrosis surface. As in other dyrosaurids, the glenoid facet is located on the lateral side of the scapula and is mainly posteroventrally facing. The glenoid facet of the scapula of *Anthracosuchus* is missing its dorsal extremity, which was presumably laterally prominent as in other dyrosaurids. The area extending from the glenoid process to the mid-length of the acromion process forms a marked recess medially corresponding to the deepest portion of the scapular fossa, as in other dyrosaurids. Anteriorly to this portion, the scapular fossa becomes shallower and extends anteriorly until the acromial crest, similar to *Co. bequaerti* but unlike *H. natator* and *Dy. maghribensis*. However, the anterior portion of the scapular fossa of *Anthracosuchus* is slightly concave as in *H. natator* differing from the slightly convex area of the scapula of *Co. bequaerti*. In its entirety, the scapular fossa of *Anthracosuchus* displays an overall triangular shape, similar to other dyrosaurids. In *Anthracosuchus*, the acromial crest is located near the dorsal margin of the acromion process, and extends dorsally until the constriction of the shaft of the scapula where it originates. In comparison, the acromial crest of the scapula of *H. natator* starts slightly more dorsally, and in *Co. bequaerti* it starts slightly more ventrally. Like *H. natator*, the acromial crest of the scapula of *Anthracosuchus* defines a dorsally facing area with the anterior margin of the scapula. This surface is mainly flat to slightly convex throughout, but it forms a deeper indentation around the neck constriction of the scapula. The peak of the acromial crest of the scapula of *Anthracosuchus* is not preserved, but was presumably located around its mid length which contrasts with the anteriorly shifted peak of *H. natator*. The acromial crest of the scapula of *Anthracosuchus* appears to further contrast with those of *H. natator* and *Co. bequaerti* as it reaches the apex of the acromion process anteriorly. In comparison, the acromial crest of the scapula of *H. natator* almost reaches the apex of the acromion process, but in *Co. bequaerti* it ends earlier.

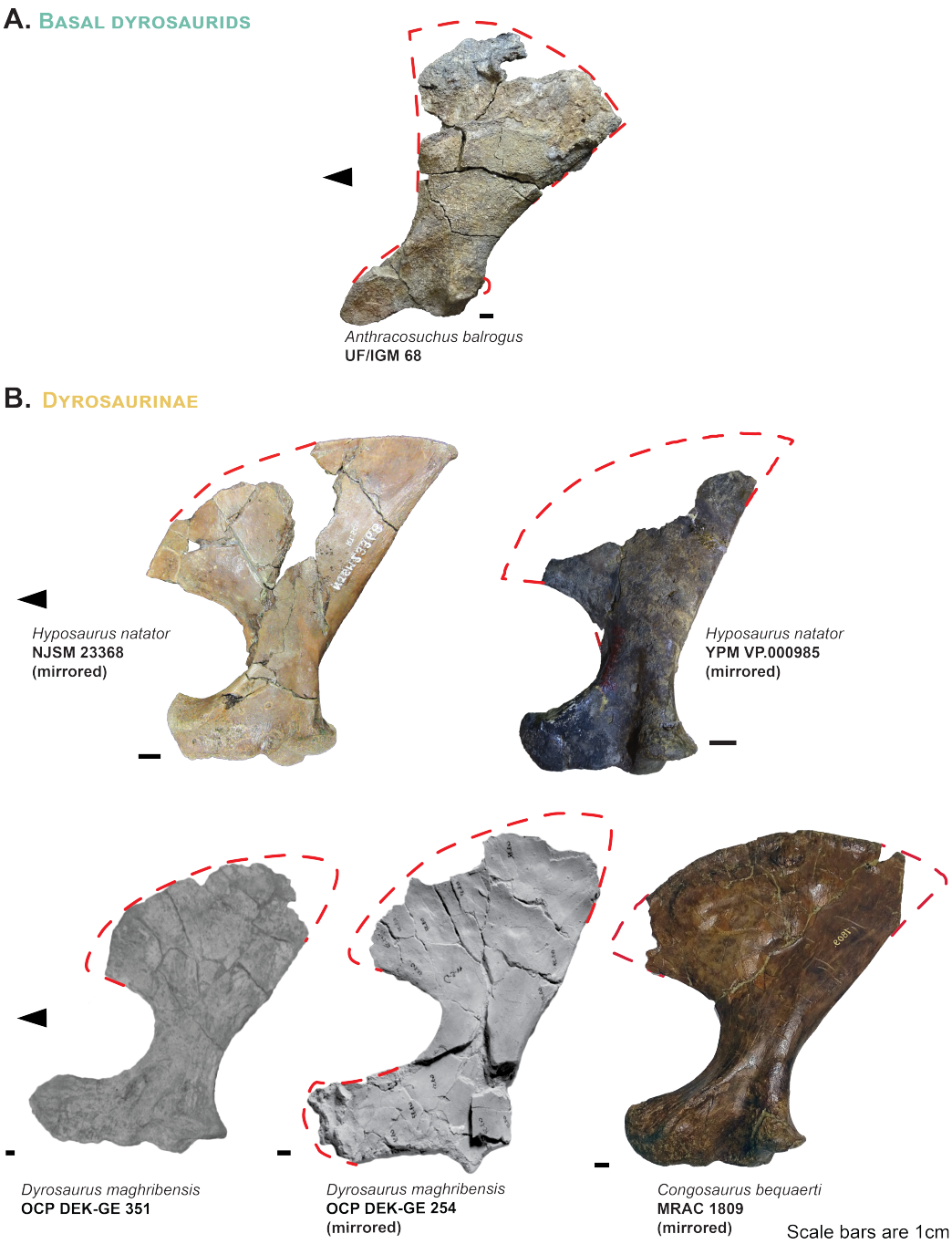


FIGURE 63. Comparative figure of dyrosaurid scapulae (photographs). **A.** Basal dyrosaurid; **B.** Dyrosaurinae. Arrow points anteriorly. Scale bars represent 1cm. Red dashed lines indicate missing parts.

9.2. ***Hyposaurus natator* Owen, 1849.** For measurements, see tables 6 and 7.

9.2.1. *Scapula.* Overall, the scapula of *Hyposaurus natator* (NJSM 23368 see figs. 63 to 65 and YPM VP.000985 see fig. 66) appears strongly similar to those of *Dy. maghribensis* and *Co. bequaerti* due to a series of traits: an expanded scapular blade and proximal region, a posteroventrally facing glenoid facet, and a strong neck constriction.

The marked dorsal flaring of the scapula of *H. natator* is more similar to other derived dyrosaurids (*e.g. Dy. maghribensis* and *Co. bequaerti*) than *Anthracosuchus*, which possesses a less expanded scapular blade. Indeed, the scapular blade of *H. natator* is almost as long anteroposteriorly as the scapula is high dorsoventrally, as in *Co. bequaerti* (and possibly *Dy. maghribensis* but the latter is incomplete). Hence, as in *Dy. maghribensis* and *Co. bequaerti*, the anterior margin of the scapula of *H. natator* is strongly concave and almost hemispherical, whereas it is more parabolic in *Anthracosuchus*. The posterior margin of the scapular blade of *H. natator* is relatively straight in comparison (dorsally to the constriction), similar to *Anthracosuchus* and *Co. bequaerti*. In comparison, the posterior margin of the scapular blade of *Dy. maghribensis* appears slightly convex in both OCP DEK-GE 252 & OCP DEK-GE 254.

The combination of the strong concavity of the anterior margin of the scapula of *H. natator* NJSM 23368 as well as the relatively upright inclination of its shaft (about 95° with the scapulocoracoid synchondrosis surface), brings the anterior corner of the scapular blade further anteriorly than the acromion process. It is possible that a comparable condition was present in *Co. bequaerti* due to a similar inclination of its shaft (about 101° with the scapulocoracoid synchondrosis surface) and proportionally short proximal region. However, the acromion process of the scapula of *Dy. maghribensis* appears markedly longer than in *H. natator* and *Co. bequaerti* as its maximum anteroposterior extension accounts for at least twice the anteroposterior thickness of the neck constriction. Furthermore, the acromion process of the scapula of *Dy. maghribensis* presumably extended further anteriorly than the scapular blade. The anterior and posterior extremities of the scapular blade of *H. natator* NJSM 23368 form two sharp and almost right-angled corners. As in *Dy. maghribensis*, the posterior corner of the scapula of *H. natator* NJSM 23368 is located further dorsally than the anterior corner. This is due to both the long posterior margin of the scapula, as well as the strong curvature of the anterior margin which brings the anterior corner more ventrally. In comparison, the difference was presumably more subtle in *Co. bequaerti* (as indicated by the curvature of the scapular blade). In *Anthracosuchus*, however, the condition is inverted as the anterior corner is slightly more dorsally located compared to the posterior one. The scapular blade of *H. natator* NJSM 23368 shows a gently convex dorsal margin which was presumably symmetrical (*i.e.* apex located at the mid-length), similarly to *Co. bequaerti*, and possibly *Dy. maghribensis*. However, in *H. natator* NJSM 23368 the posterior-most portion of the scapular blade also corresponds to the dorsal-most point of the scapula, whereas this portion is ventrally declining (*i.e.* ventrally lower) in *Co. bequaerti*. This dissimilarity between *H. natator* NJSM 23368 and *Co. bequaerti* reflect a difference in the degree of convexity of the dorsal rim of the scapular blade, with *Co. bequaerti* showing a slightly greater degree of curvature.

Ventrally, the scapular blade of *H. natator* gets markedly narrower anteroposteriorly and thicker mediolaterally to form the constriction of the shaft of the scapula. The anteroposterior width of the latter accounts for about 19% of the total dorsoventral height of the bone, which is a value closer to what is observed in *Dy. maghribensis* OCP DEK-GE 254 (about at most 18.7%) than *Co. bequaerti* (about 23%) and *Anthracosuchus* (about 27%). Similar to other dyrosaurids, the constriction of the shaft of the scapula of *H. natator* is located on the ventral half of the scapula, at around 30% of the total height of the bone. Ventrally to the scapular shaft constriction, the posterior margin of the scapula of *H. natator* YPM VP.000985 is gently concave, whereas it more angular in *H. natator* NJSM 23368. In comparison, the posterior margin of the scapula of *H. natator* is relatively straight dorsal to the constriction as in *Co. bequaerti* and *Anthracosuchus*.

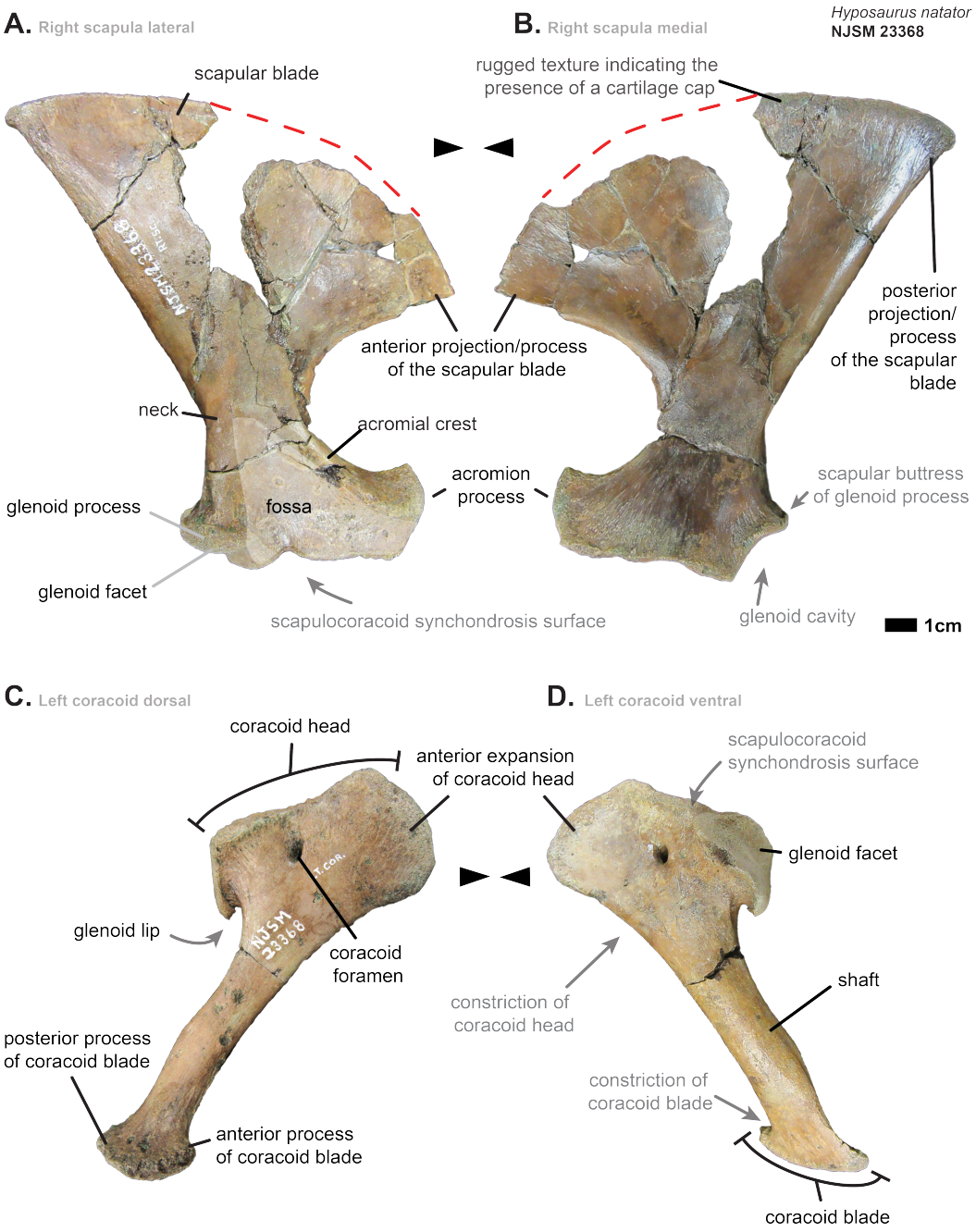


FIGURE 64. Pectoral girdle of *Hyposaurus natator* NJSM 23368, pictures courtesy of Wayne Callahan (photographs). **A.** Right scapula in lateral view ; **B.** Right scapula in medial view ; **C.** Left coracoid in dorsal view ; **D.** Left coracoid in ventral view. Arrow points anteriorly. Red dashed lines indicate missing parts. Reconstruction of missing parts based on *Congosaurus bequaerti* MRAC 1809.

The proximal region of the scapula encompasses the area ventrally to the constriction of the shaft of the scapula, and comprises three main parts anteriorly to posteriorly: the acromion process, the scapular fossa, and the glenoid process. The acromion and glenoid processes account for the mediolaterally thickest parts of the scapula of *H. natator*, as in other dyrosaurids. The acromion process of the scapula of *H. natator* bears a singular shape compared to *Anthracosuchus* and thalattosuchians, but which is found in other derived dyrosaurids: the apex is dorsally oriented, the dorsal margin is markedly concave, and the anterior margin is strongly convex almost like a human thumb in profile. The acromial crest has an overall triangular outline in dorsal view and constitutes the widest point of the acromion process mediolaterally. In lateral view, the acromial crest is recurved and displays a concave shape which does not perfectly match the shape of the anterior margin due to a difference in degree of concavity. The peak of the acromial crest is located around a little less than half of the anteroposterior length of the acromion process from the apex, which also corresponds to about one-third of the total length of the acromial crest. Indeed, the acromial crest of the scapula of *H. natator* originates on the lateral surface of the scapula slightly dorsally to the constriction of the shaft of the scapula (at around 40% of the total height of the bone). In comparison, the acromial crest of the scapula of *Anthracosuchus* starts at the same height as the neck constriction and in *Co. bequaerti* it starts more ventrally, just underneath the constriction. As in other dyrosaurids, the root of the acromial crest of the scapula of *H. natator* is not placed near the anterior margin of the scapula but is slightly posteriorly offset. However, as the acromial crest of the scapula of *H. natator* gradually protrudes laterally, its rim lines up momentarily (around its mid-length) with the anterior margin of the scapula before cutting off ventrally for the remainder anterior half. This contrasts with *Anthracosuchus* in which the acromial crest appears to follow the anterior margin of the scapula for most of its length, and it further differs from *Co. bequaerti* in which the acromial crest does not line up with the anterior margin at all. As a result, the acromial crest of the scapula of *H. natator* defines a dorsally facing surface with the anterior margin of the scapula, which is markedly concave in the area of the neck constriction, and slightly concave to flat on the remainder portion. *Anthracosuchus* displays a similar surface, but in *Co. bequaerti* the same area has a marked lateral orientation anteriorly.

Underneath the acromial crest lies the scapular fossa. The latter covers the area extending from the acromial crest anteriorly to the glenoid process posteriorly, and gradually fades away dorsally around the constriction of the shaft of the scapula as in other dyrosaurids. The scapular fossa of *H. natator* is the deepest in the area directly in line with the axis of the shaft of the scapula, similar to other dyrosaurids. However, in *H. natator*, the anterior portion of the scapular fossa directly underneath the acromial crest also forms a concave and relatively deep area as in *Dy. maghribensis*, but unlike the shallower area of *Anthracosuchus* and slightly convex one of *Co. bequaerti*.

Ventrally, the scapulocoracoid synchondrosis surface of the scapula of *H. natator* starts from the base of the glenoid process posteriorly, and extends anteriorly as far as the extremity of the acromial crest as in other dyrosaurids. Its outline is divided in two major portions: a blade-like anterior area accounting or two-thirds of the length, followed posteriorly by a sub-circular shape as in *Anthracosuchus* and *Co. bequaerti*. The junction between the two portions is marked by a deep indentation medially, which also corresponds to the deepest point of the scapular fossa on the lateral surface of the bone (as in *Co. bequaerti*). In comparison, this indentation is shallower in *Anthracosuchus*. The blade-like portion of the scapulocoracoid synchondrosis surface of the scapula of *H. natator* is slightly concave medially and bears two bulges laterally, as in *Anthracosuchus*. However, the posterior bulge of the scapulocoracoid synchondrosis surface of the scapula of *H. natator* is the largest, differing from *Anthracosuchus*. Posteriorly, the ventral surface of the scapulocoracoid synchondrosis of the scapula of *H. natator* is markedly concave, with its deepest point located at the junction between the blade-like and sub-circular portions as in other dyrosaurids. Underneath the acromion process, the facet of the scapulocoracoid synchondrosis is undulated, as in *Co. bequaerti* but differing from *Anthracosuchus*. In addition, the ventral surface of the

scapulocoracoid synchondrosis of the scapula of *H. natator* is strongly pitted throughout.

Posteriorly, the margin of the scapula of *H. natator* is straight dorsally to the neck constriction and concave underneath it. Indeed, from the neck constriction, the scapula gradually widens mediolaterally to form the glenoid process. Anteriorly, the glenoid process is delimited by the scapular fossa. The glenoid facet of the scapula of *H. natator* is similar to what is observed in other dyrosaurids: it is located on the posterolateral side of the scapulocoracoid synchondrosis, its orientation is posteroventral, and its surface is markedly concave. In *H. natator*, the glenoid facet corresponds to the mediolaterally widest part of the scapula, unlike in *Co. bequaerti* where the posterior sub-circular portion of the scapulocoracoid synchondrosis surface is the widest portion. The ventral half of the glenoid facet (underneath the inflexion point of the concavity) is mediolaterally shorter than its dorsal half, which has a strong bulbous shape in both NJSM 23368 and YPM VP.000985. The latter gives an overall mushroom shape to the glenoid facet of the scapula of *H. natator*. In comparison, the glenoid facet of the scapula of *Co. bequaerti* has a similar shape but the dorsal half is less bulbous. The specimen NJSM 23368 displays a thick and markedly protruding rim surrounding the bulbous dorsal half of the glenoid facet (as in *Dy. maghribensis* OCP DEK-GE 252), whereas YPM VP.000985 only possesses a thin rim (as in *Co. bequaerti*).

9.2.2. *Coracoid.* The coracoid of *Hyposaurus natator* (NJSM 23368 see figs. 64, 65 and 68, YPM VP.000985 see figs. 66 and 68), and *H. natator* YPM VP.000764 (see fig. 67) displays the typical dyrosaurid features: a large coracoid head, a short coracoid blade, and an elongated and rod-like shaft. The coracoid of YPM VP.000985 is partially reconstructed. The coracoid of NJSM 23368 contrasts with those of YPM VP.000985 & YPM VP.000764 in possessing a more angular outline, with prominent corners on both sides of the anterior expansion of its coracoid head and acute and sharp corners at the extremities of its coracoid blade. YPM VP.000985 also shows an angular anterior expansion of the coracoid head but YPM VP.000764 shows an overall dulled shape.

The coracoid head of *H. natator* NJSM 23368, YPM VP.000985 & YPM VP.000764 displays an overall sub-quadrangular outline similar to *Co. bequaerti*: the scapulocoracoid synchondrosis surface and the medial margin of the head are parallel, and the articular facet of the glenoid process is set almost perpendicularly to the scapulocoracoid synchondrosis surface. The anterior margin of the coracoid head (corresponding to the rim of the anterior expansion) displays a convex shape which slightly disrupts the sub-quadrangular appearance of the head as a whole, as in *Co. bequaerti* (and possibly *Dy. maghribensis*). However, the coracoid head of *H. natator* differs from that of *Co. bequaerti* in possessing markedly less symmetrical anterior expansion: the corners of the anterior expansion of the coracoid head of *H. natator* are not aligned, with the medial corner being more anteriorly shifted. This feature is the most pronounced in NJSM 23368 and YPM VP.000985, but is also observable in YPM VP.000764. As a result, the base arch of the convex margin of the head is not perpendicular to the medial and lateral margins of the coracoid head and the apex of the convexity is not centered but slightly shifted medially in NJSM 23368 and YPM VP.000985. In comparison, the anterior margin of the coracoid head of YPM VP.000764 displays a more hemispherical appearance due to its dulled corners. In addition, the lateral corner of the anterior expansion of the coracoid head of *H. natator* NJSM 23368 and YPM VP.000985 is more protruding than in *Co. bequaerti*. This corner corresponds to the anterior extremity of the scapulocoracoid synchondrosis surface, which is a strongly pitted area covering the entire lateral margin of the coracoid head. The outline of the scapulocoracoid synchondrosis surface of the coracoid of *H. natator* NJSM 23368, YPM VP.000985 & YPM VP.000764 strongly contrasts with that of *Co. bequaerti*: it displays two similarly sized peaks ventrally, is slightly concave dorsally, and has rounded anterior and posterior extremities. The two peaks are located on the posterior half of the surface and are separated by a deep indentation which also marks the base of the glenoid facet. The posterior peak is found at one-fifth of the total length of the

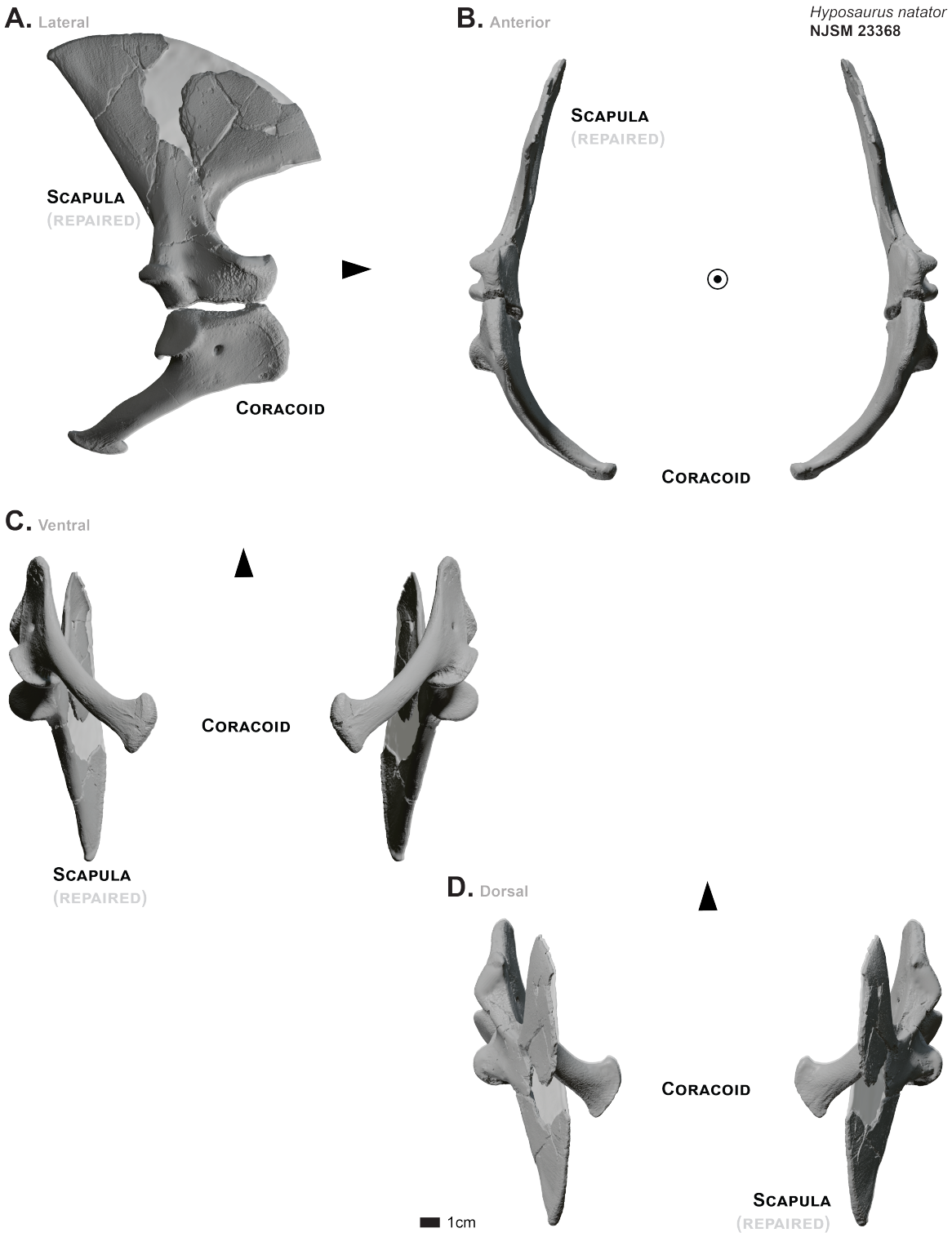


FIGURE 65. Reconstruction of the pectoral girdle of *H. natator* NJSM 23368 (3D models). **A.** Lateral view; **B.** Anterior view; **C.** Ventral view; **D.** Dorsal view. Arrow points anteriorly. Target indicates anterior. The left scapula and coracoid are mirrored. 3D models courtesy of Candice Stephanic. Reconstruction of missing parts based on *Congosaurus bequaerti* MRAC 1809.

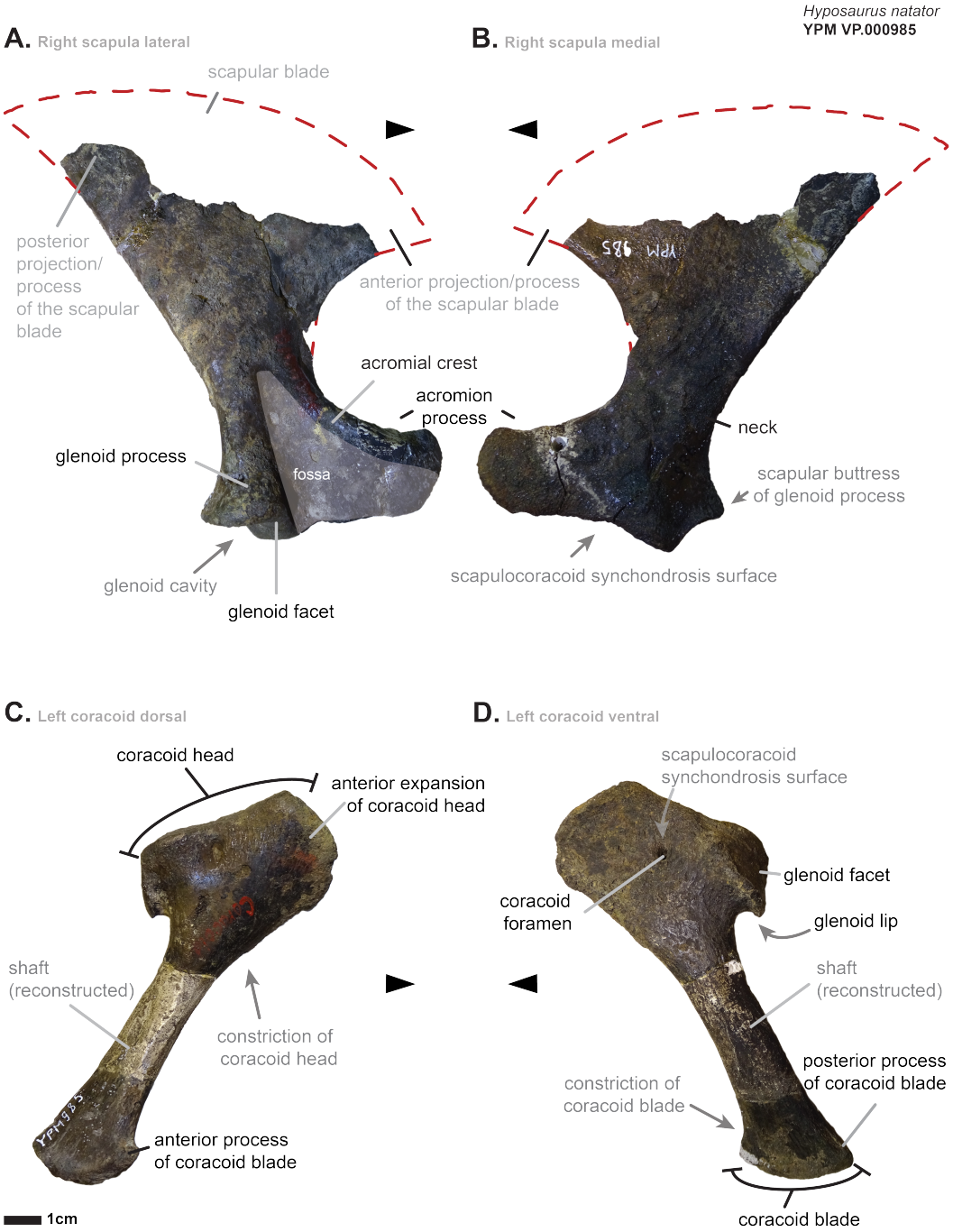


FIGURE 66. Pectoral girdle of *Hyposaurus natator* YPM VP.000985 (photographs). **A.** Right scapula in lateral view ; **B.** Right scapula in medial view ; **C.** Left coracoid in dorsal view ; **D.** Left coracoid in ventral view. The shaft of the coracoid is reconstructed. Arrow points anteriorly. Red dashed lines indicate missing parts. Reconstruction of missing parts based on *Hyposaurus natator* NJSM 23368 and *Congosaurus bequaerti* MRAC 1809.

scapulocoracoid synchondrosis surface and is borne on the glenoid process, whereas the anterior one is located directly near its base, at the mid-length of the scapulocoracoid synchondrosis surface. The anterior half of the scapulocoracoid synchondrosis surface only slightly decreases in dorsoventral thickness compared to the peaks, which contributes to the broad appearance of the surface. In comparison, *Co. bequaerti* displays a single peak corresponding to the glenoid process, and the remainder of the scapulocoracoid synchondrosis surface takes the shape of a thin undulated blade. Hence, the scapulocoracoid synchondrosis surface of the coracoid of *H. natator* is also proportionally shorter and broader than *Co. bequaerti*.

The glenoid process of the coracoid of *H. natator* NJSM 23368, YPM VP.000985 & YPM VP.000764 corresponds to dorsoventral thickest portion of the bone, as in other dyrosaurids. The glenoid process is located on the lateroposterior corner of the coracoid head and contributes to the scapulocoracoid synchondrosis surface. Ventroposteriorly, the glenoid process fans out to form the articular facet of the glenoid which meets with the humerus. The entire border of the glenoid facet of the coracoid of *H. natator* possesses a moderately thin but prominent margin which greatly protrudes from the rest of the coracoid. In *Co. bequaerti*, the margin of the glenoid facet is proportionally thicker but slightly less prominent. It is possible that *Dy. maghribensis* also displayed thick margins. The glenoid facet of the coracoid of *H. natator* is irregularly elliptical to sub-circular in shape, with its longest axis being mainly oriented mediolaterally (with a small ventral inclination as well). This contrasts with *Co. bequaerti*, in which the glenoid facet is mainly elliptical in shape with a stronger ventral dip, and an overall smaller dorsoventral thickness. Also, the anterior and posterior extremities of the glenoid facet of the coracoid of *H. natator* are more rounded than those of *Co. bequaerti*, but still culminate in a pointed apex and thus have the shape of lancet arches. In *H. natator*, the junction between the glenoid facet and the portion of the glenoid involved in the scapulocoracoid synchondrosis surface forms a marked bulge, unlike the smoother transition observed in *Co. bequaerti*. This bulge emphasizes the concavity of the underlying surface of the glenoid facet. Unlike in *Co. bequaerti* (and presumably *Dy. maghribensis*), most of the surface of the glenoid facet of the coracoid of *H. natator* is markedly concave. At around one–third of its length posteriorly, the surface of the glenoid facet of the coracoid of *H. natator* switches and becomes convex as in *Co. bequaerti* (although less markedly), so that the posterior tip of the glenoid facet is set at around a 90° angle with the anterior tip. In doing so, the posterior extremity of the glenoid also forms an anteriorly recurved rim – the glenoid lip. The latter is not directly in contact with the base of the glenoid process as both are spaced, leaving a small hollow area as in *Co. bequaerti* and *Dy. maghribensis*. The surface of the shaft of the coracoid underneath the glenoid lip is markedly concave in *H. natator* as in *Dy. maghribensis*, whereas this is less pronounced in *Co. bequaerti*.

The coracoid foramen of *H. natator* NJSM 23368, YPM VP.000985 & YPM VP.000764 forms a tilted canal as in other dyrosaurids: its dorsal aperture is closer to the scapulocoracoid synchondrosis margin than the ventral aperture. In *Co. bequaerti*, the difference in the mediolateral position of the apertures is less pronounced. On the ventral side of the coracoid, the foramen appears in line with the long axis of the shaft of the coracoid as in *Dy. maghribensis* and *Co. bequaerti*, but the dorsal aperture of the foramen of the coracoid of *H. natator* is markedly posteriorly shifted. In comparison, the dorsal aperture of the coracoid foramen of *Co. bequaerti* is only slightly posteriorly shifted and thus still appears relatively in line with the long axis of the shaft of the coracoid. In addition, the dorsal aperture of the coracoid foramen of *H. natator* is also diagonal in relation to the surface of the coracoid head, with a sharp anteromedial rim and a sloped lateroposterior side almost shaped like a half funnel as in *Co. bequaerti*. However, in *Co. bequaerti* the coracoid foramen is less strongly tilted so that the oblique shape of the dorsal aperture is slightly less marked than in *H. natator*. As in other dyrosaurids, the outline of both apertures of the coracoid foramen of *H. natator* is oval with the longest axis oriented mediolaterally.

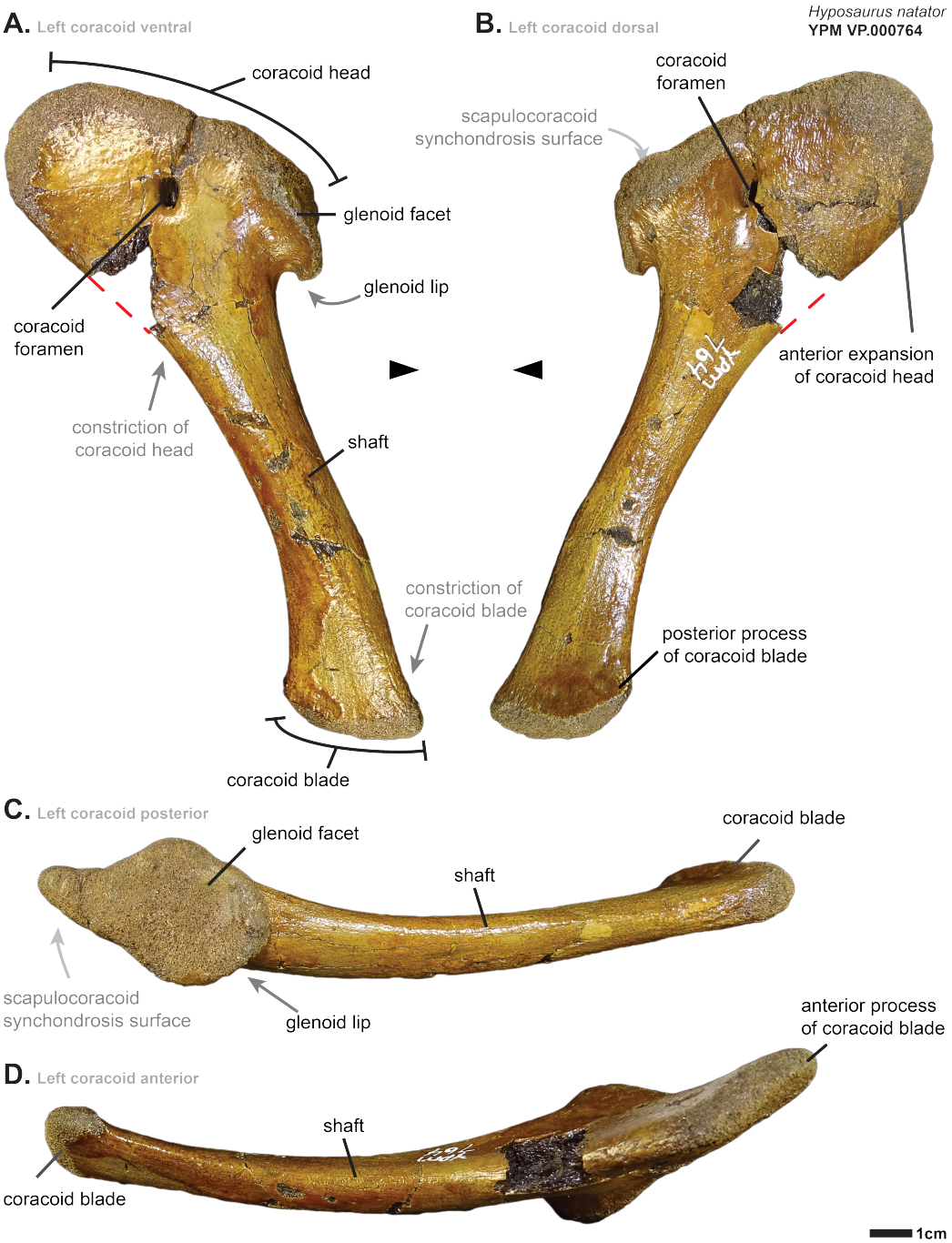


FIGURE 67. Pectoral girdle of *Hyposaurus natator* YPM VP.000764 (photographs). **A.** Left coracoid in ventral view ; **B.** Left coracoid in dorsal view ; **C.** Left coracoid in posterior view ; **D.** Left coracoid in anterior view. Arrow points anteriorly. Red dashed lines indicate missing parts. Reconstruction of missing parts based on *Hyposaurus natator* NJSM 23368.

In *H. natator* NJSM 23368, YPM VP.000985 & YPM VP.000764, the junction between the proximal head of the coracoid and the shaft of the coracoid slightly differs from what is observed in *Co. bequaerti* (and possibly *Dy. maghribensis*). Indeed, the anterior margin of the shaft of the coracoid of *H. natator* is anchored closer to the anterior extremity of the coracoid head than in *Co. bequaerti*. In addition, the anterior margin of the shaft of the coracoid of *H. natator* also appears almost in line with the medial margin of the coracoid head so that the junction between the two forms a relatively planar angle (unlike in *Co. bequaerti* and possibly *Dy. maghribensis*). As a result, the widening of the shaft of the coracoid of *H. natator* at its lateral extremity is larger than what is observed in *Co. bequaerti*. The shaft of the coracoid of *H. natator* NJSM 23368 is elongated and slender like that of *Dy. maghribensis* and *Co. bequaerti*. However, the shaft of the coracoid of *H. natator* NJSM 233368 & YPM VP.000764 displays a slightly more tortuous shape as the posterior margin of the shaft of the coracoid possesses a bulge at around one-third of its length medially. Apart from this lump, the shaft of the coracoid of *H. natator* closely resembles that of other dyrosaurids: the anterior margin of the shaft is relatively straight to slightly concave, whereas the dorsal and ventral margins are both ventrally curved giving an overall arched appearance to the bone. In *H. natator* the medial extremity of the shaft of the coracoid displays is also twisted so that the coracoid blade is posteriorly inclined, similar to *Co. bequaerti*. As a result, the orientation of the coracoid blade and that of the scapulocoracoid synchondrosis are almost parallel, as in *Co. bequaerti*.

The medial flaring of the shaft of the coracoid of *H. natator* to form the coracoid blade is limited both anteroposteriorly and mediolaterally, as in *Co. bequaerti* and *Dy. maghribensis*. Indeed, in *H. natator* the anteroposterior length of the coracoid blade only corresponds to twice the width of the shaft of the coracoid at its mid length, which is lesser than *Co. bequaerti*. Also, the medial flaring of the shaft of the coracoid is shifted towards the medial extremity of the shaft of the coracoid and is relatively condensed (*i.e.* happens over a short distance), as in *Co. bequaerti* and *Dy. maghribensis* which further contrasts to extant crocodylians and thalattosuchians. Similar to other dyrosaurids, the distal blade of the coracoid of *H. natator* NJSM 23368, YPM VP.000985 & YPM VP.000764 is shaped like an axehead: the medial margin of the blade is symmetrically convex (*i.e.* the apex is centered). In NJSM 23368 both extremities forming sharp and acute corners, but those corners are blunt in YPM VP.000985 & YPM VP.000764 (possibly worn out). The anterior corner of the distal blade is oriented laterally whereas the posterior corner points medially, as in *Co. bequaerti* (and presumably *Dy. maghribensis*). Dorsoventrally, the thickness of the coracoid blade is overall constant, but slightly increases towards the centre of the process (which also corresponds to the apex of the convexity) on the posterior side. The increase of thickness of the coracoid blade of *H. natator* is more apparent along the dorsal side where it forms a slight bulge. As a result, the coracoid blade of *H. natator* extends dorsally over the shaft of the coracoid, whereas its ventral border is in line with the shaft of the coracoid. In comparison, the coracoid blade of *Co. bequaerti* does not markedly protrude from the shaft of the coracoid. In *Co. bequaerti*, it also displays a relatively constant thickness throughout, with a small bulge located on the dorsal side near the posterior corner of the blade. The articular facet of the coracoid blade of *H. natator* NJSM 23368, YPM VP.000985 & YPM VP.000764 is markedly scarred and displays a series of ridges perpendicular to the longest axis of the blade. The rim of the articular facet of the coracoid blade forms an abrupt margin dorsally whereas it presents a more gentle bulge along the ventral side of the bone, as in *Co. bequaerti*. In addition, the dorsal rim of the articular facet closely follows the outline of the coracoid blade, whereas the ventral rim covers a portion of the ventral surface of the coracoid blade (similar to *Co. bequaerti*).

DYROSAURINAE

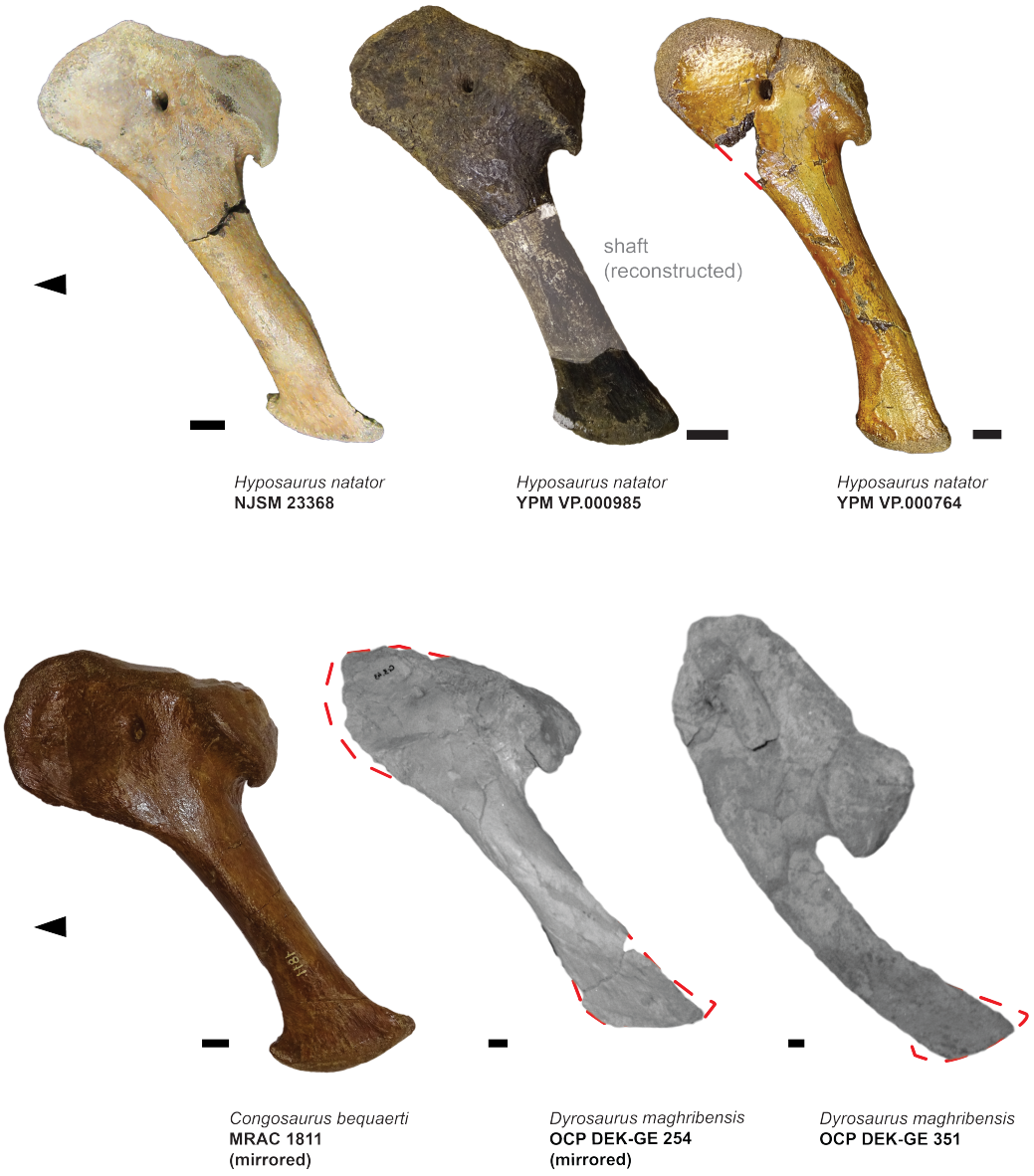


FIGURE 68. Comparative figure of Dyrosaurinae coracoids (photographs). Arrow points anteriorly. Scale bars represent 1cm. Red dashed lines indicate missing parts.

9.3. ***Dyrosaurus maghribensis*** **Jouve et al., 2006.** For measurements, see tables 6 and 7.

9.3.1. *Scapula.* The scapula of *Dyrosaurus maghribensis* OCP DEK-GE 252, OCP DEK-GE 254 & OCP DEK-GE 351 is similar to other dyrosaurids in displaying the combination of a large scapular blade, a strong neck constriction and an enlarged proximal region (see figs. 63, 69 and 70). However, due to the preservation of the specimens, the exact extent of the scapular blade and proximal region of *Dy. maghribensis* is unknown. The anterior corner of the scapular blade of *Dy. maghribensis* was presumably positioned more ventrally than the posterior one, as in *H. natator* and also *Co. bequaerti*. The slightly convex posterior margin of the scapular blade brings the posterior corner of the scapula of *Dy. maghribensis* even more dorsally (and less posteriorly) than in *H. natator* and also *Co. bequaerti*, so that the intensity of the anterior inclination of the scapular blade of *Dy. maghribensis* was presumably also greater.

As in other dyrosaurids, the anterior margin of the scapula of *Dy. maghribensis* is markedly concave and elliptic. However, as mentioned above, the posterior margin of the scapula of *Dy. maghribensis* differs from that of other dyrosaurids in being slightly convex dorsally to the constriction of the shaft of the scapula. From the shaft constriction to the tip of the glenoid process, the posterior margin of the scapula of *Dy. maghribensis* is concave, similar to other dyrosaurids. In *Dy. maghribensis*, the constriction of the shaft of the scapula appears to be located relatively more dorsally than in other dyrosaurids, and it is estimated at around at least 39% of the total dorsoventral height of the scapula for *Dy. maghribensis* OCP DEK-GE 254. The anteroposterior constriction of the shaft of the scapula of *Dy. maghribensis* OCP DEK-GE 254 possibly reached about 18% of the total dorsoventral height of the scapula (although not complete), which is a value similar to *H. natator*.

Ventrally, the shaft of the scapula of *Dy. maghribensis* anteroposteriorly flares out to form the proximal region of the scapula. As in other dyrosaurids, the anterior portion of the proximal region – the acromion process – is markedly larger than the posterior one – the glenoid process. The acromion process of the scapula of *Dy. maghribensis* OCP DEK-GE 254 and OCP DEK-GE 351 possesses a markedly concave margin dorsally and culminates anteriorly to form a thick and rounded apex, like in *H. natator* and *Co. bequaerti*. However, the anterior extremity of the acromion process of the scapula of *Dy. maghribensis* OCP DEK-GE 351 does not form a hemispherical shape like *H. natator* and *Co. bequaerti*, instead it forms a blunt and almost right-angled corner. Hence, the apex of the acromion process of the scapula of *Dy. maghribensis* constitutes the anteriormost point of the scapula as in *Anthracosuchus*, but differing from *H. natator* (and presumably *Co. bequaerti*). This is emphasized by the inclination of the shaft of the scapula in *Dy. maghribensis* (angle of 109° with the scapulocoracoid synchondrosis surface in OCP DEK-GE 252 & OCP DEK-GE 254, and about 103° in OCP DEK-GE 351), which shifts the scapular blade slightly more posteriorly than what is observed in *H. natator* and *Co. bequaerti*. In addition, the acromion process of the scapula of *Dy. maghribensis* OCP DEK-GE 351 appears proportionally longer than what is observed in *H. natator* and *Co. bequaerti*, although the exact dimensions of the scapula of *Dy. maghribensis* are unknown.

In *Dy. maghribensis* OCP DEK-GE 254 and OCP DEK-GE 351, the scapular fossa appears to extend over most of its lateral surface, similar to *H. natator* and *Anthracosuchus*. The acromial crest of the scapula of *Dy. maghribensis* runs dorsally to the scapular fossa and originates at the same level as the constriction of the shaft of the scapula, which is overall similar to other dyrosaurids. In *Dy. maghribensis*, the acromial crests aligns with the anterior margin of the scapula directly underneath the constriction of the shaft of the scapula, as in *H. natator* and *Anthracosuchus*.

The scapulocoracoid synchondrosis surface of the scapula of *Dy. maghribensis* is found on the ventral side of the scapula, and extends from the glenoid process (posteriorly) to the acromion process (anteriorly), as in other dyrosaurids. Posteriorly, its surface appears markedly concave, with its lowest point located directly anteriorly to the glenoid process, where the scapular fossa is also the deepest as in other

dyrosaurids. Underneath the acromion process, however, the scapulocoracoid synchondrosis surface is slightly convex similar to *Anthracosuchus*, and does not appear to be undulated as in *H. natator* and *Co. bequaerti*.

As in other dyrosaurids, the glenoid facet of the scapula of *Dy. maghribensis* is mainly oriented posteroventrally, and is located on the lateral side of the scapula, on the posterolateral extremity of the scapulocoracoid synchondrosis. Its surface is also markedly concave, and its dorsal half is surrounded by a thick rim as in *H. natator* NJSM 23368. The outline of the glenoid facet resembles those of *H. natator* and *Co. bequaerti* in displaying a wide and rounded dorsal half over a shorter ventral half, giving it the appearance of a mushroom.

9.3.2. *Coracoid.* The coracoid of *Dyrosaurus maghribensis* (see figs. 68 to 70) possesses the following features observed in other dyrosaurids: a slender and elongated shaft, a broad coracoid head, and a short coracoid blade.

The coracoid head of *Dy. maghribensis* OCP DEK-GE 252 & OCP DEK-GE 254 is overall shaped like a parallelepiped, similar to *Co. bequaerti* and *H. natator*. Indeed, the anterior expansion of the coracoid head of *Dy. maghribensis* is mediolaterally wide and does not taper anteriorly as seen in extant crocodylians. The lateral and medial margins of the coracoid head are parallel throughout as in *Co. bequaerti* and *H. natator*. The anterior margin of the coracoid head is not complete, but presumably displayed a curved shape as in other dyrosaurids. The scapulocoracoid synchondrosis surface covers the entire length of the lateral margin of the coracoid head. Similar to other dyrosaurids, the scapulocoracoid synchondrosis surface is the widest at the glenoid process, then it becomes narrower anteriorly. The coracoid foramen forms a diagonal canal in relation to the dorsal and ventral surfaces of the coracoid head: the aperture of the foramen is closer to the glenoid process on the dorsal surface than on the ventral one.

The glenoid process of the coracoid of *Dy. maghribensis* OCP DEK-GE 252 & OCP DEK-GE 254 is located on the posterior extremity of the coracoid head and constitutes the thickest portion of the coracoid, similar to other dyrosaurids. Indeed, the glenoid process partially contributes to the scapulocoracoid synchondrosis surface posteromedially and it bears the glenoid facet posteroventrally. In *Dy. maghribensis*, the glenoid facet also appears to possess an elliptic outline with a slightly pointed posterior corner, similar to *Co. bequaerti* and *H. natator*. The glenoid facet of the coracoid of *Dy. maghribensis* is not complete but most of its surface appears slightly concave to relatively flat, which is more similar to *Co. bequaerti* than *H. natator*. The posterior-most extremity of the glenoid facet of the coracoid of *Dy. maghribensis* is markedly bend (angle of about 90°) compared to the rest of the articular facet, as in other dyrosaurids. The edge of the glenoid facet of the coracoid of *Dy. maghribensis* is relatively thick and forms a slight bulge all around. This shape is accentuated at the posterior corner of the glenoid facet due to its recurved shape. Similar to *Co. bequaerti* and *H. natator*, the curl formed by the posterior corner of the glenoid facet – the glenoid lip – is emphasized by an underlying recess in the coracoid head. This concave alcove also marks the posterior base of the coracoid shaft.

As in other dyrosaurids, the shaft of the coracoid of *Dy. maghribensis* OCP DEK-GE 254 extends from the posteromedial corner of the coracoid head, and is set at an acute angle ($\leq 45°$) with the scapulocoracoid synchondrosis surface. The shaft of the coracoid is mediolaterally elongated and displays a relatively constant anteroposterior thickness throughout its length, giving it an overall rod-like appearance similar to *H. natator* and *Co. bequaerti*. Unlike *H. natator*, the shaft of the coracoid of *Dy. maghribensis* does not show any anteroposterior widening near its connection with the coracoid head. Instead, the shaft of the coracoid of *Dy. maghribensis* retains its thickness throughout its length which leads to a relatively more abrupt junction with the coracoid head, as in *Co. bequaerti*. Posteriorly, the shaft of the coracoid

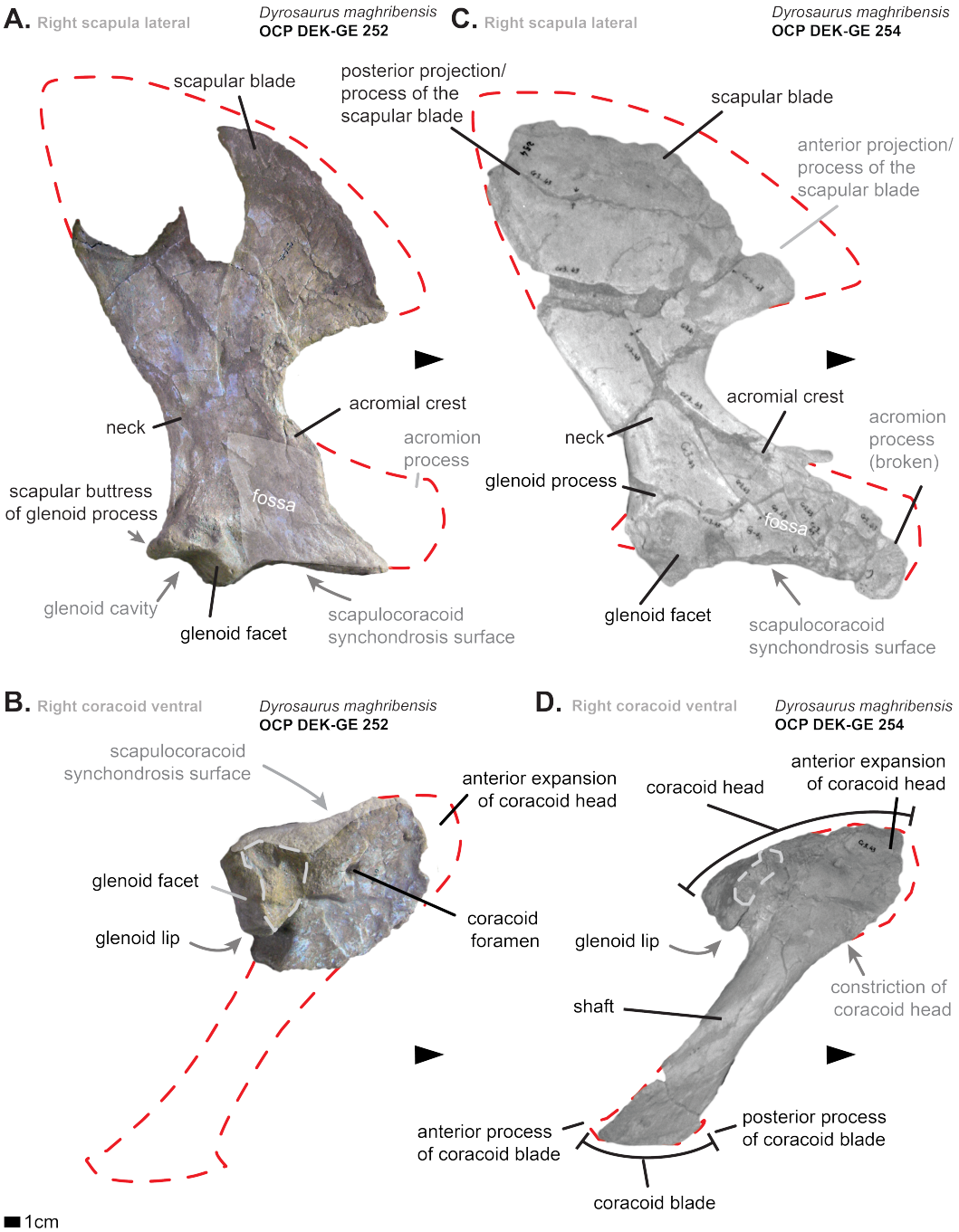


FIGURE 69. Pectoral girdle of *Dyrosaurus maghribensis* OCP DEK-GE 252 (A&B) and *Dyrosaurus maghribensis* OCP DEK-GE 254 (C&D) (photographs). **A.** Right scapula in lateral view; **B.** Right coracoid in ventral view ; **C.** Right scapula in lateral view ; **D.** Right coracoid in ventral view. Arrow points anteriorly. Red dashed lines indicate missing parts. Reconstruction of missing parts based on *Hyposaurus natator* NJSM 23368 and *Dyrosaurus maghribensis* OCP DEK-GE 351.

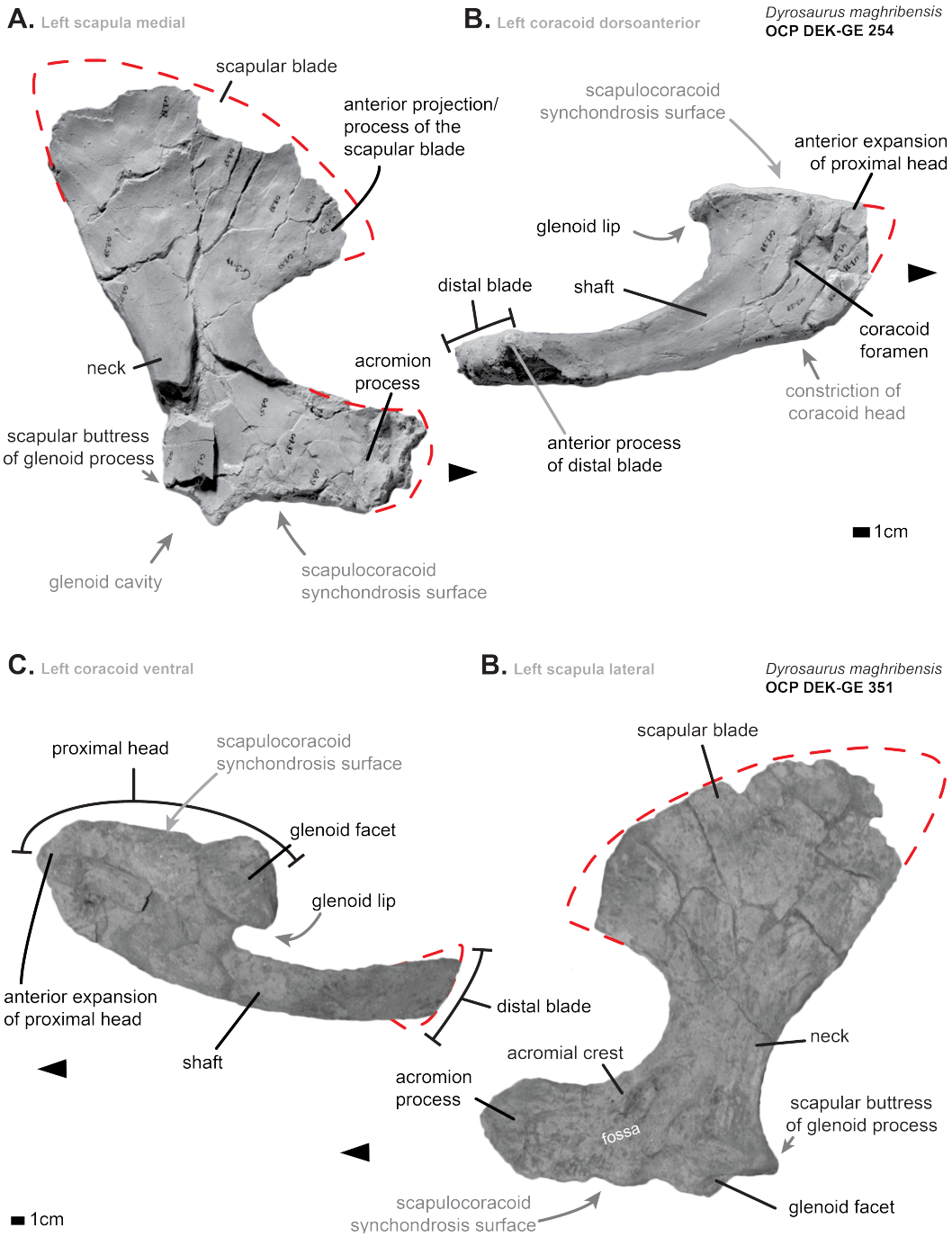


FIGURE 70. Pectoral girdle of *Dyrosaurus maghribensis* OCP DEK-GE 254 (A&B) and *Dyrosaurus maghribensis* OCP DEK-GE 351 (C&D) (photographs). **A.** Left scapula in medial view; **B.** Left coracoid in dorsoanterior view ; **C.** Left coracoid in ventral view ; **D.** Left scapula in lateral view. Arrow points anteriorly. Red dashed lines indicate missing parts. Reconstruction of missing parts of OCP DEK-GE 254 based on *Hyposaurus natator* NJSM 23368 and *Dyrosaurus maghribensis* OCP DEK-GE 351. Reconstruction of missing parts of *Dyrosaurus maghribensis* OCP DEK-GE 351 based on *Hyposaurus natator* NJSM 23368.

connects with the coracoid head below the glenoid facet, which also corresponds to the shallow recessed area underlying the glenoid lip. Anteriorly, the junction between the shaft of the coracoid and the medial margin of the coracoid head appears to form an obtuse angle as in *Co. bequaerti*. In *Dy. maghribensis*, the ventral surface of the shaft of the coracoid displays a slight diagonal ridge which runs from the anterolateral extremity of the shaft of the coracoid to the posterior medial one, similar to *Co. bequaerti* but unlike *H. natator* in which the ventral surface of the shaft is smoother. As in *Co. bequaerti*, the ridge on the ventral surface of the shaft of the coracoid of *Dy. maghribensis* becomes sharper and hence more prominent around the mid-length of the bone. There, it forms a blunt corner marking both the switch in curvature of the shaft of the coracoid (*i.e.* the apex of the concave shape of the shaft) and the decrease in dorsoventral thickness of the shaft of the coracoid towards the medial side. In addition, the medial extremity of the shaft of the coracoid of *Dy. maghribensis* is twisted which ventrally bends the posterior corner of the coracoid blade, as in *H. natator* and *Co. bequaerti*.

9.4. ***Congosaurus bequaerti* Dollo, 1914.** For measurements, see tables 6 and 7.

9.4.1. *Scapula.* The scapula of *Congosaurus bequaerti* MRAC 1809 (see figs. 63, 71 and 72) bears the distinctive dyrosaurid traits: a strong neck constriction, an anteroposteriorly expanded scapular blade, and a proportionally large proximal region, and a laterally positioned and posteroventrally facing glenoid facet. The size of its scapular blade and shape of its acromion process bring the scapula of *Co. bequaerti* closer to those of the derived dyrosaurids *H. natator* and *Dy. maghribensis*, than to *Anthracosuchus*. Indeed, the anterior margin of the scapula of *Co. bequaerti* is strongly concave, so that the anterior margin of the acromion process and scapular blade are facing one another. This configuration expands the size of the scapular blade anteriorly compared to *Anthracosuchus*. Dorsally, the rim of the scapular blade of *Co. bequaerti* displays a smoothly convex shape. The peak of the curve is relatively centered on the dorsal rim, giving the scapular blade a symmetrical appearance as in other dyrosaurids. As in *H. natator*, the scapular blade of *Co. bequaerti* is mainly dorsally oriented, with a slight anterior component in its anterior half. This contrasts with *Dy. maghribensis* in which the scapular blade has a marked anterodorsal orientation, and it further differs from the posterodorsal orientation of the scapular blade of *Anthracosuchus*. On both sides (*i.e.* lateral and medial) of the scapula of *Co. bequaerti*, the area directly surrounding the dorsal rim of the scapular blade is finely striated perpendicularly to the margin, which is itself pitted. A similar texture, presumably indicating the presence of a cartilage cap, is also observable in *H. natator* NJSM 23368 (other dyrosaurids are not well preserved in this part). As in other dyrosaurids except *Dy. maghribensis*, the posterior margin of the scapula dorsal to the constriction of the shaft of the scapula (*i.e.* the posterior margin of the scapular blade) is relatively straight, whereas it becomes slightly concave from the constriction of the shaft of the scapula to the tip of the glenoid process. In *Dy. maghribensis*, the posterior margin of the scapular blade is slightly convex. It is possible that the scapular blade of *Co. bequaerti* extended further anteriorly than the acromion process, as in *H. natator*.

The constriction of the shaft of the scapula of *Co. bequaerti* is located at around one-third of the total dorsoventral height of the bone, which is more similar to *H. natator* than to *Anthracosuchus* (about 25%) and *Dy. maghribensis* (about 40%). The intensity of the neck constriction of the scapula of *Co. bequaerti* (about 23% of the total dorsoventral height of the bone) appears slightly lesser than in *H. natator* and *Dy. maghribensis*, which gives it a stouter appearance. In comparison, the neck of the scapula of *Anthracosuchus* is even thicker than in other dyrosaurids (as it accounts for about 27% of the total dorsoventral height of the scapula). Ventrally, the neck of the scapula gradually flares out anteroposteriorly and widens lateromedially to form the proximal region. The latter is constituted by the acromion process anteriorly, followed by the glenoid process posteriorly. Both processes are separated by the scapular fossa on the lateral side of the scapula. As in *H. natator*, the acromion process of the scapula of *Co. bequaerti* has its apex dorsally oriented and its anterior margin is markedly convex. However, the dorsal margin of the acromion process of the scapula of *Co. bequaerti* is only slightly concave, whereas the concavity of this area is greater in *H. natator*. The acromial crest of the scapula of *Co. bequaerti* differs from what is observed in other dyrosaurids: it displays a relatively straight shape and is strongly offset from the anterior margin of the scapula. In this way, the acromial crest of the scapula of *Co. bequaerti* almost divides the acromion process in two sub-equal laterally oriented parts. In other dyrosaurids, the acromial crest follows more or less closely the shape of the anterior margin of the scapula, so that it splits the acromion process into a dorsal portion and a lateral portion (which corresponds to the shallow area of the scapular fossa) instead. In *Co. bequaerti*, the base length of the acromial crest is also proportionally shorter than in *Anthracosuchus* and *H. natator*, as it originates ventrally to the neck constriction and ends before reaching the apex of the acromion process (it ends near the base arch of the convex anterior margin of the acromion process). The lateral expansion of the acromial crest is unknown in *Co. bequaerti*.

The area directly underneath the acromial crest of the scapula of *Co. bequaerti* is slightly convex as in *Anthracosuchus*, and corresponds to the shallower portion of the scapular fossa. The latter is a hollow area extending from the glenoid process to the acromial crest (laterally), and is the deepest directly anteriorly to the glenoid process as in other dyrosaurids. Due to the relatively low position of the acromial crest, the scapular fossa of *Co. bequaerti* is also proportionally narrower than in other dyrosaurids. The glenoid process of the scapula *Co. bequaerti* constitutes the mediolaterally thickest portion of the scapula, similar to other dyrosaurids. The glenoid facet is well developed and markedly concave; its dorsal half has a rounded outline and is slightly wider than the ventral half, which has slightly concave margins. This contrasts with *Dy. maghribensis* and *H. natator* in which the dorsal half of the glenoid facet is markedly wider than the ventral half, resulting in a mushroom-shaped facet. The dorsal half of the glenoid facet of the scapula of *Co. bequaerti* possesses a relatively thick and rounded rim which slims down medially, whereas the ventral half only displays a thin rim. This mediolateral change in thickness of the dorsal rim of the glenoid facet is also observed in *H. natator*, which possesses an overall bulkier rim than *Co. bequaerti*. Similar to other dyrosaurids, the glenoid facet of the scapula of *Co. bequaerti* is positioned on the lateral surface of the scapula, and extends from the posterolateral corner of the scapulocoracoid synchondrosis surface.

The scapulocoracoid synchondrosis surface of the scapula of *Co. bequaerti* displays the same overall shape as found in other dyrosaurids: it is constituted of a slender blade anteriorly and a posterior sub-circular portion, separated by a marked indentation on the lateral side of the bone. This indentation also indicates the deepest portion of the scapular fossa. The posterior sub-circular portion is mediolaterally thick, and corresponds to the ventral surface of the glenoid process. It is also more intensely pitted than the anterior blade, and its surface is relatively flat. The anterior blade is mediolaterally thinner than the posterior portion, and covers the ventral surface of the acromion process. Its surface is more finely pitted, and is also slightly undulated (which is similar to *H. natator*). In comparison, the entire ventral surface of the anterior blade of the scapulocoracoid synchondrosis surface of the scapula of *Anthracosuchus* and *Dy. maghribensis* is markedly concave. In *Co. bequaerti*, the lateral margin of the anterior blade of the scapulocoracoid synchondrosis surface is slightly convex throughout (differing from the undulated margin of the scapulocoracoid synchondrosis surface of the scapulae of *Anthracosuchus* and *H. natator*), whereas its medial margin is slightly concave. In *Co. bequaerti*, the anterior blade also markedly tapers anteriorly, whereas the anterior extremity of scapulocoracoid synchondrosis remains bulkier in *H. natator* and *Anthracosuchus*. Hence, the posterior sub-circular portion of the scapulocoracoid synchondrosis surface of the scapula of *Co. bequaerti* is markedly wider than the anterior blade, unlike in *H. natator* and *Anthracosuchus*. Furthermore, the posterior sub-circular portion of the scapulocoracoid synchondrosis surface of the scapula of *Co. bequaerti* is also as wide as the dorsal half of the glenoid facet, which further contrasts with *H. natator*.

9.4.2. *Coracoid.* The coracoid of *Congosaurus bequaerti* MRAC 1811 (see figs. 68, 71 and 72) possesses the typical characteristics of dyrosaurids: the scapulocoracoid synchondrosis surface and the long axis of the shaft of the coracoid form an acute angle, a thick and rounded anterior expansion of the proximal head, a long and rod-like shaft, and a large glenoid facet with a markedly recurved lip ventrally (*e.g.*. *Dy. maghribensis* and *H. natator*).

Similar to *Dy. maghribensis* and *H. natator*, the coracoid of *Co. bequaerti* is strongly asymmetrical: the anteroposterior length of the distal blade accounts for about half of the length of the proximal head. In comparison, the proximal and distal extremities of the coracoid of extant crocodylians and thalattosuchians are more similarly sized. In *Co. bequaerti*, the overall shape of the proximal head of the coracoid of is sub-quadrangular as in *H. natator* and *Dy. maghribensis*. Indeed, the lateral margin (comprising the

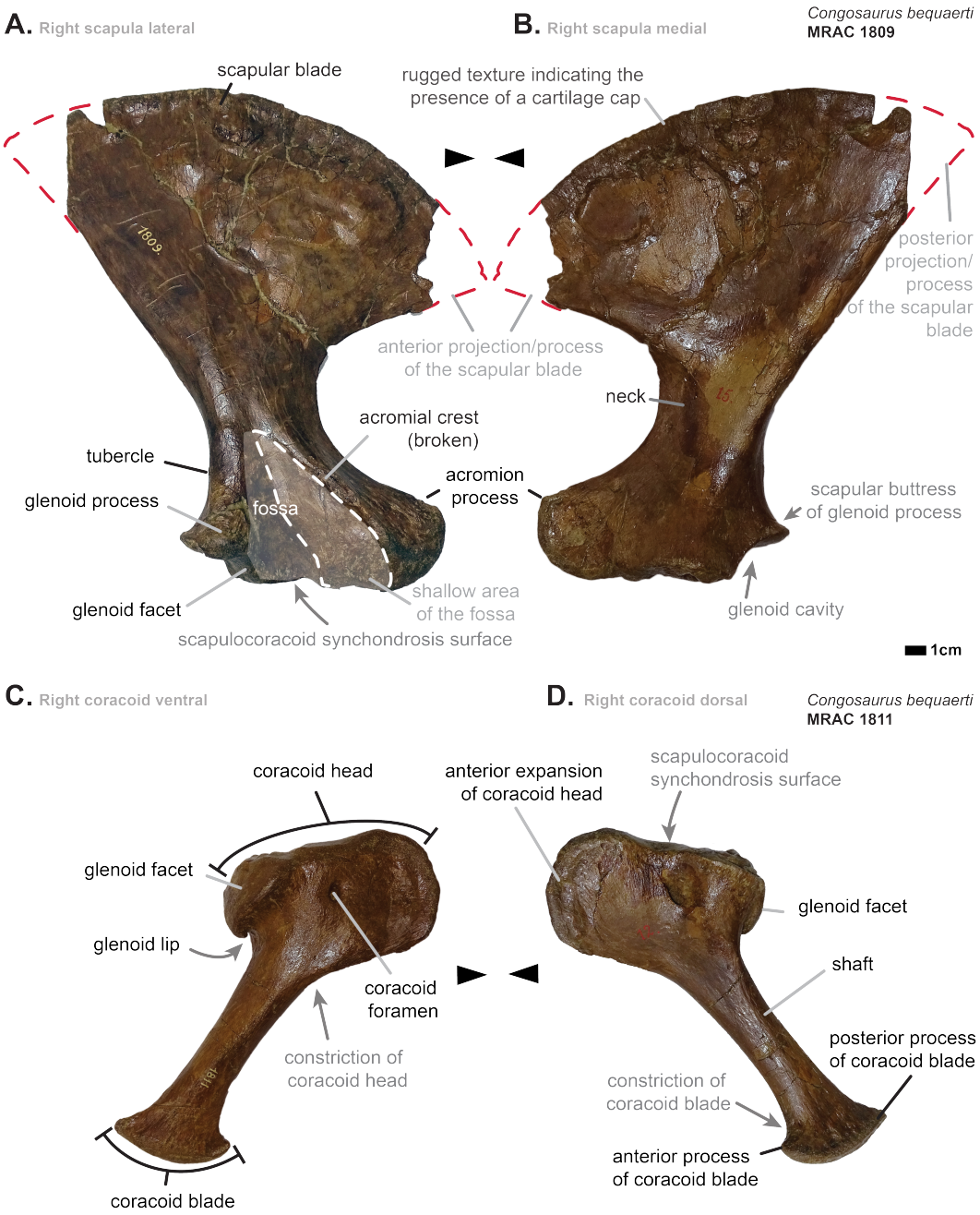


FIGURE 71. Pectoral girdle of *Congosaurus bequaerti* MRAC 1809 (A&B) and MRAC 1811 (C&D) (photographs). **A.** Right scapula in lateral view ; **B.** Right scapula in medial view ; **C.** Right coracoid in ventral view ; **D.** Right coracoid in dorsal view. Arrow points anteriorly. Red dashed lines indicate missing parts. Reconstruction of missing parts based on *Hyposaurus natator* NJSM 23368.

scapulocoracoid synchondrosis surface) and medial margin of the proximal head are parallel throughout until the glenoid process, which results in an overall constant mediolateral thickness. Also, another feature adding to the sub-quadrangular appearance of the proximal head is the shape and short projection of its anterior margin. The latter is semi-circular and relatively symmetrical and does not taper anteriorly, as in *H. natator* and *Dy. maghribensis* (unlike extant crocodylians and thalattosuchians). As a result, the expansion of the proximal head anteriorly to the scapulocoracoid synchondrosis surface – the anterior expansion of the proximal head – is anteroposteriorly short but mediolaterally thick. The junctions between the anterior margin of the coracoid head and the lateral and medial margins is achieved through smooth and rounded corners in *Co. bequaerti*, whereas the lateral corner is markedly angular in *H. natator*. The dorsoventral thickening of the coracoid head marks the start of the glenoid process.

As in other dyrosaurids, the scapulocoracoid synchondrosis surface of the coracoid of *Co. bequaerti* is proportionally large as it extends nearly over the entire anteroposterior length of the proximal head. Anteriorly, the tip of the scapulocoracoid synchondrosis surface forms a blunt corner which also marks the base of the curvature of the semicircular anterior margin of the proximal head. In comparison, the tip of the scapulocoracoid synchondrosis surface of the coracoid of *H. natator* forms a prominent corner. As in other dyrosaurids, the outline of the scapulocoracoid synchondrosis surface is complex and almost resembles a tadpole: it is composed of an undulated and dorsoventrally thin blade anteriorly, and a bulky oval portion posteriorly whose surface is markedly scarred (belonging to the glenoid process). Comparatively, in *H. natator* and *Dy. maghribensis* the difference in thickness and shape between the two sections is lesser. In *Co. bequaerti* the junction between the anterior blade-like portion and posterior oval part (belonging to the glenoid process) is marked by a dorsoventral constriction as well as the smoothening of the articular surface anteriorly. In comparison, the same junction is indicated by a strong ventral indentation in *H. natator*, whereas the entire scapulocoracoid synchondrosis surface does not show any change in surface texture. The oval posterior section of the scapulocoracoid synchondrosis surface constitutes the dorsoventrally thickest portion of the coracoid: it corresponds to the glenoid process which also bears the glenoid facet posteroventrally. The remainder of the proximal head of the coracoid of *Co. bequaerti* is markedly thinner dorsoventrally, and becomes finer toward the anterior margin of the bone. The coracoid foramen of *Co. bequaerti* forms a tilted canal not perpendicular to the dorsal and ventral surfaces of the proximal head, as in other dyrosaurids. Dorsally, the aperture of the foramen is wider and deeper than ventrally, and is also located closer to the glenoid-bearing area of the coracoid similar to other dyrosaurids.

In *Co. bequaerti*, the articular facet of the glenoid is ovoid in shape and is longer mediolaterally than dorsoventrally similar to *Dy. maghribensis*, but differing from the more circular one of *H. natator*. The articular facet of the glenoid of the coracoid of *Co. bequaerti* possesses a thick margin bordering it as in other dyrosaurids, and is subtly convex over three-quarters of its surface (which contrasts with the concave one of *H. natator*). Medially, the last quarter of the articular facet of the glenoid of the coracoid of *Co. bequaerti* is markedly recurved towards the anterior side of the bone, so that its apex is perpendicularly positioned in relation to the rest of the surface. This recurved area forms the glenoid lip. As in other dyrosaurids and extant crocodylians, the glenoid lip of the coracoid of *Co. bequaerti* possesses an underlying curved buttress which prevents the connection between the rim of the glenoid lip and the shaft of the coracoid. As mentioned above, dorsally to the articular facet of the glenoid lies the portion of the glenoid process involved in the scapulocoracoid synchondrosis. In *Co. bequaerti* the junction between the two is smooth and almost forms a right-angle corner, whereas in *H. natator* this junction forms a marked bulge emphasizing the concave appearance of the underlying articular facet of the glenoid.

As in other crocodyliforms, the shaft of the coracoid of *Co. bequaerti* extends from the medial margin of the coracoid head and leads to the distal blade medially. In *Co. bequaerti* the junction between the medial margin of the coracoid head and the shaft forms a marked obtuse angle, whereas this junction is

smoother and almost planar in *H. natator*. In *Dy. maghribensis*, the junction appears to form an angle similar to *Co. bequaerti*. In addition, the anchoring point of the shaft of the coracoid of *Co. bequaerti* on the coracoid head is located on the same level as the base of the glenoid process: the distance from the anterior tip of the coracoid head to the base of the shaft on the medial margin is similar to that from the anterior tip of the coracoid head to the base of the glenoid process on the lateral margin. Similar to other dyrosaurids, the shaft of the coracoid of *Co. bequaerti* is long and rod-like with its anterior and posterior margins being parallel throughout (it accounts for around 56% of the total length of the bone). The shaft of the coracoid is also ventrally curved and drastically decreases in dorsoventral thickness directly after its mid-length medially. The dorsal surface of the shaft of the coracoid is smooth whereas the ventral surface shows the presence of a shallow ridge uniting the anterolateral and posteromedial base of the shaft of the coracoid. This ridge intercepts the centre of the shaft of the coracoid at its maximal dorsoventral thickness before its reduction. In comparison, the ventral surface of the shaft of the coracoid of *H. natator* possesses an even less prominent ridge ventrally, but still displays a relatively angular ventral surface whereas the dorsal surface of the shaft of the coracoid remains smooth. Furthermore, the shaft of the coracoid of *Co. bequaerti* presents a torsion medially which tilts the distal blade posteriorly in relation to the longest axis of the section of the shaft of the coracoid (which is anteroposteriorly oriented), as in *H. natator*. In this way, the distal blade presents an inclination which is overall parallel to that of the scapulocoracoid synchondrosis surface.

The rod-like and elongated appearance of the shaft of the coracoid of *Co. bequaerti* also results in a more localised distal flaring (*i.e.* widening occurring over a short distance) to form the coracoid blade, differing from extant crocodylians and thalattosuchians. The intensity of the distal flaring of the shaft of the coracoid of *Co. bequaerti* is also relatively minor (only expands by two-and-a-half of its width) and leads to a proportionally short coracoid blade (which reaches around half of the anteroposterior length of the coracoid head), as in other dyrosaurids. However, the coracoid blade of *Co. bequaerti* is proportionally larger than in *H. natator*. The coracoid blade of *Co. bequaerti* is shaped like an axehead: its distal margin is slightly convex and its extremities form two sharp and acute corners, similar to *H. natator* and presumably *Dy. maghribensis*. In comparison, the distal blade of the coracoid of thalattosuchians and extant crocodylians is also fan-shaped, but only the former present acute and sharp corners at both extremities. The dorsoventral thickness of the coracoid blade of *Co. bequaerti* is relatively constant, with a slight increase towards the posterior corner. Comparatively, the dorsoventral thickness of the coracoid blade of *H. natator* is proportionally larger than in *Co. bequaerti*, which displays a slender blade. The articular facet of the coracoid blade of *Co. bequaerti* is markedly scarred throughout its length, as in *H. natator*. In anterior and posterior views, the articular facet of the coracoid blade of *Co. bequaerti* is perpendicular to the longest axis of the shaft of the coracoid and also appears relatively centered, which differs from *H. natator* in which the coracoid blade is more dorsally expanded. The rim of the articular facet of the coracoid blade forms a slight bulge (which is of greater intensity dorsally) and is hence easily observable. Unlike the dorsal rim, the ventral rim of the articular facet of the coracoid blade of *Co. bequaerti* does not follow the outline of the bone. Instead, it is ventrally deflected and almost divides the ventral surface of the coracoid blade in half, as in *H. natator*.

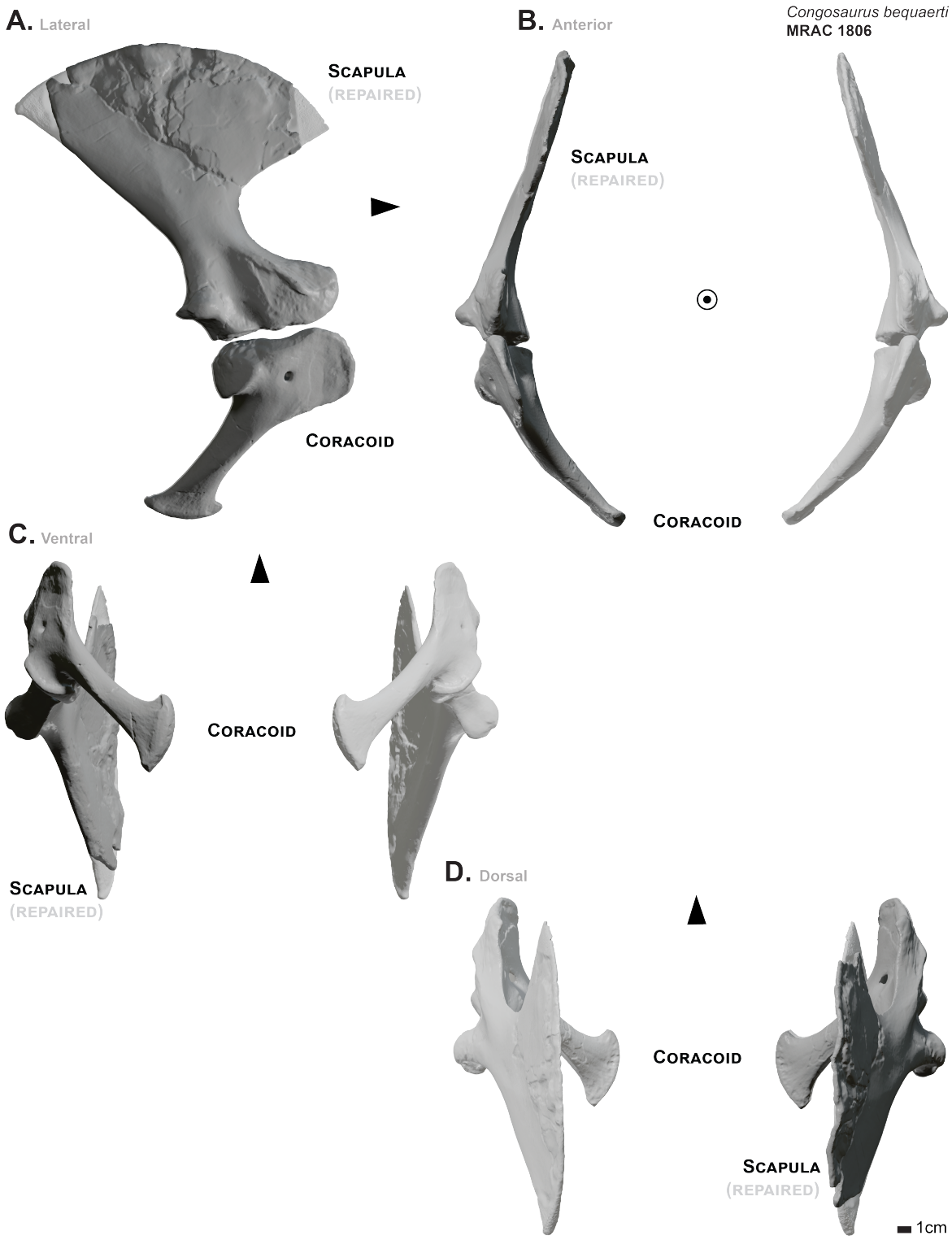


FIGURE 72. Reconstruction of the pectoral girdle of *Congosaurus bequaerti* MRAC 1809 (A&B) and MRAC 1811 (3D models). **A.** Lateral view; **B.** Anterior view; **C.** Ventral view; **D.** Dorsal view. Arrow points anteriorly. Target indicates anterior. The left scapula and coracoid are mirrored. Reconstruction of missing parts based on *Hyposaurus natator* NJSM 23368.

10. RESULTS

10.1. **Myology.** Muscle architecture is a general term encompassing the concepts of muscle fascicle length (which dictate working range), muscle fascicle cross-section (which determine force-exerting capacity) and muscle mass. The latter represents muscle work and power as it corresponds to the inverse relation of the two first concepts. Crocodylidae have longer muscle fascicles but smaller muscle physiological cross-sectional area than Alligatoridae. Longer fascicles mean increased working range whereas larger cross sectional area means higher force-exerting capacity. The use of asymmetrical gait in extant crocodylians appears intertwined with the ability to rapidly produce movement of the thoracic limbs rather than exert large limb forces (Allen et al., 2014).

As noted above, the strong disparity in size, shape and relative orientation of pectoral girdle elements (and also the humerus; see Scavezzoni and Fischer (2023)) within Metriorhynchoidea and Teleosauroidea, and between Thalattosuchia, Dyrosauridae and Crocodylia impacts the position, size of insertions and origins and overall geometry of the musculature. The angles between muscles, and hence muscle work and power and locomotor abilities. The latter can only be determined through biomechanical reconstructions including the whole limb.

However, precise estimation of muscle work and power are complicated by the fact that most muscles connecting to the pectoral girdle of extant crocodylians lack clear-cut osteological correlates (Otero et al., 2017), so that the distribution and outlines of muscle insertions and origins in our reconstructions of dyrosaurids and thalattosuchians should be seen as qualitative appearance (see fig. 73), and a thorough base for future biomechanical endeavours.

In extant crocodylians, the scapulocoracoid synchondrosis surface accounts for almost the totality of the anteroposterior extension of the coracoid head as the scapula bears a large proximal portion. In most teleosauroids and metriorhynchids, the scapulocoracoid synchondrosis surface is reduced, due to a shortened proximal region of the scapula. Nevertheless, the coracoid head remains large and mirrors the coracoid blade; this likely resulted in a relative extension of the area of origin of shoulder extensors (*m. supracoracoideus* complex see tables 4 and 5), which help increase the angle between the limb and trunk. The large extremities of the coracoid are retained throughout Thalattosuchia, although humeral shape and size greatly varies (Scavezzoni and Fischer, 2023), contrasting with the integrated pair it forms within Crocodylia (Chamero et al., 2013).

Several relatively basal metriorhynchids (excluding *Tyrannoneustes*) are unique in displaying an open coracoid foramen (*e.g. Thalattosuchus*, *G. leedsi*, *'Me.' brachyrhynchus* NHMUK PV R 4696, *Tyrannoneustes*). This feature, presumably lost in more derived metriorhynchids, enlarges the size of the coracoid foramen and separates the coracoid head into two distinct portions. This feature appears associated with a relatively slender scapula and humerus (although reduced in size). This implies a distinct distribution of muscle origins and insertions in concerned taxa, notably shortening the medial/dorsal origin of the shoulder extensor (*m. supracoracoideus longus*) to the immediate surroundings of the acromion process of the scapula, rather than extending over the coracoidal perforation to reach the tip of the anterior expansion of the coracoid head.

In dyrosaurids, the reduced coracoid blade likely decreased the overall breadth of the origin of the shoulder and limb adductor *m. coracobrachialis brevis ventralis*. However, the long and rod-like shaft of the coracoid possibly resulted in proportionably more elongated origin of *m. coracobrachialis brevis ventralis* as well as the extensor of the girdle (*m. costocoracoideus* complex see tables 4 and 5). In comparison, the relatively broad coracoid head would have offered additional space for shoulder extensors (*m. supracoracoideus* complex) as well as *m. omohyoideus* (allowing the retraction of the hyoid).

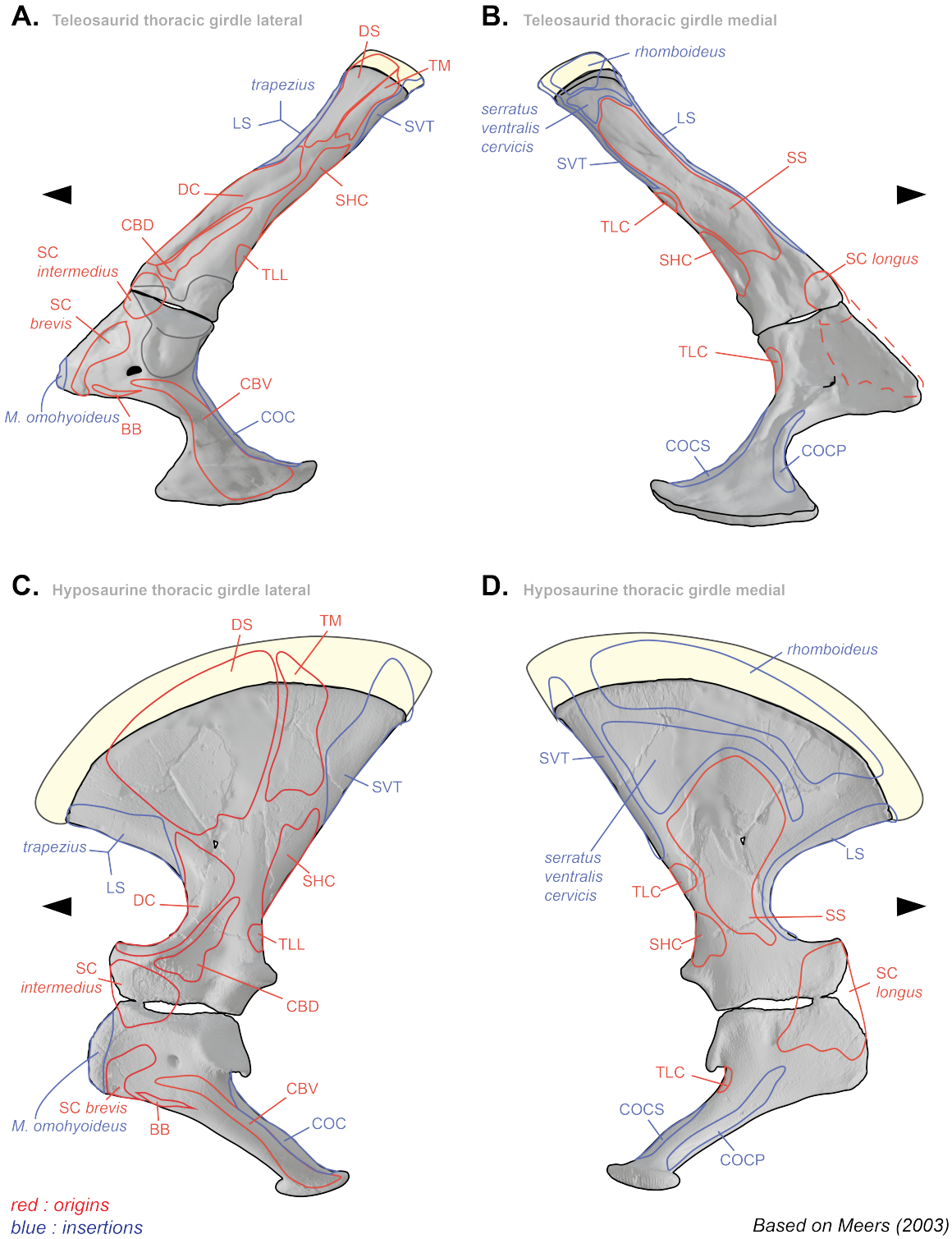


FIGURE 73. Schematic representation of the pectoral girdle with approximated distribution of muscles origins and insertions based on Meers (2003). **A.** Teleosauroid pectoral girdle in lateral view; **B.** Teleosauroid pectoral girdle in medial view; **C.** Dyrosaurid pectoral girdle in lateral view; **D.** Dyrosaurid pectoral girdle in medial view. Arrow points anteriorly. Cartilaginous structures represented in yellow. Muscles origins are colored in red; muscles insertions are colored in blue. As most muscles involved in the pectoral girdle of extant crocodylians lack clear osteological correlates (Otero et al., 2017), these reconstructions only bear a qualitative appearance. See tables 4 and 5 for abbreviation and definition.

Unlike in extant crocodylians, the anterior margin of the scapula of hyposaurine dyrosaurids is markedly concave, which strongly impacts the geometry and line of action of the muscles *m. levator scapulae* and *m. trapezius*, involved in pectoral girdle rotation, neck abduction, and forelimb protraction. The large and fan-like scapular blade of dyrosaurids, and especially in hyposaurines, certainly permitted extended surfaces for muscle origins and insertions which lies on the lateral and medial surfaces of the scapula in extant crocodylians. Those enlarged muscle areas would include the origins for the shoulder abductor and flexor (*e.g. m. deltoideus scapularis*, *m. teres major*) and for the shoulder extensor (and shoulder stabiliser) *m. subscapularis*. It would also encompass the muscle insertions for *serratus ventralis thoracis* (pectoral girdle extensor) and *rhomboideus* (pectoral girdle adductor, elevator and stabilizer) (see table 5). Those differences likely resulted in powerful limbs, supporting previous assumptions (Jouve et al., 2006; Langston, 1995; Schwarz-Wings et al., 2009; Troxell, 1925).

10.2. **Phylogeny.** The phylogenetic analyses of our different datasets bear significant differences (see figs. 74 to 76 and see supplementary information 'SUPP INF' 3 to 5). Crocodylia does not retain the same topology throughout the various analyses, due to gavialids forming a polytomy with other longirostrine taxa in our analyses centered on cranial data. Intraclade relationships are not resolved for Dyrosauroidae in both isolated cranial and postcranial datasets due to the scarcity of scorable material. Thalattosuchia is exploded in our analyses centered on cranial data but shows more resolved affinities in our postcranial results (see Johnson et al. (2020); Sachs et al. (2021); Young et al. (2020a, 2024) for most recent comparisons). In our combined dataset, the three clades as distinct from one-another, but Thalattosuchia shows less resolution in Equal Weighting (EW) compared to Implied Weighting (IW) (see fig. 76 and see supplementary information 'SUPP INF 4').

Indeed, in both IW and EW, the cranial dataset fails to recover the three clades – Thalattosuchia, Dyrosauroidae, and Crocodylia – which form a polytomy (see supplementary information 'SUPP INF 3' and fig. 74). The base of the polytomy encompasses teleosauroid taxa, basal metriorhynchoids with the basal thalattosuchian *Turnersuchus*, dyrosauroids and gavialids. Metriorhynchids and remaining crocodylians form two distinct branched groups also rooted on the polytomy. Most crocodylian affinities (see Pan et al. (2021); Rio and Mannion (2021)) are recovered although *Mecistops* taxa are found outside of Crocodylidae. Metriorhynchid subfamilies (Metriorhynchiinae and Geosaurinae) are almost accurately recovered (see Sachs et al. (2021); Young et al. (2020a, 2024)), but with minor exceptions: rhacheosaurine taxa form a polytomy, *Thalattosuchus* is found as a basal geosaurine, and Geosaurini is constituted of two main branches instead of three (*Torvoneustes* and *Geosaurus –Dakosaurus* merged).

In comparison, the postcranial dataset (see fig. 75 and see supplementary information 'SUPP INF 5') displays a better resolution than the cranium in both EW and IW analyses, as it recovers the three clades as distinct from one-another. In both EW and IW analyses, Crocodylia and Dyrosauroidea bear the same topology but not Thalattosuchia. The intraclade relationships within Dyrosauroidae are unresolved and *Elosuchus cherifiensis* is found outside, on the same node as Dyrosauroidea and Crocodylia. The usual relationships of Crocodylia are not recovered (see Pan et al. (2021); Rio and Mannion (2021)): Gavialidae is split with *Gavialis* and *Tomistoma* successively recovered as the most basal taxa, Crocodylidae forms a polytomy, and *Mecistops* taxa are found as a sister clade to Alligatoridae. In EW, Thalattosuchia forms a massive polytomy but with racheosaurines and teleosaurines forming two distinct clusters. In IW, *Plagiophthalmosuchus gracilirostris*, *Macrospondylus*, *Turnersuchus* and teleosaurines (*Te. cadomensis* and *Platysuchus* in Johnson et al. (2020); Young et al. (2024)) form a polytomy at the base of Thalattosuchia, and are thus recovered as sister-taxa to Teleosauroidea and Metriorhynchoidea. In comparison, *Plagiophthalmosuchus gracilirostris* is a basal thalattosuchian outside Metriorhynchoidea and Teleosauroidea in Young et al. (2024), but is previously a basal-most teleosauroid (Johnson et al., 2020; Wilberg et al., 2023). The basal position of *Turnersuchus* within Thalattosuchia is preserved (Wilberg et al., 2023;

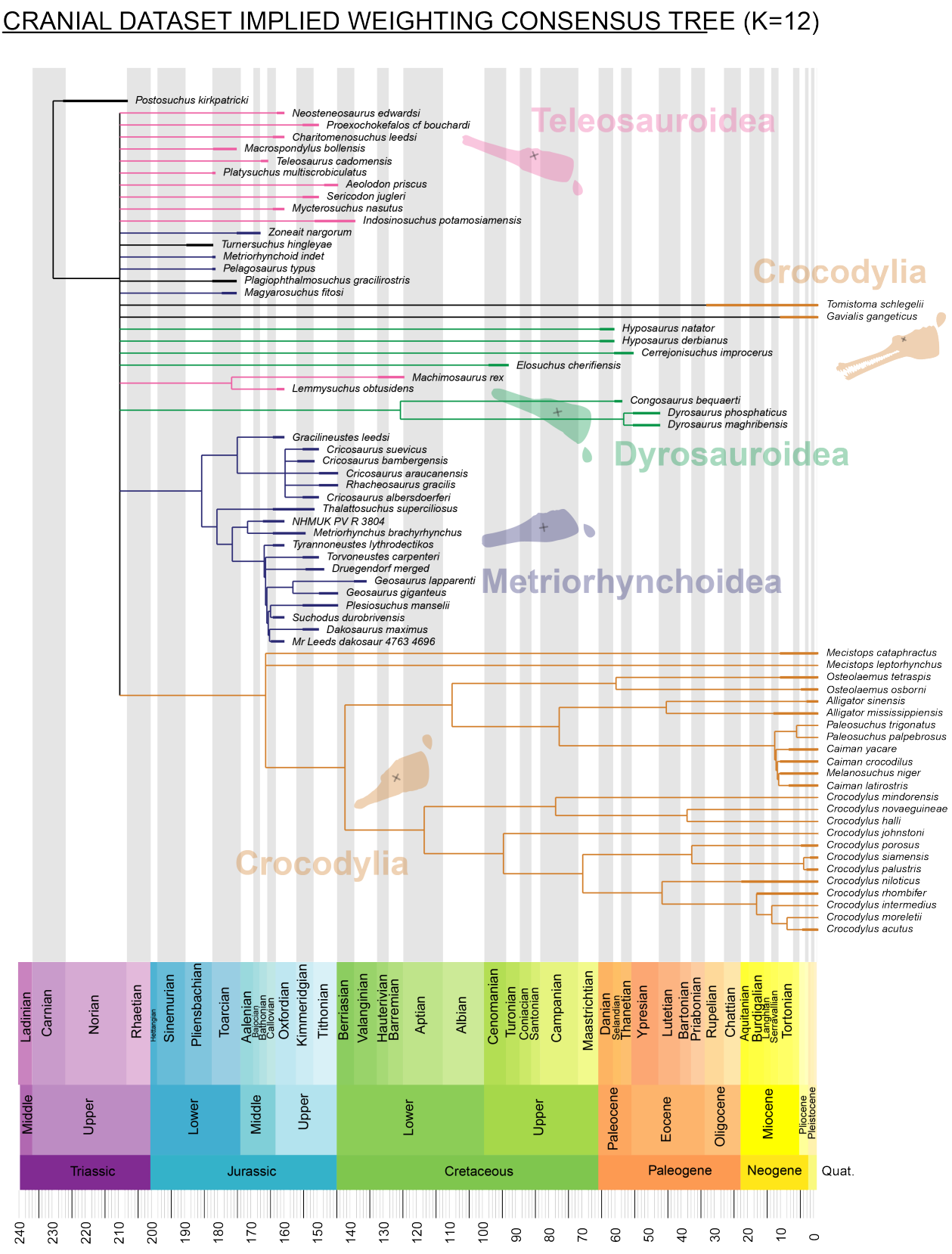


FIGURE 74. Implied weighting (k=12) consensus tree of our cranial dataset. Crocodylomorphs silhouettes: Metriorhynchoidea and Teleosauroidea (c) Gareth Monger – Licence CC BY 3.0; Dyrosauridae (c) Nobu Tamura, vectorized by Zimices – Licence CC BY-SA 3.0; Crocodylia original picture (c) Thesupermart – License CC BY-SA 3.0; Gharial – License CC0 1.0 Universal Public Domain Dedication.

POSTCRANIAL DATASET IMPLIED WEIGHTING CONSENSUS TREE (K=12)

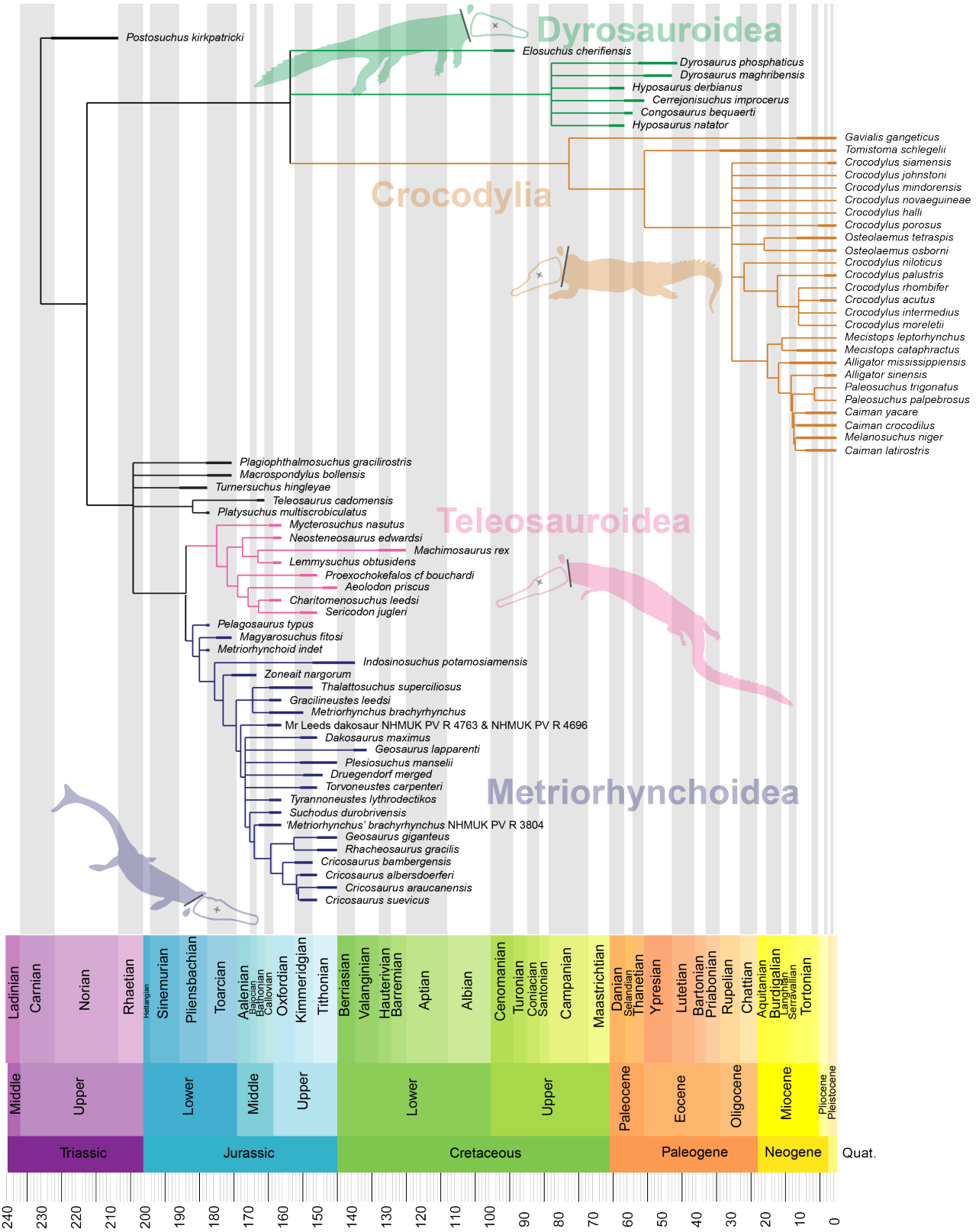


FIGURE 75. Implied weighting (k=12) consensus tree of our postcranial dataset. Crocodylomorphs silhouettes: Metriorhynchoidea and Teleosauroidea (c) Gareth Monger – Licence CC BY 3.0; Dyrosauridae (c) Nobu Tamura, vectorized by Zimices – Licence CC BY-SA 3.0; Crocodylia original picture (c) Thesupermart – License CC BY-SA 3.0.

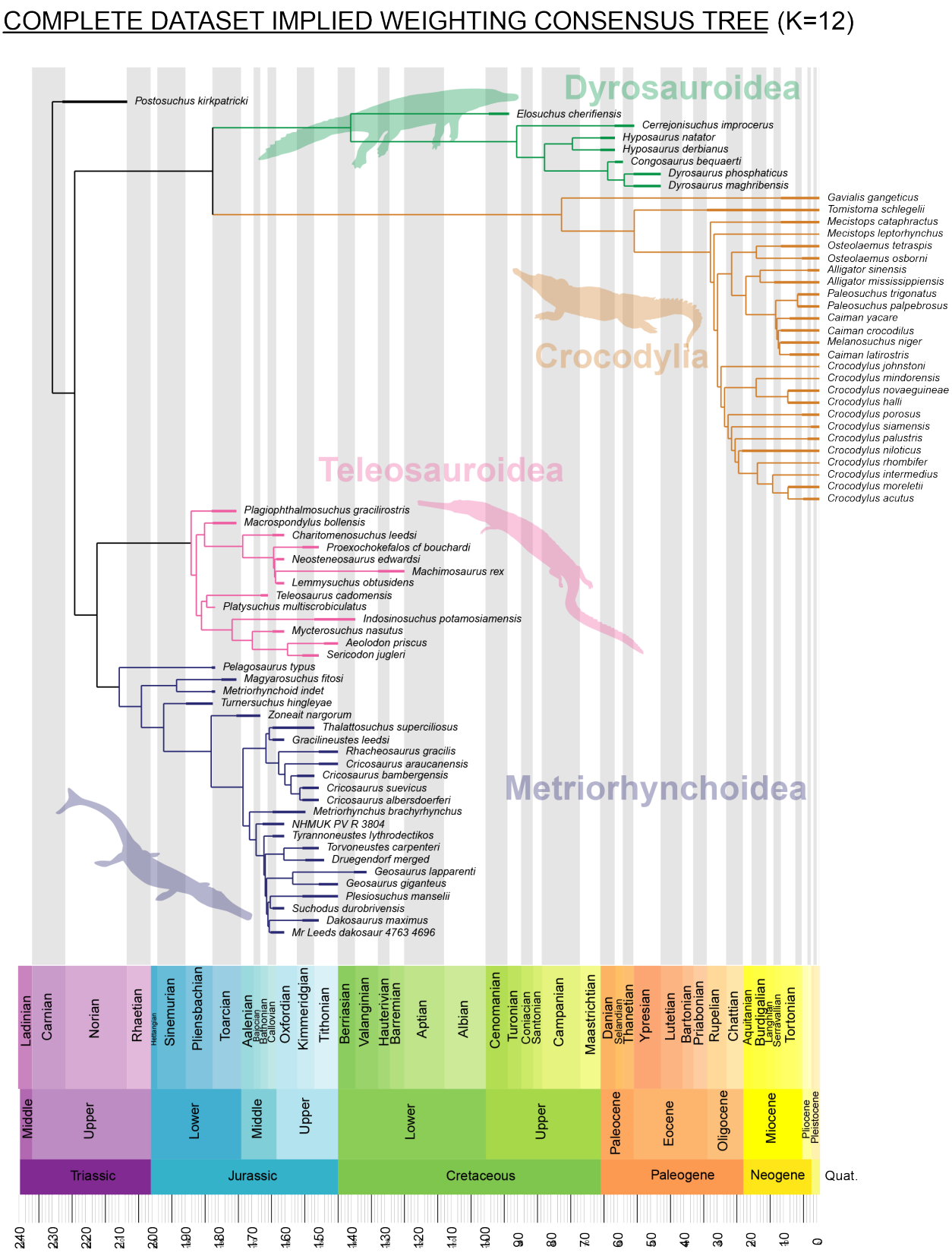


FIGURE 76. Implied weighting (k=12) consensus tree of our complete dataset (cranial and postcranial merged). Crocodylomorphs silhouettes: Metriorhynchoidea and Teleosauroidea (c) Gareth Monger – Licence CC BY 3.0; Dyrosauridae (c) Nobu Tamura, vectorized by Zimices – Licence CC BY-SA 3.0; Crocodylia original picture (c) Thesupermart – License CC BY-SA 3.0.

Young et al., 2024), but *Macrospondylus* is usually present at the base of Machimosauridae (Johnson et al., 2020; Young et al., 2024). In our analysis, Teleosauroidea possesses *Mycterosuchus* at its base and then branches into two subgroups: a mixed-up group of aeolodontines (*Aeolodon–Sericodon*) and basal machimosaurids (*Proexochokefalos* cf. *bouchardi –Charitomenosuchus*); and a subsample of derived machimosaurids (*Neosteneosaurus, Lemmysuchus* and *Machimosaurus*; see Johnson et al. (2020); Wilberg et al. (2023); Young et al. (2024)).

Similar to most recent phylogenetic analyses, the taxa *Pelagosaurus*, *Magyarosuchus* and *Zoneait nargorum* are recovered outside of Metriorhynchidae, with *Pelagosaurus* still occupying the basal-most position (Young et al., 2020a, 2024). However, the freshwater teleosaurid *Ind. potamosiamensis* (Martin et al., 2019b) is also nested among basal metriohynchoids unlike in Johnson et al. (2020); Martin et al. (2019b); Young et al. (2024). Furthermore, the usual taxonomic content of metriorhynchid subfamilies is altered in our results and forms two new main branches. The first one comprises the basal metriorhynchids *Thalattosuchus* and *Gracilineustes leedsi* along with *'Me.' brachyrhynchus* (previously a basal geosaurine; Young et al. (2020a, 2024)) which cluster to form a clade sister to all other derived metriorhynchids. The second branch mainly comprises a reworking of geosaurine taxa with rhacheosaurines (Sachs et al., 2021; Young et al., 2020a, 2024) positioned as the new most derived geosaurine subclade. Usual Geosaurini branches (*i.e.: Torvoneustes–Dakosaurus–Geosaurus*; (Sachs et al., 2021; Young et al., 2020a, 2024)) are split and mainly form a polytomy at the base of the new most derived geosaurine subclade. The latter is constituted of *Suchodus durobrivensis* (Sachs et al., 2021; Young et al., 2020a, 2024) and *'Me.' brachyrhynchus* NHMUK PV R 3804 at its base, followed by a dichotomy: *Rhacheosaurus* and *Ge. giganteus* are found as sister taxa to all *Cricosaurus* species Sachs et al. (2021); Young et al. (2020a, 2024)).

In the IW analysis of our combined dataset (see fig. 76), dyrosauroid affinities are resolved and similar to results from Jouve et al. (2021). The intraclade relationships within Metriorhynchoidea and Teleosauroidea are analogous to results from recent phylogenetic analyses of Thalattosuchia Johnson et al. (2020); Sachs et al. (2021); Young et al. (2020a, 2024). Notably, compared to the IW result of our postcranial dataset, *Ind. potamosiamensis* is nested among teleosaurids like in Johnson et al. (2020); Martin et al. (2019b); Young et al. (2024). Within Metriorhynchoidea, major differences concern *Tyrannoneustes* and *Turnersuchus*. The former is found just outside of Geosaurini along with *'Metriorhynchus'* unlike in (Young et al., 2020a, 2024), and *Turnersuchus* is not recovered as a basal thalattosuchian unlike in (Wilberg et al., 2023), but is closer to *Zoneait*.

11. Discussion

11.1. **A range of shapes and movements.** Few recent studies have looked into the functional morphology of the postcranium of Thalattosuchia (Hua and De Buffrenil, 1996; Molnar et al., 2015) and Dyrosauridae (Schwarz-Wings et al., 2009), or both (Hua, 2003), to infer biomechanical implications and possible locomotor modes. However, those works have mainly focused their attention on the flexibility of the trunk as a whole, through the investigation of the range of motion of the axial skeleton – including osteoderms if any – (Hua, 2003; Molnar et al., 2015; Schwarz et al., 2006; Schwarz-Wings et al., 2009), and also theoretical muscle mass reconstructions (Schwarz et al., 2006; Schwarz-Wings et al., 2009). Despite a rich morphological disparity (Scavezzoni and Fischer, 2023) conveying major differences in locomotor capabilities across Thalattosuchia and Dyrosauridae, the functional morphology of the pectoral girdle and forelimb of those clades remains to be fully investigated.

The shoulder girdle of extant crocodylians displays a relatively important mobility. Indeed, only 70% of the complete (fore-and-aft) limb excursion – or stride length – of a walking American alligator is complete by limb joints (Baier et al., 2018); the rest is driven by movements pectoral girdle (about 20%) and flexion of the axial skeleton (about 10%) (Baier and Gatesy, 2013; Baier et al., 2018). About half of the movement of the pectoral girdle is permitted by rotation of the sternum and the other half by motion of

the sternocoracoid joint (Baier et al., 2018), where the coracoids rotate independently (Baier and Gatesy, 2013; Baier et al., 2018). At the beginning of the stride stance of the high-walk in *Alligator mississippiensis*, the coracoid is positioned anteriorly and the scapula is tilted posteriorly. During the stance phase of a single stride, the coracosternal joint slides posteriorly of about half its total anteroposterior width, then rotates so that the scapula is more vertically oriented and abducted. As a result, the glenoid facet – which faces posteriorly in extant crocodylians – is moved more posteriorly and vertically. In *Alligator mississippiensis*, the total rotation of the glenoid facet averages 18% of the anteroposterior width of the humeral head (Baier and Gatesy, 2013), yet the total motion of the glenoid is limited by muscles anchoring the scapula to the thorax (Baier et al., 2018). Both the translation of the coracoid along the coracosternal joint and the flexion of the axial skeleton are presumably plesiomorphic features of archosaurians (or even diapsids; Baier and Gatesy (2013); Gray (1968)), and the vertebral flexure as well as humeral sliding at the glenoid are likely ancestral archosaurian traits (Baier and Gatesy, 2013). Given the global structural similarity of pectoral girdles in thalattosuchians, dyrosaurids, and crocodylians, it is safe to assume that extinct clades started their evolutionary histories with the same kind of intragirdle mobility.

The scapula and coracoid of extant crocodylians form a stiff mass with no individual motion during locomotion called the scapulocoracoid (Baier and Gatesy, 2013; Baier et al., 2018). The intertwined suture seen on the scapulocoracoid synchondrosis surface of the scapula and coracoid of *H. natator*, reveals that the pectoral girdle of dyrosaurids likely formed a tight synostosis in mature individuals. However, in most thalattosuchians, the scapulocoracoid synchondrosis is less ossified than in mature crocodylians (Brochu, 1992, 1995), with rough but usually mismatched surfaces and therefore extensive cartilage caps, which may have offered additional flexibility. It is readily observed in most metriorhynchids (which could not possibly perform terrestrial locomotion) and also in aquatic teleosauroids (*i.e.* those lacking an elongated and slender humerus and a large scapula). Nevertheless, complete kinematics remain to be tested to determine the full range of motion of the forelimb, as well as the possible postures (*i.e.* locomotive types) and different joint contributions (*i.e.* relative but also absolute) during each stride stance phase for terrestrial locomotion.

It appears indisputable from our extensive survey that the reconstruction of the pectoral girdle of fossil thalattosuchians and dyrosaurids strongly differs, notably in terms of relative spacing and inclination between the coracoids and the sternum and the scapula–coracoid angle, leading to several possible angular relations of the girdle as a whole. As a result, the scapula often presents several plausible positions from more upright to relatively more posteriorly plunging or from strictly laterally facing to anterolaterally oriented, which, in turn, creates a more or less constricted area for the thoracic region. In parallel, the scapula of extant crocodylians is under constant mediolateral twist *in vivo*, inevitably resulting in inconsistent orientations in osteological reconstructions (Baier et al., 2018). Caution is therefore needed when orienting or drawing the pectoral girdle in extinct crocodylomorphs.

An important feature distinguishing thalattosuchians from dyrosaurids is the glenoid facet. At first glance, the glenoid facet of dyrosaurids (*e.g. Anthracosuchus* UF/IGM 68, *H. natator* NJSM 23368 & YPM VP.000985, *Dy. maghribensis* OCP DEK-GE 252 & OCP DEK-GE 254, *Co. bequaerti* MRAC 1809) appears similar to that of extant crocodylians (*e.g. Palaeosuchus palpebrosus* RVC-JRH-PP1, *Mecistops cataphractus* RBINS 18374, *Caiman crocodylus* NMW 30900, etc.), however its is facing slightly more posteriorly. In addition, the surface of the scapular glenoid facet of dyrosaurids shows a stronger concavity than extant crocodylians, which creates in a medially deeper glenoid cavity. As a result, the glenoid cavity possesses a marked dorsal overhang which culminates into a thick and prominent lip. The strongly concave shape of the scapular glenoid facet of dyrosaurids mirrors the prominent and bulbous shape of the dorsal capitular tuberosity of their humerus. In parallel, it is possible that this configuration hampered dorsal excursion of the humerus, reducing its overall flexibility compared to extant

crocodylians. A similarly shaped and positioned glenoid facet is found in several terrestrial mesoeucrocodylians *Araripesuchus tsangatsangana* Turner, 2006 (Turner, 2006), *Burkesuchus mallingrandensis* Novas et al., 2021 (Novas et al., 2021), *Mahajangasuchus insignis* Buckley and Brochu, 1999 (Buckley and Brochu, 1999), *Simosuchus clarki* Buckley et al., 2000 (Sertich and Groenke, 2010), *Yacarerani boliviensis* Novas et al., 2009 (Leardi et al., 2015), and also in the potentially cursorial baurusuchids *Baurusuchus albertoi* Nascimento and Zaher, 2010 (Nascimento and Zaher, 2010) as well as in *Notosuchus terrestris* Woodward, 1896 (Pol, 2005). The more terrestrial teleosauroid *Platysuchus* SMNS 9930 also possesses a similarly shaped and positioned glenoid facet and hence departs from other members of the clade.

In comparison, the size and overall position of the glenoid facet shows an even greater variability within Thalattosuchia. In teleosauroids, the glenoid facet invariably displays a relatively large surface, noticeably concave on the scapula and weakly concave on the coracoid, which is most similar to extant crocodylians, especially compared to metriorhynchoids and dyrosaurids. However, the relative position of the scapular glenoid facet changes back-and-forth several times throughout the clade between posterior (*e.g. Te. cadomensis* NHMUK PV OR 31836, *Platysuchus* SMNS 9930, *Neosteneosaurus* NHMUK PV R 3701, *Machimosaurus* spp.) and lateral (*e.g. Mycterosuchus* NHMUK PV R 2617, *Macrospondylus* SMNS 9428, *Charitomenosuchus* NHMUK PV R 3806, *Lemmysuchus* NHMUK PV R 3168). These switches in position appear to be independent from the overall modifications undergone by the scapula, coracoid or humerus, which each seem to pursue different trends (Scavezzoni and Fischer, 2023). These complex sets of morphological modifications presumably reflect habitat preferences, with possibly several distinct combinations of characters leading to similar locomotive capabilities or mechanical advantages.

In basal members of Thalattosuchia (see figs. 77 and 78; Johnson et al. (2020); Young et al. (2020a, 2024)), the relative dimensions of the glenoid facet on both the scapula and coracoid is small (*e.g. Turnersuchus* LRM 2021/45, *Pelagosaurus* BRLSI M.1418 & BRLSI M.3578, *Magyarosuchus* (Ősi et al., 2018), *G. leedsi* NHMUK PV R 3014 & NHMUK PV R 3015) and increases in size in more derived metriorhynchids (*e.g. D. maximus* SMNS 8203, *Cricosaurus* species, *Ge. lapparenti* UJF-ID.11847j & UJF-ID.11852f), echoing the relative broadening (and shortening) of the humerus (Scavezzoni and Fischer, 2023). Also and as in dyrosaurids, the glenoid cavity of the basal thalattosuchian *Turnersuchus* LRM 2021/45 and metriorhynchoids faces more posteriorly than in extant crocodylians, possibly preventing the humerus from doing excessive dorsal movements. The glenoid facet in both the scapula and coracoid of the basal thalattosuchian *Turnersuchus* LRM 2021/45 and metriorhynchoids is relatively flat, strongly contrasting with extant crocodylians and dyrosaurids. The relatively straight appearance of the articular facets of the glenoid in metriorhynchoids is a reflection of the proximal surface of the humerus, which possesses flatter surfaces markedly less curved than in extant crocodylians and dyrosaurids. Although the relative position of the glenoid facet remains relatively constant throughout Metriorhynchoidea, the bones participating in that articulation strongly vary in size and shape, with more derived members generally showing shorter, stouter bones (Scavezzoni and Fischer, 2023). This greater disparity can possibly be seen as a release from the constraints of terrestrial walking in thalattosuchians (Herrera et al., 2009; Massare, 1988; Mazin, 1996; Wilberg, 2015a; Wilkinson et al., 2008).

11.2. **Phylogeny.** Despite being recently brought to light (Blanco, 2021; Godoy et al., 2016; Jouve and Jalil, 2020; Jouve et al., 2021; Martin et al., 2016, 2019b; Pol et al., 2012; Scavezzoni and Fischer, 2021, 2023; Scavezzoni et al., 2024), the rich morphological disparity of Crocodylomorpha is still globally obscured by a profusion of studies centered on cranial and dental anatomy, which is a complex issue stemming from historically-related lack of collected postcranial material as well as an overall neglect towards postcranial remains (Godoy et al., 2016; Martin et al., 2016; Mannion et al., 2019; Scavezzoni and Fischer, 2021, 2023). This habit is reflected in phylogenetic analyses of this group, which incorporate

ever-expanding datasets brimming with craniodental characters (usually above 70%) (Godoy et al., 2016; Martin et al., 2016; Mannion et al., 2019; Blanco, 2021), although the morphology of crocodylomorph skulls are notoriously malleable (Pierce et al., 2009) and subject to convergence (Young et al., 2010; Godoy et al., 2016; Martin et al., 2016; McCurry et al., 2017; Martin et al., 2019a; Young et al., 2020b; Stubbs et al., 2021).

Our phylogenetic analyses focused on postcranial characters manage to differentiate each clade – Crocodylia, Thalattosuchia and Dyrosauridae – from one another (see fig. 75) whereas our cranial-centered dataset fails to produce enough resolution (see fig. 74). Furthermore, it succeeds in recognizing the proportionally closer phylogenetic relationship existing between tethysuchians and eusuchians than with Thalattosuchia (see Larsson and Sues (2007); Montefeltro et al. (2013); Wilberg et al. (2019)). However, Dyrosauridae suffers from a lack of resolution which presumably reflects the incomplete state of several taxa (namely *Hyposaurus derbianus*, *Dyrosaurus phosphaticus* and *Cerrejonisuchus improcerus*; see also fig. 79 for comparison).

In addition, our phylogenetic analysis in implied weighting focused on postcranial characters retrieves the presence of two subfamilies within Thalattosuchia – Metriorhynchoidea and Teleosauroidea – yet with several finer taxa relationships reorganized compared with other results issued from cranial dominant datasets (*e.g.* see figs. 77 and 78 and Johnson et al. (2020); Sachs et al. (2021); Young et al. (2020a, 2024)). These rearrangements have noticeably clustered resembling morphologies and are undoubtedly exacerbated by the relative proportion of missing data (with strongly incomplete taxa clinging on any available data whether it is acute or superficial resemblance, homologous or homoplasic). These modifications convey the presence of several similar structures within each family, which were either inherited or convergently acquired. Such examples include the regrouping of more aquatic teleosauroids (*e.g. Sericodon jugleri*, *Aeolodon*, *Proexochokefalos* cf. *bouchardi* and *Charitomenosuchus*) which show a relatively slender scapula but a large coracoid head and blade, a proportionally shortened and twisted humerus but a relatively long femur, or an ilium with a proportionally small postacetabular process. *Macrospondylus* is fairly complete but not *Turnersuchus*, which shows a relatively wide scapular blade as well as a large scapulocoracoid synchondrosis surface on the coracoid just like *Macrospondylus*. The freshwater teleosauroid *Ind. potamosiamensis*, which is relatively incomplete, has a slender scapula, humerus and femur and hence is recovered near basal metriorhynchoids which superficially resemble teleosauroids. In Metriorhynchoidea, several taxa with an open coracoid foramen, slender scapula as well as a short but slender humerus (*e.g. 'Me.' brachyrhynchus*, *Thalattosuchus*, Mr Leed's dakosaur and *G. leedsi*) form the base Metriorhynchidae. *Tyrannoneustes*, which also has an open coracoid foramen has a less complete pectoral girdle, is found amongst the polytomy. In comparison, metriorhynchids with a closed coracoid foramen, as well as a short and broad scapula and humerus are placed amongst more derived members of Metriorhynchidea (*e.g. Ge. lapparenti*, *D. maximus*, *To. carpenteri*, and *Cricosaurus* species). The geosaurini subclades centered around *D. maximus* and *Ge. lapparenti* are not recovered in our analyses and form a polytomy. Both taxa possess a markedly broadened and shortened humerus and scapula although strongly dissimilar in shape. *Suchodus durobrivensis* and *'Me.' brachyrhynchus* NHMUK PV R 3804 both lack a pectoral girdle but show similarities in their pelvic girdle, and are found at the base of the new most derived geosaurine subclade. The position of *'Me.' brachyrhynchus* NHMUK PV R 3804 apart from other specimens referred to as *'Me.' brachyrhynchus* (*e.g.* notably NHMUK PV R 4763) reveals its marked distinction. The new most derived geosaurine subclade is mainly composed of rhacheosaurines and comprises taxa with a closed coracoid foramen as well as a reduced pubic symphysis. *Geosaurus giganteus* clusters with *Rhacheosaurus gracilis* possibly due to their reduced pubic symphysis and overall fragmentary state.

Overall, the relative height of the coracoid and scapula always remains the same throughout Thalattosuchia, so that when the scapula globally shortens so does the coracoid. Indeed, Thalattosuchia presents

several modifications of the shape of the scapula and humerus, but tends to preserve a large coracoid head and blade. Metriorhynchids almost invariably display a broad coracoid whereas it is more gracile in basal thalattosuchians (*Turnersuchus*) and metriorhynchoids (*Pelagosaurus*). In parallel, two subfamilies of metriorhynchids (metriorhynchines and geosaurines) appear to have developed an open coracoid foramen which is later closed in more derived members. Basal metriorhynchids present a rod-like scapula, which becomes markedly shorter and stouter in rhacheosaurines. In geosaurines, the scapula follows two trends: either stout and short like rhacheosaurines, or relatively more slender but with a proportionally large scapular blade. Teleosauroids tend to develop a more slender coracoid than metriorhynchoids (namely due to a longer coracoid shaft), with a markedly triangular anterior expansion of the coracoid head. Concerning the scapula, teleosauroids show two major trends, with more terrestrial taxa presenting an enlarged scapular blade and proximal region (but shorter anterior expansion of the coracoid head) and more aquatic taxa displaying a slender scapula (and proportionally longer anterior expansion of the coracoid head). In comparison, Dyrosauridae shows a major widening of the scapular blade, especially in derived members, but the coracoid shows a slender appearance with a shortened blade but wide head.

Young et al. (2024) – which have a heavily cranial dataset – have highlighted the difficulty to discern convergence from homology due to the existence of considerable traits highlighting clade specialization within Thalattosuchia and the subsequent absence of sufficient characters interconnecting them (=the clades). Our results reveal the high potential of postcranial characters in phylogenetic analyses of crocodylomorphs. However, those data are not aimed to be employed of their own (at the risk of falling into the same traps as cranium-dominated datasets) but should serve as a basis for future more comprehensive phylogenetic analyses. Hence, by creating a more comprehensive dataset (*i.e.* better balancing the proportion of postcranial and cranial characters, especially to avoid repurposed matrices), we believe that the influence missing data has in our current dataset will diminish, and also that homologies and homoplasies residing in the postcranium will become more discernible and useful in providing unambiguous synapomorphies. Such an ambitious endeavour requires a paradigm shift in the skeletal regions sampled for phylogenetic analyses.

12. CONCLUSIONS

Anatomical descriptions, diagnoses, and phylogenetic studies centered on extinct crocodylomorphs have often neglected the postcranial anatomy in favour of craniodental morphology. We offer a thorough reinvestigation of the pectoral girdle anatomy of two of the most iconic aquatic clades of Crocodylomorpha – Thalattosuchia and Dyrosauridae – highlighting several major morphological dissimilarities previously unreported between and within the clades, such as the expansion of the scapular and coracoid blade, the relative extension of the scapular shaft and overall slender or robust appearance of the bone, the presence of an open or closed coracoid foramen, the relative inclination of the scapular and coracoid shaft in relation to the scapulocoracoid synchondrosis surface, the relative positioning and size of the glenoid facet on the scapula, the overall size and shape of the anterior expansion of the coracoid head. Our work also provides insights into the intraspecific variability of extinct Crocodylomorpha, which is rarely acknowledged possibly due to the complexity of its nature depending on both the quantity and quality of specimens.

To address this issue of extreme dominance of craniodental features in phylogenetic relationships, we have built a new postcranial-only phylogenetic dataset of Thalattosuchia, Dyrosauridae, and extant Crocodylia. This dataset contains 191 characters, including new important features such as the position of the glenoid facet on the scapula, the perforation of the coracoid head, or the extension of the pubic symphysis. Our results reveal the phylogenetic potential of postcranial anatomy, as it recovers many clades and subclades, often with different taxonomic content than in skull-dominated datasets. Therefore,

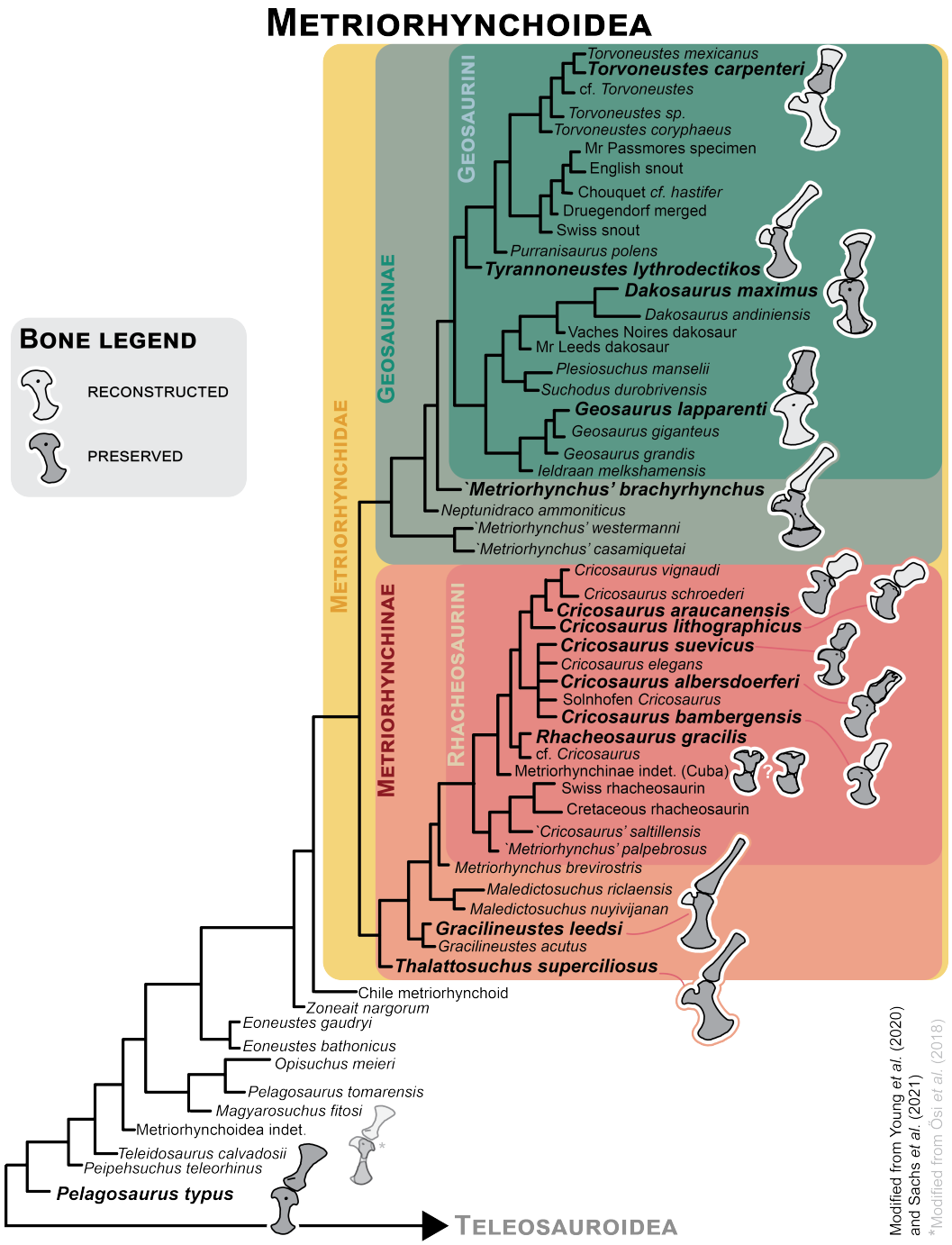
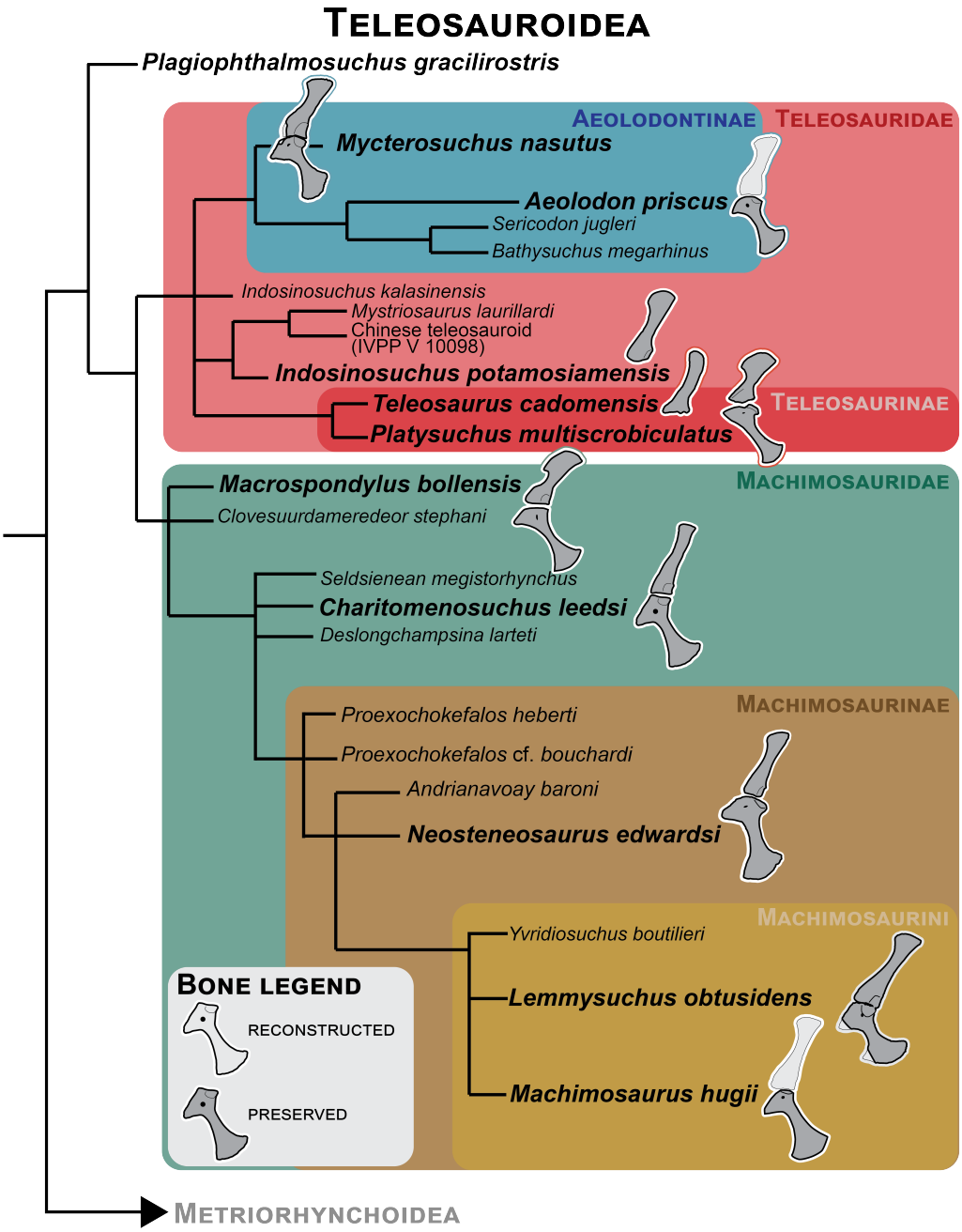


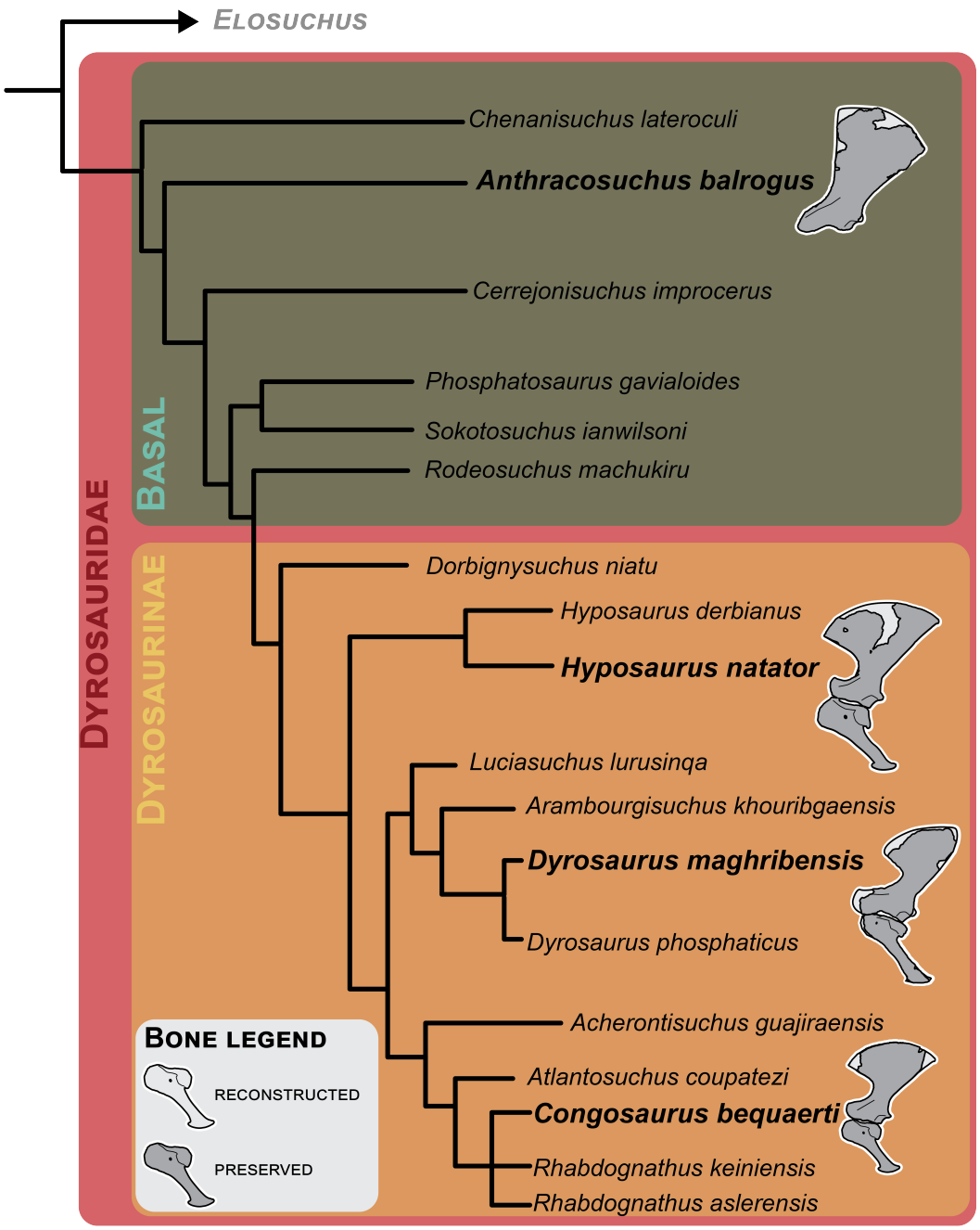
FIGURE 77. Figure illustrating the phylogeny of Metriorhynchoidea including a summary of the different pectoral girdle morphology. Figure modified from Young et al. (2020a) for the global phylogeny; the relationships of *C. suevicus*,*Cricosaurus albersdoerferi* and *C. bambergensis* modified from Sachs et al. (2021).

it appears clear that the postcranial anatomy not only aids in understanding the evolutionary connections among extinct crocodylomorphs but also sheds light on their development, ecology, and biomechanics.



MODIFIED FROM JOHNSON *ET AL.* 2020

FIGURE 78. Figure illustrating the phylogeny of Teleosauroidea including a summary of the different pectoral girdle morphology. Figure modified from Johnson et al. (2020).



Modified from Jouve & Jalil (2020)

FIGURE 79. Figure illustrating the phylogeny of Dyrosauridae including a summary of the different pectoral girdle morphology. Figure modified from Jouve and Jalil (2020).

13. ACKNOWLEDGEMENTS

We would like to thank all the museum staff for smoothly granting us the access of the crocodyliformes collections. We thank Dr. Jonathan Bloch, Dr. Richard Hulbert, and the rest of the staff at the Florida Museum (Florida Museum, Gainesville, USA); Dr. David Parris and Dr. Dana Ehret (New Jersey State Museum, Trenton, USA); collection manager Ned Gilmore (Academy of Natural Sciences of Drexel University, Philadelphia, USA); Dr. Daniel Brinkman (Yale Peabody Museum, New Haven, USA); Dr. Susannah Maidment & Dr. Mike Day (Natural History Museum, London, UK); Dr. Fabienne Giraud (Joseph Fourier University, France); Dr. Neil Clark (Hunterian Museum and Art Gallery, Glasgow, UK); Dr. Deborah Hutchinson (Bristol City Museum and Art Gallery, Bristol, UK); Matt Williams (Bath Royal Literary and Scientific Institute, Bath, UK); Dr. Erin Maxwell (Staatliches Museum für Naturkunde Stuttgart, Stuttgart, Germany); Dr. Matthew Parkes (Natural History Museum of Ireland, Republic of Ireland); Dr. Olivier Pauwels (Royal Belgian Institute of Natural Sciences, Belgium) for the help and care. We thank Dr. Yanina Herrera for her 3D models of *C. araucanensis* (MLP 72-IV-7-1); Dr Jérémy Anquetin for his 3D models of *Proexochokefalos cf. bouchardi* (SCR010-374) and *Sericodon jugleri* (SCR010-312); Dr. Rebecca Bennion, Dr. Narimane Chatar, Dr. Christophe Mallet, Dr. Roland Sookias, Romain Cottereaux and Antoine Laboury for scanning specimens during their visits; and Candice Stephanic for sharing her scans of NJSM 23368.

We would like to warmly thank our reviewers for their kind and thorough review.

REFERENCES

2023. — NHMUK Data Portal.

Aiglstorfer, M., Havlik, P., and Herrera, Y. 2019. — The first metriorhynchoid crocodyliform from the Aalenian (Middle Jurassic) of Germany, with implications for the evolution of Metriorhynchoidea. *Zoological Journal of the Linnean Society*, 188(2):522–551.

Allen, V., Molnar, J., Parker, W., Pollard, A., Nolan, G., and Hutchinson, J. R. 2014. — Comparative architectural properties of limb muscles in Crocodylidae and Alligatoridae and their relevance to divergent use of asymmetrical gaits in extant Crocodylia. *Journal of Anatomy*, 225:569–582.

Andrews, C. W. 1909. — XXXVIII - On some new Steneosaurs from the Oxford Clay of Peterborough. *Annals and Magazine of Natural History*, 3:299–308.

Andrews, C. W. 1913. *A descriptive catalogue of the marine reptiles of the Oxford Clay. Part II*. Order the the Trustees of the British Museum, London.

Baier, D. B., Garrity, B. M., Moritz, S., and Carney, R. M. 2018. — Alligator (*Alligator mississippiensis*) sternal and shoulder girdle mobility increase stride length during high walks. *Journal of Experimental Biology*, page jeb.186791.

Baier, D. B. and Gatesy, S. M. 2013. — Three-dimensional skeletal kinematics of the shoulder girdle and forelimb in walking *Alligator* . *Journal of Anatomy*, 223(5):462–473.

Bapst, D. W. 2012. — paleotree: an R package for paleontological and phylogenetic analyses of evolution. *Methods in Ecology & Evolution*, 3:803–807.

Barbosa, J. A., Kellner, A. W. A., and Viana, M. S. S. 2008. — New dyrosaurid crocodylomorph and evidences for faunal turnover at the K-P transition in Brazil. *Proceedings of the Royal Society B: Biological Sciences*, 275(1641):1385–1391.

Bell, M. A. and Lloyd, G. T. 2015. — strap: an R package for plotting phylogenies against stratigraphy and assessing their stratigraphic congruence. *Palaeontology*, 58:379–389.

Benson, R. B. J. and Druckenmiller, P. S. 2014. — Faunal turnover of marine tetrapods during the Jurassic-Cretaceous transition. *Biological Reviews*, 89:1–23.

Berckhemer, F. 1929. — Beiträge zur Kenntnis der Krokodilier des schwäbischen oberen Lias. *Neues Jahrbuch für Mineralogie, Geologie und Paläontologie. Beilagen Band*, 64B:1–59.

Blanco, A. 2021. — Importance of the postcranial skeleton in eusuchian phylogeny: reassessing the systematics of allodaposuchid crocodylians. *PLOS ONE*, 16(6):e0251900.

Brochu, C. A. 1992. — Ontogeny of the postcranium in crocodylomorph archosaurs. Master's thesis, University of Texas, Austin.

Brochu, C. A. 1995. — Heterochrony in the crocodylian scapulocoracoid. *Journal of Herpetology*, 29(3):464–468.

Bronn, H. G. 1841. — Über die fossilen Gaviale der Lias-Formation und der Oolithe. *Archiv für Naturgeschichte, Berlin*, 8:77–82.

Bronzati, M., Montefeltro, F. C., and Langer, M. C. 2012. — A species-level supertree of Crocodyliformes. *Historical Biology*, 24(6):589–606.

Bronzati, M., Montefeltro, F. C., and Langer, M. C. 2015. — Diversification events and the effects of mass extinctions on Crocodyliformes evolutionary history. *Royal Society Open Science*, 2(5):140385.

Buckley, G. A. and Brochu, C. A. 1999. — An enigmatic new crocodile from the Upper Cretaceous of Madagascar. *Special Papers in Palaeontology*, 60(60):149–175.

Buckley, G. A., Brochu, C. A., Krause, D. W., and Pol, D. 2000. — A pugnosed crocodyliform from the Late Cretaceous of Madagascar. *Nature*, 405:941–944.

Buffetaut, E. 1978. — A dyrosaurid (Crocodylia, Mesosuchia) from the Upper Eocene of Burma. *Jahrbuch für Geologie und Paläontologie, Abhandlungen*, 1978:273–281.

Buffetaut, E., Bussert, R., and Brinkman, W. 1990. — A new non-marine vertebrate fauna in the Upper Cretaceous of northern Sudan. *Berliner Geowissenschaftliche*, Abhandlungen 120:183–202.

Chamero, B., Buscalioni, Á. D., and Marugán-Lobón, J. 2013. — Pectoral girdle and forelimb variation in extant Crocodylia: the coracoid-humerus pair as an evolutionary module: variation of the crocodylian skeleton. *Biological Journal of the Linnean Society*, 108(3):600–618.

Chiarenza, A., Foffa, D., Young, M. T., Insacco, G., Cau, A., Carnevale, G., and Catanzariti, R. 2015. — The youngest record of metriorhynchid crocodylomorphs, with implications for the extinction of Thalattosuchia. *Cretaceous*, 56:608–616.

de Stefano, G. 1903. — Nuovi rettili degli strati a fosfato della Tunisia. *Bollettino delle Societa Geologica Italiana*, 22:51–80.

Debelmas, J. and Strannoloubsky, A. 1957. — Découverte d'un crocodilien dans le Néocomien des environs de la Martre (VAR): *Dacosaurus lapparenti* nov. sp. *Travaux du Laboratoire de Géologie de l'Université de Grenoble*, 33:89–99.

Dollo, L. 1914. — Sur la découverte de Téléosauriens tertiaires au Congo. *Bulletin de l'Académie royale de Belgique*, pages 288–298.

Eudes-Deslongchamps, J.-A. 1867. *[posthumous work] Note sur les téléosauriens.* Le Blanc-Hardel, Caen.

Eudes-Deslongchamps, J.-A. 1868. — Remarques sur l'os de la mâchoire inférieure des Téléosauriens, désigné sous le nom de complémentaire. *Bulletin de la Societé Linnéenne de Normandie, Caen*, (1):112–118.

Eudes-Deslongchamps, J.-A. and Blainville, H. M. D. 1852. *Lettres sur les crocodiles vivants et fossiles*. A. Hardel, Caen.

Fanti, F., Miyashita, T., Cantelli, L., Mnasri, F., Dridi, J., Contessi, M., and Cau, A. 2015. — The largest thalattosuchian (Crocodylomorpha) supports teleosaurid survival across the Jurassic-Cretaceous boundary. *Cretaceous Research*, 61:263–274.

Fernández, M. and Gasparini, Z. 2008. — Salt glands in the Jurassic metriorhynchid *Geosaurus*: Implications for the evolution of osmoregulation in Mesozoic marine crocodyliforms. *Naturwissenschaften*, 95(1):79–84.

Fischer, V., Maisch, M. W., Naish, D., Kosma, R., Liston, J., Joger, U., Krüger, F. J., Pérez, J. P., Tainsh, J., and Appleby, R. M. 2012. — New ophthalmosaurid ichthyosaurs from the European Lower Cretaceous demonstrate extensive ichthyosaur survival across the Jurassic-Cretaceous boundary. *PLoS ONE*, 7(1):1–23.

Foffa, D., Johnson, M. M., Young, M. T., Stee, L., and Brusatte, S. L. 2019. — Revision of the late jurassic deep-water teleosauroid crocodylomorph *Teleosaurus megarhinus* Hulke, 1871 and evidence of pelagic adaptations in Teleosauroidea. *PeerJ*, 7:e6646.

Fraas, E. 1901. — Die Meerkrokodile (Thalattosuchia n.g.) eine Sauriergruppe der Juraformation. *Jahresheft der Vereinigung vaterländischer Naturkundler Württembergs*, 57:409–418.

Fraas, E. 1902. — Die Meer-Krocodilier (Thalattosuchia) des oberen Jura unter specieller Berücksichtigung von *Dacosaurus* und *Geosaurus*. *Palaeontographica*, 49:1–72.

Gasparini, Z. and Dellapé, D. 1976. — Un nuevo cocodrilo marino (Thalattosuchia, Metriorhynchidae) de la Formación Vaca Muerta (Tithoniano) de la Provincia de Neuquén (Argentina). *Actas 1° Congreso Geológico Chileno, Santiago, Chile*, pages C1–C21.

Godoy, P. L., Bronzati, M., Eltink, E., Marsola, J. C. d. A., Cidade, G. M., Langer, M. C., and Montefeltro, F. C. 2016. — Postcranial anatomy of *Pissarrachampsa sera* (Crocodyliformes, Baurusuchidae) from the Late Cretaceous of Brazil: insights on lifestyle and phylogenetic significance. *PeerJ*, 4:e2075.

Goloboff, P. A. and Catalano, S. A. 2016. — *TNT* version 1.5, including a full implementation of phylogenetic morphometrics. *Cladistics*, 32(3):221–238.

Goloboff, P. A., Torres, A., and Arias, J. S. 2018. — Weighted parsimony outperforms other methods of phylogenetic inference under models appropriate for morphology. *Cladistics*, 34:407–437.

Gray, SJ. 1968. *Animal locomotion*. Weidenfeld and Nicolson, London.

Hastings, A. K., Bloch, J. I., Cadena, E. A., and Jaramillo, C. A. 2010. — A new small short-snouted dyrosaurid (Crocodylomorpha, Mesoeucrocodylia) from the Paleocene of Northeastern Colombia. *Journal of Vertebrate Paleontology*, 30(1):139–162.

Hastings, A. K., Bloch, J. I., and Jaramillo, C. 2014. — A new blunt-snouted dyrosaurid, *Anthracosuchus balrogus* gen. et sp. nov. (Crocodylomorpha, Mesoeucrocodylia), from the Palaeocene of Colombia. *Historical Biology*, 27:1–23.

Hastings, A. K., Bloch, J. I., and Jaramillo, C. A. 2011. — A new longirostrine dyrosaurid (Crocodylomorpha, Mesoeucrocodylia) from the Paleocene of north-eastern Colombia: biogeographic and behavioural implications for New–World Dyrosauridae. *Palaeontology*, 54(5):1095–1116.

Hay, O. P. 1930. *Second bibliography and catalogue of the fossil vertebrata of North America*, volume 1. Carnegie Institution of Washington, Washington, D.C.

Herrera, Y., Fernández, M., Lamas, S. G., Campos, L., Talevi, M., and Gasparini, Z. 2017. — Morphology of the sacral region and reproductive strategies of Metriorhynchidae: a counter-inductive approach. *Earth and Environmental Science Transactions of the Royal Society of Edinburgh*, 106:247–255.

Herrera, Y., Fernández, M. S., and Gasparini, Z. 2013a. — Postcranial skeleton of *Cricosaurus araucanensis* (Crocodyliformes: Thalattosuchia): morphology and palaeobiological insights. *Alcheringa*, 37:285–298.

Herrera, Y., Fernández, M. S., and Varela, J. A. 2009. — Morfología del miembro anterior de *Geosaurus araucanensis* Gasparini y Dellapé, 1976 (Crocodyliformes: Thalattosuchia). *Ameghiniana46*, pages 657–667.

Herrera, Y., Gasparini, Z., and Fernández, M. S. 2013b. — A new Patagonian species of *Cricosaurus* (Crocodyliformes, Thalattosuchia): first evidence of *Cricosaurus* in Middle-Upper Tithonian lithographic limestone from Gondwana: A NEW METRIORHYNCHID FROM PATAGONIA. *Palaeontology*, 56(3):663–678.

Hua, S. 1999. — Le Crocodilien *Machimosaurus mosae* (Thalattosuchia, Teleosauridae) du Kimmeridgien du Boulonnais (Pas de Calais, France). *Palaeontographica Abteilung A Band 252 Lieferung*, 4–6:141–170.

Hua, S. 2003. — Locomotion in marine mesosuchians (Crocodylia): the contribution of the "locomotion profiles". *Neues Jahrbuch für Geologie und Paläontologie - Abhandlungenur Geologie und Palaontologie - Abhandlungen*, 227(1):139–152.

Hua, S. and Buffetaut, E. 1997. — Introduction to Part V: Crocodylia. In Callaway, J. M. and Nicholls, E. L., editors, *Ancient Marine Reptiles*, pages 357–374. Academic Press, San Diego, California.

Hua, S. and De Buffrenil, V. 1996. — Bone histology as a clue in the interpretation of functional adaptations in the Thalattosuchia (Reptilia, Crocodylia). *Journal of Vertebrate Paleontology*, 16(4):703–717.

Hua, S., Vasse, D., Buffetaut, E., Martin, M., Mazin, J.-m., and Vadet, A. 1993. — Un squelette de *Machimosaurus mosae* Sauvage et Lienard, 1879 (Crocodylia, Thalattosuchia) dans le Kimméridgien du Boulonnais. *Comptes rendus de l'Académie des Sciences de Paris*, 317:851–856.

Jäger, v. G. F. 1828. *Über die fossile Reptilien, welche in Württemberg aufgefunden worden sind*. Stuttgart: J. B. Metzler.

Johnson, M. M., Amson, E., and Maxwell, E. E. 2023. — Evaluating growth in *Macrospondylus bollensis* (Crocodylomorpha, Teleosauroidea) in the Toarcian Posidonia Shale, Germany. *Papers in Palaeontology*, 9(2):e1529.

Johnson, M. M., Young, M. T., and Brusatte, S. L. 2020. — The phylogenetics of Teleosauroidea (Crocodylomorpha, Thalattosuchia) and implications for their ecology and evolution. *PeerJ*, 8:e9808.

Johnson, M. M., Young, M. T., Brusatte, S. L., Thuy, B., and Weis, R. 2018. — A catalogue of teleosauroids (Crocodylomorpha: Thalattosuchia) from the Toarcian and Bajocian (Jurassic) of southern Luxembourg. *Historical Biology*, 31(9):1179–1194.

Johnson, M. M., Young, M. T., Steel, L., Foffa, D., Smith, A. S., Hua, S., Havlik, P., Howlett, E. A., and Dyke, G. 2017. — Re-description of *'Steneosaurus' obtusidens* Andrews, 1909, an unusual

macrophagous teleosaurid crocodylomorph from the Middle Jurassic of England. *Zoological Journal of the Linnean Society*, 182(2):385–418.

Jouve, S. 2007. — Taxonomic revision of the dyrosaurid assemblage (Crocodyliformes: Mesoeucrocodylia) from the Paleocene of the Iullemmeden Basin, West Africa. *Journal of Paleontology*, 81(1):163–175.

Jouve, S. 2009. — The skull of *Teleosaurus cadomensis* (Crocodylomorpha; Thalattosuchia), and phylogenetic analysis of Thalattosuchia. *Journal of Vertebrate Paleontology*, 29:88–102.

Jouve, S. 2021. — Differential diversification through the K-Pg boundary, and post-crisis opportunism in longirostrine crocodyliforms. *Gondwana Research*, 99:110–130.

Jouve, S., Bardet, N., Jalil, N. E., Suberbiola, X. P., Bouya, B., and Amaghzaz, M. 2008a. — The oldest African crocodylian: phylogeny, paleobiogeography, and differential survivorship of marine reptiles through the Cretaceous-Tertiary boundary. *Journal of Vertebrate Paleontology*, 28(2):409–421.

Jouve, S., Bouya, B., and Amaghzaz, M. 2008b. — A long-snouted dyrosaurid (crocodyliformes, mesoeucrocodylia) from the paleocene of Morocco: phylogenetic and palaeobiogeographic implications. *Palaeontology*, 51(2):281–294.

Jouve, S., de Muizon, C., Cespedes-Paz, R., Sossa-Soruco, V., and Knoll, S. 2021. — The longirostrine crocodyliforms from Bolivia and their evolution through the Cretaceous–Palaeogene boundary. *Zoological Journal of the Linnean Society*, 192:475–509.

Jouve, S., Iarochène, M., Bouya, B., and Amaghzaz, M. 2006. — A new species of *Dyrosaurus* (Crocodylomorpha, Dyrosauridae) from the early Eocene of Morocco: phylogenetic implications. *Zoological Journal of the Linnean Society*, 148:603–656.

Jouve, S. and Jalil, N. E. 2020. — Paleocene resurrection of a crocodylomorph taxon: Biotic crises, climatic and sea level fluctuations. *Gondwana Research*, 85:1–18.

Jouve, S. and Schwarz, D. 2004. — *Congosaurus bequaerti*, a Paleocene dyrosaurid (Crocodyliformes; Mesoeucrocodylia) from Landana (Angola). *Bulletin de l'Institut Royal des Sciences Naturelles de Belgique*, 74:129–146.

Klinkhamer, A. J., Wilhite, D. R., White, M. A., and Wroe, S. 2017. — Digital dissection and three-dimensional interactive models of limb musculature in the Australian estuarine crocodile (Crocodylus porosus). *PLOS ONE*, 12(4):e0175079.

Lamouroux, M. 1820. — Sur le crocodile fossile trouvé dans les carrières du bourg d'Allemagne, à un quart de lieue de Cean. *Annales Générales des Sciences Physiques*, 3:160–164.

Langston, W. J. 1995. — Dyrosaurs (Crocodilia, Mesosuchia) from the Paleocene Umm Himar Formation, Kingdom of Saudi Arabia. In Whitmore, F. C. J. and Madden, C. T., editors, *Paleocene vertebrates from Jabal Umm Himar, Kingdom of Saudi Arabia*, volume 2093 of *US Geological Survey Bulletin*, pages F1–F36.

Larsson and Sues 2007. — Cranial osteology and phylogenetic relationships of *Hamadasuchus rebouli* (Crocodyliformes: Mesoeucrocodylia) from the Cretaceous of Morocco. *Zoological Journal of the Linnean Society*, 149:533–567.

Leardi, J. M., Pol, D., Novas, F. E., and Suárez Riglos, M. 2015. — The postcranial anatomy of *Yacarerani boliviensis* and the phylogenetic significance of the notosuchian postcranial skeleton. *Journal of Vertebrate Paleontology*, 35(6):e995187.

Li, Z. and Clarke, J. A. 2015. — New insight into the anatomy of the hyolingual apparatus of *Alligator mississippiensis* and implications for reconstructing feeding in extinct archosaurs. *Journal of Anatomy*, 227(1):45–61.

Mannion, P. D., Chiarenza, A. A., Godoy, P. L., and Cheah, Y. N. 2019. — Spatiotemporal sampling patterns in the 230 million year fossil record of terrestrial crocodylomorphs and their impact on diversity. *Palaeontology*, 62:615–637.

Martin, J. E., Delfino, M., Smith, T., Martin, J. E., Delfino, M., and Osteology, T. S. 2016. — Osteology and affinities of Dollo's goniopholidid (Mesoeucrocodylia) from the Early Cretaceous of Bernissart,

Belgium. *Journal of Vertebrate Paleontology*, 36:e1222534.

Martin, J. E., Sarr, R., and Hautier, L. 2019a. — A dyrosaurid from the Paleocene of Senegal. *Journal of Paleontology*, 93(2):343–358.

Martin, J. E., Suteethorn, S., Lauprasert, K., Tong, H., Buffetaut, E., Liard, R., Salaviale, C., Deesri, U., Suteethorn, V., and Claude, J. 2019b. — A new freshwater teleosaurid from the Jurassic of northeastern Thailand. *Journal of Vertebrate Paleontology*, 38:e1549059.

Martin, J. E. and Vincent, P. 2013. — New remains of *Machimosaurus hugii* von Meyer, 1837 (Crocodilia, Thalattosuchia) from the Kimmeridgian of Germany. *Fossil Record*, 16(2):179–196.

Martin, J. E., Vincent, P., and Falconnet, J. 2015. — The taxonomic content of *Machimosaurus* (Crocodylomorpha, Thalattosuchia). *Comptes Rendus Palevol*, 14(4):305–310.

Massare, J. A. 1988. — Swimming capabilities of Mesozoic marine reptiles: implications for method of predation. *Paleobiology*, 14(2):187–205.

Mazin, J.-M. 1996. — Mesozoic marine reptiles: an overview. In Mazin, J.-M. and De Buffrénil, V., editors, *Secondary Adaptation of Tetrapods to Life in Water*, pages 95–117.

McCurry, M. R., Evans, A. R., Fitzgerald, E. M. G., Adams, J. W., Clausen, P. D., and McHenry, C. R. 2017. — The remarkable convergence of skull shape in crocodilians and toothed whales. *Proceedings of the Royal Society B*, 284(1850):20162348.

Meers, M. B. 2003. — Crocodylian forelimb musculature and its relevance to archosauria. *Anatomical Record - Part A Discoveries in Molecular, Cellular, and Evolutionary Biology*, 274(2):891–916.

Michel, K. B., West, T. G., Daley, M. A., Allen, V. R., and Hutchinson, J. R. 2021. — Appendicular muscle physiology and biomechanics in *Crocodylus niloticus*. *Integrative Organismal Biology*, 2(1):obaa038.

Molnar, J. L., Pierce, S. E., Bhullar, B.-A. S., Turner, A. H., and Hutchinson, J. R. 2015. — Morphological and functional changes in the vertebral column with increasing aquatic adaptation in crocodylomorphs. *Royal Society Open Science*, 2:150439.

Montefeltro, F. C., Larsson, H. C. E., De França, M. A. G., and Langer, M. C. 2013. — A new neosuchian with Asian affinities from the Jurassic of northeastern Brazil. *Naturwissenschaften*, 100(9):835–841.

Nascimento, P. M. and Zaher, H. 2010. — A new species of Baurusuchus (Crocodyliformes, Mesoeucrocodylia) from the Upper Cretaceous of Brazil, with the first complete postcranial skeleton described for the family Baurusuchidae. *Papéis Avulsos de Zoologia (São Paulo)*, 50(21):323–361.

Novas, F. E., Agnolin, F. L., Lio, G. L., Rozadilla, S., Suárez, M., de la Cruz, R., de Souza Carvalho, I., Rubilar-Rogers, D., and Isasi, M. P. 2021. — New transitional fossil from late Jurassic of Chile sheds light on the origin of modern crocodiles. *Scientific Reports*, 11:14960.

Novas, F. E., Pais, D. F., Pol, D., Carvalho, I. S., Scanferla, A., Mones, A., and Suárez Riglos, M. 2009. — Bizarre notosuchian crocodyliform with associated eggs from the Upper Cretaceous of Bolivia. *Journal of Vertebrate Paleontology*, 29:1316–1320.

Ősi, A., Young, M. T., Galàcz, A., and Rabi, M. 2018. — A new large-bodied thalattosuchian crocodyliform from the Lower Jurassic (Toarcian) of Hungary, with further evidence of the mosaic acquisition of marine adaptations in Metriorhynchoidea. *PeerJ*, 6:e4668.

Otero, A., Allen, V., Pol, D., and Hutchinson, J. R. 2017. — Forelimb muscle and joint actions in Archosauria: insights from *Crocodylus johnstoni* (Pseudosuchia) and *Mussaurus patagonicus* (Sauropodomorpha). *PeerJ*, 5:e3976.

Owen, R. 1849. — Notes on remains of fossil reptiles discovered by Prof. H. Rogers in Greensand formations of New Jersey. *The Quarterly journal of the Geological Society of London*, 5:380–383.

Pan, T., Miao, J.-S., Zhang, H.-B., Yan, P., Lee, P.-S., Jiang, X.-Y., Ouyang, J.-H., Deng, Y.-P., Zhang, B.-W., and Wu, X.-B. 2021. — Near-complete phylogeny of extant Crocodylia (Reptilia) using mitogenome-based data. *Zoological Journal of the Linnean Society*, 191(4):1075–1089.

Paradis, E., Claude, J., and Strimmer, K. 2004. — APE: analyses of phylogenetics and evolution in R language. *Bioinformatics*, 20(2):289–290.

Pierce, S. E., Angielczyk, K. D., and Rayfield, E. J. 2009. — Shape and mechanics in thalattosuchian (Crocodylomorpha) skulls: implications for feeding behaviour and niche partitioning. *Journal of Anatomy*, 215:555–576.

Pierce, S. E. and Benton, M. J. 2006. — *Pelagosaurus typus* Bronn, 1841 (Mesoeucrocodylia: Thalattosuchia) from the Upper Lias (Toarcian, Lower Jurassic) of Somerset, England. *Journal of Vertebrate Paleontology*, 26(3):621–635.

Plieninger, T. 1846. — Prof. Dr. Th. Plieninger hielt nachstehenden vortrag über ein neues Sauriergenus und die Einreihung der Saurier mit flachen, schneidenden Zähnen in eine Familie. Pp. 148-154. In *Zweite Generalversammlung am 1. Mai 1846 zu Tübingen*, number 2 in Württembergische naturwissenschaftliche Jahreshefte, pages 129–183.

Pol, D. 2005. — Postcranial remains of *Notosuchus terrestris* Woodward (Archosauria: Crocodyliformes) from the upper Cretaceous of Patagonia, Argentina. *Ameghiniana*, 42(1):21–38.

Pol, D., Leardi, J. M., Lecuona, A., and Krause, M. 2012. — Postcranial anatomy of *Sebecus icaeorhinus* (Crocodyliformes, Sebecidae) from the Eocene of Patagonia. *Journal of Vertebrate Paleontology*, 32:328–354.

Rio, J. P. and Mannion, P. D. 2021. — Phylogenetic analysis of a new morphological dataset elucidates the evolutionary history of Crocodylia and resolves the long-standing gharial problem. *PeerJ*, 9:e12094.

Romão, M. F. and Santos, A. L. Q. 2023. — MUSCULAR ANATOMY OF THE THORAX AND THORACIC LIMB OF *Caiman crocodilus* (LINNAEUS, 1758) (CROCODYLIA: ALLIGATORIDAE) BY MEANS OF DIGITAL DISSECTION AND THREE-DIMENSIONAL MODELS. *Brazilian Journal of Implantology and Health Sciences*, 5(4):453–470.

Sachs, S., Young, M. T., Abel, P., and Mallison, H. 2019. — A new species of the metriorhynchid crocodylomorph *Cricosaurus* from the Upper Jurassic of southern Germany. *Acta Palaeontologica Polonica*, 64(2):343–356.

Sachs, S., Young, M. T., Abel, P., and Mallison, H. 2021. — A new species of *Cricosaurus* (Thalattosuchia, Metriorhynchidae) based upon a remarkably well-preserved skeleton from the Upper Jurassic of Germany. *Palaeontologia Electronica*, 24(2):a24.

Salih, K. A. O., Evans, D. C., Bussert, R., Klein, N., Nafi, M., and Muller, J. 2015. — First record of *Hyposaurus* (Dyrosauridae, Crocodyliformes) from the Upper Cretaceous Shendi Formation of Sudan. *Journal of Vertebrate Paleontology*, 36(1):1–9.

Sauvage, H. E. and Liénard, F. 1879. — Mémoire sur le genre *Machimosaurus*. *Mémoires de la Société Géologique de France 3ème série*, 4:32.

Scavezzoni, I. and Fischer, V. 2021. — The postcranial skeleton of *Cerrejonisuchus improcerus* (Crocodyliformes: Dyrosauridae) and the unusual anatomy of dyrosaurids. *PeerJ*, 9:e11222.

Scavezzoni, I. and Fischer, V. 2023. — Limited convergence in the postcranium of aquatic Crocodylomorpha. *Palaeontology*, (e12678):13.

Scavezzoni, I., Fischer, V., Johnson, M. M., and Jouve, S. 2024. — Form and function of the pelvic girdle of Thalattosuchia and Dyrosauridae (Crocodyliformes). *Geodiversitas*, 46(6):135–326.

Schwarz, D., Frey, E., and Martin, T. 2006. — The postcranial skeleton of the Hyposaurinae (Dyrosauridae; Crocodyliformes). *Palaeontology*, 49(4):695–718.

Schwarz-Wings, D., Frey, E., and Martin, T. 2009. — Reconstruction of the bracing system of the trunk and tail in hyposaurine dyrosaurids (Crocodylomorpha; Mesoeucrocodylia). *Journal of Vertebrate Paleontology*, 29(2):453–472.

Sertich, J. J. W. and Groenke, J. R. 2010. — Appendicular skeleton of *Simosuchus clarki* (Crocodyliformes: Notosuchia) from the Late Cretaceous of Madagascar. *Journal of Vertebrate Paleontology*, 30(sup1):122–153.

Sertich, J. J. W., Manthi, F. K., Sampson, S. D., Loewen, M. A., and Getty, M. A. 2006. — Rift valley dinosaurs: a new Late Cretaceous vertebrate fauna from Kenya [Conference presentation] 124A. *Journal of Vertebrate Paleontology*, 26:124A.

Smith, M. R. 2019. — Bayesian and parsimony approaches reconstruct informative trees from simulated morphological datasets. *Biology Letters*, 15:20180632.

Stubbs, T. L., Pierce, S. E., Elsler, A., Anderson, P. S. L., Rayfield, E. J., and Benton, M. J. 2021. — Ecological opportunity and the rise and fall of crocodylomorph evolutionary innovation. *Proceedings of the Royal Society B*, 288:20210069.

TEAM, R. C. 2013. — R: a language and environment for statistical computing. R Foundation for Statistical Computing.

Tennant, J. P., Mannion, P. D., and Upchurch, P. 2016. — Environmental drivers of crocodyliform extinction across the Jurassic/Cretaceous transition. *Proceedings of the Royal Society B*, 283:20152840.

Tiercelin, J.-J., Potdevin, J.-L., Thuo, P. K., Abdelfettah, Y., Schuster, M., Bourquin, S., Bellon, H., Clément, J.-P., Guillou, H., Nalpas, T., and Ruffet, G. 2012. — Stratigraphy, sedimentology and diagenetic evolution of the Lapur Sandstone in northern Kenya: Implications for oil exploration of the Meso–Cenozoic Turkana depression. *Journal of African Earth Sciences*, 71–72:43–79.

Troxell, E. L. 1925. — *Hyposaurus*, a marine crocodilian. *American Journal of Science*, 9(54):489–514.

Turner, A. H. 2006. — Osteology and phylogeny of a new species of *Araripesuchus* (Crocodyliformes: Mesoeucrocodylia) from the Late Cretaceous of Madagascar. *Historical Biology*, 18(3):255–369.

von Meyer, H. 1831. — Neue fossile Reptilien, aus der Ordnung der Saurier. *Nova Acta Academiae Leopoldino-Carolinae Curios*, 15(2):173–184.

von Meyer, H. 1837. — Mittheilungen, an Professor Bronn gerichtet. *Neues Jahrbuch für Mineralogie, Geognosie, Geologie und Petrefaktenkunde*, 1837:557–562.

von Sömmerring, S. T. 1814. — Über den *Crocodilus priscus*, oder ein in Baiern versteint gefundenes schmalkie-feriges Krokodil, Gavial der Vorwelt. *Denkschriften der Königlichen Akademie der Wisseschaften zu München. Classe der Mathematik und Naturwissenschaften*, 5:9–82.

Wagner, A. 1858. — Zur Kenntniss der Sauier aus den lithographischen Schiefen. *Abhandlungen der Mathematisch-Physikalischen Classe der Königlich Bayerischen Akademie der Wissenschaften*, (8):415–528.

Westphal, F. 1961. — Zu Systematik der deutschen und englischen Lias Krokodilier. *Neues Jahrbuch für Geologie und Paläontologie - Abhandlungen*, 113(2):207–218.

Wilberg, E. W. 2015a. — A new metriorhynchoid (Crocodylomorpha, Thalattosuchia) from the Middle Jurassic of Oregon and the evolutionary timing of marine adaptations in thalattosuchian crocodylomorphs. *Journal of Vertebrate Paleontology*, 35:902846.

Wilberg, E. W. 2015b. — What's in an outgroup? The impact of outgroup choice on the phylogenetic position of Thalattosuchia (Crocodylomorpha) and the origin of Crocodyliformes. *Systematic Biology*, 64:621–637.

Wilberg, E. W., Godoy, P. L., Griffiths, E. F., Turner, A. H., and Benson, R. B. J. 2023. — A new early diverging thalattosuchian (Crocodylomorpha) from the Early Jurassic (Pliensbachian) of Dorset, U.K. and implications for the origin and evolution of the group. *Journal of Vertebrate Paleontology*, 42(3):24.

Wilberg, E. W., Turner, A. H., and Brochu, C. A. 2019. — Evolutionary structure and timing of major habitat shifts in Crocodylomorpha. *Scientific Reports*, 9:514.

Wilkinson, L. E., Young, M. T., and Benton, M. J. 2008. — A new metriorhynchid crocodilian (Mesoeucrocodylia: Thalattosuchia) from the Kimmeridgian (Upper Jurassic) of Wiltshire, UK. *Palaeontology*, 51(6):1307–1333.

Woodward, A. S. 1896. — On two Mesozoic crocodilians *Notosuchus* (genus novum) and *Cynodontosuchus* (genus novum) from the Red Sandstones of the Territory of Neuquén (Argentina Republic). *Anales del Museo de La Plata, Paleontología*, 4:1–20.

Young, M. T., Bell, M. A., de Andrade, M. B., and Brusatte, S. L. 2011. — Body size estimation and evolution in metriorhynchid crocodylomorphs: implications for species diversification and niche partitioning. *Zoological Journal of the Linnean Society*, 163:1199–1216.

Young, M. T., Brignon, A., Sachs, S., Hornung, J. J., Foffa, D., Kitson, J. J. N., Johnson, M. M., and Steel, L. 2020a. — Cutting the Gordian knot: a historical and taxonomic revision of the Jurassic crocodylomorph *Metriorhynchus*. *Zoological Journal of the Linnean Society*, 192:510–553.

Young, M. T., Brusatte, S. L., Ruta, M., and de Andrade, M. B. 2010. — The evolution of Metriorhynchoidea (Mesoeucrocodylia, Thalattosuchia): an integrated approach using geometric morphometrics, analysis of disparity, and biomechanics. *Zoological Journal of the Linnean Society*, 158:801–859.

Young, M. T. and de Andrade, M. B. 2009. — What is *Geosaurus*? Redescription of *Geosaurus giganteus* (Thalattosuchia: Metriorhynchidae) from the Upper Jurassic of Bayern, Germany. *Zoological Journal of the Linnean Society*, 157:551–585.

Young, M. T., de Andrade, M. B., Brusatte, S. L., Sakamoto, M., and Liston, J. 2012. — The oldest known metriorhynchid super-predator: a new genus and species from the Middle Jurassic of England, with implications for serration and mandibular evolution in predacious clades. *Journal of Systematic Palaeontology*, 11(4):475–513.

Young, M. T., Hua, S., Steel, L., Foffa, D., Brusatte, S. L., Thüring, S., Mateus, O., Ruiz-Omeñaca, J. I., Havlik, P., Lepage, Y., and De Andrade, M. B. 2014. — Revision of the Late Jurassic teleosaurid genus *Machimosaurus* (Crocodylomorpha, Thalattosuchia). *Royal Society Open Science*, 1(2):140222.

Young, M. T., Rabi, M., Bell, M. A., Foffa, D., Steel, L., Sachs, S., and Peyer, K. 2016. — Big-headed marine crocodyliforms and why we must be cautious when using extant species as body length proxies for long-extinct relatives. *Palaeontologia Electronica*, 19:1–14.

Young, M. T., Sachs, S., Abel, P., Foffa, D., Herrera, Y., and Kitson, J. J. 2020b. — Convergent evolution and possible constraint in the posterodorsal retraction of the external nares in pelagic crocodylomorphs. *Zoological Journal of the Linnean Society*, 189(2):494–520.

Young, M. T., Wilberg, E. W., Johnson, M. M., Herrera, Y., De Andrade, M. B., Brignon, A., Sachs, S., Abel, P., Foffa, D., Fernández, M. S., Vignaud, P., Cowgill, T., and Brusatte, S. L. 2024. — The history, systematics, and nomenclature of Thalattosuchia (Archosauria: Crocodylomorpha). *Zoological Journal of the Linnean Society*, 200(2):547–617.

List of Figures

1 Schematic representation of a dyrosaurid (*Cerrejonisuchus improcerus*) illustrating the conventions of bone orientation based on the presumed resting pose of said taxa. Artwork by I.S. Picture modified from Scavezzoni and Fischer (2023). 4

2 Schematic left teleosaurid and metriorhynchid pectoral girdle in lateral view as laying on a flat surface illustrating the orientation of each bone. **A & B** based on *Charitomenosuchus leedsi* NHMUK PV R 3806 and **C & D** based on the reconstruction of *Thalattosuchus* GLAHM V1146 from below. **A.** Stylized left scapula in lateral view; **B.** Stylized left scapula in lateral view; **C.** Stylized left coracoid in ventral view; **D.** Stylized left coracoid in ventral view. Terms in parentheses correspond to an alternative designation. The dark blue line indicates the anterior expansion of the coracoid head, which is measured from the anterior extremity of the scapulocoracoid synchondrosis surface. 6

3 Schematic left alligatorid and hyposaurine pectoral girdle in lateral view as laying on a flat surface illustrating the orientation of each bone. **A & B** based on *Caiman crocodylus* NMW 30900 and **C & D** based on the reconstruction of *Congosaurus bequaerti* MRAC 1809 & MRAC 1811. **A.** Stylized left scapula in lateral view; **B.** Stylized left scapula in lateral view; **C.** Stylized left coracoid in ventral view; **D.** Stylized left coracoid in ventral view. Terms in parentheses correspond to an alternative designation. The dark blue line indicates the anterior expansion of the coracoid head, which is measured from the anterior extremity of the scapulocoracoid synchondrosis surface. 7

4 A snapshot of the pectoral girdle of the alligatoroid *Palaeosuchus palpebrosus* RVC-JRH-PP1 (3D models). **A.** In anterior view; **B.** In lateral view. Note the orientation of the scapula/coracoid. Target indicates anterior view. Grey arrow points anteriorly. CT scan courtesy of Professor John Hutchinson. Link: https://skfb.ly/6ByyV 15

5 Right pectoral girdle of *Mecistops cataphractus* RBINS 18374 (photographs). **A.** Scapula in lateral view; **B.** Scapula in medial view; **C.** Coracoid in ventral view; **D.** Coracoid in dorsal view. Arrow points anteriorly. 16

6 Left pectoral girdle of *Caiman crocodylus* NMW 30900 (photographs). **A.** Scapula in medial view; **B.** Coracoid in ventral view; **C.** Thoracic girlde in anterior view; **D.** Pectoral girdle in posterior view. Target indicates anterior. Cross indicates posterior. Arrow points anteriorly. Red dashed lines indicate missing parts. 17

7 Left pectoral girdle of *Crocodylus niloticus* NMW 31137 (A&B) and *Crocodylus rhombifer* AMNH FARB 16694 (C&D) (photographs). **A.** Scapula in lateral view; **B.** Scapula in posterior view; **C.** Coracoid in ventral view; **D.** Coracoid in dorsal view. Cross indicates posterior. Arrow points anteriorly. 18

8 Left pectoral girdle of *Osteolaemus tetraspis* NMW 39338:2 (photographs). **A.** Scapula and coracoid in lateral view; **B.** Coracoid in ventral view. Arrow points anteriorly. 19

9 Pectoral girdle of *Turnersuchus hingleyae* LRM 2021/45 (3D models) (Wilberg et al., 2023). **A.** Left scapula in lateral view ; **B.** Left coracoid in ventral view ; **C.** Left scapula in medial view ; **D.** Left coracoid in ventral view. Arrow points anteriorly. 3D models from Wilberg et al. (2023). Red dashed lines indicate missing parts. Reconstruction of missing parts based on *Macrospondylus bollensis* PMU 35980. 29

10 Reconstruction of the pectoral girdle of *Turnersuchus hingleyae* LRM 2021/45 (3D models). **A.** Lateral view; **B.** Anterior view; **C.** Ventral view; **D.** Dorsal view. Arrow points anteriorly. Target indicates anterior. The left scapula and coracoid are mirrored. Reconstruction of missing parts based on *Macrospondylus* PMU 35980. 31

11 Comparative figure of basal thalattosuchian and metriorhynchoid scapulae. **A.** Thalattosuchia (3D model); **B.** Metriorhynchoidea (photograph); **C.** Metriorhynchinae (photograph and 3D models); **D.** Rhacheosaurini (photographs); **E.** Geosaurini (photographs). Arrow points anteriorly. Scale bars represent 1cm. Red dashed lines indicate missing parts. 32

12 Comparative figure of basal thalattosuchian and metriorhynchoid coracoids. **A.** Thalattosuchia (3D model); **B.** Metriorhynchoidea (photograph); **C.** Metriorhynchinae (photographs first row – 3D models second row); **D.** Rhacheosaurini (photographs); **E.** Geosaurinae (photograph); **F.** Geosaurini (photographs). Arrow points anteriorly. Scale bars represent 1cm. Red dashed lines indicate missing parts. 35

13 Pectoral girdle of *Pelagosaurus typus* BRLSI M.1418 (A&B) and *Pelagosaurus typus* BRLSI M.3578 (C&D) (photographs). **A.** Left coracoid in dorsal view; **B.** Left scapula in lateral view; **C.** Left scapula in lateral view; **D.** Left coracoid in ventral view. 38

14 Reconstruction of the pectoral girdle of *Pelagosaurus* BRLSI M.3578 (3D models). **A.** Lateral view; **B.** Anterior view; **C.** Ventral view; **D.** Dorsal view. Arrow points anteriorly. Target indicates anterior. The right scapula and coracoid are mirrored. 40

15 Pectoral girdle of *Thalattosuchus superciliosus* GLAHM V1005 (A&B; reconstruction of missing parts based on GLAHM V1146) and *Thalattosuchus superciliosus* GLAHM V1146 (C, D, E & F; reconstruction of missing parts based on GLAHM V1005) (photographs). **A.** Right coracoid in dorsal view ; **B.** Right coracoid in ventral view ; **C.** Left scapula in medial view ; **D.** Left scapula in lateral view ; **E.** Left coracoid in dorsal view ; **F.** Left coracoid in ventral view.

Arrow points anteriorly. Red dashed lines indicate missing parts. Reconstruction of missing parts based on *Thalattosuchus superciliosus* GLAHM V1005. 43

16 Pectoral girdle of *Thalattosuchus superciliosus* PMU 35988 (A&B) and *Thalattosuchus superciliosus* NHMUK PV R 1530 (C&D) (3D models). **A.** Right scapula in lateral view ; **B.** Left coracoid in ventral view ; **C.** Left coracoid in dorsal view ; **D.** Left coracoid in ventral view. Arrow points anteriorly. Red dashed lines indicate missing parts. Reconstruction of missing parts based on *Thalattosuchus superciliosus* GLAHM V1146 & GLAHM V1005. 46

17 Pectoral girdle of *Thalattosuchus superciliosus* GLAHM V1143 (photographs). **A.** Right scapula in lateral view ; **B.** Right scapula in medial view ; **C.** Right coracoid in ventral view ; **D.** Right coracoid in dorsal view. Arrow points anteriorly. Red dashed lines indicate missing parts. Reconstruction of missing parts based on *Thalattosuchus superciliosus* GLAHM V1146. 47

18 Reconstruction of the pectoral girdle of *Thalattosuchus superciliosus* GLAHM V1005 (A, C & E; reconstruction of missing parts based on GLAHM V1146) and *Thalattosuchus superciliosus* GLAHM V1146 (B, D, & F; reconstruction of missing parts based on GLAHM V1005) (3D models). **A.** Right lateral view GLAHM V1005; **B.** Right lateral view GLAHM V1146; **C.** Anterior view GLAHM V1005; **D.** Anterior view GLAHM V1146; **E.** Ventral view GLAHM V1005; **F.** Ventral view GLAHM V1146. Target indicates anterior. Arrow points anteriorly. The left scapula and coracoid of GLAHM V1005 are mirrored. The right scapula and coracoid of GLAHM V1146 are mirrored. 51

19 Reconstruction of the pectoral girdle of *Thalattosuchus superciliosus* PMU 35988 (A, C & E) and *Thalattosuchus superciliosus* NHMUK PV R 1530 (B, D, & F) (3D models). **A.** Right lateral view PMU 35988; **B.** Right lateral view NHMUK PV R 1530; **C.** Anterior view PMU 35988; **D.** Anterior view NHMUK PV R 1530; **E.** Ventral view PMU 35988; **F.** Ventral view NHMUK PV R 1530. Target indicates anterior. Arrow points anteriorly. The left scapula and right coracoid of PMU 35988 are mirrored. The right coracoid of NHMUK PV R 1530 is mirrored, and the scapula of *Thalattosuchus superciliosus* GLAHM V1146 is used in the reconstruction. 52

20 Reconstruction of the pectoral girdle of *Thalattosuchus superciliosus* GLAHM V1143 (3D models). **A.** Lateral view; **B.** Anterior view; **C.** Ventral view; **D.** Dorsal view. Arrow points anteriorly. Target indicates anterior. The left scapula and coracoid are mirrored. Reconstruction of missing parts based on *Thalattosuchus superciliosus* GLAHM V1146 & *Thalattosuchus superciliosus* GLAHM V1005. 53

21 Pectoral girdle of *Gracilineustes leedsi* Andrews, 1913 NHMUK PV R 3014 (3D models). **A.** Right scapula in lateral view ; **B.** Right scapula in medial view ; **C.** Right coracoid in dorsal view ; **D.** Right coracoid in ventral view. Arrow points anteriorly. Scans courtesy of (c) The Trustees of the Natural History Museum, London. Red dashed lines indicate missing parts. Reconstruction of missing parts based on *Thalattosuchus superciliosus* GLAHM V1146. 56

22 Pectoral girdle of *Gracilineustes leedsi* Andrews, 1913 NHMUK PV R 3015 (3D models). **A.** Right scapula in lateral view ; **B.** Right scapula in medial view ; **C.** Right coracoid in ventral view ; **D.** Right coracoid in dorsal view. Arrow points anteriorly. Scans courtesy of (c) The Trustees of the Natural History Museum, London. Red dashed lines indicate missing parts. Reconstruction of missing parts based on *Thalattosuchus superciliosus* GLAHM V1146 & *Gracilineustes leedsi* NHMUK PV R 3014. 57

23 Reconstruction of the pectoral girdle of *Gracilineustes leedsi* NHMUK PV R 3014 (A, C & E) and *Gracilineustes leedsi* NHMUK PV R 3015 (B, D, & F) (3D models). **A.** Right lateral view NHMUK PV R 3014; **B.** Right lateral view NHMUK PV R 3015; **C.** Anterior view NHMUK PV R 3014; **D.** Anterior view NHMUK PV R 3015; **E.** Ventral view NHMUK PV R 3014; **F.** Ventral

view NHMUK PV R 3015. Target indicates anterior. Arrow points anteriorly. The left scapula and coracoid of NHMUK PV R 3014 and NHMUK PV R 3015 are mirrored. The anterior expansion of the coracoid of *Thalattosuchus* GLAHM V1146 was used to reconstruction the coracoid of NHMUK PV R 3014 and NHMUK PV R 3015. The exact dimensions of the ventral spacing between the coracoids is uncertain so two reconstitutions are offered. 60

24 Pectoral girdle of *Rhacheosaurus gracilis* NHMUK PV R 3948 (photographs). **A.** Right coracoid in ventral view ; **B.** Right coracoid reconstructions with a closed (based on *Cricosaurus suevicus* SMNS 9808) and opened coracoid foramen (based on *Thalattosuchus superciliosus* GLAHM V1146) ; **C.** Overview of right pectoral girdle ; **D.** Overview of entire skeleton. Arrow points anteriorly. Red dashed lines indicate missing parts. 62

25 Pectoral girdle of *Cricosaurus albersdoerferi* BMMS-BK 1-2 (photographs). **A.** Left coracoid in ventral view ; **B.** Left scapula in lateral view ; **C.** Right coracoid in ventral view ; **D.** Overview of pectoral girdle. Arrow points anteriorly. Red dashed lines indicate missing parts. Reconstruction of missing parts based on *Cricosaurus suevicus* SMNS 9808. 64

26 Pectoral girdle of *Cricosaurus bambergensis* NKMB-P-Watt14/274 (photographs). **A.** Left coracoid in ventral view ; **B.** Left scapula in medial view ; **C.** Overview of pectoral girdle. Arrow points anteriorly. Red dashed lines indicate missing parts. Reconstruction of missing parts based on *Cricosaurus suevicus* SMNS 9808. 69

27 Pectoral girdle of *Cricosaurus suevicus* SMNS 9808 (photographs). **A.** Left scapula in lateral view ; **B.** Left coracoid in ventral view ; **C.** Overview of left pectoral girdle ; **D.** Overview of right pectoral girdle ; **E.** Right coracoid in dorsal view and right scapula in medial view ; **F.** Reconstruction of the left forelimb laying flat (forelimb modified from Fraas (1902)). Arrow points anteriorly. Red dashed lines indicate missing parts. Reconstruction of missing parts based on *Cricosaurus bambergensis* NKMB-P-Watt14/274. 71

28 Pectoral girdle of *Cricosaurus lithographicus* MOZ-PV 5787 (Herrera et al., 2013b) Wagner, 1858 (photographs). **A.** Right coracoid in ventral view ; **B.** Overview of pectoral girdle. Arrow points anteriorly. Pictures courtesy of Dr. Yanina Herrera. Red dashed lines indicate missing parts. Reconstruction of missing parts based on *Cricosaurus araucanensis* MLP 72-IV-7-1. 75

29 Pectoral girdle of *Cricosaurus araucanensis* MLP 72-IV-7-1 (Gasparini and Dellapé, 1976) Wagner, 1858 (photographs). **A.** Right coracoid in ventral view ; **B.** Overview of pectoral girdle. Arrow points anteriorly. Pictures courtesy of Dr. Yanina Herrera. 78

30 Pectoral girdle of *'Metriorhynchus'* NHMUK PV R 4696, forelimb of *'Metriorhynchus' brachyrhynchus* NHMUK PV R 4763 (photographs). **A.** Left coracoid in dorsal view ; **B.** Left coracoid in ventral view ; **C.** Right coracoid in dorsal view ; **D.** Right coracoid in ventral view. Arrow points anteriorly. Pictures (c) The Trustees of the Natural History Museum, London. Red dashed lines indicate missing parts. Reconstruction of missing parts based on *Thalattosuchus superciliosus* GLAHM V1146. 80

31 Reconstruction of the pectoral girdle of *'Metriorhynchus'* NHMUK PV R 4696 (3D models). **A.** Lateral view; **B.** Anterior view; **C.** Ventral view; **D.** Dorsal view. Arrow points anteriorly. Target indicates anterior. The right coracoid of *'Metriorhynchus'* NHMUK PV R 4696 is mirrored. The reconstitution of the scapula is based on *Thalattosuchus superciliosus* GLAHM V1146. Reconstruction of missing parts based on *Thalattosuchus superciliosus* GLAHM V1146. 83

32 Pectoral girdle of *Geosaurus lapparenti* UJF-ID.11847j (A&B) and *Geosaurus lapparenti* UJF-ID.11852f (C&D) (photographs). **A.** Left scaoula in lateral view; **B.** Left scapula in medial view; **C.** Right scapula in lateral view; **D.** Right scapula in ledial view. Cross indicates posterior. Arrow points anteriorly. Red dashed lines indicate missing parts. Reconstruction of missing

parts based on *Torvoneustes carpenteri* BRSMG Cd7203 and *Dakosaurus maximus* SMNS 8203. 85

33 Reconstruction of the pectoral girdle of *Geosaurus lapparenti* UJF-ID.11847j & UJF-ID.11852f (3D models). **A.** Lateral view; **B.** Anterior view; **C.** Posterior view; **D.** Dorsal view. Arrow points anteriorly. Target indicates anterior. Cross indicates posterior. The reconstitution of the coracoid is putative and is based on *Torvoneustes carpenteri* BRSMG Cd7203 and *Dakosaurus maximus* SMNS 8203. Reconstruction of missing parts of the scapula is based on *Torvoneustes carpenteri* BRSMG Cd7203 and *Dakosaurus maximus* SMNS 8203. 86

34 Pectoral girdle of *Dakosaurus maximus* SMNS 8203 (photographs). **A.** Left scapula in lateral view ; **B.** Left scapula in medial view ; **C.** Left coracoid in ventral view ; **D.** Left coracoid in dorsal view. Cross indicates posterior. Arrow points anteriorly. Red dashed lines indicate missing parts. Reconstruction of missing parts based on *Dakosaurus sp.* DMA-JP-2009/001. 88

35 Reconstruction of the pectoral girdle of *Dakosaurus maximus* SMNS 8203 (3D models). **A.** Lateral view; **B.** Anterior view; **C.** Posterior view; **D.** Dorsal view. Arrow points anteriorly. Target indicates anterior. Cross indicates posterior. The reconstitution of the coracoid is putative and is based on *Dakosaurus sp.* DMA-JP-2009/001. 90

36 Pectoral girdle of *Tyrannoneustes lythrodectikos* GLAHM V1145 (photographs). **A.** Left coracoid in dorsal view ; **B.** Left coracoid in ventral view. Arrow points anteriorly. Red dashed lines indicate missing parts. Reconstruction of missing parts based on *Thalattosuchus superciliosus* GLAHM V1146. 93

37 Reconstruction of the pectoral girdle of *Tyrannoneustes lythrodectikos* GLAHM V1145 (3D models). **A.** Lateral view; **B.** Anterior view; **C.** Ventral view; **D.** Dorsal view. Arrow points anteriorly. Target indicates anterior. The right coracoid of *Tyrannoneustes* GLAHM V1145 is mirrored. The reconstitution of the scapula is based on *Thalattosuchus superciliosus* GLAHM V1146. Reconstruction of missing parts based on *Thalattosuchus superciliosus* GLAHM V1146. 95

38 Pectoral girdle of *Torvoneustes carpenteri* BRSMG Cd7203 (photographs). **A.** Left scapula in medial view ; **B.** Left scapula in lateral view ; **C.** Right scapula in lateral view ; **D.** Right scapula in medial view. Arrow points anteriorly. Red dashed lines indicate missing parts. Reconstruction of missing parts based on *Dakosaurus maximus* SMNS 8203. 97

39 Reconstruction of the pectoral girdle of *Torvoneustes carpenteri* BRSMG Cd7203 (3D models). **A.** Lateral view; **B.** Anterior view; **C.** Ventral view; **D.** Dorsal view. Arrow points anteriorly. Target indicates anterior. Both the right and left fragments of the scapula of *To. carpenteri* BRSMG Cd7203 were combined to build the reconstructed version. The reconstitution of the coracoid is putative and is based on *Dakosaurus maximus* SMNS 8203. Reconstruction of missing parts based on *Dakosaurus maximus* SMNS 8203. 98

40 Pectoral girdle of *Mycterosuchus nasutus* NHMUK PV R 2617 (photographs). **A.** Left scapula in medial view ; **B.** Left coracoid in dorsal view ; **C.** Left scapula in lateral view ; **D.** Left coracoid in ventral view. Arrow points anteriorly. Red dashed lines indicate missing parts. Reconstruction of missing parts based on *Macrospondylus bollensis* SMNS 54063. 101

41 Comparative figure of teleosauroid scapulae. **A.** Aeolodontinae (3D model); **B.** Teleosauridae (3D model); **C.** Teleosaurinae (photographs); **D.** Machimosauridae (photograph and 3D model); **E.** Machimosaurinae (photographs); **F.** Machimosaurini (photograph). Arrow points anteriorly. Scale bars represent 1cm. Red dashed lines indicate missing parts. 102

42 Reconstruction of the pectoral girdle of *Mycterosuchus nasutus* NHMUK PV R 2617 (3D models). **A.** Lateral view; **B.** Anterior view; **C.** Ventral view; **D.** Dorsal view. Arrow points

anteriorly. Target indicates anterior. The right scapula and coracoid are mirrored. Scapula and coracoid have been slightly repaired based on *Macrospondylus* SMNS 54063, SMNS 9428 & PMU 35980. 104

43 Comparative figure of teleosauroid coracoids. **A.** Aeolodontinae (3D model and photograph); **B.** Teleosaurinae (photograph); **C.** Machimosauridae (photograph and 3D models); **D.** Machimosaurinae (photographs); **E.** Machimosaurini (3D model and photographs). Arrow points anteriorly. Scale bars represent 1cm. Red dashed lines indicate missing parts. 107

44 Pectoral girdle of *Aeolodon priscus* MNHN.F.CNJ 78 (photographs). **A.** Right pectoral girdle with the scapula mainly in anterior view and the coracoid in dorsal view; **B.** Overview of right pectoral girdle. Arrow points anteriorly. 109

45 Pectoral girdle of *Aeolodon priscus* NHMUK PV R 1086 (photographs). **A.** Right coracoid in dorsal view ; **B.** Overview of the pectoral girdle. Arrow points anteriorly. 110

46 Reconstruction of the pectoral girdle of *Aeolodon priscus* NHMUK PV R 1086 (3D models). **A.** Lateral view; **B.** Anterior view; **C.** Ventral view; **D.** Dorsal view. Arrow points anteriorly. Target indicates anterior. The left coracoid is mirrored. The scapula has been putatively reconstituted based on *Aeolodon* MNHN.F.CNJ 78 and *Te. cadomensis* NHMUK PV OR 31836. The ventral surface of the coracoid has been reconstructed. 112

47 Pectoral girdle of *Indosinosuchus potamosiamensis* PRC-24 (3D models). **A.** Right scapula in lateral view ; **B.** Right scapula in ventral view ; **C.** Right scapula in posterior view ; **D.** Right scapula in medial view. Arrow points anteriorly. Cross indicates posterior view. 3D model courtesy of Suravech Suteethorn. 115

48 Pectoral girdle of *Teleosaurus cadomensis* NHMUK PV OR 31836 (photograph). **A.** Left scapula in medial view. Arrow points anteriorly. 118

49 Pectoral girdle of *Platysuchus multiscrobiculatus* SMNS 9930 (**A** and **B**) & UMH-0005 (**C**) (photographs). **A.** Right scapula in lateral view; **B.** Right coracoid in ventral view; **C.** Left scapula of UMH-0005 mirrored not to scale. Arrow points anteriorly. Red dashed lines indicate missing parts. Reconstruction of missing parts of the scapula of SMNS 9930 based on UMH-0005. Reconstruction of missing parts of the coracoid based on *Macrospondylus bollensis* SMNS 54063. 120

50 Pectoral girdle of *Platysuchus multiscrobiculatus* from Kloster Banz (unnumbered) (3D models). **A.** Pectoral girdle; **B.** Overview of the entire skeleton. Arrow points anteriorly. 122

51 Reconstruction of the pectoral girdle of *Platysuchus multiscrobiculatus* SMNS 9930 (3D models). **A.** Lateral view; **B.** Anterior view; **C.** Ventral view; **D.** Dorsal view. Arrow points anteriorly. Target indicates anterior. The left scapula and coracoid are mirrored. The scapula has been reconstructed based on *Platysuchus multiscrobiculatus* UMH-0005, and the coracoid based on *Platysuchus multiscrobiculatus* Kloster Banz unnumbered specimen. 124

52 Pectoral girdle of *Macrospondylus bollensis* SMNS 54063 (A&B; photographs), *Macrospondylus bollensis* SMNS 9428 (C&D; photographs) and *Macrospondylus bollensis* PMU 35980 (E; 3D model). **A.** Right scapula in medial view; **B.** Right coracoid in dorsal view; **C.** Left scapula in lateral view; **D.** Left coracoid in ventral view; **E.** Overview of right pectoral girdle. Arrow points anteriorly. Red dashed lines indicate missing parts. Reconstruction of missing parts of the scapula of *Macrospondylus bollensis* SMNS 9428 based on *Macrospondylus bollensis* SMNS 54063 and *Macrospondylus bollensis* PMU 35980. Reconstruction of missing parts of the coracoids of *Macrospondylus bollensis* SMNS 54063 and *Macrospondylus bollensis* SMNS 9428 based on *Macrospondylus bollensis* PMU 35980. 127

53 Reconstruction of the pectoral girdle of *Macrospondylus bollensis* PMU 35980 (3D models). **A.** Lateral view; **B.** Anterior view; **C.** Ventral view; **D.** Dorsal view. Arrow points anteriorly. Target indicates anterior. The left scapula and coracoid are mirrored. The scapula has been reconstructed based on *Macrospondylus bollensis* SMNS 54063, and the coracoid based on *Macrospondylus bollensis* SMNS 9428. 130

54 Pectoral girdle of *Charitomenosuchus leedsi* NHMUK PV R 3806 (3D models). **A.** Right scapula in medial view ; **B.** Right scapula in lateral view ; **C.** Left coracoid in dorsal view ; **D.** Left coracoid in ventral view. Arrow points anteriorly. Red dashed lines indicate missing parts. 133

55 Reconstruction of the pectoral girdle of *Charitomenosuchus leedsi* NHMUK PV R 3806 (3D models). **A.** Lateral view; **B.** Anterior view; **C.** Ventral view; **D.** Dorsal view. Arrow points anteriorly. Target indicates anterior. The left scapula and coracoid are mirrored. Reconstruction of missing parts of the right girdle based on the left one (NHMUK PV R 3806). 137

56 Pectoral girdle of *Neosteneosaurus edwardsi* NHMUK PV R 3701 (photographs). **A.** Left scapula in lateral view ; **B.** Left scapula in medial view ; **C.** Right coracoid in dorsal view ; **D.** Right coracoid in ventral view. Arrow points anteriorly. Red dashed lines indicate missing parts. Reconstruction of missing parts based on *Neosteneosaurus edwardsi* PETMG R178. 139

57 Pectoral girdle of *Neosteneosaurus edwardsi* PETMG R178 (photographs). **A.** Right scapula in lateral view ; **B.** Right scapula in medial view ; **C.** Left coracoid in ventral view ; **D.** Left coracoid in dorsal view. Arrow points anteriorly. Red dashed lines indicate missing parts. Reconstruction of missing parts based on *Neosteneosaurus edwardsi* NHMUK PV R 3701. 141

58 Reconstruction of the pectoral girdle of *Neosteneosaurus edwardsi* NHMUK PV R 3701 (3D models). **A.** Lateral view; **B.** Anterior view; **C.** Ventral view; **D.** Dorsal view. Arrow points anteriorly. Target indicates anterior. The left scapula and coracoid are mirrored. Reconstruction of missing parts based on *Neosteneosaurus edwardsi* PETMG R178. 145

59 Pectoral girdle of *Lemmysuchus obtusidens* NHMUK PV R 3168 (A & B; photographs) and *Lemmysuchus* NHMUK PV R 3169 (C & D; 3D models). **A.** Left scapula in lateral view ; **B.** left scapula in medial view; **C.** Left coracoid in ventral view ; **D.** Left coracoid in dorsal view. Arrow points anteriorly. Red dashed lines indicate missing parts. Reconstruction of missing parts based on *Neosteneosaurus edwardsi* PETMG R178. 149

60 Reconstruction of the pectoral girdle of *Lemmysuchus obtusidens* (3D models). Scapula from *Lemmysuchus obtusidens* NHMUK PV R 3168 & coracoid from *Lemmysuchus obtusidens* NHMUK PV R 3169. **A.** Lateral view; **B.** Anterior view; **C.** Ventral view; **D.** Dorsal view. Arrow points anteriorly. Target indicates anterior. The left scapula and coracoid are mirrored. Reconstruction of missing parts based on *Neosteneosaurus edwardsi* PETMG R178 and *Neosteneosaurus edwardsi* NHMUK PV R 3701. 152

61 Pectoral girdle of *Machimosaurus* spp.: *Machimosaurus mosae* Neotype (lost during WWII) (A&B) and *Machimosaurus buffetauti* SMNS 91415 (C) (photographs). **A.** Right coracoid in dorsal view ; **B.** Right humerus in dorsal view ; **C.** Left coracoid in ventral view. Arrow points anteriorly. Red dashed lines indicate missing parts. Reconstruction of missing parts based on *Lemmysuchus obtusidens* NHMUK PV R 3168. 155

62 Pectoral girdle of *Anthracosuchus balrogus* UF/IGM 68 (photographs). **A.** Left scapula in lateral view ; **B.** Left scapula in medial view. Arrow points anteriorly. Red dashed lines indicate missing parts. Reconstruction of missing parts based on *Hyposaurus natator* NJSM 23368. 157

63 Comparative figure of dyrosaurid scapulae (photographs). **A.** Basal dyrosaurid; **B.** Dyrosaurinae. Arrow points anteriorly. Scale bars represent 1cm. Red dashed lines indicate missing parts. 159

64 Pectoral girdle of *Hyposaurus natator* NJSM 23368, pictures courtesy of Wayne Callahan (photographs). **A.** Right scapula in lateral view ; **B.** Right scapula in medial view ; **C.** Left coracoid in dorsal view ; **D.** Left coracoid in ventral view. Arrow points anteriorly. Red dashed lines indicate missing parts. Reconstruction of missing parts based on *Congosaurus bequaerti* MRAC 1809. 161

65 Reconstruction of the pectoral girdle of *H. natator* NJSM 23368 (3D models). **A.** Lateral view; **B.** Anterior view; **C.** Ventral view; **D.** Dorsal view. Arrow points anteriorly. Target indicates anterior. The left scapula and coracoid are mirrored. 3D models courtesy of Candice Stephanic. Reconstruction of missing parts based on *Congosaurus bequaerti* MRAC 1809. 164

66 Pectoral girdle of *Hyposaurus natator* YPM VP.000985 (photographs). **A.** Right scapula in lateral view ; **B.** Right scapula in medial view ; **C.** Left coracoid in dorsal view ; **D.** Left coracoid in ventral view. The shaft of the coracoid is reconstructed. Arrow points anteriorly. Red dashed lines indicate missing parts. Reconstruction of missing parts based on *Hyposaurus natator* NJSM 23368 and *Congosaurus bequaerti* MRAC 1809. 165

67 Pectoral girdle of *Hyposaurus natator* YPM VP.000764 (photographs). **A.** Left coracoid in ventral view ; **B.** Left coracoid in dorsal view ; **C.** Left coracoid in posterior view ; **D.** Left coracoid in anterior view. Arrow points anteriorly. Red dashed lines indicate missing parts. Reconstruction of missing parts based on *Hyposaurus natator* NJSM 23368. 167

68 Comparative figure of Dyrosaurinae coracoids (photographs). Arrow points anteriorly. Scale bars represent 1cm. Red dashed lines indicate missing parts. 169

69 Pectoral girdle of *Dyrosaurus maghribensis* OCP DEK-GE 252 (A&B) and *Dyrosaurus maghribensis* OCP DEK-GE 254 (C&D) (photographs). **A.** Right scapula in lateral view; **B.** Right coracoid in ventral view ; **C.** Right scapula in lateral view ; **D.** Right coracoid in ventral view. Arrow points anteriorly. Red dashed lines indicate missing parts. Reconstruction of missing parts based on *Hyposaurus natator* NJSM 23368 and *Dyrosaurus maghribensis* OCP DEK-GE 351. 172

70 Pectoral girdle of *Dyrosaurus maghribensis* OCP DEK-GE 254 (A&B) and *Dyrosaurus maghribensis* OCP DEK-GE 351 (C&D) (photographs). **A.** Left scapula in medial view; **B.** Left coracoid in dorsoanterior view ; **C.** Left coracoid in ventral view ; **D.** Left scapula in lateral view. Arrow points anteriorly. Red dashed lines indicate missing parts. Reconstruction of missing parts of OCP DEK-GE 254 based on *Hyposaurus natator* NJSM 23368 and *Dyrosaurus maghribensis* OCP DEK-GE 351. Reconstruction of missing parts of *Dyrosaurus maghribensis* OCP DEK-GE 351 based on *Hyposaurus natator* NJSM 23368. 173

71 Pectoral girdle of *Congosaurus bequaerti* MRAC 1809 (A&B) and MRAC 1811 (C&D) (photographs). **A.** Right scapula in lateral view ; **B.** Right scapula in medial view ; **C.** Right coracoid in ventral view ; **D.** Right coracoid in dorsal view. Arrow points anteriorly. Red dashed lines indicate missing parts. Reconstruction of missing parts based on *Hyposaurus natator* NJSM 23368. 177

72 Reconstruction of the pectoral girdle of *Congosaurus bequaerti* MRAC 1809 (A&B) and MRAC 1811 (3D models). **A.** Lateral view; **B.** Anterior view; **C.** Ventral view; **D.** Dorsal view. Arrow points anteriorly. Target indicates anterior. The left scapula and coracoid are mirrored. Reconstruction of missing parts based on *Hyposaurus natator* NJSM 23368. 180

73 Schematic representation of the pectoral girdle with approximated distribution of muscles origins and insertions based on Meers (2003). **A.** Teleosauroid pectoral girdle in lateral view; **B.** Teleosauroid pectoral girdle in medial view; **C.** Dyrosaurid pectoral girdle in lateral view; **D.** Dyrosaurid pectoral girdle in medial view. Arrow points anteriorly. Cartilaginous structures represented in yellow. Muscles origins are colored in red; muscles insertions are colored in blue.

As most muscles involved in the pectoral girdle of extant crocodylians lack clear osteological correlates (Otero et al., 2017), these reconstructions only bear a qualitative appearance. See tables 4 and 5 for abbreviation and definition. 182

74 Implied weighting (k=12) consensus tree of our cranial dataset. Crocodylomorphs silhouettes: Metriorhynchoidea and Teleosauroidea (c) Gareth Monger – Licence CC BY 3.0; Dyrosauridae (c) Nobu Tamura, vectorized by Zimices – Licence CC BY-SA 3.0; Crocodylia original picture (c) Thesupermart – License CC BY-SA 3.0; Gharial – License CC0 1.0 Universal Public Domain Dedication. 184

75 Implied weighting (k=12) consensus tree of our postcranial dataset. Crocodylomorphs silhouettes: Metriorhynchoidea and Teleosauroidea (c) Gareth Monger – Licence CC BY 3.0; Dyrosauridae (c) Nobu Tamura, vectorized by Zimices – Licence CC BY-SA 3.0; Crocodylia original picture (c) Thesupermart – License CC BY-SA 3.0. 185

76 Implied weighting (k=12) consensus tree of our complete dataset (cranial and postcranial merged). Crocodylomorphs silhouettes: Metriorhynchoidea and Teleosauroidea (c) Gareth Monger – Licence CC BY 3.0; Dyrosauridae (c) Nobu Tamura, vectorized by Zimices – Licence CC BY-SA 3.0; Crocodylia original picture (c) Thesupermart – License CC BY-SA 3.0. 186

77 Figure illustrating the phylogeny of Metriorhynchoidea including a summary of the different pectoral girdle morphology. Figure modified from Young et al. (2020a) for the global phylogeny; the relationships of *C. suevicus,Cricosaurus albersdoerferi* and *C. bambergensis* modified from Sachs et al. (2021). 192

78 Figure illustrating the phylogeny of Teleosauroidea including a summary of the different pectoral girdle morphology. Figure modified from Johnson et al. (2020). 193

79 Figure illustrating the phylogeny of Dyrosauridae including a summary of the different pectoral girdle morphology. Figure modified from Jouve and Jalil (2020). 194